UNIVERSIDAD COMPLUTENSE DE MADRID

FACULTAD DE CIENCIAS BIOLÓGICAS

TESIS DOCTORAL

Diseño racional de peroxidasas ligninolíticas

Rational design of ligninolytic peroxidases

MEMORIA PARA OPTAR AL GRADO DE DOCTOR

PRESENTADA POR

Verónica Sáez Jiménez

Directores

Ángel Tomás Martínez Ferrer
Francisco Javier Ruiz Dueñas

Madrid, 2016

DISEÑO RACIONAL DE PEROXIDASAS LIGNINOLÍTICAS

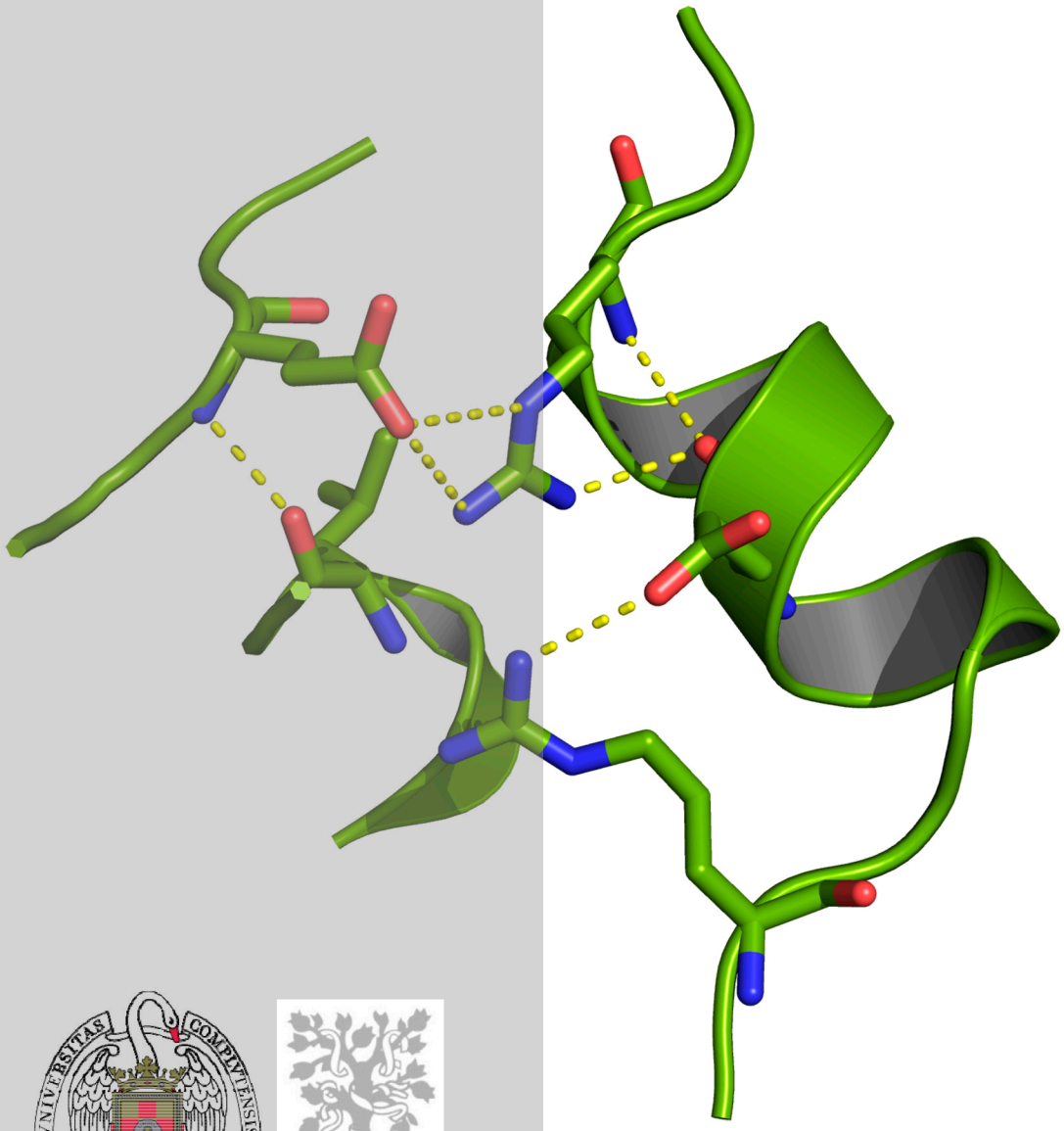

Verónica Sáez Jiménez

DISEÑO RACIONAL DE PEROXIDASAS LIGNINOLÍTICAS

TESIS DOCTORAL

Verónica Sáez Jiménez

Centro de Investigaciones Biológicas
CSIC

Facultad de Ciencias Biológicas
Universidad Complutense de Madrid

Madrid, 2015

DISEÑO RACIONAL DE PEROXIDASAS LIGNINOLÍTICAS

RATIONAL DESIGN OF LIGNINOLYTIC PEROXIDASES

Tesis doctoral presentada por
Verónica Sáez Jiménez para optar al grado de
Doctor por la Universidad Complutense de Madrid

Directores:

Dr. Ángel Tomás Martínez Ferrer
Profesor de Investigación, CSIC

Dr. Francisco Javier Ruiz Dueñas
Investigador, CSIC

Madrid, 2015

A Javi

A Sofía

AGRADECIMIENTOS

La presente tesis doctoral ha sido realizada en el Centro de Investigaciones Biológicas (CSIC) y en la universidad de Siena durante una estancia breve. Ha sido financiada por una beca predoctoral de Formación de Personal Investigador (FPI, Ref. BES-2009-014246) y una beca para estancia breve, así como por los proyectos europeos "Novel and more robust fungal peroxidases as industrial biocatalysts" (PEROXICATS, KBBE-2010-4-265397) y "Optimized oxidoreductases for medium and large scale industrial biotransformations" (INDOX, KBBE-2013-613549), junto a los proyectos del plan nacional de I+D+i "Búsqueda e ingeniería de nuevas peroxidasas fúngicas de alto potencial redox" (HIPOP, BIO2011-26694) y "Nuevas enzimas oxidativas para una industria sostenible" (NOESIS, BIO2014-56388-R).

Dicen que la felicidad se encuentra en el camino, y no en el destino. Debe ser cierto, pues durante el "camino" recorrido en todos estos años, he atesorado muchas vivencias preciosas. Por ello quiero agradecer a todas las personas con las que me he cruzado en esta aventura y que han contribuido con su talento y cariño a la realización de esta tesis.

En primer lugar, al Dr. Ángel T. Martínez, que me dio la oportunidad de realizarla en su grupo de investigación y del que he aprendido tanto (eres una fuente inacabable de conocimientos). Gracias por el tiempo dedicado, tus consejos y tu humor irónico. Sin ti, este trabajo y las publicaciones no habrían visto la luz.

Al Dr. Francisco J. Ruiz Dueñas (Javi), siempre compresivo, alentador y preciso como buen científico, que me ha contagiado su pasión por este trabajo. Gracias por tu dedicación y entrega, fundamentales para la realización de toda esta labor.

También me gustaría dar las gracias a todos los colaboradores imprescindibles que han contribuido a completar este trabajo: el Dr. Francisco J. Medrano y el Dr. Antonio Romero, que cristalizaron varias variantes de VP; las Dras. Rebecca Pogni y Camilla Baratto, que nos han ayudado con los análisis de EPR; igualmente al Dr. Jorge Rencoret, la Dra. Ana Gutiérrez y el Dr. José Ignacio Santos, expertos en NMR; al Dr.

Victor Guallar, la Dra. Fatima Lucas y Sandra Acebes, que aportaron su visión computacional al trabajo; a la Dra. Vivian de los Rios, mi agradecimiento por los análisis de espectrometría de masas; y a la Dra. Emilia Aporta, que realizó los análisis de aminoácidos.

En especial a las Dras. Rebecca Pogni y Camilla Baratto quienes, durante mi estancia en Siena, me recibieron con los brazos abiertos y con las que me fue tan fácil y ameno trabajar.

A todos mis compañeros del CIB, ¡con los que se trabaja muy a gusto! A las Dras. María Jesús Martínez y Alicia Prieto, siempre con una sonrisa en la boca. A la Dra. Marta Pérez Boada, siempre dispuesta a escuchar y ayudar (¡eres un sol!) y a la Dra. Susana Camarero, pendiente y resolutiva. A Lola, por sus impagables consejos para ser una súper mami. A Cris y sus deliciosísimas tartas. A Iván, el compañero de labo y de pádel perfecto. A Juan, irónico y divertido. A Ana, tan eficiente. A David, con sus prisas y sus risas. A Meme y su alegría contagiosa. Y a José María Barrasa, con su sabiduría fúngica. También a mis compañeros de los laboratorios 249 y 245: a Mariu, con la que he sufrido el final de la interminable tesis. Gracias por tus consejos y los buenos momentos (eres un cielo). A Laura-Lidem, con tu humor irrepetible y tus riquísimas recetas. A Manolito, con tu manera de ser única e irrepetible. Y a Emmanuel, su alter ego. A Isa Pardo, eficiente y positiva. A Felipe, amable y divertido. A María, con su pasión contagiosa por la ciencia. A Jorge, con sus chistes malos de los cafés. A Úrsula, siempre positiva y divertida a pesar de todo. A Rosa, tan amable. A Juanan, tan discreto. Y a Gerard y a Jose. No quisiera dejarme en el tintero a todos los que hace tiempo que no veo, pero que fueron parte fundamental del grupo BioLig: Elena, con la que he compartido tantos buenos momentos; Aitor y Yuta, y a sus sabios consejos que me enseñaron mucho sobre peroxidasas; Bea Balcells, que sabe vivir la vida; Mario (coccus); Jesús, mi bloguero científico favorito; Davinia, con sus chistes a dúo con Juan; MariJose, que le ponía mucha marcha al labo. Y por supuesto, a Lorea, Erick, Xiomara, Ledys, Zayra, Deborah, Craig, Mario Saparrat (con sus mates y su labia), Leandro, Beatriz Casas, Miguel, Amaia, Victor, Rita, Gisela, Dalel, Belén, Elda, Xueyu (Sueño José)… A mis otros compañeros del 209, Fran y Tomás que nos acogieron tan bien a los nuevos del 248. También a mis

compañeros del ICP: Isa Vicente (siempre de buen humor), David, Patricia, Miguel, Eva, Javi y Bernardo.

Y a Alessio, Silvia, Caterina, Federico, Daniele, Andrea, Alice y Adalgisa, que me enseñaron la cultura toscana y con los que compartí muy buenos momentos. ¡Grazie mille, amici!

A las increíbles BioLocas: Eva, Paloma, Sara, Gloria, Emi, Marian y Marta, que comparten conmigo su amistad y la pasión por la ciencia y con quienes comencé hace años, esta andadura. Y por supuesto, a Silvia.

Y en última instancia, pero no menos importantes, a mi familia: mis padres, Julio y Paula, y a Julio y Natalia, que siempre, siempre están ahí, que me han dado todo el apoyo e ilusión del mundo y a los que quiero con locura. A "Los Salaos", mi familia a lo grande, con los que he pasado tantos buenísimos momentos (también malos, aunque éstos se hacen menos malos con ellos al lado), también os quiero con locura. En especial a mis primas, Paula y Mari Carmen, que comparten conmigo su pasión por la biología; Irene, una de las personas más especiales que conozco; Elena, la más audaz y viajera; Raquel, la súper mami; y Martina, que va para veterinaria, seguro. También a Bárbara, sensible y única; y a Belén, activa y risueña. A mi tío Juan Carlos, permanentemente preocupado por mi tesis. A la familia Pino Balce, divertidos y acogedores.

Y muy especialmente, a Javi y Sofía, que sois las dos personas más importantes de mi vida, y que hacéis de mi día a día una aventura fascinante. Javi, que siempre has estado ahí, desde antes del comienzo de esta tesis, que me haces tan feliz y haces de mi vida una continua ilusión. Que me das los más valiosos consejos y me aportas otras perspectivas. Espero tener la gran fortuna de compartir mil aventuras más contigo. ¡Te quiero con toda mi alma! A Sofía, que eres lo más increíble que me ha ocurrido y que llenas de ilusión y alegría mi vida. Y que con tu mágica perspectiva del mundo, haces que valore lo realmente importante. ¡Te quiero con locura mi niña!

¡Muchas gracias a todos!

ÍNDICE

RESUMEN **1**

1. Antecedentes 1
2. Objetivos 3
3. Resultados 3
   - 3.1 Estudio y mejora de la estabilidad oxidativa de la VP 3
   - 3.2 Estudio y mejora de la estabilidad a pH de la VP 4
   - 3.3 Investigando las propiedades mejoradas de una variante evolucionada de la VP 5
   - 3.4 Estudio de la capacidad de la VP para oxidar lignosulfonatos y de la transferencia electrónica entre la VP y la lignina 6
4. Conclusiones 7

ABSTRACT **9**

1. Background 9
2. Aims 11
3. Results 11
   - 3.1 Study and improvement of the oxidative stability of VP 11
   - 3.2 Study and improvement of the pH stability of VP 12
   - 3.3 Investigating the basis of stability in an evolved VP 13
   - 3.4 Study on the lignin-to-peroxidase direct electron transfer and the ability of VP to oxidize technical lignins 14
4. Conclusions 15

ABREVIATURAS **17**

INTRODUCCIÓN **19**

1. Hacia una nueva bioeconomía 21
   - 1.1 Biotecnología blanca 21
   - 1.2 Biorrefinerías de la lignocelulosa 22
   - 1.3 Importancia de los hongos que degradan la biomasa vegetal 25
2. Peroxidasas ligninolíticas 28
   - 2.1 Aspectos generales 28
   - 2.2 Diferentes familias (y nuevas superfamilias) 31
3. Peroxidasa versátil 34
   - 3.1 Sitio de oxidación del manganeso (Mn^{2+}) 35
   - 3.2 Triptófano catalítico 36

3.3 Canal principal de acceso al hemo 38
3.4 Ciclo catalítico global 39
3.5 Características espectroscópicas 40
4. Aplicaciones de las PODs ligninolíticas 44
4.1 Deslignificación industrial 44
4.2 Biorremediación 45
4.3 Síntesis 46
5. Optimización de las PODs como biocatalizadores 46
5.1 Aspectos generales 46
5.2 Mejora de la estabilidad oxidativa de la VP 48
5.3 Mejora de la estabilidad al pH de la VP 50
6. Bibliografía 52
OBJETIVOS 61
CHAPTER 1: Improving the Oxidative Stability of a High Redox Potential Fungal Peroxidase by Rational Design 65
Abstract 67
1. Introduction 67
2. Materials and methods 70
2.1 Chemicals 70
2.2 Amino acid analysis 70
2.3 Design of mutated variants at the heme distal side 70
2.4 Site-directed mutagenesis 71
2.5 Enzyme production, activation and purification 72
2.6 Steady-state kinetics 72
2.7 Transient-state kinetics 72
2.8 Oxidative stability studies 73
2.9 Spectral analysis of transient states in H_2O_2 reactions 73
3. Results 74
3.1 Strategies to improve the VP oxidative stability and kinetic analysis of the designed variants 74
3.2 Oxidative stabilization 78
3.3 Spectral analyses 81
4. Discussion 85
4.1 Stability improvement by substituting oxidizable methionines 86

4.2 Stability improvement by decreasing enzyme reactivity with H_2O_2 87
4.3 Final improvement by combining two stabilization strategies 88
5. References 90
CHAPTER 2: Improving the pH-stability of Versatile Peroxidase by Comparative Structural Analysis with a Naturally-stable Manganese Peroxidase 95
Abstract 97
1. Introduction 97
2. Materials and methods 100
2.1 Chemicals 100
2.2 Design of VP variants 100
2.3 Enzyme production, activation and purification 101
2.4 Kinetic studies 102
2.5 Optimum pH determination 103
2.6 pH stability studies 103
2.7 Thermal stability studies 103
2.8 Crystallization 103
2.9 Data collection and processing 104
3. Results 106
3.1 Rational design strategy 106
3.2 Effect of the mutations on VP catalytic properties 109
3.3 pH and thermal stability of VP variants 112
3.4 Crystal structure analysis of the VP variants 117
4. Discussion 120
5. Conclusions 126
6. References 128
CHAPTER 3: Investigating the basis of stability in an evolved versatile peroxidase variant .. 133
Abstract 135
1. Introduction 135
2. Material and Methods 137
2.1 Chemicals 137
2.2 Directed mutagenesis 137
2.3 Heterologous expression 138
2.4 pH stability studies 139
2.5 Kinetic constants 140

2.6 Crystallization, data collection and crystal structure determination 140
3. Results 142
3.1 pH stability of the different variants 142
3.2 pH effect on the UV-visible spectra 145
3.3 Catalytic constants 146
3.4 Analysis of crystal structures 148
4. Discussion 151
4.1 Explaining the alkaline stability 152
4.2 Explaining the modified catalytic properties 155
4.3 Conclusions 156
5. References 157
CHAPTER 4: Demonstration of Lignin-to-Peroxidase Direct Electron Transfer: A Transient-state Kinetics, Directed Mutagenesis, EPR and NMR Study 161
Abstract 163
1. Introduction 163
2. Material and methods 166
2.1 Enzyme production 166
2.2 Softwood and hardwood lignins 167
2.3 Enzyme (transient-state) kinetics 167
2.4 EPR of VP reactions with lignin 169
2.5 Lignosulfonate treatment under steady-state conditions 170
2.6 SEC and GC-MS analyses 170
2.7 Lignin NMR 171
3. Results 172
3.1 Transient-state kinetics of electron abstraction from lignin 172
3.2 EPR detection of VP and lignin radicals 175
3.3 Fluorescence changes during the VP treatments 176
3.4 Changes of lignin molecular mass 177
3.5 NMR analyses of lignosulfonates after VP treatment 178
4. Discussion 182
4.1 Lignin oxidation by VP 182
4.2 Role of VP Trp-164 184
4.3 Importance of the Trp-164 environment 185
4.4 Concluding remarks 187

5. References 189
DISCUSIÓN GENERAL 193
1. Estudio y mejora de la estabilidad oxidativa. 195
2. Estudio y mejora de la estabilidad a pH. 197
3. Demostración de la transferencia electrónica entre la VP y la lignina 199
4. References 201
CONCLUSIONES/ CONCLUSIONS 203
ANEXO I 209

RESUMEN

1. Antecedentes

Las peroxidasas ligninolíticas son enzimas que tienen una gran potencial biotecnológico debido a sus propiedades catalíticas que les permiten oxidar una gran variedad de sustratos recalcitrantes. Son producidas por los hongos de podredumbre blanca, los principales responsables de la degradación de la lignina en la naturaleza. La lignina es el material aromático renovable más abundante en la naturaleza y, junto con la celulosa y la hemicelulosa, compone la biomasa lignocelulósica. Estructuralmente, es un polímero aromático muy heterogéneo, y recalcitrante. Para degradar la lignina, los hongos de podredumbre blanca secretan un conjunto de oxidorreductasas al medio, entre las que se encuentran las peroxidasas ligninolíticas, que juegan un papel central en este proceso.

Las peroxidasas ligninolíticas son hemo peroxidasas de alto potencial redox. Se clasifican en tres familias: lignina peroxidasas (LiP), manganeso peroxidasas (MnP) y peroxidasas versátiles (VP). Las VP se caracterizan por la presencia de tres sitios catalíticos: i) un triptófano catalítico expuesto en superficie, que puede formar un radical de proteína a través de una ruta de transferencia electrónica desde el hemo y es capaz de oxidar compuestos de alto potencial redox; ii) el sitio de oxidación de manganeso, que le permite oxidar Mn^{2+} a Mn^{3+}; y iii) el canal principal de acceso al hemo en el que se oxidan compuestos de bajo potencial redox. Entre las distintas peroxidasas ligninolíticas, la VP presenta un especial interés debido a que combina las propiedades catalíticas propias de LiP, MnP y las peroxidasas genéricas y, además, no necesita de la presencia de mediadores para su actuación. Por ello, la VP, en concreto la variante alélica VPL2 de *Pleurotus eryngii*, fue la peroxidasa escogida para realizar los trabajos de la presente tesis doctoral.

Las propiedades catalíticas de la VP y demás peroxidasas ligninolíticas les permiten oxidar compuestos aromáticos fenólicos y no fenólicos, así como diferentes tintes industriales y pesticidas. Por ello, las reacciones de oxidación que llevan a cabo estas enzimas son interesantes desde un punto de vista biotecnológico. Además, estas peroxidasas tienen la ventaja de ser autosuficientes, en el sentido de que son activadas por

H_2O_2, un oxidante de fácil adquisición. Por tanto, la utilización de peroxidasas ligninolíticas como biocatalizadores en diferentes procesos industriales representa una alternativa sostenible y respetuosa con el medio ambiente frente al uso de métodos químicos convencionales. Sin embargo, muy pocas de ellas se comercializan y su aplicación industrial es modesta. Esto es debido, principalmente, a que no son aplicables tal cual se producen en la naturaleza, ya que no presentan una adecuada selectividad y compatibilidad con los rigurosos procesos industriales. Por ello, algunas de sus propiedades han de ser optimizadas antes de su aplicación.

La estabilidad frente a H_2O_2 (estabilidad oxidativa) es uno de los principales obstáculos a superar para el uso biotecnológico de las peroxidasas ligninolíticas. El H_2O_2, necesario para el funcionamiento de las peroxidasas, es un fuerte oxidante que tiene efectos deletéreos sobre estas enzimas. La inactivación por H_2O_2 es un proceso irreversible, especialmente importante cuando existe un exceso de peróxido o no existe sustrato reductor. Su mecanismo no se conoce por completo, aunque se sabe que es consecuencia de diferentes reacciones de oxidación que afectan a distintos componentes de la enzima, incluyendo aminoácidos y el anillo de porfirina del cofactor.

La estabilidad a pH es otro de los factores clave que a menudo necesita ser optimizado. La inactivación de las peroxidasas ligninolíticas debida al pH alcalino, o incluso neutro, se produce como consecuencia de la pérdida de los calcios estructurales responsables del mantenimiento de la correcta conformación del bolsillo del hemo. La ausencia de los calcios conduce al colapso de la estructura, lo que lleva a que el hierro del hemo quede hexacoordinado y la enzima inactiva. De igual forma, estas enzimas también se inactivan a pH ácido, aunque en este caso como consecuencia de la rotura del enlace entre el hierro del hemo y la histidina proximal.

Por otra parte, aunque las propiedades de la VP y las otras peroxidasas ligninolíticas están ampliamente estudiadas, todavía hay aspectos catalíticos que no se conocen claramente. Por todo ello, es necesario comprender las bases estructurales que determinan y regulan la estabilidad y catálisis de estas enzimas para que su optimización y empleo sea una opción real.

2. Objetivos

Los principales objetivos de la presente tesis fueron: i) el diseño de una VP que presente unas características más adecuadas para su uso biotecnológico, y ii) la profundización en el conocimiento de las bases estructurales que regulan la catálisis y estabilidad de la VP. Para ello, se abordaron las siguientes tareas:

i) El estudio de la estabilidad oxidativa de la VP y de las bases estructurales que determinan esta propiedad, así como el diseño de una variante mutada que presente mayor resistencia oxidativa.
ii) El diseño de una variante de VP con mayor estabilidad a pH mediante la transferencia de motivos estabilizantes encontrados en peroxidasas relacionadas (Fernández-Fueyo et al. Biotechnology for Biofuels 2014, 7:2).
iii) El análisis de la variante VP 2-1B obtenida por evolución dirigida (García-Ruiz et al. Biochem. J. (2012) 441, 487–498) con objeto de averiguar qué determinantes estructurales generados por las mutaciones introducidas regulan sus propiedades catalíticas y estabilidad mejoradas.
iv) Profundizar en el conocimiento del funcionamiento del triptófano catalítico, estudiar la transferencia electrónica entre la peroxidasa y la lignina durante la oxidación de ésta, y mostrar la capacidad de la VP para oxidar ligninas técnicas.

Para realizar estas tareas, se utilizó un enfoque racional y se diseñaron diferentes variantes mutadas, que posteriormente fueron evaluadas.

3. Resultados

3.1 Estudio y mejora de la estabilidad oxidativa de la VP

El estudio de la estabilidad oxidativa de la VP demostró que la enzima se inactiva fácilmente por H_2O_2. Durante la inactivación, las cuatro metioninas presentes en la VP se oxidaron a derivados de metionina. Teniendo en cuenta la proximidad de estos residuos a los sitios catalíticos de la enzima es probable que su oxidación provoque una alteración en la conformación de la enzima con un efecto directo sobre su actividad catalítica y estabilidad. De acuerdo con estas evidencias, la primera

estrategia utilizada para mejorar la estabilidad oxidativa de la VP consistió en el diseño de variantes en las que las metioninas fueron sustituidas por residuos más resistentes a la oxidación.

Asimismo, se diseñó una segunda estrategia consistente en la modificación del entorno de la histidina distal (His47) mediante la introducción de las mutaciones T45A e I103T. Los dos aminoácidos mutados se localizan por encima del área ocupada por la histidina 47, que está implicada, junto con la arginina 43, en la ruptura heterolítica del H_2O_2 durante la activación de la enzima. Las mutaciones se seleccionaron con la intención de provocar cambios sutiles en la posición de His47 y Arg43 que lleven a la ralentización de la velocidad de reacción con el H_2O_2 y, como consecuencia, a una menor inactivación. Finalmente, las dos estrategias se combinaron en la variante quíntuple T45A/I103T/M152F/M262F/M265L.

Ambas estrategias dieron lugar a variantes mutadas con mayor estabilidad oxidativa. Los mejores resultados se obtuvieron con la variante quíntuple, ya que su velocidad de inactivación por H_2O_2 disminuyó 11 veces. Además, en presencia de un exceso de 2000 equivalentes de H_2O_2, la vida media de esta variante se incrementó hasta los 30 minutos, comparados con los 5 minutos de la enzima nativa. Finalmente, la mejora de la estabilidad del compuesto III (Fe^{III}-$O_2^{\cdot-}$), un intermediario catalítico relacionado con la inactivación por H_2O_2, parece ser la causa de las mejoras observadas asociadas a estas mutaciones.

3.2 Estudio y mejora de la estabilidad a pH de la VP

Con la intención de mejorar la estabilidad a pH de la VP, se llevó a cabo un análisis comparativo de las estructuras cristalográficas de la VP y de una manganeso peroxidasa (MnP4) de *Pleurotus ostreatus* que presenta una elevada estabilidad a pH (Fernández-Fueyo et al. Biotechnology for Biofuels 2014, 7:2). Durante este análisis, se identificaron diferentes motivos estructurales, como redes de puentes de hidrógeno, puentes salinos o la presencia de un gran número de residuos cargados en superficie, que se presentaban como posibles determinantes de la elevada estabilidad de la MnP4. Por ello, fueron introducidos en la VP mediante mutagénesis dirigida, lo que permitió el diseño de diferentes

variantes. Además, se diseñó un puente disulfuro extra cerca del calcio distal y su efecto en la estabilidad de la VP también fue estudiado. Las variantes resultantes presentaron una estabilidad a pH mayor que la enzima nativa. El análisis de sus estructuras cristalográficas reveló que estas variantes presentaban nuevos motivos estructurales que fueron asociados a las mejoras en estabilidad. Los nuevos puentes de hidrógeno y puentes salinos introducidos estabilizaron el hemo y su entorno dando lugar a una variante que retuvo hasta un 61% de actividad después de 24 horas de incubación a pH 3.5, y de un 55% de actividad tras 5 días a pH 7, mientras que en estas condiciones la enzima nativa se inactivó completamente. La introducción de residuos básicos expuestos al solvente y del puente disulfuro extra aumentó aun más la estabilidad a pH ácido. El análisis de las estructuras cristalográficas aportó una explicación racional a los resultados obtenidos.

3.3 Investigando las propiedades mejoradas de una variante evolucionada de la VP

La variante 2-1B de la VP es una variante obtenida por evolución dirigida de la VP de *Pleurotus eryngii* (García-Ruiz et al. Biochem. J. (2012) 441, 487–498). Como consecuencia del proceso de evolución, esta variante incorporó 7 mutaciones en su secuencia que le confirieron una mayor estabilidad a pH alcalino y temperatura, así como una mayor eficiencia en la oxidación de sustratos de bajo potencial rédox.

Con objeto de investigar de qué manera las mutaciones introducidas en 2-1B regulan y mejoran su estabilidad y propiedades catalíticas, se diseñaron (en *Escherichia coli*) diferentes variantes mutadas que contenían una o varias de las mutaciones presentes en 2-1B, y sus propiedades fueron evaluadas. Además, se obtuvieron las estructuras cristalográficas de 2-1B y una de las variantes diseñadas (EHG). Con los datos obtenidos, se observó que la introducción de tres residuos básicos en VP 2-1B (Lys37, Arg39 and Arg330) condujo a la formación de nuevas interacciones no presentes en la VP nativa, como una nueva conexión del propionato del hemo con la apoenzima, la existencia de nuevos puentes salinos y la eliminación de interacciones desestabilizantes entre residuos ácidos. Estos nuevos determinantes estructurales estabilizaron el hemo y su entorno, y mantuvieron a la enzima activa bajo condiciones alcalinas

moderadas. Además, los nuevos puentes de hidrógeno superficiales generados en el entorno de la Gln305 como consecuencia de la mutación Q202L también contribuyeron al aumento de la estabilidad. Por otra parte, la introducción de la metionina 184 en la variante 2-1B mejoró la oxidación de sustratos de bajo potencial redox en el sitio de baja eficiencia. Además, el canal de acceso del manganeso estaba más expuesto al solvente en la variante 2-1B que en la enzima nativa. Los datos disponibles sugirieren que la oxidación de sustratos de bajo potencial redox podría ocurrir en la sitio de oxidación del manganeso en la variante 2-1B.

3.4 Estudio de la capacidad de la VP para oxidar lignosulfonatos y de la transferencia electrónica entre la VP y la lignina

La capacidad de la VP para oxidar ligninas técnicas se estudió utilizando lignosulfonatos provenientes de *Picea abies* y de *Eucalyptus grandis*. La VP fue capaz de aceptar electrones de ambos lignosulfonatos con una eficiencia similar. Por el contrario, la variante W164S, en la que el triptófano catalítico fue sustituido por una serina, mostró peores constantes cinéticas demostrando la implicación del triptófano catalítico en la actuación sobre los lignosulfonatos. Además, se llevaron a cabo experimentos de resonancia paramagnética electrónica con objeto de conocer qué radicales se forman durante la reacción con la lignina. Se observó la aparición de un radical triptofanilo tras la activación de la VP por H_2O_2. Cuando el sustrato fue añadido a la reacción, la señal correspondiente al triptófano fue sustituida por la del radical de lignina. Así, se demostró que el radical de triptófano formado en la VP es catalíticamente activo y responsable de la oxidación de la lignina. Además, se realizaron tratamientos en estado estacionario en los que los productos de la reacción de los lignosulfonatos con la VP fueron analizados. Los espectros de resonancia magnética nuclear mostraron la desaparición de las señales aromáticas de la lignina, confirmando las capacidades ligninolíticas de la VP. Simultáneamente, experimentos de cromatografía de exclusión molecular revelaron un aumento del peso molecular de los lignosulfonatos, indicando que tras la degradación de los lignosulfonatos por la VP los productos de oxidación tienden a polimerizar. Finalmente, la variante R257A/A260F, que presenta dos mutaciones en aminoácidos del entorno del triptófano catalítico, mostró

una mejora en las constantes cinéticas para la reacción con los lignosulfonatos, lo que indicó que cambios en el entorno del triptófano catalítico modulan la actividad de éste.

4. Conclusiones

El trabajo llevado a cabo en esta tesis ha permitido profundizar en el conocimiento del mecanismo catalítico de la VP así como avanzar en el conocimiento de las bases estructurales que regulan algunas de sus propiedades como la estabilidad oxidativa, alcalina o ácida. Asimismo, se obtuvieron variantes mutadas que presentaron una mayor estabilidad frente a peróxido y pH, que son algunos de los principales factores que actualmente dificultan el uso biotecnológico de estas peroxidasas. La mejora en la estabilidad a pH ácido es especialmente importante teniendo en cuenta que la VP presenta un pH óptimo ácido para la oxidación de compuestos aromáticos de alto potencial redox. Además, el éxito de la estrategia consistente en transferir motivos estructurales estabilizadores de unas peroxidasas a otras sugiere que esta metodología se podría usar para el diseño de biocatalizadores de interés. Por otra parte, se confirmó la capacidad de la VP para degradar lignosulfonatos y se estudió el patrón de degradación de estas ligninas producido por la enzima. Además, se puso de manifiesto la transferencia electrónica que se produce entre el polímero de lignina y la peroxidasa, que fue caracterizada cinéticamente en condiciones de flujo detenido (*stopped flow*) y se asoció a la presencia del triptófano 164, el cual forma una radical catalíticamente activo.

ABSTRACT

1. Background

Ligninolytic peroxidases are enzymes of biotechnological interest due to their ability to oxidize high redox potential aromatic compounds, including the recalcitrant lignin polymer. They are produced by white-rot fungi, the main organisms being able to mineralize lignin in nature. Lignin is the second most abundant polymer in nature. Due to its aromatic and heterogeneous nature, it is very recalcitrant and its degradation is difficult. White-rot fungi secrete a battery of oxidoreductases to the extracellular medium that, together with low molecular redox mediators, attack the lignin and achieve its degradation. Ligninolytic peroxidases play a key role in this process oxidizing the aromatic units of lignin.

Ligninolytic peroxidases can be classified into three families: lignin peroxidases (LiP), manganese peroxidases (MnP) and versatile peroxidases (VP). VPs are characterized by the presence of three catalytic sites: i) the catalytic tryptophan, a solvent exposed residue that forms a protein radical trough a long range electron transfer from the heme, able to oxidize high redox potential compounds; ii) the manganese oxidation site, able to oxidize Mn^{2+} to Mn^{3+}, which acts as a diffusible oxidizer, and iii) the main heme access channel where low redox potential compounds are oxidized. Among the different ligninolytic peroxidases, VP shows a special interest since it gathers the catalytic properties of LiP, MnP and generic peroxidases and, in addition, the enzyme does not need redox mediators to develop its activity. For these reasons, the VP from *Pleurotus eryngii* (isoenzyme VPL2) was the enzyme selected and studied in this thesis.

The above catalytic properties allow VP to oxidize not only lignin but also other aromatic phenolic and non-phenolic (high or low redox potential) compounds, dyes and pesticides. The oxidative reactions VP and other ligninolytic peroxidases catalyze led to the break of lignin bonds or to the formation of new ones by radical condensation, or even indirectly to oxygenation reactions. All these reactions are of interest from a biotechnological point of view. On the other hand, ligninolytic

peroxidases use hydrogen peroxide as substrate, which is cheap and of easy acquisition. Therefore, the use of these enzymes as biocatalysts in different industrial processes is very attractive as a sustainable and eco-friendly alternative to the conventional chemical methods. However, in spite of the high potential of ligninolytic peroxidases, they are not applicable as they are produced by natural organisms, since they do not present a proper selectivity and/or compatibility with the conditions under which the industrial processes are carried out. For these reasons, an optimization of the catalytic properties and stability of these enzymes is necessary previous to their biotechnological use. Among the drawbacks that limit the application of these peroxidases, the relative low stability towards pH, temperature and H_2O_2, or the insufficient production levels are found.

The low stability of ligninolytic peroxidases towards H_2O_2 (their natural co-substrate) is one of the reasons delaying the development of applications based on these fungal enzymes. H_2O_2 is involved in enzyme inactivation by a mechanism-based process described as a suicide inactivation. This irreversible oxidative inactivation is produced in absence of reducing substrates or when the enzyme is exposed to a high excess of peroxide, and it is a consequence of multiple oxidization events affecting different components of the enzyme, including amino acids and the porphyrin ring.

The relatively low pH stability of this and other fungal peroxidases is another drawback for their application. Under alkaline or even neutral conditions, ligninolytic peroxidases lose the structural calcium ions, which leads to a relaxation of the structure and the hexacoordination of the heme iron, resulting in an inactive enzyme. In a similar way, at acidic pH, the heme environment of these enzymes is affected being the interaction between the heme iron and the proximal histidine broken and the enzyme inactivated.

On the other hand, although the catalytic properties of VP have been thoroughly studied, there are still catalytic aspects that are not clearly understood. Taking all this into account, studying the bases that regulate the stability and the catalytic properties of ligninolytic peroxidases is of interest for the future design of useful biocatalysts.

2. Aims

The main aims of the present doctoral thesis were: i) the design of a VP with more adequate properties for its biotechnological application, and ii) the acquisition of an in-depth knowledge about the structural determinants that govern the catalysis and the stability of the enzyme. With this in mind, the following issues were addressed:

i) The study of the oxidative inactivation of VP, and the factors that influence this process, as well as the design of a VP with improved H_2O_2-stability.
ii) The design of a VP variant with optimized pH stability through the transfer of stabilizing structural motifs found in other peroxidases (Fernández-Fueyo et al. Biotechnology for Biofuels 2014, 7:2).
iii) The analysis of the evolved variant 2-1B, obtained by directed evolution of VP (García-Ruiz et al. Biochem. J. (2012) 441, 487–498), to determine which structural determinants generated by the mutations introduced improved its catalytic and stability properties.
iv) To obtain an in-depth knowledge of the function of the catalytic tryptophan of VP, characterize the electron transfer between the peroxidase and the lignin, and study the ability of VP to oxidize technical lignins.

Thanks to the structural-function information existing about VP and other ligninolytic peroxidases, and the availability of the crystal structure of VP, the optimization of VP using a rational approach has been possible. In this way, several VP variants were designed and produced and their properties were evaluated.

3. Results

3.1 Study and improvement of the oxidative stability of VP

The oxidative inactivation of VP by H_2O_2 was studied and different strategies were evaluated with the aim of improving its H_2O_2 stability. The studies performed demonstrated that VP is easily inactivated by H_2O_2 and that, during the inactivation process, the four methionine residues of VP are oxidized to methionine derivatives. Substitution of

these residues, located in a sensitive region of the enzyme (near the heme cofactor and the catalytic tryptophan), rendered a variant with a 7.8-fold decreased oxidative inactivation rate. A second strategy was developed consisting in mutating two residues (Thr45 and Ile103) near the catalytic distal histidine (His47) with the aim of modifying the reactivity of the enzyme with H_2O_2 and consequently, slowing down the inactivation process. The T45A/I103T variant showed a 2.9-fold slower reaction rate with H_2O_2 and 2.8-fold enhanced oxidative stability. Finally, both strategies were combined in the T45A/I103T/M152F/M262F/M265L variant, whose stability in the presence of H_2O_2 was improved 11.7-fold. This variant showed an increased half-life, over 30 min compared with 3.4 min of the native enzyme, under an excess of 2000 equivalents of H_2O_2. Interestingly, the stability improvement achieved was related with the slower formation, subsequent stabilization and slower bleaching of the enzyme Compound III (Fe^{III}-$O_2^{\cdot-}$), a peroxidase intermediate that is not part of the catalytic cycle and leads to the inactivation of the enzyme.

3.2 Study and improvement of the pH stability of VP

A strategy based on the comparative analysis of the crystal structures of VP and the highly pH-stable manganese peroxidase isoenzyme 4 (MnP4) from *Pleurotus ostreatus* (Fernández-Fueyo et al. Biotechnology for Biofuels 2014, 7:2) was followed with the intention of improving the pH stability of VP. Several hydrogen bonds, salt bridges and charged residues exposed to the solvent were identified as putatively contributing to the high pH stability of MnP4. The eight amino acid residues responsible for these hydrogen and salt bonds, and seven surface basic residues were introduced into VP by directed mutagenesis. An extra disulfide bond was also designed in VP to explore its effect stabilizing the distal structural Ca^{2+} region. The different VP variants obtained showed improved pH stability to different extents. Three designed variants were crystallized and the new structural determinants found were correlated with the improvement in pH stability of the VP variants. The extra hydrogen bonds and salt bridges stabilized the heme pocket as revealed by electronic absorption spectroscopy. They led to a VP variant that retained a 61 % of the initial activity after 24 h incubation at pH 3.5, and 55 % of activity after a 5-day incubation at pH 7, meanwhile, the native VP was almost inactivated. The introduction of extra solvent-exposed basic

residues and an additional disulfide bond further improved the stability at acidic pH (85% of residual activity at pH 3.5 after 24 h when introduced separately, and 64% of activity after 1-h incubation at pH 3 when introduced together, compared with 1-5% of activity of the native VP under these conditions). The analysis of the results provided a rational explanation to the improvement achieved.

3.3 Investigating the basis of stability in an evolved VP

2-1B is a variant obtained by directed evolution of the *Pleurotus eryngii* VP (García-Ruiz et al. Biochem. J. (2012) 441, 487–498). 2-1B incorporates 7 mutations in its sequence introduced during the evolution process. As a consequence, this variant exhibits improved alkaline and thermal stability together with enhanced catalytic properties for the oxidation of low redox potential substrates.

In the present thesis, several VP variants containing some of the mutations present in 2-1B were designed and expressed in *Escherichia coli*, and their stability and biochemical properties were determined with the intention of investigating the structural bases that regulate the enhanced properties of VP 2-1B (a study that could not be performed using the original expression system in *Saccharomyces cerevisiae*). In addition, the crystal structures of 2-1B and other designed VP variant (EHG) were obtained. Analyzing the data acquired, it was observed that the introduction of three basic residues in VP 2-1B (Lys37, Arg39 and Arg330) led to the formation of a new interaction with the heme, new salt bridges and the removal of acid-acid destabilizing interactions. These new structural determinants stabilized the heme and its environment and maintained the enzyme active under moderate alkaline conditions. Moreover, the reinforcement of the solvent-exposed area around Gln305 in the proximal side, prompted by the Q202L mutation, further enhanced the stability. On the other hand, the introduction of Met184 (T184M mutation) was responsible for the improved activity observed for the oxidation of low redox potential substrates in this variant. In addition, VP 2-1B exhibited a more exposed manganese channel than native VP. The data available suggested that the oxidation of low redox potential substrates would happen at the manganese oxidation site of the 2-1B variant, being their oxidation more efficient.

3.4 Study on the lignin-to-peroxidase direct electron transfer and the ability of VP to oxidize technical lignins

The ability of VP to oxidize water-soluble lignins (lignosulfonates) from softwood and hardwood was studied by a combination of directed mutagenesis and spectroscopic techniques. The direct electron transfer produced between the peroxidase and the lignin macromolecule was kinetically characterized under stopped-flow conditions. VP W164S variant, in which the catalytic tryptophan was substituted by a serine, was used to show that this reaction strongly depends on the presence of the solvent-exposed tryptophan residue 164. Moreover, the tryptophanyl radical detected by electronic paramagnetic resonance spectroscopy of H_2O_2-activated VP (being absent from the W164S variant) was identified as catalytically active, since it was reduced during lignosulfonate oxidation resulting in the appearance of a lignin radical. In addition, VP was shown to be able to act on both technical lignins. A decrease of lignin fluorescence (excitation 355 nm/emission 400 nm) was observed during lignosulfonate treatment with VP under steady-state conditions, which was accompanied by a decrease of the lignin (aromatic nuclei and side chains) signals in nuclear magnetic resonance spectra, confirming the ligninolytic capabilities of the enzyme. Simultaneously, size-exclusion chromatography of the reactions products was performed. The results showed an increase of the molecular mass of the modified residual lignin, especially for the hardwood lignosulfonate, revealing that the oxidation products tend to repolymerizate during the VP treatment. Finally, mutagenesis of selected residues neighbour to Trp164 (in the VP R257A/A260F variant) resulted in improved apparent second-order rate constants for the reduction of the intermediate states of the catalytic cycle of the enzyme by lignosulfonates, revealing that changes in its protein environment (modifying the net negative charge and/or substrate accessibility/binding) can modulate the reactivity of the catalytic tryptophan.

4. Conclusions

The work carried out in this thesis allowed to get an in-depth knowledge about the catalytic mechanism of the VP as well as about the structural bases that govern some properties such as the oxidative stability or the pH stability. Wild VP was not well suited for its biotechnological

application regarding the stability properties. Using a rational approach, the design of some VP variants with enhanced properties concerning the oxidative and pH stability was possible. The success of the approach, consisting in the transfer of stabilizing motifs from a more stable peroxidase to VP, suggests that it could be applied for the design and improvement of other enzymes of biotechnological interest. On the other hand, the ability of VP to directly act on technical lignins was demonstrated and the direct electron transfer produced between the polymer of lignin and the peroxidase was established and unequivocally related to the presence of the solvent-expose tryptophan (Trp164) that forms a catalytically active radical.

ABREVIATURAS

ABTS	2,2-azinobis (3-etilbenzotiazolin-6-sulfonato)
CI	Compuesto I / *Compound I*
CII	Compuesto II/ *Compound II*
CIII	Compuesto III/ *Compound III*
CPMAS	*Cross polarization and magic-angle spinning*
CT	Bandas de transferencia de carga/ *Charge transfer bands*
DHP	*Dehydrogenation (lignin) polymer*
DMP	*2,6-dimethoxyphenol*
DyP	Peroxidasa decolorante de tintes/ *Dye-Decolorizing peroxidase*
EPR	Resonancia paramagnética electrónica/ *Electron paramagnetic resonance*
GP	Peroxidasa genérica/ *Generic peroxidase*
HPLC	Cromatografía líquida de alta resolución/ *High-performance liquid chromatography*
HRP	Peroxidasa de rábano/ *Horseradish peroxidase*
HSQC	*Heteronuclear single-quantum correlation*
HTP	Hemo-tiolato peroxidasa/ *Heme-thiolate peroxidase*
IPTG	Isopropil tio-β-D-galactósido
k_{app}	Constante de velocidad aparente de segundo orden/ *Apparent second-order rate constant*
k_{cat}	Constante catalítica/ *Catalytic constant*
k_{cat}/ K_m	Eficiencia catalítica/ *Catalytic efficiency*
K_D	Constante de disociación/ *Dissociation constant*
K_m	Constante de Michaelis/ *Michaelis constant*
k_{obs}	Constante de velocidad de pseudo-primer orden/ *Pseudo first-order rate constants*
$k_1/ k_2/ k_3$	Constante de velocidad de primer orden para la formación del C-I/ reducción del C-I/ reducción del C-II / *First-order rate constant for CI formation/CI reduction/ CII reduction*
k_i	Constante de velocidad de inactivación de primer orden/ *First-order inactivation rate constant*
K_I	Tasa de inactivación mitad de la máxima/ *Half maximal inactivation rate*
LiP	Lignina peroxidasa / *Lignin peroxidase*
LRET	Transferencia electrónica de largo recorrido/ *Longe range electron transfer*
MALLS	*Multi-angle laser light scattering*
MnP	Manganeso peroxidasa/ *Manganese peroxidase*
Mp	Pico principal/ *Main peak*
NMR	Resonancia paramagnética nuclear/ *Nuclear paramagnetic resonance*
PDB	*Protein Data Bank*

POD	Peroxidasas fúngicas de clase II/ *Class-II fungal peroxidases*
RI	Índice de refacción*/ Refraction Index*
RB5	*Reactive Black 5*
RS	Estado de reposo/ *Resting state*
SEC	Cromatografía de exclusión molecular/ *Size-exclusion chromatography*
T_{50}	Temperatura a la que la actividad es mitad de la máxima/ *Temperature at which the activiy is half the initial*
VA	Alcohol veratrílico (alcohol 3,4-dimetoxibencílico)/ *Veratryl alcohol*
VP	Peroxidasa versátil/ *Versatile peroxidase*

INTRODUCCIÓN

1. Hacia una nueva bioeconomía

1.1 Biotecnología blanca

La biotecnología blanca es la rama de la biotecnología dedicada a optimizar los procesos industriales mediante el empleo de organismos vivos y sus enzimas, buscando reemplazar las tecnologías convencionales, a menudo contaminantes, por otras más limpias y sostenibles.

La aplicación de enzimas en la industria atrae mucho interés ya que estos biocatalizadores actúan sobre una amplia gama de moléculas, suelen ser selectivos, trabajan en unas condiciones energéticamente menos costosas que las utilizadas en los procesos químicos convencionales y además, son biodegradables. Por todo ello, representan una alternativa medioambientalmente más aceptable para una industria que busca el desarrollo sostenible mediante procesos bioindustriales y energías renovables (Schmid et al., 2001; Martínez et al., 2009).

Aunque los recientes avances en biotecnología permiten a las empresas la producción más segura y barata de enzimas con una efectividad mejorada, en general, la aplicación de estos biocatalizadores es comparativamente escasa. Hoy en día, la mayoría de enzimas comercializadas por las empresas biotecnológicas pertenecen al grupo de las hidrolasas (Barredo, 2005; Polaina and MacCabe, 2007). Sin embargo, las oxidorreductasas, uno de los grupos de enzimas con mayor potencial, todavía tienen una baja representación en la industria química a pesar de que suponen una alternativa atrayente en procesos industriales que requieren transformaciones oxidativas. Ello es debido a que estos biocatalizadores no presentan una adecuada selectividad, disponibilidad y compatibilidad con los procesos industriales (Ruiz-Dueñas and Martínez, 2009).

Actualmente se están abordando los principales problemas que dificultan el uso de las enzimas oxidativas a nivel industrial, entre los que se encuentran la estabilidad a diferentes factores y los bajos niveles de expresión obtenidos. También se busca modular las propiedades

catalíticas más interesantes para adaptarlas a las diferentes aplicaciones industriales. Por otra parte, la gran cantidad de información genómica disponible hoy en día permite la búsqueda y caracterización de nuevas enzimas con propiedades de especial interés (Martínez et al., 2014). Como resultado de todos estos estudios, en pocos años podremos disponer de biocatalizadores oxidativos optimizados para una amplia variedad de procesos industriales.

1.2 Biorrefinerías de la lignocelulosa

La alta demanda de energía a nivel mundial, junto con la limitación que supone el uso de fuentes de energía derivadas del petróleo, así como la creciente preocupación por el cambio climático han llevado a un resurgimiento del interés por las fuentes de energía renovables (Himmel et al., 2007), además de tecnologías que maximicen el rendimiento en la producción de de combustibles, materiales y productos químicos a partir de dichas fuentes. En este marco, surgen las biorrefinerías lignocelulósicas, un nuevo concepto industrial que supone la transformación de la biomasa lignocelulósica en diferentes productos de valor añadido, de una manera integrada, sostenible y respetuosa con el medio ambiente (Martínez et al., 2009) (**Fig. 1**). Las biorrefinerías pretenden sustituir a las refinerías convencionales, basadas en el uso de petróleo, y llegar a obtener básicamente los mismos tipos de productos que actualmente se consiguen a partir de éstas.

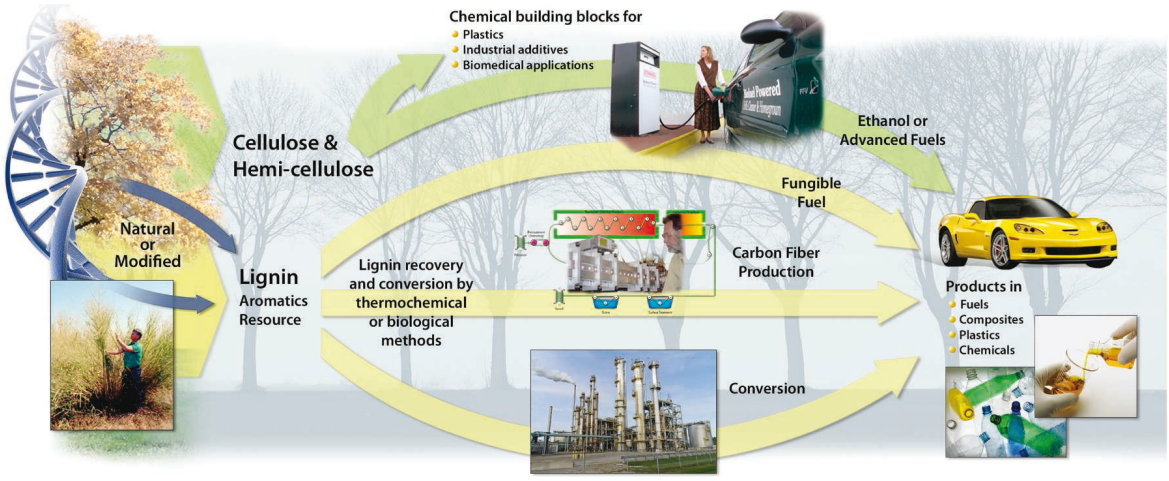

Figura 1. Funcionamiento esquemático de una biorrefinería lignocelulósica en la que los diferentes componentes de la biomasa son separados y transformados en biocombustibles y distintos materiales y productos químicos de valor añadido. Tomado de Ragauskas *et al*., 2014.

A principios del siglo XX, numerosos productos industriales como tintes, solventes o fibras se producían a partir de plantas y residuos vegetales provenientes de la actividad agrícola. Sin embargo, hacia finales de los años 60, muchos de estos productos fueron reemplazados por derivados del petróleo. La dependencia de fuentes fósiles, que son finitas, no es una opción a largo plazo (Ragauskas et al., 2006), por lo que el desarrollo de las biorrefinerías se presenta como una opción atractiva. La biomasa vegetal tiene la ventaja de que, al ser un material altamente oxigenado, se puede emplear para la producción de una gran variedad de productos químicos, como alcoholes, ácidos carboxílicos o esteres, compuestos que apenas se obtienen de las refinerías del petróleo en las que solo el 5% del material utilizado va destinado a la obtención de productos químicos (Ragauskas et al., 2006). Además, la conversión de esta biomasa en biocombustibles es una alternativa medioambientalmente sostenible, ya que el balance de carbono entre el dióxido de carbono fijado por las plantas y el liberado en el proceso de combustión es próximo a cero. Por tanto, la biomasa lignocelulósica, que es el material renovable más abundante en los ecosistemas terrestres, representa una excelente fuente de carbono para la producción de bioenergía, productos químicos y biomateriales, y su "buen uso" permitirá abordar muchas necesidades de nuestra sociedad actual (Amidon et al., 2008).

La biomasa lignocelulósica está formada por tres componentes principales: celulosa, hemicelulosas y lignina (**Fig. 2**). La celulosa representa alrededor de un 50% de la biomasa y está constituida por cadenas de D-glucosa unidas mediante enlaces glicosídicos β -(1,4) que forman un polímero lineal ordenado. A diferencia de ésta, las hemicelulosas son heteropolisacáridos ramificados formados tanto por hexosas como pentosas, a menudo acetiladas. Por último, la lignina es el material aromático renovable más abundante en la naturaleza, y el segundo polímero más cuantioso en ecosistemas terrestres, después de la celulosa (supone entre un 15 y un 40% de la biomasa) (Ragauskas et al., 2014). Estructuralmente es un polímero aromático heterogéneo formado por la polimerización deshidrogenativa de los alcoholes *p*-hidroxicinamílicos (*p*-cumarílico, coniferílico y sinapílico) que dan lugar a las subunidades *p*-hidroxifenilo (no metoxilada), guaiacilo (monometoxilada) y siringilo (dimetoxilada). Estas subunidades se

disponen formando una compleja red tridimensional con diversas subestructuras unidas por diferentes enlaces, siendo mayoritarios los enlaces alquil-aril éter β-O-4' (Boerjan et al., 2003). Por su naturaleza, la lignina es una material muy recalcitrante y difícil de degradar. En la pared secundaria de la células de las plantas vasculares, la lignina se organiza formando una matriz en la que queda embebida la fracción polisacarídica (**Fig. 2**). Entre sus funciones, cabe destacar, la rigidez y consistencia que aporta a la pared celular, la protección que ofrece a las plantas frente a ataques patógenos y la impermeabilidad que aporta a los elementos vasculares (Gellerstedt and Henriksson, 2008).

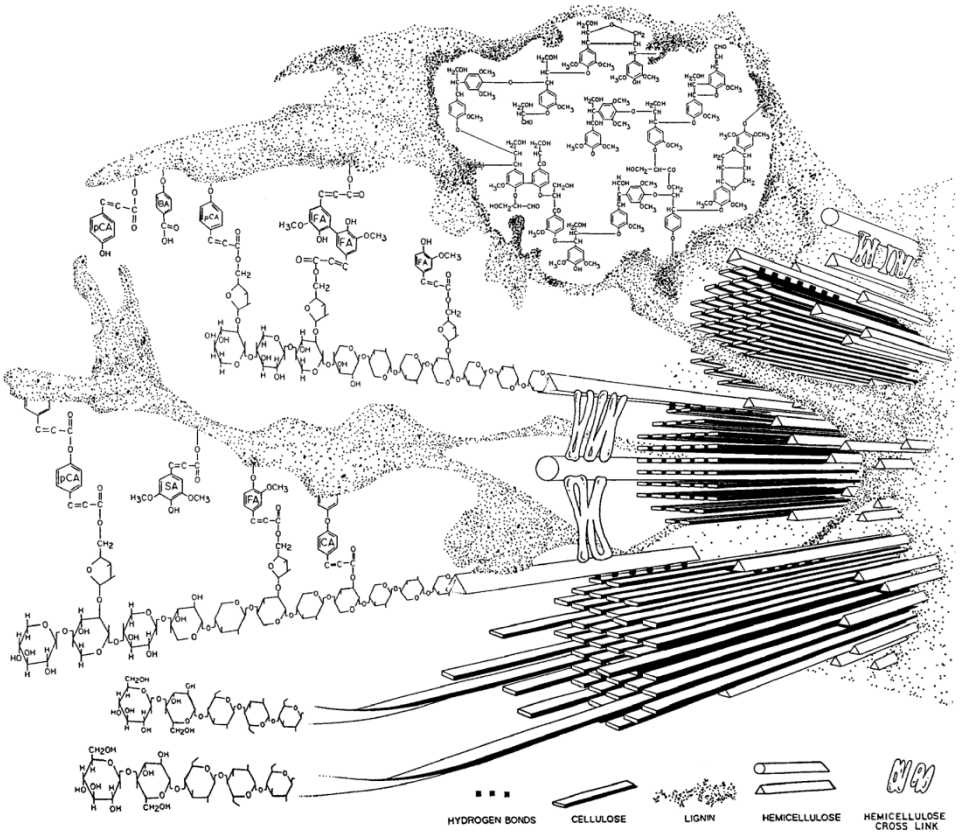

Figura 2. Estructura de la pared secundaria de plantas en la que se observan las cadenas de celulosa (formando microfibrillas ordenadas) y de hemicelulosa embebidas dentro del polímero de lignina. Tomado de Bidlack *et al.*, 1992.

La complejidad y naturaleza recalcitrante de la lignina plantean uno de los mayores retos en el uso de la biomasa lignocelulósica, ya que dificultan la separación de los diferentes componentes que la constituyen y su posterior transformación en productos de interés (Hammel and Cullen, 2008). En este sentido, los avances que se están

realizando en campos como la genética, la química o la ingeniería de proteínas contribuyen a afrontar este reto. Estos avances no solo afectan al empleo de la biotecnología blanca, aportando biocatalizadores adaptados y diseñados para una mejor deslignificación, sino también al empleo de la biotecnología verde (aplicada a cultivos agrícolas y forestales) suministrando materias primas más manejables (Martínez et al., 2009).

Tradicionalmente, en los procesos industriales en los que se utiliza la biomasa lignocelulósica, la lignina se quema para generar energía. En el caso de las biorrefinerías, éstas generan más lignina de la necesaria para la producción de energía (alrededor de un 60% más) por lo que existe un excedente que se puede utilizar como fuente aromática para la obtención de productos de valor añadido. Entre éstos se incluyen plásticos, fibra de carbono, espumas poliméricas, combustibles y productos químicos que actualmente se obtienen a partir del petróleo (Ragauskas et al., 2014).

Por todo lo anterior, se puede concluir que, para que el desarrollo de las biorrefinerías lignocelulósicas sea viable y económicamente rentable, el tratamiento de la lignina es un paso clave que ha de ser estudiado (Martínez et al., 2009). Aunque se han hecho muchos avances en este campo, todavía quedan importantes retos tecnológicos y económicos que superar (Ragauskas et al., 2014; Ruiz-Dueñas et al., 2009a).

1.3 Importancia de los hongos que degradan la biomasa vegetal

Algunos hongos basidiomicetos son los principales responsables de la degradación de la biomasa lignocelulósica en la naturaleza. Estos organismos son capaces de superar las dificultades que conlleva este proceso, incluidas entre otras la presencia de compuestos tóxicos y antibióticos en la madera, el bajo contenido en nitrógeno de la misma o la presencia del polímero recalcitrante de lignina (Martínez et al., 2005). Estos hongos actúan sobre la biomasa lignocelulósica siguiendo diferentes estrategias que dan lugar a distintos patrones de degradación, entre los que destacan la podredumbre blanca y la

podredumbre parda (**Fig. 3**) (Eriksson et al., 1990; Zabel and Morrell, 1992; Schwarze et al., 2000).

Figura 3. Aspecto de la madera tras la actuación de hongos de podredumbre parda (A) y hongos de podredumbre blanca (B).

Los hongos de podredumbre parda degradan los polisacáridos de la madera. Su actuación da lugar a un producto de color marronáceo enriquecido en lignina debido a su incapacidad para degradarla (Martínez et al., 2011) (**Fig. 3A**). Esta estrategia de degradación se basa en el ataque al polímero de celulosa a través de radicales hidroxilo. Éstos se producen mediante una reacción basada en la química de Fenton, en la que el peróxido de hidrógeno, generado por distintas oxidasas, es reducido por el Fe^{2+}, generado por enzimas reductoras de hierro. Los radicales libres de tipo hidroxilo formados son capaces de oxidar la celulosa y, en menor medida, la lignina (Martinez et al., 2009; Baldrian and Valaskova, 2008; Gómez-Toribio et al., 2009).

En contraposición, los hongos de podredumbre blanca son los únicos organismos en la naturaleza capaces de degradar de manera sustancial (mineralizar) la lignina. Reciben este nombre debido al color blanquecino de la celulosa que queda en la madera tras el proceso de deslignificación (Eriksson et al., 1990; Martínez et al., 2005) (**Fig. 3B**). Para superar la barrera que supone el polímero de lignina, estos hongos secretan un conjunto de oxidorreductasas al medio, entre las que se encuentran peroxidasas, lacasas y oxidasas productoras de peróxido. Estas últimas son activadas por el O_2 y generan el H_2O_2 requerido para la activación de las peroxidasas ligninolíticas (las lacasas también son activadas por el O_2 pero generan H_2O como producto reducido). Estas enzimas están asistidas por compuestos aromáticos, cationes metálicos,

lípidos y especies reactivas de oxígeno que actúan como mediadores redox (Martínez et al., 2009; Ruiz-Dueñas and Martínez, 2009). Cabe resaltar el papel fundamental de estos mediadores de bajo peso molecular durante el ataque inicial a la lignina, ya que la arquitectura compacta y la baja porosidad de la pared celular dificultan el acceso inicial de las enzimas (Flournoy et al., 1993).

La degradación de la lignina se ha definido como una combustión enzimática (Kirk and Farrell, 1987) en la que peroxidasas de alto potencial redox juegan un papel clave en la oxidación inespecífica de las unidades aromáticas que constituyen este polímero. Esta oxidación conduce a la generación de radicales aromáticos inestables dentro del polímero, que evolucionan dando lugar a la rotura de diferentes enlaces y estructuras. La consecuencia final, tras la actuación conjunta de oxidorreductasas y mediadores, es la despolimerización y modificación oxidativa de la lignina.

Se pueden describir dos patrones de degradación de la lignocelulosa por los hongos de podredumbre blanca: i) degradación simultánea, en la que tanto lignina como celulosa son degradados; y ii) degradación preferente, en la que mayoritariamente se degrada el polímero de lignina, quedando la mayor parte de la celulosa disponible (Otjen and Blanchette, 1986). Este último patrón representa un modelo de degradación con gran potencial industrial en aplicaciones que requieren de la deslignificación de la biomasa para el aprovechamiento de sus polisacáridos como, por ejemplo, la producción de bioetanol (Young and Akhtar, 1998; Salvachúa et al., 2011).

Es interesante comentar que recientemente se ha fijado en el tiempo la aparición de los hongos degradadores de biomasa lignocelulósica (Floudas et al., 2012). Evolutivamente, la capacidad de degradar el polímero de lignina fue adquirida por los ancestros de los Agaricomicetes en el carbonífero tardío. La aparición de estos primeros basidiomicetos ligninolíticos coincide en el tiempo con un descenso brusco en la acumulación de carbón en la tierra. Teniendo en cuenta que la lignina es el principal precursor del carbón, todo parece indicar que estos organismos podrían haber contribuido a detener la acumulación de carbono en forma de carbón a finales del periodo carbonífero. A

partir de estos ancestros, los basidiomicetos de podredumbre blanca habrían evolucionado ampliando y diversificando el número y tipo de peroxidasas ligninolíticas, así como de enzimas activas sobre carbohidratos responsables de los dos patrones de degradación mencionados anteriormente. Posteriormente, a partir de éstos habrían evolucionado los basidiomicetos de podredumbre parda por pérdida de genes codificantes de enzimas ligninolíticas y celulolíticas (Floudas et al., 2012).

Finalmente, es importante resaltar que el impacto ecológico de los basidiomicetos de podredumbre blanca es inmenso, ya que facilitan el acceso a los polisacáridos a otros microorganismos y permiten el reciclaje del carbono orgánico fijado por la plantas en los ecosistemas terrestres (Lundell et al., 2010).

2. Peroxidasas ligninolíticas

2.1 Aspectos generales

Entre el conjunto de enzimas secretadas por los hongos de podredumbre blanca, implicadas en la degradación de lignina, encontramos diferentes hemoperoxidasas que juegan un papel central en este proceso (Hammel and Cullen, 2008; Ruiz-Dueñas and Martínez, 2009). Éstas se incluyen dentro de las denominadas peroxidasas fúngicas de clase II (PODs) que a su vez pertenecen a la superfamilia de peroxidasas-catalasas (Zámocký et al., 2014). Las PODs se clasifican en cuatro familias: las lignina peroxidasas (LiPs), manganeso peroxidasas (MnPs) y peroxidasas versátiles (VPs), que se caracterizan por presentar un elevado potencial redox que les permite oxidar (directa o indirectamente) no solo el polímero de lignina, sino también otros compuestos aromáticos fenólicos y no fenólicos (Ruiz-Dueñas and Martínez, 2010); y las peroxidasas genéricas (GPs) que, a diferencia de las anteriores, son PODs de bajo potencial redox que no están directamente implicadas en el proceso de degradación de lignina (Ruiz-Dueñas et al., 2013).

Las PODs se caracterizan por ser enzimas globulares con 11 ó 12 α -hélices distribuidas en dos dominios que delimitan una cavidad central

en la que se localiza un grupo hemo (**Fig. 4**). La estructura molecular de estas enzimas se encuentra estabilizada por la presencia de dos iones de calcio, uno en cada dominio (situados por encima y por debajo del hemo), y cuatro o cinco puentes disulfuro. El grupo hemo es de tipo b (ferriprotoporfirina IX), con un ion férrico (Fe^{3+}) en forma de alto spin (en la enzima en estado de reposo), pentacoordinado por los cuatro nitrógenos del anillo tetrapirrólico y el nitrógeno de una histidina axial, denominada histidina proximal (Martínez, 2002).

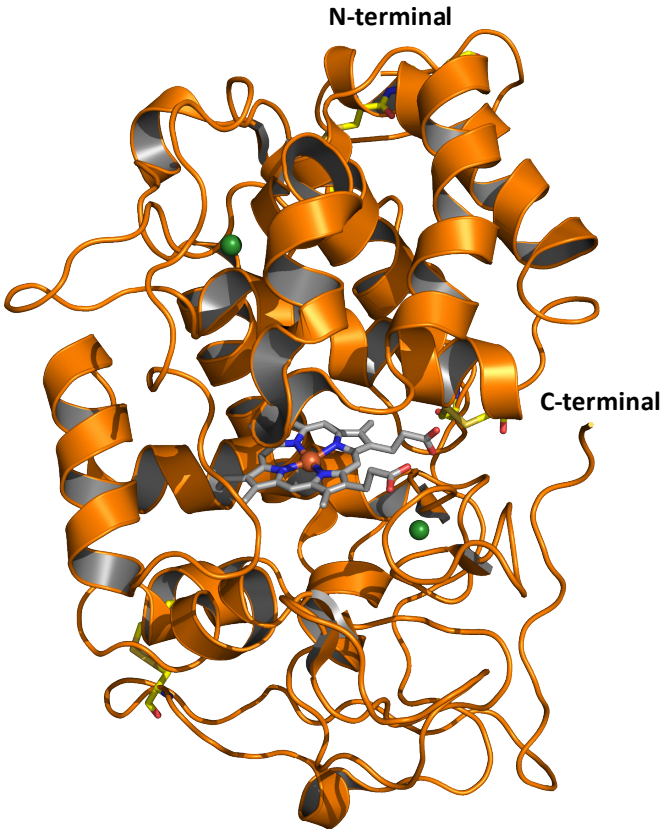

Figura 4. Estructura de las peroxidasas ligninolíticas en la que se destaca el grupo hemo (barras en colores CPK con el hierro como esfera roja), los calcios estructurales (esferas verdes), los puentes disulfuro (barras en colores CPK) y los extremos C-terminal y N-terminal. Modelo basado en la estructura de la VP de *P. eryngii* (PDB:3FJW).

Hay una serie de residuos conservados en la estructura de todas las PODs ligninolíticas (**Fig. 5**). En la región distal encontramos una segunda histidina axial, denominada histidina distal, y una arginina (His47 y Arg43 en la isoenzima VPL de la VP de *P. eryngii*) que juegan un papel clave en la reacción de la enzima con el H_2O_2, así como en la estabilización de los diferentes estados de oxidación del hierro a lo largo del ciclo catalítico (Hiner et al., 2002; Erman et al., 1993; Vitello et al.,

1993). En esta región también aparecen conservados una fenilalanina, un glutámico y una asparagina (Phe46, Glu72 y Asn78 en la VPL de *P. eryngii*) que forman una red de puentes de hidrógeno que contribuyen a mantener la posición relativa de la histidina distal (Martínez, 2002)

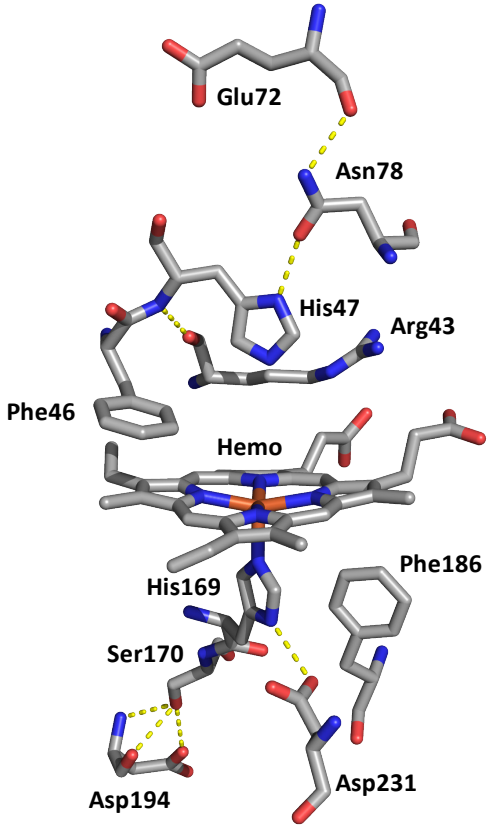

Figura 5. Residuos conservados en los lados distal y proximal del hemo en las peroxidasas ligninolíticas (ubicados por encima y por debajo del plano del hemo, respectivamente). Las líneas discontinuas representan puentes de hidrógeno. Modelo basado en la estructura de la VPL2 de *P. eryngii* (PDB:2BOQ).

En el lado opuesto del hemo, encontramos la histidina proximal, que recibe este nombre por estar implicada en la coordinación del hierro del hemo (His169 en la VPL de *P. eryngii*). La fuerza de interacción entre el hierro y el nitrógenoε del anillo imidazólico de este residuo determina el elevado potencial redox de las peroxidasas ligninolíticas (Banci et al., 1991; Banci et al., 2003). Esta interacción parece estar modulada por un puente de hidrógeno entre la serina contigua a la histidina proximal y un aspártico (Ser170 y Asp194 en la VPL de *P. eryngii*), que condiciona la posición de la hélice donde se encuentra el residuo de histidina (Piontek et al., 1993). También aparece conservado otro aspártico (Asp231 en la VPL de *P. eryngii*) que forma un puente de hidrógeno con la histidina

proximal, y una fenilalanina (Phe186 en la VPL de *P. eryngii*) que parece no tener un papel fundamental en la catálisis pero sí en la estabilidad de estas enzimas (Kishi et al., 1997).

2.2 Diferentes familias (y nuevas superfamilias)

Las primeras PODs ligninolíticas descritas fueron la LiP y la MnP, que fueron aisladas del hongo de podredumbre blanca *Phanerochaete chrysosporium* en la década de los 80 (Glenn et al., 1983; Tien and Kirk, 1983; Tien and Kirk, 1983). Desde entonces, se han descrito enzimas de tipo LiP y MnP en un gran número de especies. Debido a su gran interés biotecnológico, la LiP fue la segunda peroxidasa en ser cristalizada (Piontek et al., 1993; Poulos et al., 1993) seguida por la MnP (Sundaramoorthy et al., 1994). Hoy en día disponemos de la estructura cristalográfica de diferentes PODs producidas por distintos hongos ligninolíticos (Miki et al., 2011; Fernández-Fueyo et al., 2014a; Fernández-Fueyo et al., 2014b), lo que ha facilitado su estudio y la compresión de sus mecanismos catalíticos.

Las LiPs (EC 1.11.1.13) se caracterizan por ser capaces de oxidar compuestos aromáticos no fenólicos de alto potencial redox, como el alcohol veratrílico (3,4-dimetoxibencílico), otros compuestos modelo de lignina, y lignina polimérica en presencia de este alcohol (Harvey et al., 1986; Tien and Kirk, 1983; Schoemaker et al., 1994; Mester et al., 2001). Estas reacciones las llevan a cabo a través de un residuo de superficie, generalmente un triptófano, que en forma de radical capta los electrones de la lignina y demás sustratos, y los transfiere al hemo activado por el H_2O_2 a través de una ruta de transferencia electrónica de largo recorrido (LRET) (Mester et al., 2001; Ruiz-Dueñas and Martínez, 2009; Blodig et al., 2001; Du et al., 1992; Ruiz-Dueñas and Martínez, 2009) (**Fig. 6B**).

Las MnPs (EC 1.11.1.14) se caracterizan por ser capaces de oxidar Mn^{2+} en un sitio específico de unión del manganeso. Una vez unido, el Mn^{2+} es oxidado a Mn^{3+} en contacto con el propionato interno del hemo (Gold et al., 2000; Sundaramoorthy et al., 2005) (**Fig. 6C**). El Mn^{3+} resultante es quelado por ácidos dicarboxílicos producidos por los mismos hongos que secretan estas enzimas, estabilizándolo en solución y permitiendo su difusión hasta alcanzar las unidades fenólicas de la lignina que son finalmente oxidadas. Además, el Mn^{3+} quelado es capaz

de iniciar un proceso de peroxidación de lípidos insaturados del que derivan radicales muy reactivos que también actúan sobre las unidades no fenólicas, contribuyendo así al proceso de degradación de lignina (Jensen et al., 1996; Bao et al., 1994; Kapich et al., 2005). Recientemente, las MnPs se han clasificado en dos subfamilias, denominadas MnP cortas y MnPs largas/extralargas, en función de la longitud de su extremo C-terminal que es responsable de sus diferentes propiedades catalíticas y estabilidad (Fernández-Fueyo et al., 2014a). Las MnP cortas son capaces de oxidar Mn^{2+} y compuestos de bajo potencial redox como el ABTS, mientras que las MnP largas y extralargas únicamente oxidan Mn^{2+}, aunque son más eficientes que las MnPs cortas oxidando este catión.

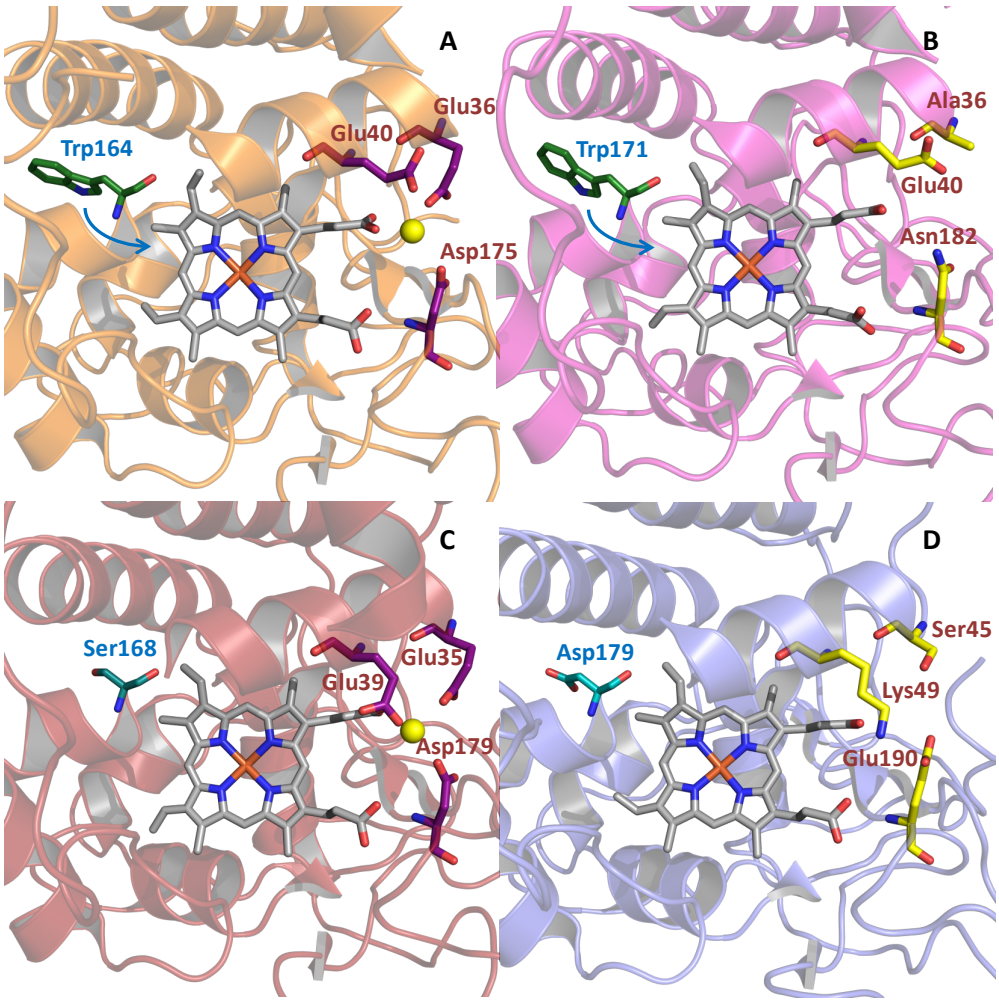

Figura 6. Detalle de la estructura de las PODs: A, VP; B, LiP; C, MnP y D, GP. Se aprecia el Trp catalítico en la VP (Trp164) y la LiP (Trp171), y el sitio de unión a manganeso en la VP (Glu36, Glu40 y Asp175) y la MnP (Glu35, Glu39 y Asp179). El manganeso unido se representa como esferas amarillas. Modelos basados en la estructuras de la VP (PDB:2BOQ), LiP (PDB:1LGA), MnP (PDB:1YYD) y GP (PDB:1ARX).

Las VPs (EC 1.11.1.16) constituyen la tercera familia de PODs ligninolíticas. Inicialmente se describieron como MnPs con actividad independiente de manganeso en el hongo *Pleurotus eryngii* (Martínez and Martínez, 1996), pero poco después se reconocieron como representantes de una nueva familia de peroxidasas ligninolíticas (Camarero et al., 1999; Ruiz-Dueñas et al., 1999; Ruiz-Dueñas et al., 1999). Su estructura cristalográfica también ha sido resuelta (Fernández-Fueyo et al., 2014b; Pérez-Boada et al., 2005). Catalíticamente se caracterizan por presentar propiedades híbridas de tipo LiP y MnP, debido a que en su estructura presentan un sitio de oxidación de Mn^{2+} y un triptófano catalítico capaz de oxidar compuestos de alto potencial redox (Ruiz-Dueñas et al., 2009a) (**Fig. 6A**). Además, las VPs comparten con las GPs la capacidad de oxidar compuestos de bajo potencial redox (p.ej. fenoles). Sin embargo, a diferencia de éstas, los oxidan en dos sitios catalíticos diferentes. El triptófano expuesto al solvente actúa como sitio de alta eficiencia, mientras que el canal principal de acceso al hemo funciona como sitio de baja eficiencia (Morales et al., 2012).

Recientemente se ha descrito el origen y la historia evolutiva de las distintas familias de peroxidasas ligninolíticas. Esto ha sido posible gracias a un estudio basado en las PODs identificadas en más de treinta genomas de hongos (Floudas et al., 2012; Ruiz-Dueñas et al., 2013). En este estudio se concluyó que una GP debió ser el ancestro común a partir del cual surgieron el resto de PODs. Esta peroxidasa ancestral evolucionó dando lugar a una enzima de tipo MnP por aparición del sitio de oxidación de manganeso, siendo ésta la primera peroxidasa ligninolítica. Más tarde, a partir de la MnP surgió la primera VP gracias a la adquisición de un triptófano catalítico. Finalmente, la VP debió perder el sitio de oxidación del manganeso dando lugar a una LiP.

El análisis de los genomas de basidiomicetos secuenciados también ha revelado la existencia de nuevos tipos de peroxidasas que eran prácticamente desconocidas hasta hace poco (Hofrichter et al., 2010; Ruiz-Dueñas and Martínez, 2010; Ruiz-Dueñas and Martínez, 2010). Se identificaron tanto hemotiolato peroxidasas (HTPs) como peroxidasas degradadoras de tintes ("dye-decolorizing peroxidases", DyPs) (Ruiz-Dueñas et al., 2013; Floudas et al., 2012) cuyo papel en el proceso de

degradación de lignina o de los productos derivados de ésta aun bien definido. Ambas enzimas son hemoperoxidasas, pero su estructura general difiere radicalmente de la de las PODs, lo que las sitúa en dos superfamilias diferentes de las peroxidasas-catalasas (Sugano et al., 2007 Piontek et al., 2010; Zubieta et al., 2007) (**Fig. 7**). Es interesante resaltar que las HTPs presentan actividad peroxigenasa además de actividad peroxidasa, hecho que hace que estas enzimas sean atractivas desde un punto de vista biotecnológico al catalizar reacciones de transferencia de oxígeno sobre sustratos aromáticos y alifáticos de baja reactividad (Ullrich et al., 2004; Ullrich and Hofrichter, 2007), difíciles de conseguir mediante métodos químicos convencionales. Por otro lado, las DyPs pueden oxidar tintes de alto y bajo potencial redox, compuestos fenólicos y β-carotenos (Liers et al., 2010), entre otros sustratos, lo que también las hace atractivas como biocatalizadores industriales.

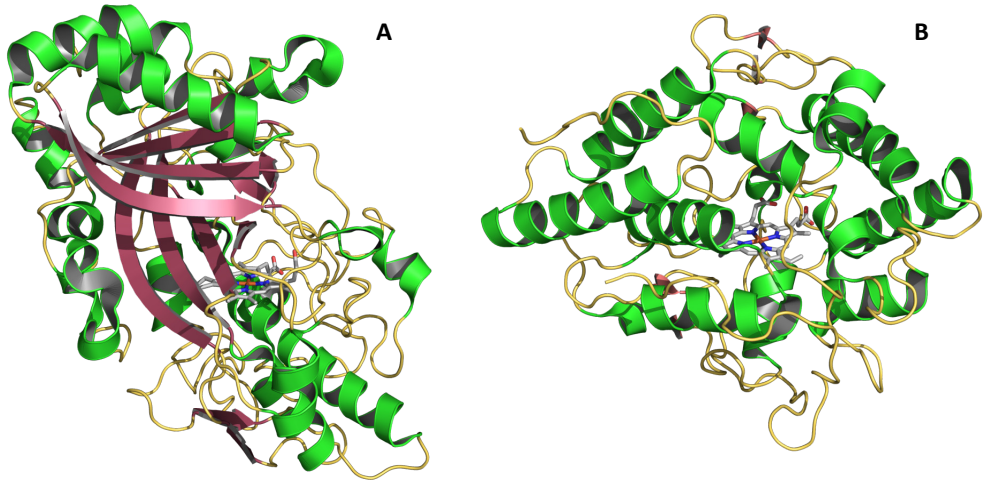

Figura 7. Estructura cristalográfica de: A) DyP de *Auricularia auricula-judae* (PDB:4AU9); y B) UPO de *Agrocybe aegerita* (PDB:2YP1). Las α-hélices se muestran en verde, las láminas β en granate, los *loops* en amarillo y el grupo hemo en colores CPK con los átomos de carbono en gris.

3. Peroxidasa versátil

Las VPs son peroxidasas de alto potencial redox capaces de oxidar Mn^{2+} y una variedad de sustratos, entre los que encontramos compuestos aromáticos y tintes de alto y bajo potencial redox. Como se ha descrito anteriormente, las VPs presentan tres sitios catalíticos responsables de su gran versatilidad catalítica. Estos son: i) el sitio de oxidación de manganeso, también presente en las MnPs; ii) el triptófano catalítico,

también presente en las LiPs; y iii) el sitio de oxidación de compuestos de bajo potencial redox, localizado en el canal del hemo, también presente en las GPs.

3.1 Sitio de oxidación del manganeso (Mn^{2+})

El sitio de oxidación del Mn^{2+} se encuentra en un pequeño canal formado por tres residuos ácidos (Glu36, Glu40 y Asp175 en la VPL de *P. eryngii*) que da acceso al propionato interno del hemo (Ruiz-Dueñas et al., 2007) (**Fig. 8**). La disposición de los tres residuos ácidos da lugar a dos configuraciones del canal: i) configuración de "puerta abierta", en la que los carboxilatos de Glu36 y Glu40 apuntan al solvente manteniendo el canal abierto, a la espera de un ión de Mn^{2+}; y ii) configuración de "puerta cerrada", en la que el canal queda cerrado tras la unión de este ión por los carboxilatos de los tres residuos ácidos y del propionato interno del hemo (dos moléculas de agua completan la coordinación). Una vez unido, el Mn^{2+} es oxidado, transfiriéndose un electrón al hemo activado a través del propionato interno (Ruiz-Dueñas et al., 2007). El Mn^{3+}, una vez quelado, es un agente oxidante difusible capaz de penetrar en la matriz lignocelulósica, contribuyendo al proceso de degradación de lignina, tal como se describió anteriormente para la MnP.

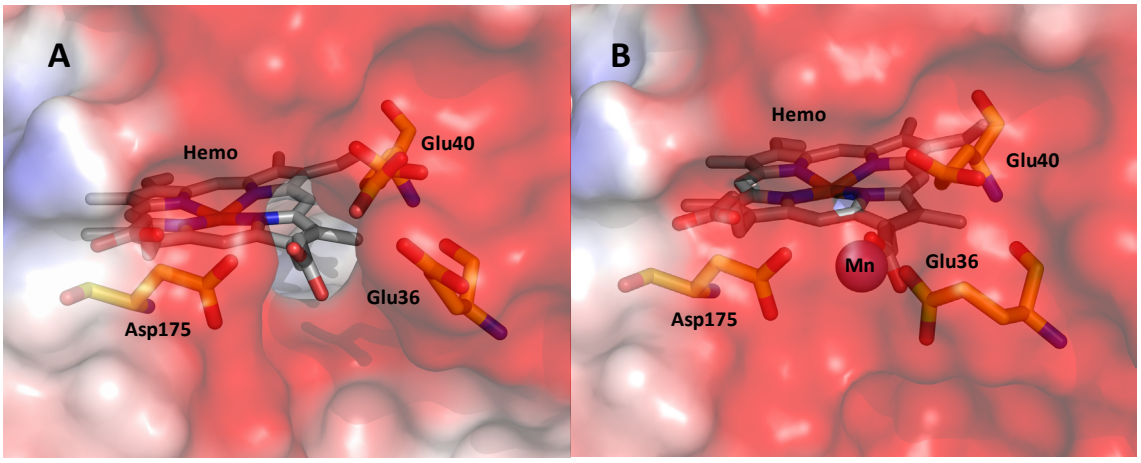

Figura 8. Sitio de oxidación del manganeso en la VP de *P. eryngii* formado por el aspártico 175 y los glutámicos 36 y 40. A, configuración de "puerta abierta" en la que las carboxilos de Glu36 y Glu40 apuntan al solvente permitiendo el acceso de un ión de Mn^{2+} y B, configuración de "puerta cerrada" en la que el un ión de Mn^{2+} aparece unido y coordinado por los tres residuos ácidos y el propionato interno del hemo.

Aunque VPs y MnPs comparten la presencia de un sitio de oxidación de Mn^{2+}, existen algunas diferencias entre las propiedades de dicho sitio en ambos tipos de peroxidasas. En este sentido, las VPs son capaces de actuar sobre el Mn^{2+}, aunque con menor eficiencia, cuando solo están presentes dos (o incluso 1) de los tres residuos ácidos (tras mutagénesis dirigida) (Ruiz-Dueñas et al., 2007). Por el contrario, las MnPs requieren de la presencia de los tres residuos ácidos para oxidar el Mn^{2+} (Kishi et al., 1996; Whitwam et al., 1997). Estas diferencias podrían tener su origen en la presencia de algunos residuos en el entorno de este sitio de oxidación en la MnP, ausentes en la VP, que interaccionan con los ligandos del Mn^{2+} limitando su movilidad (Gelpke et al., 2000).

La oxidación enzimática de Mn^{2+} a Mn^{3+} no es una característica única de las VPs y MnPs de basidiomicetos. Magliozzo y Marcinkeviciene (1997) describieron una peroxidasa-catalasa procariótica que también oxida este catión, y más recientemente se han descrito DyPs bacterianas y fúngicas con esta capacidad catalítica (Brown et al., 2012; Ahmad et al., 2011; Rahmanpour and Bugg, 2015; Singh et al., 2013; Santos et al., 2014; Fernández-Fueyo et al., 2015).

3.2 Triptófano catalítico

El triptófano catalítico (Trp164 en la VPL de *P. eryngii*), localizado en la superficie de la enzima, es el sitio responsable de la oxidación de sustratos de alto potencial redox, y también es el sitio de oxidación de alta eficiencia para sustratos de bajo potencial redox (p.ej. fenoles) (**Fig. 9A**). Tras la activación de las VPs por peróxido, los equivalentes de oxidación inicialmente localizados en el grupo hemo se desplazan hasta este residuo a través de una ruta LRET generándose un radical de triptófano. Una vez formado, el radical puede oxidar, entre otros, compuestos aromáticos no fenólicos (p.ej. alcohol veratrílico), y tintes industriales recalcitrantes (como el *Reactive Black 5*, RB5) (Pérez-Boada et al., 2005).

La implicación del triptófano catalítico en la oxidación de compuestos de alto potencial redox se ha demostrado a través de estudios en los que el Trp164 se sustituyó por mutagénesis dirigida. Además, la formación

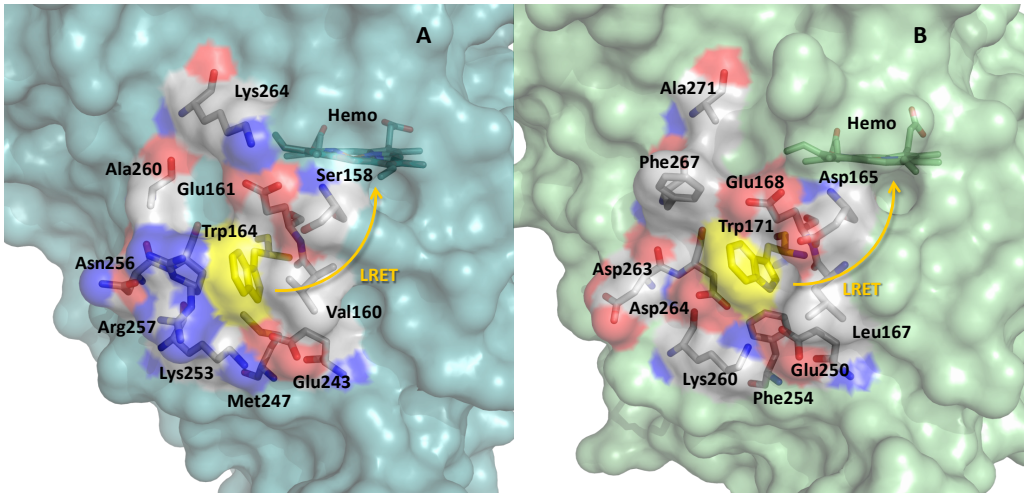

Figura 9. Entorno del triptófano catalítico de la VP (A) y la LiP (B). Representación de la superficie de las peroxidasas, del triptófano catalítico (en amarillo), del grupo hemo (en verde) y de los residuos del entorno del Trp (con colores CPK). Modelos basados en las estructuras de la VP (PDB:2BOQ) y de la LiP (PDB:1LGA).

del radical de triptófano en la VP de *P. eryngii* ha sido confirmada mediante estudios de resonancia paramagnética electrónica (EPR) (Pérez-Boada et al., 2005; Ruiz-Dueñas et al., 2009b; Pogni et al., 2006). La formación de este radical en una posición equivalente también se ha identificado en la VP de *Bjerkandera adusta* (Pogni et al., 2005), y más recientemente en la LiP de *P. chrysosporium* tras modificar los residuos del entorno (Smith et al., 2009).

En relación con esto último, es interesante resaltar el papel que juegan los residuos de superficie cercanos al triptófano catalítico. Estos residuos son responsables de algunas de las diferencias encontradas entre el funcionamiento de la VP y la LiP (Ruiz-Dueñas et al., 2008). Así, la VP es capaz de oxidar directamente compuestos recalcitrantes como el RB5, mientras que la LiP solo es capaz de oxidar estos dos compuestos en presencia de mediadores como el alcohol veratrílico. Esto es debido a que en la VP, el área que rodea al triptófano se encuentra cargada positivamente (**Fig. 9A**), lo que ayuda en la unión y oxidación de sustratos aniónicos (como el RB5). El triptófano de la LiP, por el contrario, está rodeado de residuos que aportan una carga parcialmente negativa al entorno (**Fig. 9B**), que estabiliza el radical catiónico del alcohol veratrílico, que es el producto de su oxidación por la enzima y, además, actúa como mediador en la oxidación de otros sustratos (Ruiz-Dueñas et al., 2008).

La evolución de las VPs y LiPs a partir de una MnP ancestral (Floudas et al., 2012) parece estar específicamente dirigida hacia la oxidación de la molécula de lignina. Ésta no sólo es difícil de oxidar por el elevado potencial redox necesario para sustraer un electrón de sus anillos bencénicos, sino que además es un polímero voluminoso que no puede acceder a través del canal principal de acceso al hemo. Gracias a que el triptófano catalítico está expuesto al solvente, VPs y LiPs son capaces de actuar sobre este polímero y otros sustratos de gran tamaño (Ruiz-Dueñas et al., 2009a).

3.3 Canal principal de acceso al hemo

El tercer sitio de oxidación presente en las VPs es el canal principal por el que accede el H_2O_2 para activar a la enzima. En dicho canal se oxidan, en contacto directo con el hemo, sustratos de bajo potencial redox, como por ejemplo fenoles sencillos y tintes como el ABTS (Morales et al., 2012) (**Fig. 10**). Este canal está conservado en todas las hemoperoxidasas y es el único sitio de oxidación que encontramos en las GPs, que no son capaces de oxidar sustratos de alto potencial redox o sustratos muy voluminosos debido a la ausencia de un residuo catalítico similar al triptófano expuesto al solvente, característico de VPs y LiPs (Smith and Veitch, 1998; Dunford, 1999).

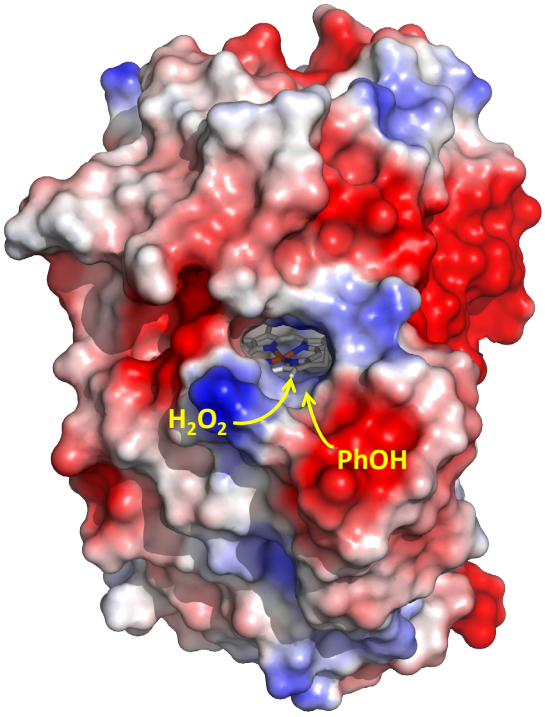

Figura 10. Canal principal de acceso al hemo de la VP de *P. eryngii* por el que accede el peróxido y otros sustratos de pequeño tamaño y bajo potencial redox, como por ejemplo fenoles.

Existen diferencias significativas entre las GPs y las PODs ligninolíticas en cuanto al tamaño del canal principal de acceso al hemo. En las PODs ligninolíticas éste es más estrecho y no permite el acceso de sustratos aromáticos voluminosos. Se ha descrito que la ampliación del canal en la VP de *P. eryngii* da lugar a una enzima que es capaz de oxidar este tipo de sustratos (Morales et al., 2012). Sin embargo, esta oxidación genera radicales catiónicos aromáticos altamente reactivos que llevan a la inactivación de la enzima al reaccionar con el hemo. De acuerdo con estos resultados, podría pensarse que las PODs ligninolíticas han evolucionado estrechando el canal principal de acceso al hemo para evitar daños oxidativos a la enzima.

3.4 Ciclo catalítico global

Como en todas las peroxidasas, el ciclo catalítico de la VP se inicia con la activación de la enzima por peróxido de hidrógeno (**Fig. 11**). En esta reacción, la peroxidasa en estado de reposo (con el hierro del hemo como Fe^{3+}) sufre una oxidación de dos electrones dando lugar al Compuesto I. Este primer intermediario del ciclo catalítico se caracteriza por presentar dos equivalentes de oxidación en forma de complejo Fe^{4+}-oxo y radical catiónicoπ de la porfirina (Compuesto IA). A través de la oxidación de una molécula de sustrato, la enzima recupera un electrón en la porfirina y pasa a estar en forma de Compuesto II, manteniendo el complejo Fe^{4+}-oxo (Compuesto IIA). Finalmente, con la oxidación de una segunda molécula de sustrato, la enzima recupera el segundo electrón volviendo al estado de reposo. Además, los Compuestos IA y IIA pueden desplazar un equivalente de oxidación desde el hemo al triptófano catalítico, que queda como radical (intermediarios denominados IB y IIB). Para la VP, se ha calculado que, en las condiciones utilizadas para la EPR (a baja temperatura), el 25% de las moléculas en forma de Compuesto I, lo están como Compuesto IB; y que el 3% de las moléculas en forma de Compuesto II lo están como Compuesto IIB (Ruiz-Dueñas et al., 2009b). Los Compuestos IB y IIB serían los responsables de la oxidación de compuestos de alto potencial redox a través del triptófano catalítico (Pérez-Boada et al., 2005; Ruiz-Dueñas et al., 2009b).

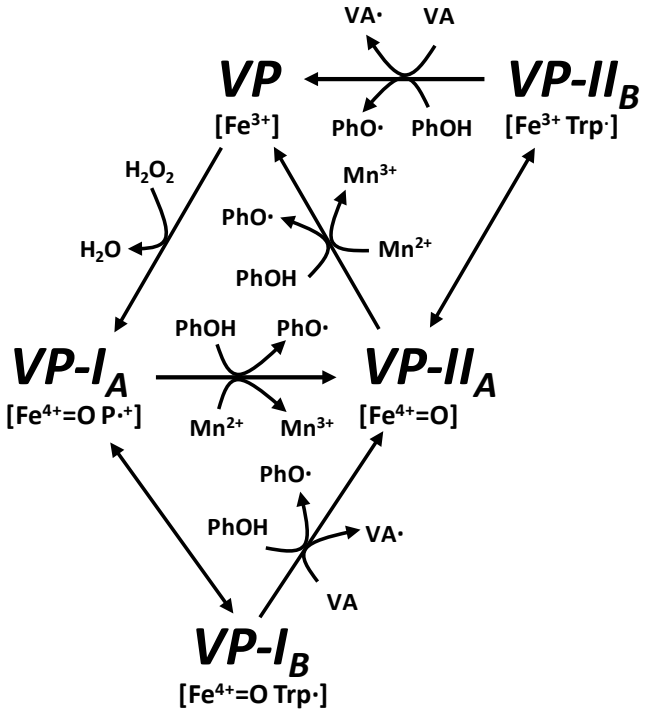

Figura 11. Ciclo catalítico de la VP. La VP en estado de reposo (con Fe^{3+}) es oxidada por el peróxido de hidrógeno dando lugar al Compuesto I, VP-I_A (con Fe^{4+}=O y radical de porfirina, $P^{\cdot+}$), el cual puede derivar a VP-I_B desplazando un equivalente de oxidación al Trp catalítico. VP-I_A cataliza la oxidación de sustratos en contacto directo con el hemo, como el Mn^{2+} o sustratos de bajo potencial redox, como por ejemplo, fenoles (PhOH). VP-I_B cataliza la oxidación de sustratos de alto potencial redox, por ejemplo el VA, a través del Trp catalítico en superficie. Tras la reducción del Compuesto I se forma el Compuesto II, VP-II_A (con Fe^{4+}=O), que igualmente puede desplazar un equivalente de oxidación dando lugar a VP-II_B. El compuesto II también puede oxidar sustratos en contacto directo con el hemo (VP-II_A) o a través del Trp catalítico (VP-II_B) recuperando el estado de reposo.

3.5 Características espectroscópicas

Los estudios espectroscópicos de la enzima nos aportan información valiosa sobre el estado de coordinación y oxidación en el que se encuentra el hemo y su entorno, así como sobre la formación de radicales en la proteína. Por tanto, son una herramienta muy útil en el estudio de las hemoperoxidasas.

La VP en estado de reposo se caracteriza por presentar un espectro de absorción UV-Visible con máximos a 407 nm (banda de Soret), 505 nm y 637 nm (bandas de transferencia de carga CT2 y CT1, respectivamente) y dos hombros a 532 nm y 560 nm correspondientes a las bandas β y α

(Pérez-Boada et al., 2005) (**Fig. 12A**). Este espectro es reflejo de un hemo con el Fe^{3+} en forma de alto spin y pentacoordinado por los cuatro nitrógenos del anillo tetrapirrólico y el nitrógeno ε de la histidina proximal. También puede presentar el hemo hexacoordinado en forma de alto spin con una molécula de agua ocupando la sexta posición de coordinación, conformación en la cual la enzima sigue siendo activa (Ayala-Aceves et al., 2001).

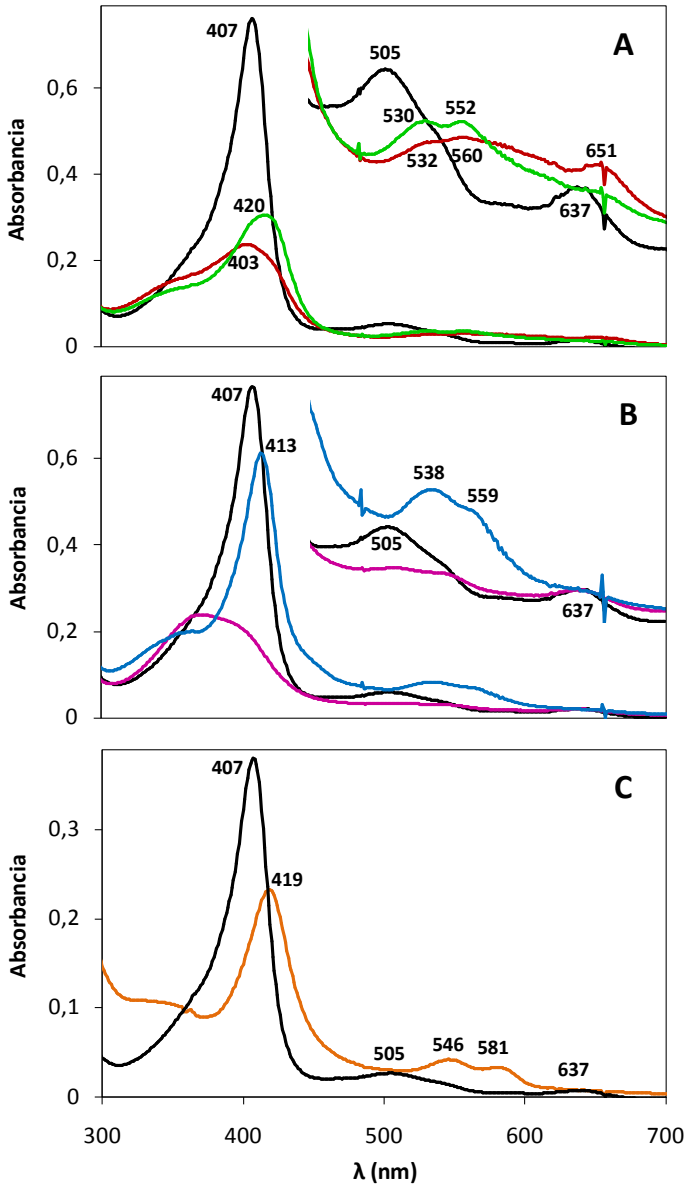

Figura 12. Espectros de absorción UV-visible de la VP (isoenzima VPL2) de *P. eryngii*. A) Espectros del estado de reposo (negro), Compuesto I (rojo) y Compuesto II (verde). B) VP en estado de reposo (negro), con el hemo hexacoordinado debido a la inactivación alcalina (azul) e inactivada a pH ácido (rosa). C) VP en estado de reposo (negro) y en forma de Compuesto III (naranja).

Cuando se forma el Compuesto I, tras la reacción con el H_2O_2, la banda de Soret se desplaza hasta los 403 nm, disminuyendo su intensidad de manera considerable, y aparecen nuevos máximos a 532 nm, 560 nm y 651 nm (**Fig. 12A**). El espectro de la enzima en forma de Compuesto II presenta el máximo de la banda de Soret a 420 nm y máximos a 530 nm y 552 nm. Los espectros de estos dos intermediarios catalíticos son similares a los encontrados en otras PODs ligninolíticas.

Igualmente, es posible estudiar la VP y demás PODs en estados diferentes de los encontrados en el ciclo catalítico, por ejemplo, estados en que las enzimas se encuentran inactivadas. La inactivación alcalina o térmica de las PODs ligninolíticas implica la pérdida de uno o los dos calcios estructurales, responsables de mantener la conformación del bolsillo del hemo. Esta pérdida lleva a la hexacoordinación del hemo con el nitrógeno ε de la histidina distal ocupando la sexta posición de coordinación, quedando el hierro en conformación de bajo spin. Espectroscópicamente, esto se refleja en un desplazamiento de la banda de Soret a los 413 nm y en la aparición de nuevos máximos a 538 nm y 559 nm (Youngs et al., 2000; George et al., 1999) (**Fig. 12B**). Por otra parte, la inactivación ácida de la VP produce el blanqueamiento del enzima, hecho que queda reflejado en el espectro por la desaparición de la banda de Soret.

Por otro lado, el Compuesto III es un intermediario que presenta un anión superóxido ($O_2^{\cdot -}$) unido al Fe^{3+} del hemo. No forma parte del ciclo catalítico normal y su aparición está relacionada con el proceso de inactivación oxidativa de la VP y otras PODs. Se caracteriza por presentar el máximo de la banda de Soret desplazado a 419 nm, y dos máximos en la región visible del espectro a 546 nm y 581 nm (Wariishi and Gold, 1990; Valderrama et al., 2002) (**Fig. 12C**).

También es posible caracterizar espectroscópicamente las hemoperoxidasas utilizando la técnica de EPR. En el caso de la VP, es útil para determinar el estado de oxidación del hierro y los radicales de proteína formados a lo largo del ciclo catalítico. Además, en algunos casos, también se han podido observar radicales de sustratos tras su oxidación enzimática. El espectro de EPR de la VP en estado de reposo

se caracteriza por presentar señales en g=6 y g=2 correspondientes al Fe^{3+} en forma de alto spin (**Fig. 13A**).

Cuando la enzima reacciona con peróxido de hidrógeno y se forma el Compuesto I, en el espectro de EPR se pueden distinguir las señales correspondientes al radical triptófano ($Trp^{\cdot}$, g=2.0031) y al radical catiónico π formado en la porfirina ($P^{\cdot+}$, g_{iso} =2.00(1)) (Pogni et al., 2006; Pogni et al., 2005; Verdín et al., 2006) (**Fig. 13B**). Esta última señal es similar a la descrita en la HRP (Schulz et al., 1979). La señal correspondiente al Fe^{3+} que se observaba en la enzima en estado de reposo desaparece ya que el hierro ahora está en forma de Fe(IV)=O y esta especie no es observable por EPR. El radical del triptófano catalítico ha sido directamente detectado tanto en el compuesto I (B) como en el compuesto II (B) de la VP (Ruiz-Dueñas et al., 2009b).

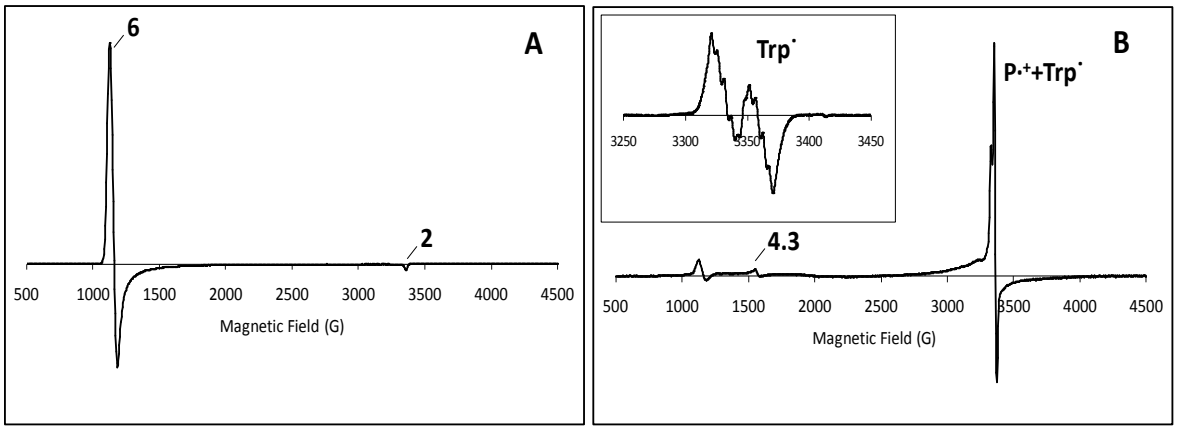

Figura 13. Espectros de resonancia paramagnética electrónica (EPR) de banda X de la VP en estado de reposo (A) y tras la adición de 8 equivalentes de H_2O_2 (B). En A se aprecian las señales de g=6 y g=2 correspondientes al Fe^{3+} en forma de alto spin. En B, la principal señal que se aprecia corresponde a una mezcla de los radicales de la porfirina y del triptófano, la señal de g=6 al Fe^{3+} en forma de alto spin y la señal de g=4.3 corresponde a hierro no unido al hemo. El espectro del recuadro muestra la señal correspondiente al radical triptófano ampliada. Los espectros se tomaron en las siguientes condiciones: ν=9.4 GHz; frecuencia de modulación, 100 kHz; amplitud de modulación, 4G; temperatura, 4K y potencia de microondas, 2 mW. El espectro del recuadro se tomó con una potencia de microondas de 1mW, una frecuencia de modulación de 2G y una temperatura de 20K.

4. Aplicaciones de las PODs ligninolíticas

Las peroxidasas ligninolíticas están naturalmente diseñadas para superar la heterogeneidad y naturaleza polimérica y recalcitrante de la lignina ya que presentan un alto potencial redox y la capacidad de transferir el potencial oxidativo a un residuo expuesto al solvente que sustrae un electrón de anillo bencénico de las diferentes unidades y subestructuras del polímero (Martínez et al., 2009). Estas características les permiten oxidar una variedad de sustratos aromáticos fenólicos y no fenólicos (de bajo y alto potencial redox, respectivamente) así como diferentes tintes industriales y pesticidas. Además, las PODs son autosuficientes, en el sentido de que son activadas por H_2O_2, un oxidante de fácil adquisición, de tal manera que no necesitan proteínas auxiliares o caros co-sustratos para su funcionamiento. Por otra parte, las reacciones de oxidación que llevan a cabo las PODs pueden conducir a la rotura de enlaces o la formación de otros por condensación de radicales, así como reacciones de oxigenación indirectas debido a la reacción de los radicales formados con especies de oxígeno. Todas estas reacciones son interesantes industrialmente (Burton, 2003). Por todo ello, las PODs ligninolíticas son herramientas muy interesantes y prometedoras para gran diversidad de aplicaciones biotecnológicas.

4.1 Deslignificación industrial

Una de las principales aplicaciones de las peroxidasas ligninolíticas se encuentra en su uso en procesos de deslignificación de la biomasa vegetal. Se trata de un paso determinante en la utilización de esta materia prima, ya que permite la separación de sus diferentes componentes, el acceso a los carbohidratos de la madera y el aprovechamiento de los mismos (Martínez et al., 2009).

En este sentido, el potencial biotecnológico de estas enzimas, así como el de los microorganismos productores, se ha probado en distintos procesos relacionados con la producción sostenible de biocombustibles y productos químicos en las biorrefinerías lignocelulósicas o en procesos relacionados con la producción de papel (Young and Akhtar, 1998; Ragauskas et al., 2006; Himmel et al., 2007). Por ejemplo, en el "biopulping", proceso en el que se tratan astillas de madera con la intención de eliminar la lignina para la separación de las fibras

celulósicas, se podría realizar un pretratamiento con PODs ligninolíticas reduciendo de este modo el consumo de productos químicos y energía (Fackler et al., 2006; Hakala et al., 2004). También, en la industria papelera, durante el blanqueo de la pasta de papel, el uso de enzimas ligninolíticas podría sustituir el empleo de compuestos clorados, tradicionalmente utilizados, los cuales son altamente contaminantes para el medio ambiente, aumentando así la sostenibilidad del proceso (Marques et al., 2010; Sigoillot et al., 2005; Moreira et al., 2003).

4.2 Biorremediación

Las peroxidasas ligninolíticas también tienen potencial biotecnológico en el campo de la biorremediación ya que son capaces de oxidar y degradar un amplio rango de compuestos xenobióticos como hidrocarburos policíclicos aromáticos (Rodríguez et al., 2004), compuestos aromáticos y sus derivados halogenados (Dávila-Vázquez et al., 2005), fenoles, dioxinas (Hammel et al., 1986), pesticidas y diferentes tintes (Heinfling et al., 1998; Ollikka et al., 1993), incluyendo los de tipo azo que se encuentran entre los más comercializados (Robinson et al., 2001) (**Fig. 14**).

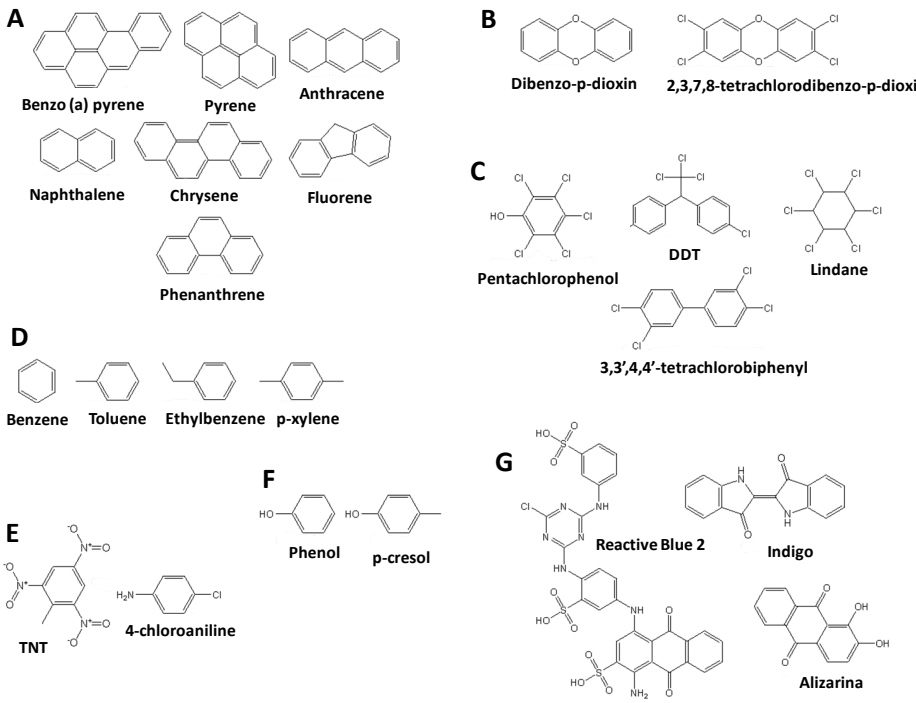

Figura 14: Distintos sustratos recalcitrantes sobre los que actúan las PODs ligninolíticas. A, hidrocarburos policíclicos aromáticos (PAHs); B, dioxinas; C, compuestos clorados; D, derivados del benceno; E, compuestos nitroaromáticos; F, compuestos fenólicos; G, colorantes.

Debido a la capacidad para degradar esta gran diversidad de compuestos, las PODs ligninolíticas podrían sustituir a los métodos físico-químicos tradicionalmente utilizados en el tratamiento de determinados residuos industriales. Estos tratamientos son normalmente costosos y contaminantes y, además, dejan un sedimento concentrado. Los métodos biológicos suponen una alternativa más sostenible que ayudará a cumplir las legislaciones cada vez más restrictivas con respecto al tratamiento y eliminación de residuos industriales de manera que no supongan un peligro para el medio ambiente (Robinson et al., 2001).

4.3 Síntesis

Las peroxidasas ligninolíticas están capacitadas para llevar a cabo reacciones de oxidación que las hacen interesantes también en el campo de la síntesis de diferentes compuestos químicos.

Se ha estudiado su uso en la polimerización de lignanos, péptidos y polisacáridos dando lugar a diferentes compuestos de valor añadido y materiales con nuevas propiedades (Salvachúa et al., 2013). También son útiles en la producción de resinas fenólicas sintéticas que pueden reemplazar a las basadas en fenol-formaldehido (Schmid et al., 2001). Además se estudia el uso de la VP y otras peroxidasas ligninolíticas para la transformación de β -carotenos y otros carotenoides en iononas, compuestos aromáticos ampliamente utilizados en perfumería y como saborizantes en alimentos (Zorn et al., 2003).

5. Optimización de las PODs como biocatalizadores

5.1 Aspectos generales

Como se ha mencionado, la utilización de peroxidasas ligninolíticas como biocatalizadores en diferentes procesos industriales es muy prometedora (Martínez et al., 2009). Sin embargo, a pesar del interés que despiertan estas enzimas, muy pocas se comercializan actualmente y su aplicación industrial es modesta. Esto es debido, al menos en parte, a que no son aplicables tal como se producen en la naturaleza, ya que no presentan una adecuada selectividad y compatibilidad con las

condiciones agresivas (de pH, temperatura, etc) que caracterizan los procesos industriales.

Los principales requisitos que ha de cumplir un biocatalizador para su aplicación industrial son: i) su obtención a unos niveles suficientemente elevados; ii) una alta selectividad que permita la obtención del producto de interés con una baja o nula producción de compuestos secundarios; y iii) una estabilidad adecuada en las condiciones del proceso en el que se va a emplear, lo que incluye estabilidad frente a diferentes factores (pH, temperatura, solventes orgánicos o concentración de peróxido en el caso de las peroxidasas) (Ayala et al., 2008). También es importante que el proceso en sí sea más sostenible medioambientalmente que el proceso químico clásico que se pretende sustituir con el uso del biocatalizador.

Por tanto, para que el empleo de las PODs sea una opción real, es necesaria la optimización de las mismas, es decir, la adaptación y refinamiento de sus propiedades catalíticas y operacionales (Schmid et al., 2001). Este proceso es hoy posible gracias a la existencia de técnicas de ingeniería de proteínas que abarcan abordajes racionales, basados en la información estructura-función existente, y no racionales, como la evolución molecular dirigida, que no necesitan esta información. También es posible utilizar una combinación de ambas aproximaciones y además éstas se pueden complementar con métodos computacionales (Chaput et al., 2008;Yang et al., 2014). El diseño racional se basa en el conocimiento de las bases estructurales que subyacen a la propiedad a mejorar. Hoy en día, disponemos de una gran cantidad de estructuras cristalográficas de PODs, además de un gran conocimiento sobre los mecanismos de reacción de estas peroxidasas (Ruiz-Dueñas and Martínez, 2009; Wong, 2009; Kersten and Cullen, 2007; Ruiz-Dueñas et al., 2009a). Considerando toda la información disponible, la mejora y el diseño de las propiedades que interesan a través de esta metodología es posible, así como la transferencia de las características más favorables de unas enzimas a otras. Por otra parte, la evolución molecular dirigida se basa en la generación de diversidad genética mediante la introducción de mutaciones de manera aleatoria y/o la recombinación del material genético que codifica para las proteínas de interés, seguidos de la selección de la mejor variante en base a las características

buscadas (Bloom et al., 2005; Dougherty and Arnold, 2009). Es un arma poderosa dentro de la ingeniería de enzimas, sobre todo cuando las bases estructurales que subyacen a una propiedad no se conocen bien. Por último, cabe resaltar el papel de las técnicas de modelado molecular que se usan cada vez con más frecuencia. Se pueden aplicar en tres aspectos fundamentales de la optimización de oxidorreductasas: i) en el estudio del proceso catalítico de oxidación; ii) en el estudio de la difusión y unión de sustratos; y iii) en el estudio de la estabilidad de las proteínas. Podemos encontrar numerosos ejemplos de cómo la combinación de estas técnicas con la ingeniería de proteínas es una herramienta exitosa para el diseño de biocatalizadores (Borrelli et al., 2005; Dougherty and Arnold, 2009).

5.2 Mejora de la estabilidad oxidativa de la VP

La estabilidad a peróxido de hidrógeno es uno de los principales parámetros a mejorar antes del uso industrial de las peroxidasas ligninolíticas (Valderrama et al., 2002). El peróxido de hidrógeno, necesario para el funcionamiento de las peroxidasas, es un fuerte oxidante que puede tener efectos deletéreos sobre células y proteínas. En la naturaleza, la presencia del H_2O_2 implicado en la degradación de lignina no supone un problema para el funcionamiento de las peroxidasas, ya que en condiciones de exceso es destruido por catalasas. Sin embargo, en la aplicación de las PODs como biocatalizadores, la inactivación por H_2O_2 es un evento a tener muy en cuenta. Éste es un proceso complejo ya que puede implicar una gran variedad de reacciones y su mecanismo no se conoce por completo, aunque se sabe que es especialmente importante cuando existe un exceso de peróxido o no existe sustrato reductor (Valderrama et al., 2006;Arnao et al., 1990;Valderrama et al., 2002;Hiner et al., 2000; Hiner et al., 1995).

La inactivación de las peroxidasas por H_2O_2 se ha relacionado con la formación del Compuesto III (**Fig. 15**), un intermediario que no forma parte del ciclo catalítico pero que lleva a la pérdida de actividad y al blanqueo de estas enzimas (Valderrama et al., 2006; Valderrama et al., 2002; Hiner et al., 2000; Hiner et al., 1995). En ausencia de sustrato reductor, los Compuestos I y II, que son muy reactivos, pueden llegar a oxidar el H_2O_2 dando lugar al Compuesto III, que presenta un anión

superóxido ($O_2^{\cdot-}$) unido al Fe^{3+}del hemo (Wariishi and Gold, 1990). El sustrato reductor tiene un papel protector ya que previene (o ralentiza) la formación del Compuesto III compitiendo eficazmente con el H_2O_2 por el Compuesto II (Valderrama et al., 2002). Una vez formado, el Compuesto III puede seguir diferentes rutas, incluyendo (**Fig. 15**): i) la oxidación y ruptura del anillo de porfirina del hemo causando el blanqueo de la enzima y la inactivación irreversible de la misma (Hiner et al., 2001; Nakajima and Yamazaki, 1980); ii) la oxidación de otros componentes de la proteína, permitiendo a la enzima retornar al estado de reposo a costa de la acumulación de daño oxidativo; y iii) la liberación del radical superóxido que puede transformarse en otras especies reactivas como radicales hidroxilo que difunden y pueden oxidar otras zonas de la enzima (Valderrama et al., 2002). Los componentes más vulnerables a estos daños serían los residuos más fácilmente oxidables, como tirosinas, cisteínas y metioninas y triptófanos. La oxidación de estos residuos tiene diferentes consecuencias que a menudo provocan la pérdida de la actividad y la inactivación de la enzima (Villegas et al., 2000).

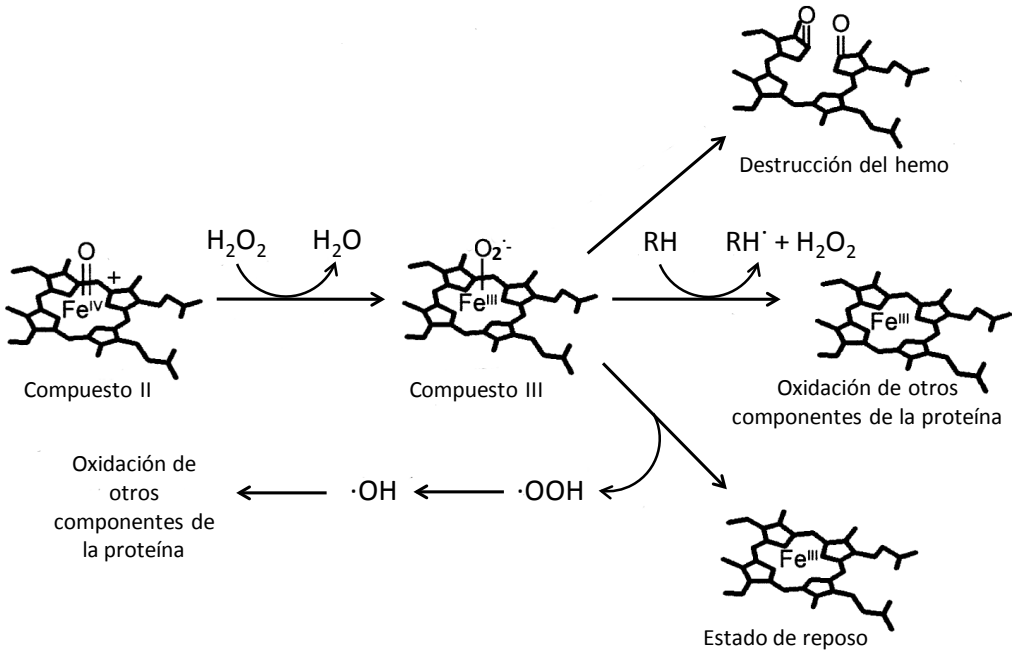

Figura 15. Distintas rutas de inactivación que derivan de la formación del Compuesto III. Adaptado de Valderrama *et a*l., 2002.

Las peroxidasas ligninolíticas no presentan o tienen un bajo número de tirosinas en su secuencia, un hecho que parecería indicar que estas enzimas habrían evolucionado tratando de reducir el contenido en este

tipo de residuos con objeto de minimizar los daños oxidativos como consecuencia del ambiente oxidante en el que se produce la degradación de lignina en la naturaleza. Un caso curioso es el de la LiP de *Trametes cervina,* que no solo presenta una tirosina sino que además es el residuo catalítico expuesto al solvente (Miki et al., 2011). Por lo que respecta a los residuos de metionina, su oxidación por exceso de peróxido da lugar a la formación de metionina sulfóxido y metionina sulfona, lo que implica un incremento del tamaño de la cadena lateral, una reducción de la hidrofobicidad del residuo, así como un incremento en la capacidad de formar puentes de hidrógeno del mismo. Esto ocasiona cambios estructurales que pueden afectar no solo a la región donde se encuentran ubicadas las metioninas sino también a otras regiones de la proteína con consecuencias impredecibles. La oxidación de metioninas y otros residuos se ha descrito durante la inactivación por peróxido de diferentes peroxidasas (Vogt, 1995; Kim and Erman, 1988; Stadtman et al., 2003).

La sustitución de los residuos más sensibles por otros más resistentes a la oxidación puede prevenir, ralentizar o eliminar el proceso de inactivación. Esta estrategia ha sido utilizada en varios trabajos (Ogola et al., 2010; Cherry et al., 1999). Sin embargo, no es la única solución propuesta. Otras aproximaciones, distintas al empleo de la ingeniería de proteínas, pasan por suministrar el H_2O_2 en forma continua para evitar su acumulación, la inmovilización de las peroxidasas, o la adición de aditivos que las protejan (Hernandez et al., 2012).

5.3 Mejora de la estabilidad al pH de la VP

La estabilidad a pH es otro de los factores clave para el uso industrial de biocatalizadores que a menudo necesita ser mejorada. La inactivación de las peroxidasas ligninolíticas debida al pH alcalino, o incluso neutro, se produce como consecuencia de la pérdida de los dos iones de calcio estructurales responsables del mantenimiento de la correcta conformación del bolsillo del hemo (Martínez, 2002). La ausencia de los calcios conduce al colapso de la estructura de dicho bolsillo, lo que lleva a que el hierro del hemo quede hexacoordinado con los residuos de histidina proximal y distal (**Fig. 16**), en estado de bajo spin, de tal manera la enzima es incapaz de reaccionar con el H_2O_2 (Youngs et al.,

2000; George et al., 1999). De igual forma, el pH ácido también afecta a las PODs, aunque en este caso parece que se producen cambios conformacionales a nivel de toda la estructura, lo que lleva al desplegado y desnaturalización de las peroxidasas con su consecuente blanqueo e inactivación (Hargrove and Olson, 1996; McEldoon et al., 1995). El refuerzo del área de coordinación de los calcios, así como la adición de elementos estructurales, como puentes disulfuro o puentes de hidrógeno, en zonas clave de la enzima pueden ser algunas de las estrategias a utilizar para conseguir una mayor estabilidad a pH de estos biocatalizadores (Sakharov and Sakharova, 2002).

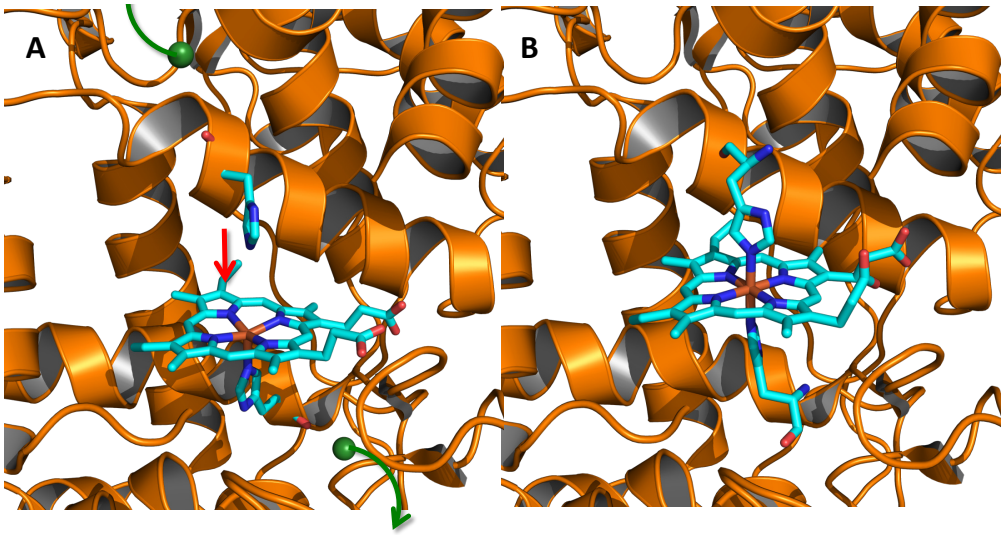

Figura 16. Inactivación alcalina y térmica de las PODs. La enzima con el hierro del hemo pentacoordinado (A) pierde uno o los dos calcios estructurales (esferas verdes y flechas verdes) a pH alcalino o elevada temperatura, de tal manera que la estructura del bolsillo del hemo colapsa (representado por la flecha roja) y la histidina distal pasa a coordinar el hierro del hemo quedando hexacoordinado sin posibilidad de reaccionar con H_2O_2 (B).

6. Bibliografía

Ahmad, M., J.N.Roberts, E.M.Hardiman, R.Singh, L.D.Eltis, and T.D.H.Bugg. 2011. Identification of DypB from *Rhodococcus jostii* RHA1 as a lignin peroxidase. *Biochemistry* 50:5096-5107.

Amidon, T.E., C.D.Wood, A.M.Shupe, Y.Wang, M.Graves, and S.J.Liu. 2008. Biorefinery: Conversion of woody biomass to chemicals, energy and materials. *J. Biobased Mater. Bio.* 2:100-120.

Arnao, M.B., M.Acosta, J.A.del Río, R.Varón, and F.García-Cánovas. 1990. A kinetic study on the suicide inactivation of peroxidase by hydrogen peroxide. *Biochim. Biophys. Acta* 1041:43-47.

Ayala, M., M.A.Pickard, and R.Vázquez-Duhalt. 2008. Fungal enzymes for environmental purposes, a molecular biology challenge. *J. Mol. Microbiol. Biotechnol.* 15:172-180.

Ayala-Aceves, M., M.C.Baratto, R.Basosi, R.Vázquez-Duhalt, and R.Pogni. 2001. Spectroscopic characterization of a manganese-lignin peroxidase hybrid isozyme produced by *Bjerkandera adusta* in the absence of manganese: evidence of a protein centred radical by hydrogen peroxide. *J. Mol. Catal. B-Enzym.* 16:159-167.

Baldrian, P. and V.Valaskova. 2008. Degradation of cellulose by basidiomycetous fungi. *FEMS Microbiol. Rev.* 32:501-521.

Banci, L., I.Bertini, P.Turano, M.Tien, and T.K.Kirk. 1991. Proton NMR investigation into the basis for the relatively high redox potential of lignin peroxidase. *Proc. Natl. Acad. Sci. USA* 88:6956-6960.

Banci, L., S.Camarero, A.T.Martínez, M.J.Martínez, M.Pérez-Boada, R.Pierattelli, and F.J.Ruiz-Dueñas. 2003. NMR study of Mn(II) binding by the new versatile peroxidase from the white-rot fungus *Pleurotus eryngii*. *J. Biol. Inorg. Chem.* 8:751-760.

Bao, W.L., Y.Fukushima, K.A.Jensen, M.A.Moen, and K.E.Hammel. 1994. Oxidative degradation of non-phenolic lignin during lipid peroxidation by fungal manganese peroxidase. *FEBS Lett.* 354:297-300.

Barredo, J.L. 2005. Microbial enzymes and biotransformations. Humana Press, Totowa.

Blodig, W., A.T.Smith, W.A.Doyle, and K.Piontek. 2001. Crystal structures of pristine and oxidatively processed lignin peroxidase expressed in *Escherichia coli* and of the W171F variant that eliminates the redox active tryptophan 171. Implications for the reaction mechanism. *J. Mol. Biol.* 305:851-861.

Bloom, J.D., M.M.Meyer, P.Meinhold, C.R.Otey, D.MacMillan, and F.H.Arnold. 2005. Evolving strategies for enzyme engineering. *Curr. Opin. Struct. Biol.* 15:447-452.

Boerjan, W., J.Ralph, and M.Baucher. 2003. Lignin biosynthesis. *Annu. Rev. Plant Biol.* 54:519-546.

Borrelli, K.W., A.Vitalis, R.Alcantara, and V.Guallar. 2005. PELE: Protein energy landscape exploration. A novel Monte Carlo based technique. *J. Chem. Theory Comput.* 1:1304-1311.

Brown, M.E., T.Barros, and M.C.Y.Chang. 2012. Identification and characterization of a multifunctional dye peroxidase from a lignin-reactive bacterium. *ACS Chemical Biology* 7:2074-2081.

Burton, S.G. 2003. Oxidizing enzymes as biocatalysts. *Trends Biotechnol.* 21:543-549.
Camarero, S., S.Sarkar, F.J.Ruiz-Dueñas, M.J.Martínez, and A.T.Martínez. 1999. Description of a versatile peroxidase involved in natural degradation of lignin that has both Mn-peroxidase and lignin-peroxidase substrate binding sites. *J. Biol. Chem.* 274:10324-10330.
Chaput, J.C., N.W.Woodbury, L.A.Stearns, and B.A.R.Williams. 2008. Creating protein biocatalysts as tools for future industrial applications. *Expert* 8:1087-1098.
Cherry, J.R., M.H.Lamsa, P.Schneider, J.Vind, A.Svendsen, A.Jones, and A.H.Pedersen. 1999. Directed evolution of a fungal peroxidase. *Nat. Biotechnol.* 17:379-384.
Dávila-Vázquez, G., R.Tinoco, M.A.Pickard, and R.Vázquez-Duhalt. 2005. Transformation of halogenated pesticides by versatile peroxidase from *Bjerkandera adusta*. *Enzyme Microb. Technol.* 36:223-231.
Dougherty, M.J. and F.H.Arnold. 2009. Directed evolution: new parts and optimized function. *Curr. Opin. Biotechnol.* 20:486-491.
Du, P., J.R.Collins, and G.H.Loew. 1992. Homology modeling of a heme protein, lignin peroxidase, from the crystal structure of cytochrome *c* peroxidase. *Protein Eng.* 5:679-691.
Dunford, H.B. 1999. Heme peroxidases. Wiley-VCH, New York.
Eriksson, K.-E.L., R.A.Blanchette, and P.Ander. 1990. Microbial and enzymatic degradation of wood components. Springer-Verlag, Berlin.
Erman, J.E., L.B.Vitello, M.A.Miller, A.Shaw, K.A.Brown, and J.Kraut. 1993. Histidine 52 is a critical residue for rapid formation of cytochrome *c* peroxidase compound I. *Biochemistry* 32:9798-9806.
Fackler, K., C.Gradinger, B.Hinterstoisser, K.Messner, and M.Schwanninger. 2006. Lignin degradation by white rot fungi on spruce wood shavings during short-time solid-state fermentations monitored by near infrared spectroscopy. *Enzyme Microb. Technol.* 39:1476-1483.
Fernández-Fueyo, E., S.Acebes, F.J.Ruiz-Dueñas, M.J.Martínez, A.Romero, F.J.Medrano, V.Guallar, and A.T.Martínez. 2014a. Structural implications of the C-terminal tail in the catalytic and stability properties of manganese peroxidases from ligninolytic fungi. *Acta Crystallogr. D. Biol. Crystallogr.* 70:3253-3265.
Fernández-Fueyo, E., D.Linde, D.Almendral, M.F.López-Lucendo, F.J.Ruiz-Dueñas, and A.T.Martínez. 2015. Description of the first fungal dye-decolorizing peroxidase oxidizing manganese(II). *Appl. Microbiol. Biotechnol.* (online).
Fernández-Fueyo, E., F.J.Ruiz-Dueñas, M.J.Martínez, A.Romero, K.E.Hammel, F.J.Medrano, and A.T.Martínez. 2014b. Ligninolytic peroxidase genes in the oyster mushroom genome: Heterologous expression, molecular structure, catalytic and stability properties and lignin-degrading ability. *Biotechnol. Biofuels* 7:2.
Floudas, D., M.Binder, R.Riley, K.Barry, R.A.Blanchette, B.Henrissat, A.T.Martínez, R.Otillar, J.W.Spatafora, J.S.Yadav, A.Aerts, I.Benoit, A.Boyd, A.Carlson, A.Copeland, P.M.Coutinho, R.P.de Vries, P.Ferreira, K.Findley, B.Foster, J.Gaskell, D.Glotzer, P.Górecki, J.Heitman, C.Hesse, C.Hori, K.Igarashi, J.A.Jurgens, N.Kallen, P.Kersten, A.Kohler, U.Kües, T.K.A.Kumar, A.Kuo, K.LaButti, L.F.Larrondo, E.Lindquist, A.Ling, V.Lombard, S.Lucas, T.Lundell, R.Martin, D.J.McLaughlin, I.Morgenstern, E.Morin, C.Murat, M.Nolan, R.A.Ohm, A.Patyshakuliyeva, A.Rokas, F.J.Ruiz-Dueñas, G.Sabat, A.Salamov, M.Samejima, J.Schmutz, J.C.Slot, F.St.John, J.Stenlid, H.Sun, S.Sun, K.Syed, A.Tsang,

A.Wiebenga, D.Young, A.Pisabarro, D.C.Eastwood, F.Martin, D.Cullen, I.V.Grigoriev, and D.S.Hibbett. 2012. The Paleozoic origin of enzymatic lignin decomposition reconstructed from 31 fungal genomes. *Science* 336:1715-1719.

Flournoy, D.S., J.A.Paul, T.K.Kirk, and T.L.Highley. 1993. Changes in the size and volume of pores in sweetgum wood during simultaneous rot by *Phanerochaete chrysosporium* Burds. *Holzforschung* 47:297-301.

Gellerstedt, G. and G.Henriksson. 2008. Lignins: Major sources, structure and properties. *In* Monomers, polymers and composites from renewable resources. M.Belgacem and A.Gandini, editors. Elsevier, Amsterdam. 201-224.

Gelpke, M.D.S., H.L.Youngs, and M.H.Gold. 2000. Role of arginine 177 in the Mn^{II} binding site of manganese peroxidase. Studies with R177D, R177E, R177N, and R177Q mutants. *Eur. J. Biochem.* 267:7038-7045.

George, S.J., M.Kvaratskhelia, M.J.Dilworth, and R.N.F.Thorneley. 1999. Reversible alkaline inactivation of lignin peroxidase involves the release of both the distal and proximal site calcium ions and bishistidine co-ordination of the haem. *Biochem. J.* 344:237-244.

Glenn, J.K., M.A.Morgan, M.B.Mayfield, M.Kuwahara, and M.H.Gold. 1983. An extracellular H_2O_2-requiring enzyme preparation involved in lignin biodegradation by the white rot basidiomycete *Phanerochaete chrysosporium*. *Biochem. Biophys. Res. Commun.* 114:1077-1083.

Gold, M.H., H.L.Youngs, and M.D.Gelpke. 2000. Manganese peroxidase. *Met. Ions Biol. Syst.* 37:559-586.

Gómez-Toribio, V., A.B.García-Martín, M.J.Martínez, A.T.Martínez, and F.Guillén. 2009. Induction of extracellular hydroxyl radical production by white-rot fungi through quinone redox cycling. *Appl. Environ. Microbiol.* 75:3944-3953.

Hakala, T.K., P.Maijala, J.Konn, and A.Hatakka. 2004. Evaluation of novel wood-rotting polypores and corticioid fungi for the decay and biopulping of Norway spruce (*Picea abies*) wood. *Enzyme Microb. Technol.* 34:255-263.

Hammel, K.E. and D.Cullen. 2008. Role of fungal peroxidases in biological ligninolysis. *Curr. Opin. Plant Biol.* 11:349-355.

Hammel, K.E., B.Kalyanaraman, and T.K.Kirk. 1986. Oxidation of polycyclic aromatic hydrocarbons and dibenzo[p]-dioxins by *Phanerochaete chrysosporium* ligninase. *J. Biol. Chem.* 261:16948-16952.

Hargrove, M.S. and J.S.Olson. 1996. The stability of holomyoglobin is determined by heme affinity. *Biochemistry* 35:11310-11318.

Harvey, P.J., H.E.Schoemaker, and J.M.Palmer. 1986. Veratryl alcohol as a mediator and the role of radical cations in lignin biodegradation by *Phanerochaete chrysosporium*. *FEBS Lett.* 195:242-246.

Heinfling, A., F.J.Ruiz-Dueñas, M.J.Martínez, M.Bergbauer, U.Szewzyk, and A.T.Martínez. 1998. A study on reducing substrates of manganese-oxidizing peroxidases from *Pleurotus eryngii* and *Bjerkandera adusta*. *FEBS Lett.* 428:141-146.

Hernandez, K., A.Berenguer-Murcia, R.C.Rodrigues, and R.Fernandez-Lafuente. 2012. Hydrogen Peroxide in Biocatalysis. A Dangerous Liaison. *Curr. Org. Chem.* 16:2652-2672.

Himmel, M.E., S.Y.Ding, D.K.Johnson, W.S.Adney, M.R.Nimlos, J.W.Brady, and T.D.Foust. 2007. Biomass recalcitrance: Engineering plants and enzymes for biofuels production. *Science* 315:804-807.

Hiner, A.N.P., J.Hernández-Ruíz, F.García-Cánovas, A.T.Smith, M.B.Arnao, and M.Acosta. 1995. A comparative study of the inactivation of wild-type, recombinant and two mutant horseradish peroxidase isoenzymes C by hydrogen peroxide and *m*-chloroperoxybenzoic acid. *Eur. J. Biochem.* 234:506-512.

Hiner, A.N.P., J.Hernández-Ruíz, J.N.Rodríguez-López, M.B.Arnao, R.Varon, F.García-Cánovas, and M.Acosta. 2001. The inactivation of horseradish peroxidase isoenzyme A2 by hydrogen peroxide: an example of partial resistance due to the formation of a stable enzyme intermediate. *J. Biol. Inorg. Chem.* 6:504-516.

Hiner, A.N.P., E.L.Raven, R.N.F.Thorneley, F.García-Canovas, and J.N.Rodríguez-López. 2002. Mechanisms of compound I formation in heme peroxidases. *J. Inorg. Biochem.* 91:27-34.

Hiner, A.N.P., J.N.Rodríguez-López, M.B.Arnao, E.L.Raven, F.García-Cánovas, and M.Acosta. 2000. Kinetic study of the inactivation of ascorbate peroxidase by hydrogen peroxide. *Biochem. J.* 348:321-328:321-328.

Hofrichter, M., R.Ullrich, M.J.Pecyna, C.Liers, and T.Lundell. 2010. New and classic families of secreted fungal heme peroxidases. *Appl. Microbiol. Biotechnol.* 87:871-897.

Jensen, K.A., W.Bao, S.Kawai, E.Srebotnik, and K.E.Hammel. 1996. Manganese-dependent cleavage of non-phenolic lignin structures by *Ceriporiopsis subvermispora* in the absence of lignin peroxidase. *Appl. Environ. Microbiol.* 62:3679-3686.

Kapich, A.N., K.T.Steffen, M.Hofrichter, and A.Hatakka. 2005. Involvement of lipid peroxidation in the degradation of a non-phenolic lignin model compound by manganese peroxidase of the litter-decomposing fungus *Stropharia coronilla*. *Biochem. Biophys. Res. Commun.* 330:371-377.

Kersten, P. and D.Cullen. 2007. Extracellular oxidative systems of the lignin-degrading basidiomycete *Phanerochaete chrysosporium*. *Fungal Genet. Biol.* 44:77-87.

Kim, K. and J.E.Erman. 1988. Methionine modification in cytochrome-*c* peroxidase. *Biochim. Biophys. Acta* 954:95-107.

Kirk, T.K. and R.L.Farrell. 1987. Enzymatic "combustion": The microbial degradation of lignin. *Annu. Rev. Microbiol.* 41:465-505.

Kishi, K., D.P.Hildebrand, M.Kusters-van Someren, J.Gettemy, A.G.Mauk, and M.H.Gold. 1997. Site-directed mutations at phenylalanine-190 of manganese peroxidase: Effect on stability, functions and coordination. *Biochemistry* 36:4268-4277.

Kishi, K., M.Kusters-van Someren, M.B.Mayfield, J.Sun, T.M.Loehr, and M.H.Gold. 1996. Characterization of manganese(II) binding site mutants of manganese peroxidase. *Biochemistry* 35:8986-8994.

Liers, C., C.Bobeth, M.Pecyna, R.Ullrich, and M.Hofrichter. 2010. DyP-like peroxidases of the jelly fungus *Auricularia auricula-judae* oxidize nonphenolic lignin model compounds and high-redox potential dyes. *Appl. Microbiol. Biotechnol.* 85:1869-1879.

Lundell, T.K., M.R.Makela, and K.Hildén. 2010. Lignin-modifying enzymes in filamentous basidiomycetes: Ecological, functional and phylogenetic review. *J. Basic Microb.* 50:5-20.

Magliozzo, R.S. and J.A.Marcinkeviciene. 1997. The role of Mn(II)-peroxidase activity of mycobacterial catalase-peroxidase in activation of the antibiotic isoniazid. *J. Biol. Chem.* 272:8867-8870.

Marques, G., J.A.F.Gamelas, F.J.Ruiz-Dueñas, J.C.del Río, D.V.Evtuguin, A.T.Martínez, and A.Gutiérrez. 2010. Delignification of eucalypt kraft pulp with manganese-substituted polyoxometalate assisted by fungal versatile peroxidase. *Bioresource Technol.* 101:5935-5940.

Martínez, A.T. 2002. Molecular biology and structure-function of lignin-degrading heme peroxidases. *Enzyme Microb. Technol.* 30:425-444.

Martínez, A.T., J.Rencoret, L.Nieto, J.Jiménez-Barbero, A.Gutiérrez, and J.C.del Río. 2011. Selective lignin and polysaccharide removal in natural fungal decay of wood as evidenced by *in situ* structural analyses. *Environ. Microbiol.* 13:96-107.

Martínez, A.T., F.J.Ruiz-Dueñas, A.Gutiérrez, J.C.del Río, M.Alcalde, C.Liers, R.Ullrich, M.Hofrichter, K.Scheibner, L.Kalum, J.Vind, and H.Lund. 2014. Search, engineering and applications of new oxidative biocatalysts. *Biofuels Bioprod. Biorefining* 8:819-835.

Martínez, A.T., F.J.Ruiz-Dueñas, M.J.Martínez, J.C.del Río, and A.Gutiérrez. 2009. Enzymatic delignification of plant cell wall: from nature to mill. *Curr. Opin. Biotechnol.* 20:348-357.

Martínez, A.T., M.Speranza, F.J.Ruiz-Dueñas, P.Ferreira, S.Camarero, F.Guillén, M.J.Martínez, A.Gutiérrez, and J.C.del Río. 2005. Biodegradation of lignocellulosics: Microbiological, chemical and enzymatic aspects of fungal attack to lignin. *Int. Microbiol.* 8:195-204.

Martinez, D., J.Challacombe, I.Morgenstern, D.S.Hibbett, M.Schmoll, C.P.Kubicek, P.Ferreira, F.J.Ruiz-Dueñas, A.T.Martínez, P.Kersten, K.E.Hammel, A.Vanden Wymelenberg, J.Gaskell, E.Lindquist, G.Sabat, S.S.Bondurant, L.F.Larrondo, P.Canessa, R.Vicuña, J.Yadav, H.Doddapaneni, V.Subramanian, A.G.Pisabarro, J.L.Lavín, J.A.Oguiza, E.Master, B.Henrissat, P.M.Coutinho, P.Harris, J.K.Magnuson, S.E.Baker, K.Bruno, W.Kenealy, P.J.Hoegger, U.Kües, P.Ramaiya, S.Lucas, A.Salamov, H.Shapiro, H.Tu, C.L.Chee, M.Misra, G.Xie, S.Teter, D.Yaver, T.James, M.Mokrejs, M.Pospisek, I.V.Grigoriev, T.Brettin, D.Rokhsar, R.Berka, and D.Cullen. 2009. Genome, transcriptome, and secretome analysis of wood decay fungus *Postia placenta* supports unique mechanisms of lignocellulose conversion. *Proc. Natl. Acad. Sci. USA* 106:1954-1959.

Martínez, M.J. and A.T.Martínez. 1996. Characterization of MnP isoenzymes of *Pleurotus eryngii* exhibiting Mn-independent activities on 2,6-dimethoxyphenol and veratryl alcohol. *In* Biotechnology in the pulp and paper industry: Recent advances in applied and fundamental research. K.Messner and E.Srebotnik, editors. Facultas-Universitätsverlag, Vienna. 417-420.

McEldoon, J.P., A.R.Pokora, and J.S.Dordick. 1995. Lignin peroxidase-type activity of soybean peroxidase. *Enzyme Microb. Technol.* 17:359-365.

Mester, T., K.Ambert-Balay, S.Ciofi-Baffoni, L.Banci, A.D.Jones, and M.Tien. 2001. Oxidation of a tetrameric nonphenolic lignin model compound by lignin peroxidase. *J. Biol. Chem.* 276:22985-22990.

Miki, Y., F.R.Calviño, R.Pogni, S.Giansanti, F.J.Ruiz-Dueñas, M.J.Martínez, R.Basosi, A.Romero, and A.T.Martínez. 2011. Crystallographic, kinetic, and

spectroscopic study of the first ligninolytic peroxidase presenting a catalytic tyrosine. *J. Biol. Chem.* 286:15525-15534.

Morales, M., M.J.Mate, A.Romero, M.J.Martínez, A.T.Martínez, and F.J.Ruiz-Dueñas. 2012. Two oxidation sites for low redox-potential substrates: A directed mutagenesis, kinetic and crystallographic study on *Pleurotus eryngii* versatile peroxidase. *J. Biol. Chem.* 287:41053-41067.

Moreira, M.T., G.Feijoo, J.Canaval, and J.M.Lema. 2003. Semipilot-scale bleaching of Kraft pulp with manganese peroxide. *Wood Sci. Technol.* 37:117-123.

Nakajima, R. and I.Yamazaki. 1980. The conversion of horseradish peroxidase C to a verdohemoprotein by a hydroperoxide derived enzymatically from indole-3-acetic acid and by m-nitroperoxybenzoic acid. *J. Biol. Chem.* 255:2067-2071.

Ogola, H.J.O., N.Hashimoto, S.Miyabe, H.Ashida, T.Ishikawa, H.Shibata, and Y.Sawa. 2010. Enhancement of hydrogen peroxide stability of a novel *Anabaena* sp DyP-type peroxidase by site-directed mutagenesis of methionine residues. *Appl. Microbiol. Biotechnol.* 87:1727-1736.

Ollikka, P., K.Alhonmaki, V.M.Leppanen, T.Glumoff, T.Raijola, and I.Suominen. 1993. Decolorization of azo, triphenyl methane, heterocyclic, and polymeric dyes by lignin peroxidase isoenzymes from *Phanerochaete chrysosporium*. *Appl. Environ. Microbiol.* 59:4010-4016.

Otjen, L. and R.A.Blanchette. 1986. A discussion of microstructural changes in wood during decomposition by white rot basidiomycetes. *Can. J. Bot.* 64:905-911.

Pérez-Boada, M., F.J.Ruiz-Dueñas, R.Pogni, R.Basosi, T.Choinowski, M.J.Martínez, K.Piontek, and A.T.Martínez. 2005. Versatile peroxidase oxidation of high redox potential aromatic compounds: Site-directed mutagenesis, spectroscopic and crystallographic investigations of three long-range electron transfer pathways. *J. Mol. Biol.* 354:385-402.

Piontek, K., T.Glumoff, and K.Winterhalter. 1993. Low pH crystal structure of glycosylated lignin peroxidase from *Phanerochaete chrysosporium* at 2.5 Å resolution. *FEBS Lett.* 315:119-124.

Piontek, K., R.Ullrich, C.Liers, K.Diederichs, D.A.Plattner, and M.Hofrichter. 2010. Crystallization of a 45 kDa peroxygenase/peroxidase from the mushroom *Agrocybe aegerita* and structure determination by SAD utilizing only the haem iron. *Acta Crystallogr. F* 66:693-698.

Pogni, R., M.C.Baratto, S.Giansanti, C.Teutloff, J.Verdín, B.Valderrama, F.Lendzian, W.Lubitz, R.Vázquez-Duhalt, and R.Basosi. 2005. Tryptophan-based radical in the catalytic mechanism of versatile peroxidase from *Bjerkandera adusta*. *Biochemistry* 44:4267-4274.

Pogni, R., M.C.Baratto, C.Teutloff, S.Giansanti, F.J.Ruiz-Dueñas, T.Choinowski, K.Piontek, A.T.Martínez, F.Lendzian, and R.Basosi. 2006. A tryptophan neutral radical in the oxidized state of versatile peroxidase from *Pleurotus eryngii*: a combined multi-frequency EPR and DFT study. *J. Biol. Chem.* 281:9517-9526.

Polaina, J. and A.P.MacCabe. 2007. Industrial enzymes: Structure, function and applications. Springer, Dordrecht.

Poulos, T.L., S.L.Edwards, H.Wariishi, and M.H.Gold. 1993. Crystallographic refinement of lignin peroxidase at 2 Å. *J. Biol. Chem.* 268:4429-4440.

Ragauskas, A.J., G.T.Beckham, M.J.Biddy, R.Chandra, F.Chen, M.F.Davis, B.H.Davison, R.A.Dixon, P.Gilna, M.Keller, P.Langan, A.K.Naskar, J.N.Saddler, T.Tschaplinski, G.A.Tuskan, and C.E.Wyman. 2014. Lignin valorization: improving lignin processing in the biorefinery. *Science* 344:1246843.

Ragauskas, A.J., C.K.Williams, B.H.Davison, G.Britovsek, J.Cairney, C.A.Eckert, W.J.Frederick, J.P.Hallett, D.J.Leak, C.L.Liotta, J.R.Mielenz, R.Murphy, R.Templer, and T.Tschaplinski. 2006. The path forward for biofuels and biomaterials. *Science* 311:484-489.

Rahmanpour, R. and T.D.H.Bugg. 2015. Characterisation of Dyp-type peroxidases from *Pseudomonas fluorescens* Pf-5: Oxidation of Mn(II) and polymeric lignin by Dyp1B. *Arch. Biochem. Biophys.* http://dx.doi.org/10.1016/j.abb.2014.12.022.

Robinson, T., G.McMullan, R.Marchant, and P.Nigam. 2001. Remediation of dyes in textile effluent: a critical review on current treatment technologies with a proposed alternative. *Bioresource Technol.* 77:247-255.

Rodríguez, E., O.Nuero, F.Guillén, A.T.Martínez, and M.J.Martínez. 2004. Degradation of phenolic and non-phenolic aromatic pollutants by four *Pleurotus* species: the role of laccase and versatile peroxidase. *Soil Biol. Biochem.* 36:909-916.

Ruiz-Dueñas, F.J., T.Lundell, D.Floudas, L.G.Nagy, J.M.Barrasa, D.S.Hibbett, and A.T.Martínez. 2013. Lignin-degrading peroxidases in Polyporales: An evolutionary survey based on ten sequenced genomes. *Mycologia* 105:1428-1444.

Ruiz-Dueñas, F.J. and A.T.Martínez. 2009. Microbial degradation of lignin: How a bulky recalcitrant polymer is efficiently recycled in nature and how we can take advantage of this. *Microbial Biotechnol.* 2:164-177.

Ruiz-Dueñas, F.J. and A.T.Martínez. 2010. Structural and functional features of peroxidases with a potential as industrial biocatalysts. *In* Biocatalysts based on heme peroxidases. E.Torres and M.Ayala, editors. Springer-Verlag, Berlin. 37-59.

Ruiz-Dueñas, F.J., M.J.Martínez, and A.T.Martínez. 1999. Molecular characterization of a novel peroxidase isolated from the ligninolytic fungus *Pleurotus eryngii*. *Mol. Microbiol.* 31:223-236.

Ruiz-Dueñas, F.J., M.Morales, E.García, Y.Miki, M.J.Martínez, and A.T.Martínez. 2009a. Substrate oxidation sites in versatile peroxidase and other basidiomycete peroxidases. *J. Exp. Bot.* 60:441-452.

Ruiz-Dueñas, F.J., M.Morales, M.J.Mate, A.Romero, M.J.Martínez, A.T.Smith, and A.T.Martínez. 2008. Site-directed mutagenesis of the catalytic tryptophan environment in *Pleurotus eryngii* versatile peroxidase. *Biochemistry* 47:1685-1695.

Ruiz-Dueñas, F.J., M.Morales, M.Pérez-Boada, T.Choinowski, M.J.Martínez, K.Piontek, and A.T.Martínez. 2007. Manganese oxidation site in *Pleurotus eryngii* versatile peroxidase: A site-directed mutagenesis, kinetic and crystallographic study. *Biochemistry* 46:66-77.

Ruiz-Dueñas, F.J., R.Pogni, M.Morales, S.Giansanti, M.J.Mate, A.Romero, M.J.Martínez, R.Basosi, and A.T.Martínez. 2009b. Protein radicals in fungal versatile peroxidase: Catalytic tryptophan radical in both Compound I and Compound II and studies on W164Y, W164H and W164S variants. *J. Biol. Chem.* 284:7986-7994.

Sakharov, I.Y. and T.V.Sakharova. 2002. Extremely high stability of African oil palm tree peroxidase. *BBA Proteins Proteomics* 1598:108-114.

Salvachúa, D., A.Prieto, M.Lopez-Abelairas, T.Lú-Chau, A.T.Martínez, and M.J.Martínez. 2011. Fungal pretreatment: An alternative in second-generation ethanol from wheat straw. *Bioresource Technol.* 102:7500-7506.

Salvachúa, D., A.Prieto, M.L.Mattinen, T.Tamminen, T.Liitiä, M.Lille, S.Willfor, A.T.Martínez, M.J.Martínez, and C.B.Faulds. 2013. Versatile peroxidase as a valuable tool for generating new biomolecules by homogeneous and heterogeneous cross-linking. *Enzyme Microb. Technol.* 52:303-311.

Santos, A., S.Mendes, V.Brissos, and L.O.Martins. 2014. New dye-decolorizing peroxidases from *Bacillus subtilis* and *Pseudomonas putida* MET94: towards biotechnological applications. *Appl. Microbiol. Biotechnol.* 98:2053-2065.

Schmid, A., J.S.Dordick, B.Hauer, A.Kiener, M.Wubbolts, and B.Witholt. 2001. Industrial biocatalysis today and tomorrow. *Nature* 409:258-268.

Schoemaker, H.E., T.K.Lundell, A.I.Hatakka, and K.Piontek. 1994. The oxidation of veratryl alcohol, dimeric lignin models and lignin by lignin peroxidase - The redox cycle revisited. *FEMS Microbiol. Rev.* 13:321-332.

Schulz, C.E., P.W.Devaney, H.Winkler, P.G.Debrunner, N.Doan, R.Chiang, R.Rutter, and L.P.Hager. 1979. Horseradish peroxidase compound I: evidence for spin coupling between the heme iron and a 'free' radical. *FEBS Lett.* 103:102-105.

Schwarze, F.W.M.R., J.Engels, and C.Mattheck. 2000. Fungal strategies of decay in trees. Springer, Berlin.

Sigoillot, C., S.Camarero, T.Vidal, E.Record, M.Asther, M.Pérez-Boada, M.J.Martínez, J.-C.Sigoillot, M.Asther, J.Colom, and A.T.Martínez. 2005. Comparison of different fungal enzymes for bleaching high-quality paper pulps. *J. Biotechnol.* 115:333-343.

Singh, R., J.C.Grigg, W.Qin, J.F.Kadla, M.E.P.Murphy, and L.D.Eltis. 2013. Improved manganese-oxidizing activity of DypB, a peroxidase from a lignolytic bacterium. *ACS Chemical Biology* 8:700-706.

Smith, A.T., W.A.Doyle, P.Dorlet, and A.Ivancich. 2009. Spectroscopic evidence for an engineered, catalytically active Trp radical that creates the unique reactivity of lignin peroxidase. *Proc. Natl. Acad. Sci. USA* 106:16084-16089.

Smith, A.T. and N.C.Veitch. 1998. Substrate binding and catalysis in heme peroxidases. *Curr. Opin. Chem. Biol.* 2:269-278.

Stadtman, E.R., J.Moskovitz, and R.L.Levine. 2003. Oxidation of methionine residues of proteins: Biological consequences. *Antioxidants & Redox Signaling* 5:577-582.

Sugano, Y., R.Muramatsu, A.Ichiyanagi, T.Sato, and M.Shoda. 2007. DyP, a unique dye-decolorizing peroxidase, represents a novel heme peroxidase family. Asp171 replaces the distal histidine of classical peroxidases. *J. Biol. Chem.* 282:36652-36658.

Sundaramoorthy, M., K.Kishi, M.H.Gold, and T.L.Poulos. 1994. The crystal structure of manganese peroxidase from *Phanerochaete chrysosporium* at 2.06-Å resolution. *J. Biol. Chem.* 269:32759-32767.

Sundaramoorthy, M., H.L.Youngs, M.H.Gold, and T.L.Poulos. 2005. High-resolution crystal structure of manganese peroxidase: substrate and inhibitor complexes. *Biochemistry* 44:6463-6470.

Tien, M. and T.K.Kirk. 1983. Lignin-degrading enzyme from the hymenomycete *Phanerochaete chrysosporium* Burds. *Science* 221:661-663.

Ullrich, R. and M.Hofrichter. 2007. Enzymatic hydroxylation of aromatic compounds. *Cell. Mol. Life Sci.* 64:271-293.

Ullrich, R., J.Nuske, K.Scheibner, J.Spantzel, and M.Hofrichter. 2004. Novel haloperoxidase from the agaric basidiomycete *Agrocybe aegerita* oxidizes aryl alcohols and aldehydes. *Appl. Environ. Microbiol.* 70:4575-4581.

Valderrama, B., M.Ayala, and R.Vázquez-Duhalt. 2002. Suicide inactivation of peroxidases and the challenge of engineering more robust enzymes. *Chem. Biol.* 9:555-565.

Valderrama, B., H.García-Arellano, S.Giansanti, M.C.Baratto, R.Pogni, and R.Vázquez-Duhalt. 2006. Oxidative stabilization of iso-1-cytochrome c by redox-inspired protein engineering. *FASEB J.* 20:1233-1235.

Verdín, J., R.Pogni, A.Baeza, M.C.Baratto, R.Basosi, and R.Vázquez-Duhalt. 2006. Mechanism of versatile peroxidase inactivation by Ca2+ depletion. *Biophys. Chem.* 121:163-170.

Villegas, J.A., A.G.Mauk, and R.Vázquez-Duhalt. 2000. A cytochrome c variant resistant to heme degradation by hydrogen peroxide. *Chem. Biol.* 7:237-244.

Vitello, L.B., J.E.Erman, M.A.Miller, J.Wang, and J.Kraut. 1993. Effect of Arginine-48 replacement on the reaction between cytochrome *c* peroxidase and hydrogen peroxide. *Biochemistry* 32:9807-9818.

Vogt, W. 1995. Oxidation of Methionyl Residues in Proteins - Tools, Targets, and Reversal. *Free Radic. Biol. Med.* 18:93-105.

Wariishi, H. and M.H.Gold. 1990. Lignin peroxidase compound III. Mechanism of formation and decomposition. *J. Biol. Chem.* 265:2070-2077.

Whitwam, R.E., K.R.Brown, M.Musick, M.J.Natan, and M.Tien. 1997. Mutagenesis of the Mn^{2+}-binding site of manganese peroxidase affects oxidation of Mn^{2+} by both compound I and compound II. *Biochemistry* 36:9766-9773.

Wong, D.W.S. 2009. Structure and Action Mechanism of Ligninolytic Enzymes. *Appl. Biochem. Biotechnol.* 157:174-209.

Yang, H., J.Li, H.Shin, G.Du, L.Liu, and J.Chen. 2014. Molecular engineering of industrial enzymes: recent advances and future prospects. *Appl. Microbiol. Biotechnol.* 98:23.

Young, R.A. and M.Akhtar. 1998. Environmentally-friendly technologies for the pulp and paper industry. John Wiley and Sons, New York.

Youngs, H.L., P.Moënne-Loccoz, T.M.Loehr, and M.H.Gold. 2000. Formation of a bis(histidyl) heme iron complex in manganese peroxidase at high pH and restoration of the native enzyme structure by calcium. *Biochemistry* 39:9994-10000.

Zabel, R. and J.Morrell. 1992. Wood microbiology: Decay and its prevention. Academic Press, London.

Zámocký, M., B.Gasselhuber, P.G.Furtmüller, and C.Obinger. 2014. Turning points in the evolution of peroxidase-catalase superfamily: molecular phylogeny of hybrid heme peroxidases. *Cell. Mol. Life Sci.* 71:4681-4696.

Zorn, H., S.Langhoff, M.Scheibner, M.Nimtz, and R.G.Berger. 2003. A peroxidase from *Lepista irina* cleaves b,b-carotene to flavor compounds. *Biol. Chem.* 384:1049-1056.

Zubieta, C., R.Joseph, S.S.Krishna, D.McMullan, M.Kapoor, H.L.Axelrod, M.D.Miller, P.Abdubek, C.Acosta, T.Astakhova, D.Carlton, H.J.Chiu, T.Clayton, M.C.Deller, L.Duan, Y.Elias, M.A.Elsliger, J.Feuerhelm, S.K.Grzechnik, J.Hale, G.W.Han, L.Jaroszewski, K.K.Jin, H.E.Klock, M.W.Knuth, P.Kozbial, A.Kumar, D.Marciano, A.T.Morse, K.D.Murphy, E.Nigoghossian, L.Okach, S.Oommachen, R.Reyes, C.L.Rife, P.Schimmel, C.V.Trout, H.van den Bedem, D.Weekes, A.White, Q.P.Xu, K.O.Hodgson, J.Wooley, A.M.Deacon, A.Godzik, S.A.Lesley, and I.A.Wilson. 2007. Identification and structural characterization of heme binding in a novel dye-decolorizing peroxidase, TyrA. *Proteins* 69:234-243.

OBJETIVOS

Las peroxidasas ligninolíticas son uno de los grupos de enzimas con mayor potencial biotecnológico debido a sus propiedades catalíticas que les permiten oxidar una variedad de sustratos recalcitrantes. Sin embargo, su aplicación industrial se ve frenada ya que no presentan una adecuada compatibilidad con las agresivas condiciones que caracterizan los procesos industriales. Por ello, previo a su aplicación, las características de estas enzimas han de ser optimizadas.

Entre las distintas POD ligninolíticas, la VP presenta un especial interés debido a que combina las propiedades catalíticas de LiP, MnP y GP y, además, no necesita de la presencia de mediadores para su actuación. Por ello, la VP, en concreto la variante alélica VPL2 de la isoenzima VPL de *Pleurotus eryngii*, fue la peroxidasa escogida para realizar los trabajos llevados a cabo en la presente tesis doctoral.

El objetivo general de la tesis fue el diseño de una VP que presente unas características más adecuadas para su uso biotecnológico. Para ello se abordaron las siguientes tareas:

i) La optimización de la estabilidad oxidativa de la VP, basada en un mejor conocimiento de las bases estructurales que determinan esta propiedad. Este trabajo queda reflejado en el primer capítulo de la tesis.
ii) La optimización de la estabilidad a pH de la VP, el estudio de los factores que afectan este parámetro, así como la posibilidad de trasladar motivos estructurales relacionados de unas enzimas a otras. Estos estudios quedan reflejados en los capítulos segundo y tercero de esta tesis.
iii) Profundizar en el funcionamiento del triptófano catalítico, el sitio de oxidación de compuestos de alto potencial redox en la enzima, y su implicación directa en el proceso de degradación de la lignina. Este trabajo aparece reflejado en el cuarto capítulo.

Para realizar estas tareas, se utilizó un enfoque racional basado en la información existente sobre las relaciones estructura-función de la VP. Para ello, se diseñaron diferentes variantes de la enzima mediante mutagénesis dirigida que posteriormente fueron evaluadas y caracterizadas.

CHAPTER 1

Improving the Oxidative Stability of a High Redox Potential Fungal Peroxidase by Rational Design

Abstract

Ligninolytic peroxidases are enzymes of biotechnological interest due to their ability to oxidize high redox potential aromatic compounds, including the recalcitrant lignin polymer. However, different obstacles prevent their use in industrial and environmental applications, including low stability towards their natural oxidizing-substrate H_2O_2. In this work, versatile peroxidase was taken as a model ligninolytic peroxidase, its oxidative inactivation by H_2O_2 was studied and different strategies were evaluated with the aim of improving H_2O_2 stability. Oxidation of the methionine residues was produced during enzyme inactivation by H_2O_2 excess. Substitution of these residues, located near the heme cofactor and the catalytic tryptophan, rendered a variant with a 7.8-fold decreased oxidative inactivation rate. A second strategy consisted in mutating two residues (Thr45 and Ile103) near the catalytic distal histidine with the aim of modifying the reactivity of the enzyme with H_2O_2. The T45A/I103T variant showed a 2.9-fold slower reaction rate with H_2O_2 and 2.8-fold enhanced oxidative stability. Finally, both strategies were combined in the T45A/I103T/M152F/M262F/M265L variant, whose stability in the presence of H_2O_2 was improved 11.7-fold. This variant showed an increased half-life, over 30 min compared with 3.4 min of the native enzyme, under an excess of 2000 equivalents of H_2O_2. Interestingly, the stability improvement achieved was related with slower formation, subsequent stabilization and slower bleaching of the enzyme Compound III, a peroxidase intermediate that is not part of the catalytic cycle and leads to the inactivation of the enzyme.

1. Introduction

Lignin removal is a key step for carbon recycling in terrestrial ecosystems, as well as a central issue for industrial utilization of plant biomass (Martínez et al., 2009). In nature, white-rot fungi are the main organisms responsible for lignin biodegradation in a process that has been described as an enzymatic combustion (Kirk and Farrell, 1987). These fungi have developed extracellular ligninolytic machinery made up of oxidoreductases including peroxidases, laccases and oxidases, among others (Martínez et al., 2005). Manganese peroxidases (MnP, E.C:

1.11.1.13), lignin peroxidases (LiP, E.C. 1.11.1.14), and versatile peroxidases (VP, E.C.1.11.1.16) forming part of this machinery are unique to white-rot basidiomycetes (Floudas et al., 2012) although they can be absent from some atypical or transitional species (Riley et al., 2014).

VP shares catalytic properties with MnP and LiP, and also with non-ligninolytic generic peroxidases (GP, E.C. 1.11.1.7), due to combination of the catalytic sites characterizing these enzymes (Ruiz-Dueñas et al., 2009). This results in a high redox potential peroxidase with a wide substrate specificity, able to oxidize Mn^{2+} (Ruiz-Dueñas et al., 2007) and high and low redox potential compounds (Heinfling et al., 1998; Pérez-Boada et al., 2005; Morales et al., 2012). Its catalytic promiscuity makes VP a biocatalyst of industrial and environmental interest. The use of this enzyme has been considered as an interesting possibility in lignin transformation and delignification processes (Moreira et al., 2007; Marques et al., 2010; Ruiz-Dueñas and Martínez, 2009). Its ability to transform polycyclic aromatic hydrocarbons, phenolic and non-phenolic aromatic pollutants, pesticides and industrial dyes has been confirmed (Ruiz-Dueñas and Martínez, 2010; Ayala et al., 2008). Moreover, it has been also proposed as a valuable tool for generating new biomolecules (Salvachúa et al., 2013).

However, the potential of this and the other high redox potential peroxidases cannot be exploited due to different obstacles that prevent their utilization at industrial level (Martínez et al., 2009). Of these, perhaps the most surprising is the inactivation by peroxide excess, since this compound is the substrate strictly necessary for enzyme activation. This process has been described as a suicide inactivation related to the formation of Compound III (CIII), a peroxidase intermediate that is not part of the catalytic cycle but can lead to enzyme inactivation (Wariishi and Gold, 1990; Hiner et al., 2002a; Valderrama et al., 2002). The VP catalytic cycle (**Fig. 1**, black arrows) (Morales et al., 2012) is initiated by the reaction of the enzyme resting state (RS, containing Fe^{3+} heme) with one molecule of H_2O_2 in a two-electron reaction yielding Compound I (CI). This transient state contains two oxidation equivalents, one as a ferryl-oxo iron (Fe^{4+}=O) and the other delocalized as a porphyrin radical or as a tryptophanyl radical (on Trp164). CI catalyzes the one-electron

substrate oxidation in direct contact with heme or through the tryptophanyl radical forming Compound II (CII). This intermediate retains the Fe^{4+}=O state (after porphyrin or tryptophanyl radical reduction) or transfers the remaining oxidation equivalent to the tryptophan residue as in CI. Finally, CII can also produce one-electron oxidization of substrates directly in contact with the heme or through the tryptophanyl radical restoring the enzyme resting state. Both CI and CII are very reactive intermediates that, in the absence of a normal reducing substrate and in the presence of high peroxide concentration, are finally converted to CIII, a superoxide anion ($O_2^{\cdot-}$) containing Fe^{3+} species (**Fig. 1,** red arrows) (Wariishi and Gold, 1990). Once formed, CIII can follow different decomposition pathways under excess of H_2O_2 generating reactive oxygen species able to oxidize the porphyrin moiety or amino acid side chains (such as those of methionines) leading to enzyme inactivation (Valderrama et al., 2002).

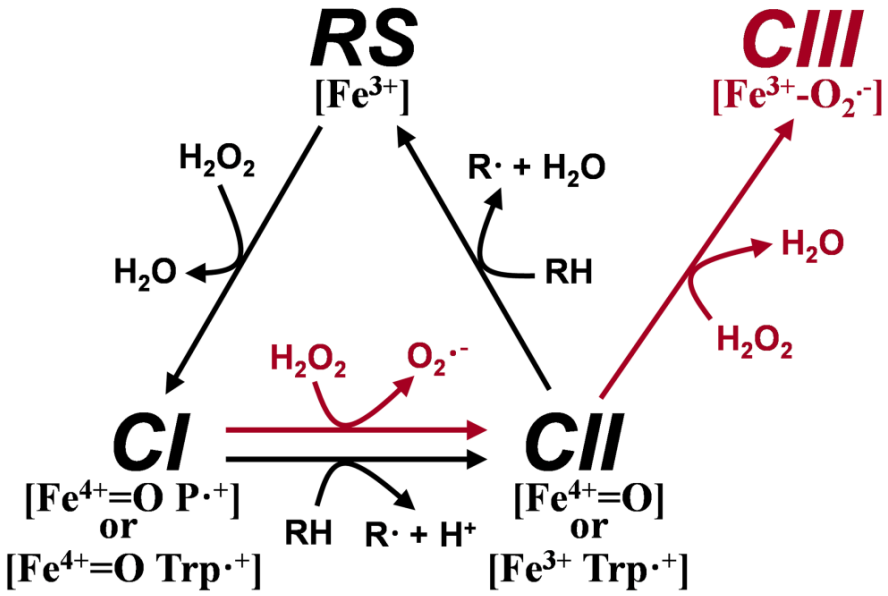

Figure 1. Versatile peroxidase catalytic cycle (black arrows) and CIII formation by hydrogen peroxide (red arrows). RS, resting state peroxidase containing Fe^{3+} heme; CI, compound I retaining two oxidizing equivalents in the form of a Fe^{4+}=O and porphyrin cation radical, P·+, or Fe^{4+}=O and tryptophanyl cation radical, Trp·+ (on Trp164); CII, compound II bearing only one oxidation equivalent on the Fe^{4+}=O or Trp·+; CIII, compound III containing Fe^{3+} and superoxide anion radical, $O_2^{\cdot-}$; and RH, reducing substrates of CI and CII.

Taking into account this information, we addressed the oxidative stability improvement in VP using different strategies consisting in: i) substituting methionines for less-oxidizable residues to prevent or minimize inactivation by formation of methionine derivatives; ii) modifying the environment of the histidine residue involved in the two-electron activation of the resting enzyme to affect the stability/reactivity of CI and CII, as CIII precursors; and iii) combining the above two strategies. In the light of the results obtained, a rational explanation is proposed for the observed oxidative stability improvements.

2. Materials and methods

2.1 Chemicals

Isopropyl-β-D-thiogalactopyranoside (IPTG), dithiothreitol, hemin, oxidized glutathione, veratryl alcohol (VA), manganese(II) sulphate and sodium tartrate were from Sigma-Aldrich; urea and H_2O_2 from Merck; and 2,2'-azino-bis (3-ethylbenzothiazoline-6-sulfonate) (ABTS) from Roche.

2.2 Amino acid analysis

The amino acid composition of the native VP incubated in the absence and in the presence of a 5000-fold stoichiometric excess of H_2O_2, at 25°C for 40 min, was determined with a Biochrom 30 amino acid analyzer. Previous to the amino acid analysis, the samples (24 μg of protein) were subjected to an acid hydrolysis (6 N HCl) for 24 h under vacuum. The H_2O_2 concentration in this and other experiments was determined using ε_{240}= 39.4 M^{-1} cm^{-1} (Nelson and Kiesow, 1972).

2.3 Design of mutated variants at the heme distal side

Residues in the contact interface between helixes D and B, the latter containing catalytic Arg43 and His47 were identified. Thr45 and Ile103 located immediately on the catalytic amino acid residues in helixes B and D, respectively, were selected for site-directed mutagenesis. Mutations at these two residues sought to reduce the distance between the two helices. Alternative amino acid residues at these positions were checked *in silico* by using the Swiss-Pdb Viewer mutation tool. Acidic, basic and easily oxidizable amino acids as well as glycine and residues

with side chains larger than those of threonine and isoleucine were excluded from the analysis. Amino acid residues with their rotamers exhibiting the lowest score were selected for subsequent site directed mutagenesis.

2.4 Site-directed mutagenesis

All VP variants were produced using the QuikChange Site-Directed Mutagenesis kit from Stratagene. Each mutation was introduced by PCR using the expression vector pFLAG1 (International Biotechnologies Inc.) harbouring the mature protein-coding sequence of *Pleurotus eryngii* VP (allelic variant VPL2; GenBank AF007222) (named pFLAG1-VPL2) (Pérez-Boada et al., 2002) as template. For each mutation, both a direct and a reverse primer were designed complementary to opposite strands of the same DNA region containing the desired mutation. Only the direct sequences with indication of the changed triplets (underlined) and the mutations introduced (bold) are listed below: (i) M152V, 5'-CC ATT CTT GCC AGA **G**TG GGT GAC GCA GGC-3'; (ii) M247F, 5'-GCC TGC GAA TGG CAG TCC **TTC** GTT AAC AAC CAA CCG-3'; (iii) M262F, 5'-C CGT TTC GCT GCT ACC **TTC** TCG AAG ATG GCT CTT CTT GGC C-3'; (iv) M265L, 5'-GCT ACC ATG TCG AAG **T**TG GCT CTT CTT GGC C-3'); (v) M262F/M265L, 5'-CGT TTC GCT GCT ACC **TTC** TCG AAG **T**TG GCT CTT CTT GGC C-3'; (vi) M152F/M262F/M265L was obtained using pFLAG1-VPL2-M262F/M265L as template and primers for the M152F mutation, 5'-CC ATT CTT GCC AGA **TTC** GGT GAC GCA GGC-3'; (vii) M152F/M247F/M262F/M265L was obtained using pFLAG1-VPL2-M152F/M262F/M265L as template and the M247F primers; (viii) T45A/I103T was obtained using pFLAG1-VPL2 as template and the T45A, 5'-C GAG TCC CTT CGT TTG **G**CT TTC CAC GAT GCA ATC GG-3', and I103T, 5'-CC GCC GGC GAC TTC A**C**T CAA TTT GCT GGC GCC G-3', primers in two consecutive PCR reactions; and (ix) T45A/I103T/M152F/M262F/M265L was obtained using pFLAG1-VPL2-M152F/M262F/M265L as template and the T45A and I103T primers in two successive PCR amplifications.

PCR reactions were carried out in an Eppendorf Mastercycler Pro S using 10 ng of template DNA, 250 μM each dNTP, 125 ng of direct and reverse primers, 2.5 units of *Pfu* Turbo DNA polymerase AD (Stratagene) and the manufacture´s reaction buffer. Reaction conditions were as follows: (i) a "hot start" of 95 °C for 1 min; (ii) 18 cycles at 95 °C

for 50 s, 55 °C for 50 s, and 68 °C for 10 min; and (iii) a final cycle at 68°C for 10 min. The mutated sequences were confirmed by DNA sequencing using an ABI 3730 DNA Analyzer (Applied Biosystem). pFLAG1-VPL2 plasmids containing mutations described above were transformed into *Escherichia coli* DH5α for propagation.

2.5 Enzyme production, activation and purification

Native recombinant VP and its site-directed variants were expressed in *E. coli* W3110. Cells were grown in Terrific Broth (Sambrook and Russell, 2001) until OD_{500}~1 (~3h). Then protein expression was induced with 1 mM IPTG and cells were grown for a further 4 h. The apoenzyme accumulated in inclusion bodies and was recovered by solubilisation in 50 mM Tris-HCl (pH 8.0) containing 8 M urea, 1 mM EDTA, and 1 mM dithiothreitol for 30 min at room temperature. The subsequent *in vitro* folding of the solubilised apoprotein and purification of the active enzyme were performed as described by Pérez-Boada et al. (2002). Enzyme concentration was determined from the absorbance of the Soret band (ε_{407}= 150 mM^{-1} cm^{-1}) (Ruiz-Dueñas et al., 1999b).

2.6 Steady-state kinetics

Oxidation of VA (veratraldehyde ε_{310}= 9300 M^{-1} cm^{-1}) was estimated at pH 3.0; that of ABTS (cation radical ε_{436}= 29300 M^{-1} cm^{-1}) at pH 3.5 and that of Mn^{2+} (Mn^{3+}-tartrate complex ε_{238}= 6500 M^{-1} cm^{-1}) at pH 5.0. All enzymatic activities were measured as initial velocities from linear increments of absorbance due to the appearance of the reaction product. Reactions were performed in 0.1 M sodium tartrate and 0.1 mM H_2O_2, at 25 °C, and followed using a Shimadzu UV-1800 spectrophotometer. Means and standard errors for apparent affinity constant (Michaelis constant, K_m) and enzyme turnover (catalytic constant, k_{cat}) were obtained by non-linear least-squares fitting of the experimental measurements to the Michaelis-Menten model. Fitting of these constants to the normalized equation $\upsilon = (k_{cat}/K_m)[S]/(1+[S]/K_m)$ yielded the catalytic efficiency values (k_{cat}/K_m) with their standard errors.

2.7 Transient-state kinetics

VP CI formation was measured at 25 °C using a stopped-flow equipment (Bio-Logic) including a three-syringe module (SFM300) synchronized

with a diode array detector (J&M), and Bio-Kine software. The resting enzyme (1 μM final concentration) was mixed with increasing concentrations of H_2O_2 in 0.1 M sodium tartrate (pH 3.0) and the reaction was followed at 397 nm (isosbestic point of VP CI and CII). All kinetic traces exhibited single-exponential character from which pseudo first-order rate constants were calculated.

2.8 Oxidative stability studies

The oxidative stability was determined by enzyme incubation in a wide range of H_2O_2:VP molar ratios in 10 mM sodium tartrate, pH 5.0. The time course of oxidative inactivation was followed by measuring the residual activity of the enzyme (0.01 μM) as the oxidation of 6 mM Mn^{2+} (saturating conditions) as described above. The enzyme incubated under the same experimental conditions in absence of H_2O_2 was used as a reference. The experimental data of residual activity *vs* time at each H_2O_2:VP ratio were fitted to an exponential decay model and a pseudo first-order inactivation rate constant (k_{obs}, s^{-1}) was obtained. The k_{obs} values for each VP variant at all the H_2O_2:VP ratios tested were fitted to a linear or a sigmoidal (Hill equation) model. From this fitting an apparent second-order inactivation rate constant (k_{app}, $s^{-1}\cdot M^{-1}$) (for linear fits), and a first-order inactivation rate constant (k_i) and the H_2O_2:VP molar ratio resulting in the half maximal inactivation rate (K_I) (for sigmoid fits) were calculated. Fitting of k_i and K_I to the normalized equation $k_{obs}= (k_i/K_I)\ K_I\ R^n/(K_I^n+R^n)$ (where n is the Hill coefficient and R is the H_2O_2:VP molar ratio) yielded the k_{app} values (k_i/K_I) with their corresponding standard errors.

2.9 Spectral analysis of transient states in H_2O_2 reactions

Spectral analyses of native VP and mutated variants (10 μM) were carried out in a millisecond to second time scale after activating the enzyme with a 5000-fold stoichiometric excess of H_2O_2 in 0.1 M sodium tartrate (pH 5.0), at 25 °C. The spectra were obtained using the stopped-flow equipment described above. The rate of CIII formation was determined at a wavelength (581 nm) at which the change in absorbance was specific for this reaction. Subsequent bleaching of 5 μM CIII, generated as previously described, was followed at its Soret maximum (419 nm) in a minute time scale using an Agilent 8454 diode array spectrophotometer. Conversion of the native VP and the T45A/

I103T/M152F/M262F/M265L variant CIII to RS was measured after removing the excess of H_2O_2 by incubation with catalase (75 mg/ml) for 1 min at 25 °C. Afterwards, 50 equivalents of Mn^{2+} were added to the reaction and the conversion to RS followed at 407 nm (Soret band). CIII formation, enzyme bleaching and CIII conversion to RS exhibited a single-exponential behaviour from which pseudo first-order rate constants (k_{obs}, s^{-1}) were calculated.

3. Results

3.1 Strategies to improve the VP oxidative stability and kinetic analysis of the designed variants

The oxidative stability of VP was investigated by enzyme incubation with increasing stoichiometric excesses of H_2O_2 (**Fig. 2**). The enzyme residual activity was measured over time, observing progressive inactivation at all the H_2O_2:VP molar ratios assayed (from 500:1 to 40000:1), although some activity remained even when the enzyme was incubated for long periods of time. The loss of activity was complete at all the H_2O_2: VP ratios when the temperature of incubation was increased at 25 °C (**Fig. 2**, rhombs).

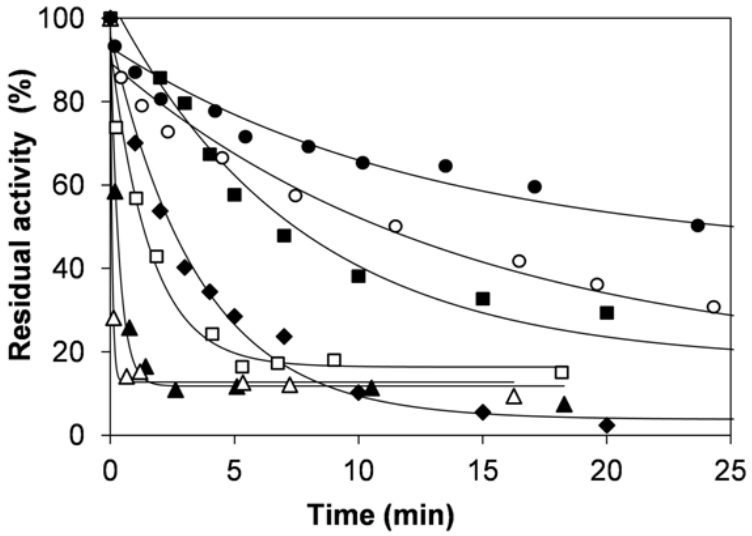

Figure 2. Oxidative stability of native VP. Time course of the residual activity of native VP incubated at 4°C with different stoichiometric excesses of H_2O_2: 1000 (●), 2000 (○), 3000 (■), 5000 (□), 10000 (▲), 40000 (Δ) equivalents, and 3000 equivalents at 25°C (♦), estimated from Mn^{2+} oxidation in 0.1 M sodium tartrate, pH 5.0.

The amino acid composition analysis of the inactivated enzyme at a 5000:1 H_2O_2:VP ratio, after 40 min incubation at 25 °C, revealed that methionine residues were oxidized to methionine sulfone (**Fig. 3**). VP contains four methionines at positions 152, 247, 262 and 265. They are buried within the enzyme molecular structure close to both the heme cofactor (at a distance between 4.2 and 12.4 Å) and the catalytic Trp164 (at a distance between 3.7 and 9.3 Å) (**Fig. 4A**). Considering that their oxidation is likely to be related to enzyme inactivation, they were replaced with less oxidizable amino acids by site-directed mutagenesis in single (M152V, M247F, M262F and M265L), double (M262F/M265L) and multiple (M152F/M262F/M265L and M152F/M247F/M262F/M265L) variants.

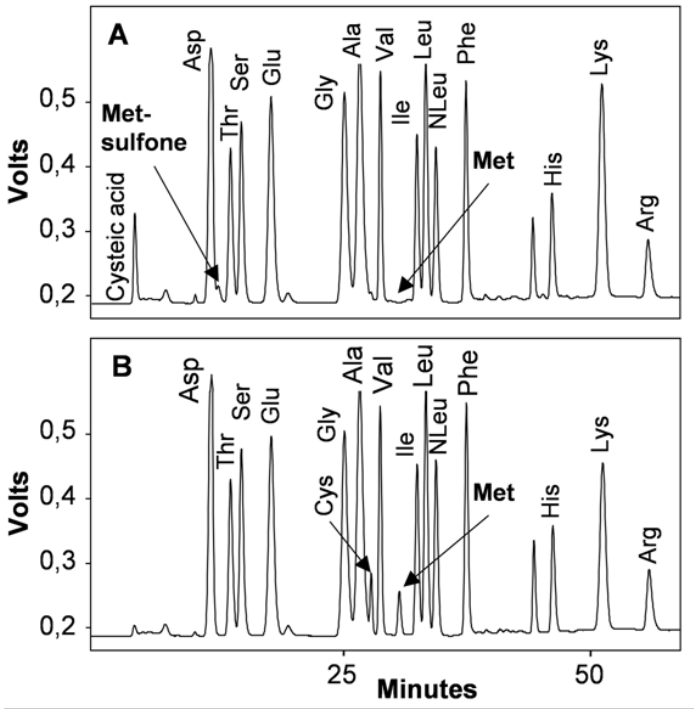

Figure 3. Amino acid analysis of native VP. Amino acid composition evaluated after enzyme incubation in the presence (**A**) and absence (**B**) of H_2O_2 (5000 equivalents). Peaks of methionine, methionine sulfone, cystine and cysteic acid are highlighted with arrows.

As an alternative to methionine substitution, a second strategy was designed based on the modification of the distal histidine (His47) environment through introduction of mutations at Thr45 and Ile103 residues. These two amino acids are located directly above the area occupied by His47 (Thr45 in helix B and Ile103 in helix D) (**Fig. 4B**) which is involved, together with Arg43, in the two-electron activation of the resting enzyme by H_2O_2 to form CI.

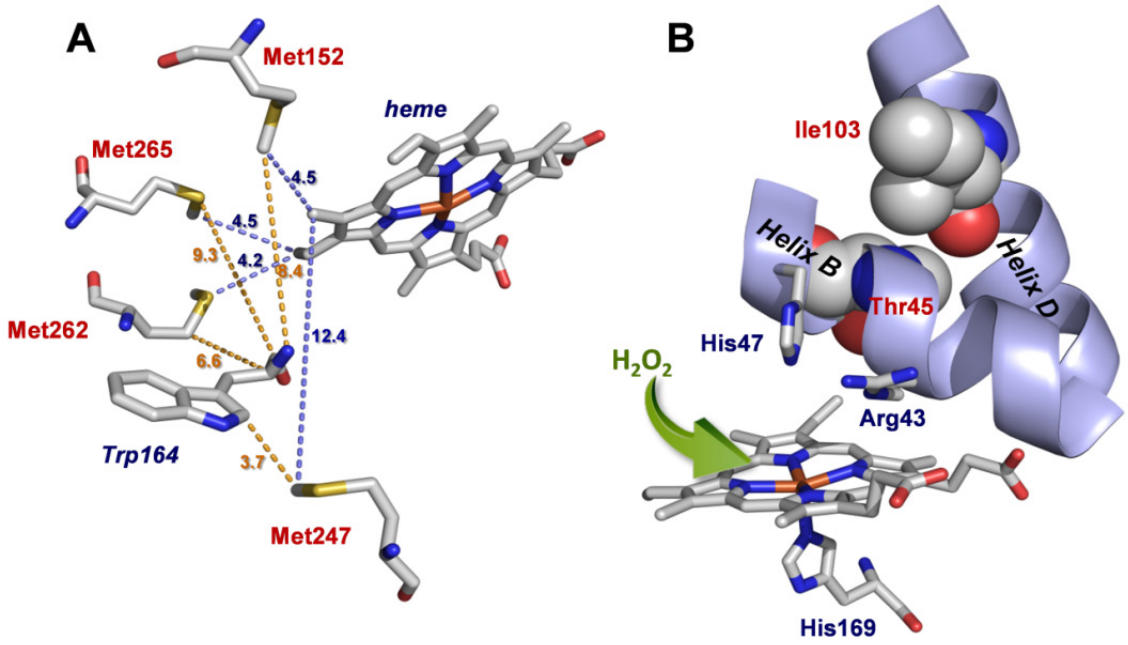

Figure 4. Details of native VP crystal structure (PDB entry 2BOQ). A, Methionine residues and their distances in Å to both the heme and the catalytic tryptophan (Trp164), shown as sticks; and **B**, distal histidine (His47) environment, including heme and Arg43 (as sticks), together with residues Thr45 and Ile103 (both as van der Waals spheres) further mutated to obtain the T45A/I103T variant (proximal His169 acting as the fifth iron ligand and H_2O_2 gaining access to the heme are also shown). PyMOL (http://pymol.org) was used for graphical analysis and image generation.

T45A and I103T substitutions were selected after *in silico* analysis with the aim of modifying the interaction between helices B and D. Changes in the enzyme oxidation rate by H_2O_2 and minimization of the inactivation rate were expected, among other effects that *a priori* could not be exactly predicted. Finally, the T45A/I103T/M152F/M262F/M265L variant, including substitution of the three methionines closer to the heme plus the two mutations located above His47 was produced, combining in a single VP molecule the two strategies previously described.

After expression and purification, the steady-state kinetic constants for VA, Mn^{2+} and ABTS oxidation (at the exposed catalytic Trp164, Mn^{2+} oxidation site and main heme access channel, respectively), by the nine VP variants designed in this work, were determined (**Table 1**) in order to investigate how the mutations affect the catalytic properties of this peroxidase.

Table 1. Steady-state kinetic constants [K_m (μM), k_{cat} (s^{-1}), and k_{cat}/K_m (s^{-1}·mM^{-1})] of native VP and variants for oxidation of VA, Mn^{2+}, and ABTS in the low-efficiency site.

		VP	M152V	M247F	M262F	M265L
	K_m	2600 ± 190	3400 ± 200	4100 ± 400	2500 ±	3900 ± 300
VA	k_{cat}	5.8 ± 0.1	5.4 ± 0.1	4.3 ± 0.2	5.6 ± 0.1	11.4 ± 0.3
	k_{cat}/K	2.2 ± 0.1	1.6 ± 0.1	1.1 ± 0.1	2.3 ± 0.1	2.9 ± 0.2
	K_m	130 ± 11	119 ± 8	70 ± 5	162 ± 26	136 ± 7
Mn^{2+}	k_{cat}	211 ± 4	219 ± 3	76 ± 1	233 ± 2	215 ± 2
	k_{cat}/K	1640 ±130	1840 ± 133	1090 ± 100	1440 ±	1580 ± 103
	K_m	1040 ± 80	1200 ± 740	869 ± 60	1740 ±	1490 ± 110
ABTS	k_{cat}	209 ± 6	223 ± 5	35 ± 1	160 ± 4	224 ± 7
	k_{cat}/K	201 ± 10	186 ± 8	40 ±2	92 ± 3	151 ± 8
		M262F/ M265L	M152F/ M262F/M265L	M152F/M247F/ M262F/M265L	T45A/ I103T	T45A/I103T/ M152F/ M262F/ M265L
	K_m	1900 ± 300	255 ± 28	622 ± 10	357 ± 30	65 ± 14
VA	k_{cat}	3.6 ± 0.2	1.8 ± 0.1	1.1 ± 0.1	1.9 ± 0.1	0.35 ± 0.01
	k_{cat}/K	1.9 ± 0.2	7.0 ± 0.6	1.8 ± 0.2	5.2 ± 0.4	5.3 ± 1.0
	K_m	185 ± 12	255 ± 15	277 ± 28	371 ± 15	789 ± 51
Mn^{2+}	k_{cat}	225 ± 3	147 ± 2	97 ± 2	158 ± 2	104 ± 2
	k_{cat}/K	1220 ±110	576 ± 34	350 ± 30	425 ± 15	132 ± 7
	K_m	1810 ± 90	1420 ± 110	1200 ± 129	932 ± 77	2030 ± 390
ABTS	k_{cat}	186 ± 4	65 ± 2	35 ± 2	55 ± 2	79 ± 7
	k_{cat}/K	103 ± 3	46 ±2	29 ± 2	59 ± 3	39 ± 5

Means and 95% confidence limits from reactions at 25 °C in 0.1 M tartrate (VA at pH 3, Mn^{2+} at pH 5 and ABTS at pH 3.5). In native VP and some variants, a double kinetics for ABTS oxidation was observed enabling calculation of a second set of constants (not shown) corresponding to a high catalytic efficiency site.

In general, the single and double methionine variants exhibited similar catalytic efficiencies when compared with native VP. The M247F variant was the exception since its ability to oxidize the three substrates assayed was significantly impaired (the efficiency values showing a 1.5 to 5-fold drop).

The rest of variants were affected in a similar way in their catalytic properties. The k_{cat} and K_m for VA oxidation suffered a decrease of 3.1 to 6-fold and 4.2 to 40-fold, respectively, resulting in mutated variants with an improvement in the catalytic efficiency as a consequence of the higher reduction in K_m (thereby increasing the affinity of the enzyme for this substrate) than in k_{cat}. The M152F/M247F/M262F/M265L variant was the only of these enzymes that retained a similar catalytic efficiency

on VA compared with the native enzyme because a similar reduction of ~4-5-fold was produced in both the K_m and k_{cat} values. Unlike what observed with VA, a decrease in the catalytic efficiency for oxidation of Mn^{2+} and ABTS by these four variants was produced: i) as a result of the decrease in k_{cat} and increase in K_m, in the case of Mn^{2+} oxidation, with a higher K_m contribution (6.1-fold increment) in the T45A/I103T/M152F/ M262F/ M265L variant; and ii) due to a significant (2.6 to 6-fold) decrease in k_{cat} in the case of ABTS, without practically changes in K_m except in the M152F/M247F/M262F/M265L variant in which the value of this constant exhibited a 2-fold increase.

Similarly, the reaction of native VP and the different variants with H_2O_2 was characterized by stopped-flow spectrophotometry to know if the enzyme activation was affected by the mutations. The observed pseudo first-order rate constants (k_{obs}) for CI formation (RS + H_2O_2 → CI +H_2O) exhibited a linear dependence on H_2O_2 concentration, as shown in **Fig. 5** for native VP and the T45A/I103T variant. The apparent second-order rate constant (k_{1app}) obtained for this variant (1.2 x 10^6 s^{-1}·M^{-1}) experienced a 2.9-fold decrease compared with the native enzyme (3.46 x 10^6 s^{-1}·M^{-1}).

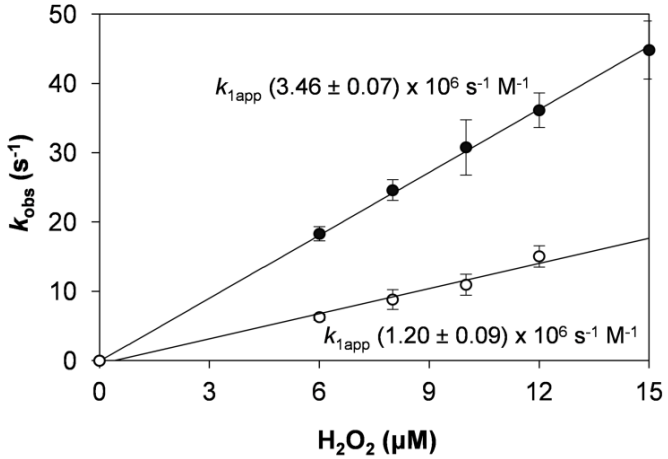

Figure 5. Transient-state kinetics of native VP (●) and T45A/I103T variant (○) for CI formation. Apparent second-order rate constants (k_{1app}) expressed in s^{-1}·M^{-1}. Reactions were carried out at 25 °C in 0.1 M sodium tartrate (pH 3.0) using 1 μM VP and increasing concentrations of H_2O_2. Means and 95% confidence limits are shown.

3.2 Oxidative stabilization

The oxidative stability of the VP variants was compared with that of the native enzyme in the presence of increasing stoichiometric excesses of

H_2O_2. The oxidative inactivation kinetics of the native VP followed a sigmoidal curve (**Fig. 6**) that was fitted to a Hill equation. This enzyme is characterized by a first-order inactivation rate constant (k_i) of 0.32 s^{-1}, a H_2O_2:VP ratio resulting in the half maximal inactivation rate (K_I) of 27.6 mM, an apparent second-order inactivation rate constant (k_{app}) of 11.7 $s^{-1}\cdot M^{-1}$ and a Hill coefficient of 1.85 (**Table 2**). Single and double variants at methionine residues evidenced the same sigmoidal behaviour (**Fig. 6A**). Their inactivation kinetic constants did not substantially differ from those of the native VP, with k_{app} values between 8.3 and 15.5 $s^{-1}\cdot M^{-1}$ (**Table 2**). Interestingly, in the triple (M152F/M262F/M265L) and quadruple (M152F/M247F/M262F/M265L) methionine variants, the inactivation kinetics fitted to a linear model (**Fig. 6B**) instead of to a sigmoidal one, with a concomitant decrease in the k_{app} value (**Table 2**). The triple variant exhibited a k_{app} of 1.8 $s^{-1}\cdot M^{-1}$, being 6.5-fold lower than the value shown by the native VP. Likewise, the quadruple variant presented a k_{app} of 1.5 $s^{-1}\cdot M^{-1}$, a value slightly lower than that found for the triple variant and 7.8-fold lower compared with the native VP.

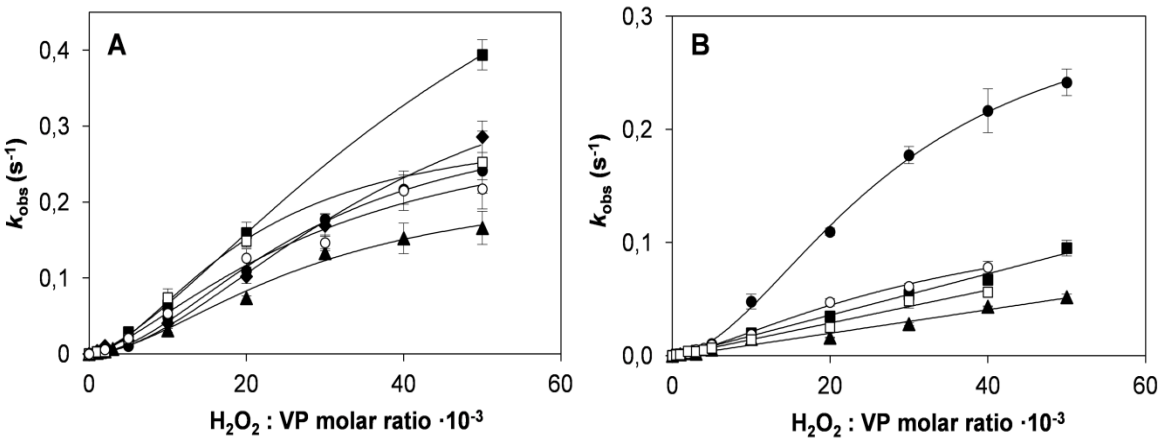

Figure 6. Inactivation kinetics under oxidative conditions. A, Native VP and single and double methionine variants: native VP (●), M247F (○), M152V (■), M265L (□), M262F (▲), M262F/M265L (♦); and **B**, native VP and multiple variants: native VP (●), T45A/I103T○], M152F/M262F/M265L (■), M152F/M247F/M262F/ M265L (□) and T45A/I103T/M152F/M262F/M265L (▲). Reactions were carried out at 25°C using 0.01 µM enzyme in 10 mM sodium tartrate (pH 5.0) in the presence of increasing H_2O_2 concentrations. Means and 95% confidence limits are shown.

A 2.9-fold decrease was also observed in the k_{app} (4.1 $s^{-1}\cdot M^{-1}$) of the T45A/I103T variant (**Table 2**), mainly due to a drop in the k_i value (0.14 s^{-1}), although without loss of the sigmoidal inactivation behaviour (**Fig. 6B**). This inactivation behaviour was lost when these two mutations were combined in the T45A/I103T/M152F/M262F/M265L quintuple variant. The k_{app} for oxidative inactivation of this variant (1.0 $s^{-1}\cdot M^{-1}$) was diminished to a greater extent (11.7-fold) than observed for any of the other variants.

Finally, the decrease in the k_{app} values observed in the above multiple variants could be related to the increase in the half-life of these enzymes, and this improvement was more significant at the lowest H_2O_2:VP ratios (**Fig. 7**). The quintuple variant exhibited the highest half-life (over 30 min at H_2O_2:VP ratios of 1000:1 and 2000:1) compared with the other variants and the native VP (3.4 min at a H_2O_2:VP ratio of 2000:1).

Table 2. Kinetic constants of the inactivation process of native VP and its mutated variants (k_i, first-order inactivation rate constant; K_I, H_2O_2 : VP molar ratio resulting in the half maximum inactivation rate; k_{app}, apparent second-order oxidative inactivation rate constant; and n, Hill coefficient).

	k_i (s^{-1})	K_I (mM)	k_{app} ($s^{-1}\cdot M^{-1}$)	n
VP	0.32 ± 0.02	27.6 ± 2.2	11.7 ± 0.2	1.85 ± 0.12
M262F	0.23 ± 0.04	27.9 ± 6.3	8.3 ± 0.5	1.73 ± 0.29
M265L	0.30 ± 0.01	20.1 ± 1.4	15.1 ± 0.5	1.75 ± 0.11
M247F	0.32 ± 0.09	29.3 ± 12.6	11.0 ± 1.7	1.35 ± 0.22
M152V	0.83 ± 0.09	53.8 ± 7.7	15.5 ± 0.5	1.46 ± 0.06
M262F/M265L	0.45 ± 0.04	38.3 ± 4.3	11.7 ± 0.4	1.80 ± 0.17
M152F/M262F/M265L	n.d.[a]	n.d.[a]	1.8 ± 0.04	n.d.[a]
M152F/M247F/M262F/M265L	n.d.[a]	n.d.[a]	1.5 ± 0.05	n.d.[a]
T45A/I103T	0.14 ± 0.02	34.4 ± 7.8	4.1 ± 0.3	1.41 ± 0.11
T45A/I103T/M152F/M262F/M265L	n.d.[a]	n.d.[a]	1.0 ± 0.04	n.d.[a]

Reactions at 25 ºC in 0.1 M tartrate, pH 5, using 0.01 µM VP, final concentration, and increasing stoichiometric excesses of H_2O_2. Means and 95 % confidence limits.

[a]n.d. Not determined because saturation was not reached.

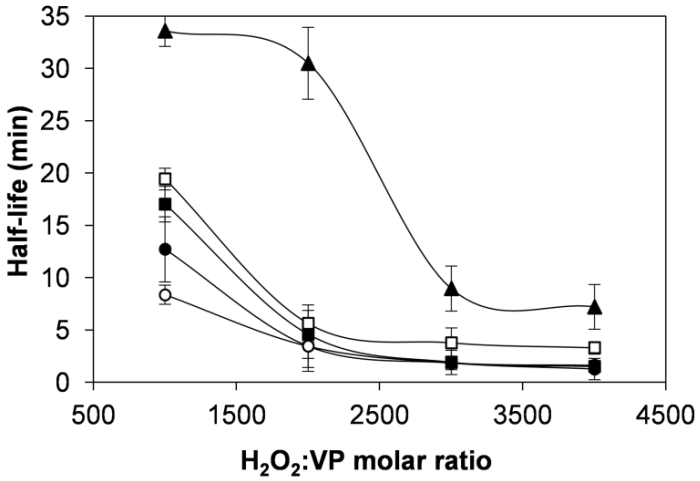

Figure 7. Half-life of native VP and multiple variants incubated with different H_2O_2: VP molar ratios. Native VP (●), T45A/I103T (○), M152F/M262F/M265L (■), M152F/M247F/M262F/M265L (□) and T45A/I103T/M152F/M262F/M265L (▲). The enzyme half-life is defined as the period of time required to inactivate the enzyme at 50% of initial activity. The residual activity of the variants (0.01 μM) was measured in 10 mM sodium tartrate (pH 5.0) using 6 mM Mn^{2+} and 0.1 mM H_2O_2.

3.3 Spectral analyses

The spectral changes of the native VP and of three variants improving oxidative stability (M152F/M262F/M265L, T45A/I103T and T45A/ I103T/M152F/M262F/ M265L) were analyzed after enzyme activation in the presence of 5000 equivalents of H_2O_2 (high enough to see the transitions between the three states of the catalytic cycle in a short period of time). The first spectrum of the native enzyme, obtained at 10 ms, exhibited typical maxima of CI including the Soret band at 403 nm and the charge transfer band CT1 at 651nm (**Fig. 8A**). Subsequently, CII was formed as observed by the displacement of the Soret band to 417 nm, the reorganization of the 500-600 nm spectral region and the disappearance of the maximum at 651 nm. Then CIII was generated exhibiting a characteristic spectrum with maxima at 419, 546 and 581 nm. Comparable spectral changes, although with different conversion rates, were obtained for the VP variants, as illustrated for the T45A/I103T/M152F/M262F/M265L variant in **Fig. 8B**. When the reaction was extended in time (up to 20 min) strong differences in CIII decay and enzyme bleaching were observed (**Fig. 9**), as discussed below together with the differences in CIII formation.

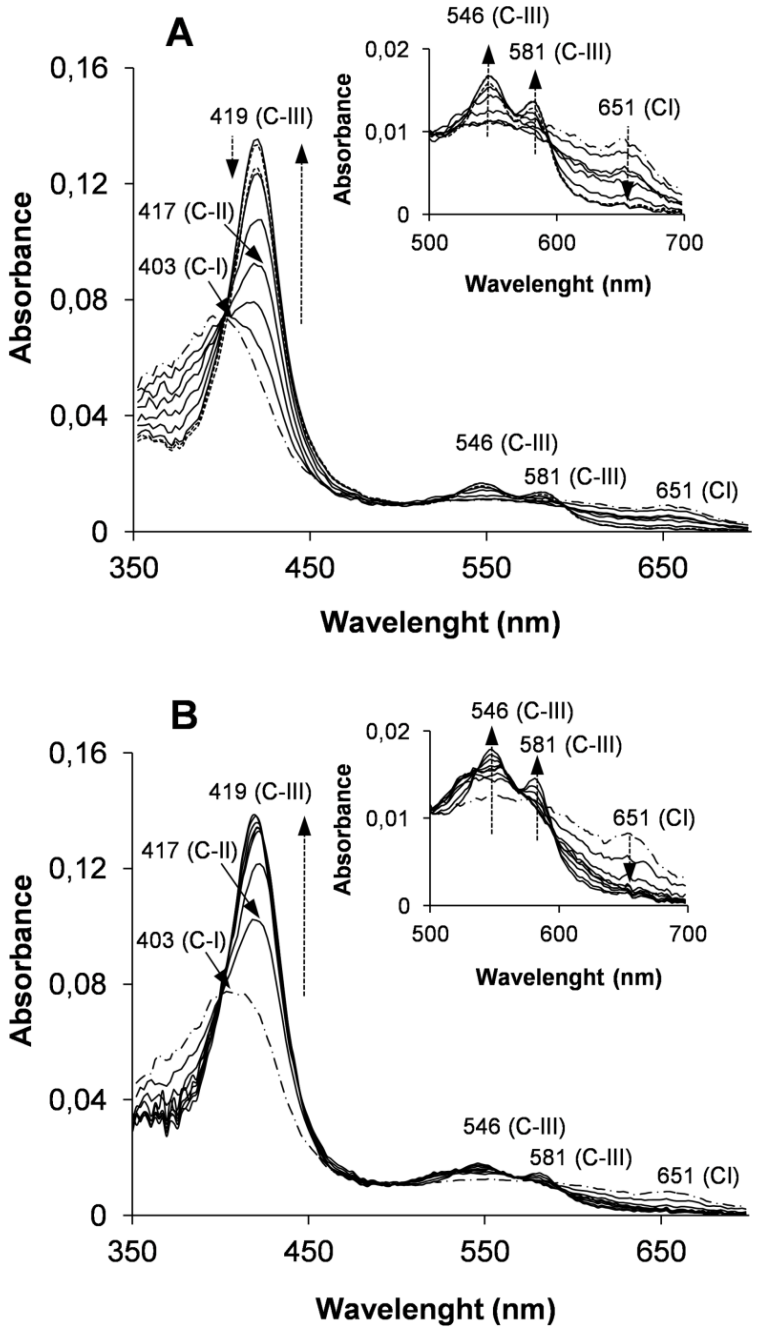

Figure 8. Turnover studies in the presence of excess of hydrogen peroxide. Kinetics of native VP (**A**) and its T45A/I103T/M152F/M262F/M265L variant (**B**) in the presence of a stoichiometric excess of 5000 equivalents of H_2O_2. Spectra were recorded at 25 °C during 20 s. The dashed arrows indicate the increase and decrease of absorbance during formation of CII (with a maximum at 417 nm) and CIII (with maxima at 419 nm, 546 nm and 581 nm, and a minimum at 651 nm), and the decrease of absorbance during heme bleaching (at 419 nm). Traces correspond respectively to 0.01 s (CI spectrum both in A and B, showed as a dashed-point line); 0.1, 0.25, 0.5, 1, 2 and 5 s (continuous lines); and 10 and 20 s (continuous lines in **B**, and discontinuous lines in **A** due to heme bleaching). Details of the 500 nm-700 nm region are shown in x8 scale.

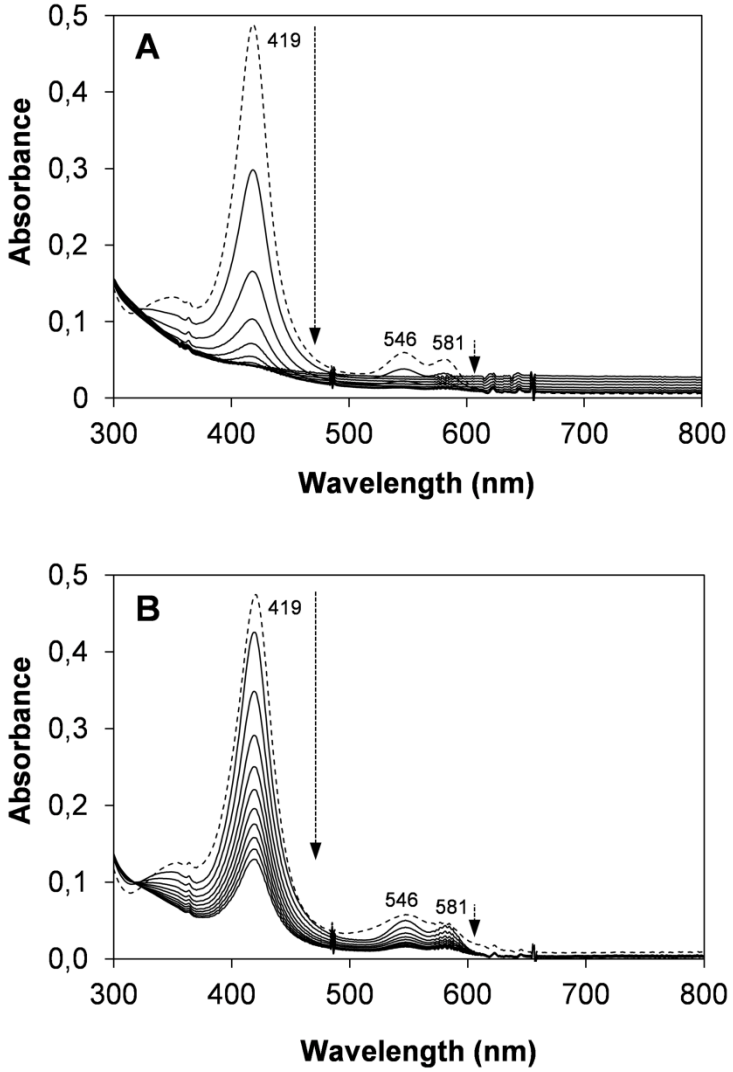

Figure 9. Bleaching of native VP (A) and the T45A/I103T/M152F/M262F/M265L variant (B) under high oxidative stress conditions. Both enzymes were incubated with 5000 equivalents of H_2O_2 at 25 °C, and spectra (in the 300-800 nm range) were recorded every 2 min for 20 min. The first spectrum, obtained after 5 s of incubation, is shown as a discontinuous line and corresponds to: **A**, native VP CIII; and **B**, a mixture of CII and CIII (the latter being the major form) of the T45A/I103T/M152F/M262F/M265L variant. The arrows indicate the direction of the spectral evolution with time.

The rate of CIII formation ($k_{CIII(obs)}$), monitored by the increase of absorbance at 581 nm (**Fig. 10A**), was slowed down by 1.3 to 2.3-fold in the three VP variants. The T45A/I103T/M152F/M262F/M265L mutant was that exhibiting the slowest one (0.12 s^{-1} *vs* 0.27 s^{-1} for the native VP) (**Table 3**). Then CIII further evolved in excess of H_2O_2 leading to enzyme inactivation (see **Table 3** for $k_{i(obs)}$ values) and heme bleaching (**Fig. 9**), which was monitored by the loss of absorbance at 419 nm (**Fig. 10B**).

The corresponding $k_{b(obs)}$ values are shown in **Table 3**. The differences observed between both sets of constants, $k_{i(obs)}$ (0.013-0.033 s^{-1}) being one order of magnitude higher than $k_{b(obs)}$ (0.0014-0.0058 s^{-1}) for the native enzyme and mutated variants, evidenced that the loss of catalytic activity precedes heme bleaching. As previously described for CIII formation, these two events were also slowed down in the improved variants compared with the native enzyme.

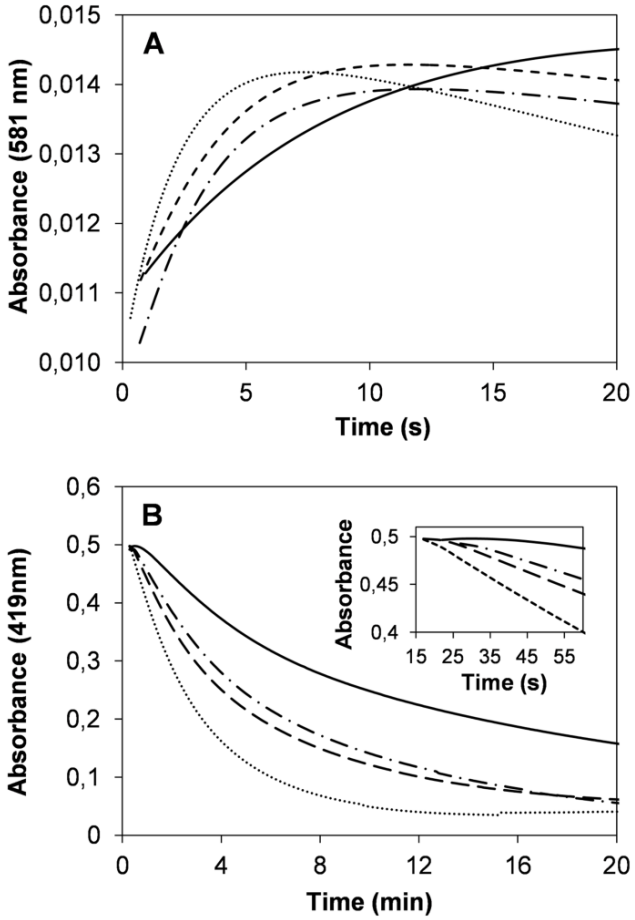

Figure 10. Time course of CIII formation and bleaching. **A**, CIII formation at 581 nm; and **B,** CIII bleaching at 419 nm of VP (⋯), VP T45A/I103T (−·−), VP M152F/M262F/M265L (---) and VP T45A/I103T/M152F/M262F/M265L (—). The variants were incubated with 5000 equivalents of H_2O_2 in 0.1M sodium tartrate (pH 5.0) at 25°C. The inset shows a detail of the CIII bleaching corresponding to the first min of incubation.

Native VP was very unstable and its CIII form started to be bleached from the moment it was formed (**Fig. 10B inset**) following the spectral evolution shown in **Fig. 9A**. By contrast, the T45A/I103T, M152F/ M262F/M265L and T45A/I103T/M152F/M262F/M265L variants

slowed the $k_{b(obs)}$ values with respect to native VP by 1.7, 2.3 and 4.2-fold, respectively. In addition, the T45A/I103T/M152F/M262F/M265L variant remained as a stable CIII form for approximately 45 s prior to the start of heme bleaching (**Fig. 10B inset**). Finally, CIII reversion to native VP and quintuple variant resting states were studied in the presence of Mn^{2+} as reducing substrate and similar conversion rates were obtained (0.70 and 0.75 s^{-1}, respectively).

Table 3. Pseudo first-order rate constants for CIII formation ($k_{CIII(obs)}$), enzyme inactivation ($k_{i(obs)}$) and heme bleaching ($k_{b(obs)}$) of native VP and three mutated variants in the presence of 5000 equivalents of H_2O_2.

	$k_{CIII(obs)}$ (s^{-1})	$k_{i(obs)}$ (s^{-1})	$k_{b(obs)}$ (s^{-1})
VP	0.27 ± 0.05	0.033 ± 0.006	0.0058 ± 0.00002
T45A/I103T	0.21 ± 0.02	0.027 ± 0.003	0.0035 ± 0.00002
M152F/M262F/M265L	0.20 ± 0.04	0.023 ± 0.004	0.0025 ± 0.00002
T45A/I103T/M152F/M262F/M265L	0.12 ± 0.02	0.013 ± 0.002	0.0014 ± 0.00001

Reactions in 50 mM sodium tartrate, pH 5, in the presence of 5000 equivalents of H_2O_2. CIII formation was measured as the absorbance increase at 581 nm (Fig. 8A) and heme bleaching as the absorbance decrease at 419 nm (Fig. 8B). The catalytic inactivation was followed by measuring the residual activity with time, oxidizing 6 mM Mn^{2+} (saturating conditions) in the presence of 0.1 mM H_2O_2 and 0.01 μM enzyme. Means and 95 % confidence limits.

4.Discussion

H_2O_2 plays different roles throughout the life of heme peroxidases in general, and ligninolytic peroxidases in particular, from "birth" to "death". So, H_2O_2 induces the natural production of these enzymes (Ruiz-Dueñas et al., 1999a; Li et al., 1995), is the enzyme-activating substrate, and is also involved in a mechanism-based process described as suicide inactivation (Valderrama et al., 2002). The studies on *P. eryngii* VP, used here as a model ligninolytic peroxidase, demonstrated that this peroxidase is inactivated at increasing H_2O_2 concentrations in the absence of reducing substrates, confirming previous results (Bao et al., 2012; García-Ruiz et al., 2012). All methionines present in VP were

oxidized to methionine sulfone containing larger and more polar side-chains, as also described for other peroxidases (Villegas et al., 2000; Valderrama et al., 2006; Kim and Erman, 1988). Considering their proximity to the heme cofactor and catalytic tryptophan, it is quite probable that a local disruption at this level causes misalignment of active site residues. This would affect electron transfer, and/or energy barriers, with an effect on the enzyme activity and stability, as shown in a variety of proteins (Vogt, 1995). However, although important, this is not the oxidative event that causes the complete oxidative inactivation of VP. The enzyme proceeds through the different transient states of the catalytic cycle under conditions of excess of H_2O_2 to reach the CIII state. This Fe^{3+}-$O_2^{\cdot-}$ species (Wariishi and Gold, 1990), spectrally identified here for the first time in VP, is not part of its normal catalytic cycle (Morales et al., 2012) and leads to the irreversible enzyme inactivation and heme destruction (bleaching) (Wariishi and Gold, 1989) in the presence of high H_2O_2 concentration.

4.1 Stability improvement by substituting oxidizable methionines

In a recent study, where VP was evolved for increased oxidative stability, methionine substitutions were not selected in the improved variant (González-Pérez et al., 2014). However, different authors have reported oxidative stability improvement after removal of methionine residues from a VP fusion protein (Bao et al., 2014), as well as from fungal MnP (Miyazaki and Takahashi, 2001), GP (Cherry et al., 1999) and dye-decolorizing peroxidase (Ogola et al., 2010). Given this background, and after verifying methionine oxidation in VP under oxidative conditions, a strategy was designed based on the replacement of methionines. This is the first time that all of them are simultaneously substituted in a heme peroxidase. The result was that the mutated variants at three or the four methionine residues behaved as the most stable ones, confirming the involvement of methionine oxidation in the inactivation process and, consequently, that our strategy has been sound.

We have also demonstrated that the native VP follows a time-dependent (with decreasing half-life values to increasing concentrations of H_2O_2) and saturation kinetic H_2O_2-mediated inactivation model, as

reported for other heme peroxidases (Timofeevski et al., 1998; Wariishi and Gold, 1989; Cai and Tien, 1989; Arnao et al., 1990; Hiner et al., 2000; Cuadrado et al., 2011; Paumann-Page et al., 2013). In addition, our studies reveal that a positive cooperativity model contributes, at least in part, to the oxidative inactivation of VP by H_2O_2, in agreement with the sigmoidal profile characterizing the inactivation kinetics. Interestingly, this model is dependent on the oxidation of the methionine residues, since it is lost in the triple and quadruple methionine variants, where the cooperativity is not possible. According to this analysis, the substitution of three or four methionines by non-oxidizable residues abolishes this inactivation mechanism. In consequence, it can be considered that this is the reason of the stability improvement towards H_2O_2 in the M152F/M262F/M265L and M152F/M247F/ M262F/M265L variants. The only negative impact lies in the enzymatic activity on the different substrates assayed, which was affected to different extents. At this respect, a correlation was found between k_{cat} and k_{app} values, both decreasing simultaneously in these variants (and also observed in the T45A/I103T and T45A/I103T/M152F/M262F/M265L mutants).

Oxidative stability of heme peroxidases has been found to be the result of a competition between productive (reducing substrate) and unproductive electron sources (enzyme components including methionines) (Valderrama et al., 2006). According to this idea, our results suggest that in the absence of reducing substrates the higher catalytic rate of native VP would result in a more rapid oxidation of methionines and other oxidizable residues leading to a faster inactivation compared with the mutated variants.

4.2 Stability improvement by decreasing enzyme reactivity with H_2O_2

The second strategy aimed to improve the stability of VP towards H_2O_2 by the simultaneous substitution of Thr45 and Ile103 most probably perturbs the interaction between helices B and D. Mutations in the same protein region of the *Coprinopsis cinerea* peroxidase during directed evolution were related with a significant improvement in thermal and oxidative stability (Cherry et al., 1999) after only minor structural changes (Houborg et al., 2003). Similarly, conformational changes due to a point mutation in the heme pocket has been also suggested to be

responsible for the higher H_2O_2 resistance of a MnP variant (Miyazaki and Takahashi, 2001). In VP, the predicted structural changes associated to the T45A and I103T substitutions would affect the mobility and/or positioning of the conserved distal His47 and Arg43. These two residues, found in all functional peroxidases of the catalase-peroxidase superfamily, play a key role in the catalytic cycle (Berglund et al., 2002) during resting enzyme activation and CI stabilization (Hiner et al., 2002b; Vitello et al., 1993; Casadei et al., 2014). Stopped-flow spectrophotometry analysis of the T45A/I103T variant revealed that CI formation is impaired. The expected structural changes due to these two mutations led to a 2.8-fold decrease in the inactivation rate by H_2O_2, retaining the positive cooperativity inactivation model because of the presence of the four methionine residues. However, the decrease in the inactivation rate was not reflected in its half-life, being similar to that of the native enzyme.

4.3 Final improvement by combining two stabilization strategies

The above two stabilization strategies were combined in the T45A/I103T/M152F/M262F/M265L variant. Only three of the four methionines present in VP were substituted in this variant since the replacement of the fourth one (Met247) did not provide any additional improvement. All the parameters evaluating the stability of the new enzyme towards H_2O_2 were improved, confirming the success of this final approach. The decrease in k_{app} was the result of the accumulative effect observed in the T45A/I103T and M152F/M262F/M265L variants, confirming that solving the oxidative instability problem of heme peroxidases has to be addressed using different (complementary) approaches. The T45A/I103T/M152F/M262F/M265L variant was by far the most stable VP under oxidative conditions. Its increased stability could be justified by the slowdown of three events that occur consecutively as deduced from the calculated velocities: i) CIII formation; ii) enzyme inactivation; and iii) heme bleaching. CIII is completely stable for circa 45 s in the presence of a 5000-fold stoichiometric excess of H_2O_2. This time should be enough to allow the enzyme to return to the RS in the presence of reducing substrates, minimizing the oxidative inactivation under operational conditions. The development of a mechanistic explanation for the improved peroxidase

stability of this variant would be too speculative with the data currently available. However, taking into account that CIII is stabilized by complex interactions with residues of the heme distal side (Berglund et al., 2002), we can hypothesize that changes at this environment due to the mutations introduced could modify these interactions increasing the CIII stability and reducing the bleaching rate of the enzyme.

In conclusion, the higher VP oxidative stability improvement obtained in this work has been achieved by substitution of amino acid residues located at specific positions near the heme group affecting formation, stabilization and decomposition of CIII. Additional changes at the heme distal side, together with the replacement of methionine residues, could further improve the stability of this enzyme towards H_2O_2. Moreover, the results presented here give insight into the strategy to be used to improve the oxidative stability of other peroxidases of biotechnological interest.

5. References

Arnao, M.B., M.Acosta, J.A.del Río, R.Varón, and F.García-Cánovas. 1990. A kinetic study on the suicide inactivation of peroxidase by hydrogen peroxide. *Biochim. Biophys. Acta* 1041:43-47.

Ayala, M., M.A.Pickard, and R.Vázquez-Duhalt. 2008. Fungal enzymes for environmental purposes, a molecular biology challenge. *J. Mol. Microbiol. Biotechnol.* 15:172-180.

Bao, X., X.N.Huang, X.F.Lu, and J.J.Li. 2014. Improvement of hydrogen peroxide stability of *Pleurotus eryngii* versatile ligninolytic peroxidase by rational protein engineering. *Enzyme Microb. Technol.* 54:51-58.

Bao, X., A.Q.Liu, X.F.Lu, and J.J.Li. 2012. Direct over-expression, characterization and H2O2 stability study of active Pleurotus eryngii versatile peroxidase in Escherichia coli. *Biotechnol. Lett.* 34:1537-1543.

Berglund, G.I., G.H.Carlsson, A.T.Smith, H.Szoke, A.Henriksen, and J.Hajdu. 2002. The catalytic pathway of horseradish peroxidase at high resolution. *Nature* 417:463-468.

Cai, D. and M.Tien. 1989. On the reactions of lignin peroxidase compound III (isozyme H8). *Biochem. Biophys. Res. Commun.* 162:464-469.

Casadei, C.M., A.Gumiero, C.L.Metcalfe, E.J.Murphy, J.Basran, M.G.Concilio, S.C.M.Teixeira, T.E.Schrader, A.J.Fielding, A.Ostermann, M.P.Blakeley, E.L.Raven, and P.C.E.Moody. 2014. Neutron cryo-crystallography captures the protonation state of ferryl heme in a peroxidase. *Science* 345:193-197.

Cherry, J.R., M.H.Lamsa, P.Schneider, J.Vind, A.Svendsen, A.Jones, and A.H. Pedersen. 1999. Directed evolution of a fungal peroxidase. *Nat. Biotechnol.* 17:379-384.

Cuadrado, N.H., G.G.Zhadan, M.G.Roig, and V.L.Shnyrov. 2011. Suicide inactivation of peroxidase from *Chamaerops excelsa* palm tree leaves. *Int. J. Biol. Macromol.* 49:1078-1082.

Floudas, D., M.Binder, R.Riley, K.Barry, R.A.Blanchette, B.Henrissat, A.T.Martínez, R.Otillar, J.W.Spatafora, J.S.Yadav, A.Aerts, I.Benoit, A.Boyd, A.Carlson, A.Copeland, P.M.Coutinho, R.P.de Vries, P.Ferreira, K.Findley, B.Foster, J.Gaskell, D.Glotzer, P.Górecki, J.Heitman, C.Hesse, C.Hori, K.Igarashi, J.A.Jurgens, N.Kallen, P.Kersten, A.Kohler, U.Kües, T.K.A.Kumar, A.Kuo, K.LaButti, L.F.Larrondo, E.Lindquist, A.Ling, V.Lombard, S.Lucas, T.Lundell, R.Martin, D.J.McLaughlin, I.Morgenstern, E.Morin, C.Murat, M.Nolan, R.A.Ohm, A.Patyshakuliyeva, A.Rokas, F.J.Ruiz-Dueñas, G.Sabat, A.Salamov, M.Samejima, J.Schmutz, J.C.Slot, F.St.John, J.Stenlid, H.Sun, S.Sun, K.Syed, A.Tsang, A.Wiebenga, D.Young, A.Pisabarro, D.C.Eastwood, F.Martin, D.Cullen, I.V.Grigoriev, and D.S.Hibbett. 2012. The Paleozoic origin of enzymatic lignin decomposition reconstructed from 31 fungal genomes. *Science* 336:1715-1719.

García-Ruiz, E., D.González-Pérez, F.J.Ruiz-Dueñas, A.T.Martínez, and M.Alcalde. 2012. Directed evolution of a temperature-, peroxide- and alkaline pH-tolerant versatile peroxidase. *Biochem. J.* 441:487-498.

González-Pérez, D., E.García-Ruiz, F.J.Ruiz-Dueñas, A.T.Martínez, and M.Alcalde. 2014. Structural determinants of oxidative stabilization in an evolved versatile peroxidase. *ACS Catal.* 4:3891-3901.

Heinfling, A., F.J.Ruiz-Dueñas, M.J.Martínez, M.Bergbauer, U.Szewzyk, and A.T.Martínez. 1998. A study on reducing substrates of manganese-oxidizing peroxidases from *Pleurotus eryngii* and *Bjerkandera adusta*. *FEBS Lett.* 428:141-146.

Hiner, A.N., J.Hernández-Ruíz, J.N.Rodríguez-López, F.Garcia-Canovas, N.C.Brisset, A.T.Smith, M.B.Arnao, and M.Acosta. 2002a. Reactions of the class II peroxidases, lignin peroxidase and *Arthromyces ramosus* peroxidase, with hydrogen peroxide. Catalase-like activity, compound III formation, and enzyme inactivation. *J. Biol. Chem.* 277:26879-26885.

Hiner, A.N.P., E.L.Raven, R.N.F.Thorneley, F.García-Canovas, and J.N.Rodríguez-López. 2002b. Mechanisms of compound I formation in heme peroxidases. *J. Inorg. Biochem.* 91:27-34.

Hiner, A.N.P., J.N.Rodríguez-López, M.B.Arnao, E.L.Raven, F.García-Cánovas, and M.Acosta. 2000. Kinetic study of the inactivation of ascorbate peroxidase by hydrogen peroxide. *Biochem. J.* 348:321-328:321-328.

Houborg, K., P.Harris, J.C.N.Poulsen, P.Schneider, A.Svendsen, and S.Larsen. 2003. The structure of a mutant enzyme of *Coprinus cinereus* peroxidase provides an understanding of its increased thermostability. *Acta Crystallogr. D. Biol. Crystallogr.* 59:997-1003.

Kim, K. and J.E.Erman. 1988. Methionine modification in cytochrome-*c* peroxidase. *Biochim. Biophys. Acta* 954:95-107.

Kirk, T.K. and R.L.Farrell. 1987. Enzymatic "combustion": The microbial degradation of lignin. *Annu. Rev. Microbiol.* 41:465-505.

Li, D., M.Alic, J.A.Brown, and M.H.Gold. 1995. Regulation of manganese peroxidase gene transcription by hydrogen peroxide, chemical stress, and molecular oxygen. *Appl. Environ. Microbiol.* 61:341-345.

Marques, G., J.A.F.Gamelas, F.J.Ruiz-Dueñas, J.C.del Río, D.V.Evtuguin, A.T.Martínez, and A.Gutiérrez. 2010. Delignification of eucalypt kraft pulp with manganese-substituted polyoxometalate assisted by fungal versatile peroxidase. *Bioresource Technol.* 101:5935-5940.

Martínez, A.T., F.J.Ruiz-Dueñas, M.J.Martínez, J.C.del Río, and A.Gutiérrez. 2009. Enzymatic delignification of plant cell wall: from nature to mill. *Curr. Opin. Biotechnol.* 20:348-357.

Martínez, A.T., M.Speranza, F.J.Ruiz-Dueñas, P.Ferreira, S.Camarero, F.Guillén, M.J.Martínez, A.Gutiérrez, and J.C.del Río. 2005. Biodegradation of lignocellulosics: Microbiological, chemical and enzymatic aspects of fungal attack to lignin. *Int. Microbiol.* 8:195-204.

Miyazaki, C. and H.Takahashi. 2001. Engineering of the H_2O_2-binding pocket region of a recombinant manganese peroxidase to be resistant to H_2O_2. *FEBS Lett.* 509:111-114.

Morales, M., M.J.Mate, A.Romero, M.J.Martínez, A.T.Martínez, and F.J.Ruiz-Dueñas. 2012. Two oxidation sites for low redox-potential substrates: A directed mutagenesis, kinetic and crystallographic study on *Pleurotus eryngii* versatile peroxidase. *J. Biol. Chem.* 287:41053-41067.

Moreira, P.R., E.Almeida-Vara, F.X.Malcata, and J.C.Duarte. 2007. Lignin transformation by a versatile peroxidase from a novel *Bjerkandera* sp strain. *Int. Biodeterior. Biodegrad.* 59:234-238.

Nelson, D.P. and L.A.Kiesow. 1972. Enthalpy of Decomposition of Hydrogen-Peroxide by Catalase at 25 Degrees C (with Molar Extinction Coefficients of H2O2 Solutions in Uv). *Anal. Biochem.* 49:474-478.

Ogola, H.J.O., N.Hashimoto, S.Miyabe, H.Ashida, T.Ishikawa, H.Shibata, and Y.Sawa. 2010. Enhancement of hydrogen peroxide stability of a novel *Anabaena* sp DyP-type peroxidase by site-directed mutagenesis of methionine residues. *Appl. Microbiol. Biotechnol.* 87:1727-1736.

Paumann-Page, M., P.G.Furtmuller, S.Hofbauer, L.N.Paton, C.Obinger, and A.J.Kettle. 2013. Inactivation of human myeloperoxidase by hydrogen peroxide. *Arch. Biochem. Biophys.* 539:51-62.

Pérez-Boada, M., W.A.Doyle, F.J.Ruiz-Dueñas, M.J.Martínez, A.T.Martínez, and A.T.Smith. 2002. Expression of *Pleurotus eryngii* versatile peroxidase in *Escherichia coli* and optimisation of *in vitro* folding. *Enzyme Microb. Technol.* 30:518-524.

Pérez-Boada, M., F.J.Ruiz-Dueñas, R.Pogni, R.Basosi, T.Choinowski, M.J.Martínez, K.Piontek, and A.T.Martínez. 2005. Versatile peroxidase oxidation of high redox potential aromatic compounds: Site-directed mutagenesis, spectroscopic and crystallographic investigations of three long-range electron transfer pathways. *J. Mol. Biol.* 354:385-402.

Riley, R., A.A.Salamov, D.W.Brown, L.G.Nagy, D.Floudas, B.W.Held, A.Levasseur, V.Lombard, E.Morin, R.Otillar, E.A.Lindquist, H.Sun, K.M.LaButti, J.Schmutz, D.Jabbour, H.Luo, S.E.Baker, A.G.Pisabarro, J.D.Walton, R.A.Blanchette, B.Henrissat, F.Martin, D.Cullen, D.S.Hibbett, and I.V.Grigoriev. 2014. Extensive sampling of basidiomycete genomes demonstrates inadequacy of the white-rot/brown-rot paradigm for wood decay fungi. *Proc. Natl. Acad. Sci. USA* 111:9923-9928.

Ruiz-Dueñas, F.J., F.Guillén, S.Camarero, M.Pérez-Boada, M.J.Martínez, and A.T.Martínez. 1999a. Regulation of peroxidase transcript levels in liquid cultures of the ligninolytic fungus *Pleurotus eryngii*. *Appl. Environ. Microbiol.* 65:4458-4463.

Ruiz-Dueñas, F.J. and A.T.Martínez. 2009. Microbial degradation of lignin: How a bulky recalcitrant polymer is efficiently recycled in nature and how we can take advantage of this. *Microbial Biotechnol.* 2:164-177.

Ruiz-Dueñas, F.J. and A.T.Martínez. 2010. Structural and functional features of peroxidases with a potential as industrial biocatalysts. *In* Biocatalysts based on heme peroxidases. E.Torres and M.Ayala, editors. Springer-Verlag, Berlin. 37-59.

Ruiz-Dueñas, F.J., M.J.Martínez, and A.T.Martínez. 1999b. Molecular characterization of a novel peroxidase isolated from the ligninolytic fungus *Pleurotus eryngii*. *Mol. Microbiol.* 31:223-236.

Ruiz-Dueñas, F.J., M.Morales, E.García, Y.Miki, M.J.Martínez, and A.T.Martínez. 2009. Substrate oxidation sites in versatile peroxidase and other basidiomycete peroxidases. *J. Exp. Bot.* 60:441-452.

Ruiz-Dueñas, F.J., M.Morales, M.Pérez-Boada, T.Choinowski, M.J.Martínez, K.Piontek, and A.T.Martínez. 2007. Manganese oxidation site in *Pleurotus eryngii* versatile peroxidase: A site-directed mutagenesis, kinetic and crystallographic study. *Biochemistry* 46:66-77.

Salvachúa, D., A.Prieto, M.L.Mattinen, T.Tamminen, T.Liitiä, M.Lille, S.Willfor, A.T.Martínez, M.J.Martínez, and C.B.Faulds. 2013. Versatile peroxidase as a

valuable tool for generating new biomolecules by homogeneous and heterogeneous cross-linking. *Enzyme Microb. Technol.* 52:303-311.

Sambrook, J. and D.W.Russell. 2001. Molecular cloning. CSHL Press, Cold Spring Harbor, New York.

Timofeevski, S.L., N.S.Reading, and S.D.Aust. 1998. Mechanisms for protection against inactivation of manganese peroxidase by hydrogen peroxide. *Arch. Biochem. Biophys.* 356:287-295.

Valderrama, B., M.Ayala, and R.Vázquez-Duhalt. 2002. Suicide inactivation of peroxidases and the challenge of engineering more robust enzymes. *Chem. Biol.* 9:555-565.

Valderrama, B., H.García-Arellano, S.Giansanti, M.C.Baratto, R.Pogni, and R.Vázquez-Duhalt. 2006. Oxidative stabilization of iso-1-cytochrome c by redox-inspired protein engineering. *FASEB J.* 20:1233-1235.

Villegas, J.A., A.G.Mauk, and R.Vázquez-Duhalt. 2000. A cytochrome c variant resistant to heme degradation by hydrogen peroxide. *Chem. Biol.* 7:237-244.

Vitello, L.B., J.E.Erman, M.A.Miller, J.Wang, and J.Kraut. 1993. Effect of Arginine-48 replacement on the reaction between cytochrome *c* peroxidase and hydrogen peroxide. *Biochemistry* 32:9807-9818.

Vogt, W. 1995. Oxidation of Methionyl Residues in Proteins - Tools, Targets, and Reversal. *Free Radic. Biol. Med.* 18:93-105.

Wariishi, H. and M.H.Gold. 1989. Lignin peroxidase compound III: Formation, inactivation, and conversion to the native enzyme. *FEBS Lett.* 243:165-168.

Wariishi, H. and M.H.Gold. 1990. Lignin peroxidase compound III. Mechanism of formation and decomposition. *J. Biol. Chem.* 265:2070-2077.

CHAPTER 2

Improving the pH-stability of Versatile Peroxidase by Comparative Structural Analysis with a Naturally-stable Manganese Peroxidase

Abstract

Versatile peroxidase (VP) from the white-rot fungus *Pleurotus eryngii* is a high redox potential peroxidase of biotechnological interest able to oxidize a wide range of recalcitrant substrates including lignin, phenolic and non-phenolic aromatic compounds and dyes. However, the relatively low stability towards pH of this and other fungal peroxidases is a drawback for their industrial application. A strategy based on the comparative analysis of the crystal structures of VP and the highly pH-stable manganese peroxidase (MnP4) from *Pleurotus ostreatus* was followed to improve the VP pH stability. Several interactions, including hydrogen bonds and salt bridges, and charged residues exposed to the solvent were identified as putatively contributing to the pH stability of MnP4. The eight amino acid residues responsible for these interactions and seven surface basic residues were introduced into VP by directed mutagenesis. Furthermore, two cysteines were also included to explore the effect of an extra disulfide bond stabilizing the distal Ca^{2+} region. Three of the four designed variants were crystallized and new interactions were confirmed, being correlated with the observed improvement in pH stability. The extra hydrogen bonds and salt bridges stabilized the heme pocket at acidic and neutral pH as revealed by UV-visible spectroscopy. They led to a VP variant that retained a significant percentage of the initial activity at both pH 3.5 (61% after 24 h) and pH 7 (55% after 120 h) compared with the native enzyme, which was almost completely inactivated. The introduction of extra solvent-exposed basic residues and an additional disulfide bond into the above variant further improved the stability at acidic pH (85% residual activity at pH 3.5 after 24 h when introduced separately, and 64% at pH 3 when introduced together). The analysis of the results provides a rational explanation to the pH stability improvement achieved.

1. Introduction

Lignin degradation has been a hot topic of research for several decades, and still actual nowadays. It is a key step for carbon recycling in land ecosystems and also a central issue for the industrial utilization of lignocellulosic biomass as a renewable feedstock (Martínez et al., 2009). In nature, the so-called white-rot fungi belonging to the group of

basidiomycetes are unique due to their ability to degrade lignin from plant biomass in an efficient way. This process begins with the unspecific oxidative attack to the aromatic units of this polymer by means of a battery of extracellular oxidoreductases among which ligninolytic peroxidases play a key role (Martínez et al., 2005).

Manganese peroxidase (MnP, EC 1.11.1.13) and lignin peroxidase (LiP, EC 1.11.1.14) are two families of ligninolytic heme peroxidases described 30-years ago (Tien and Kirk, 1983; Kuwahara et al., 1984). The first one is characterized by having a Mn-binding site, formed by three acidic residues (two glutamates and one aspartate) and the internal propionate of heme, where Mn^{2+} is oxidized (Kishi et al., 1996). The resulting Mn^{3+} acts as a diffusible oxidizer after being chelated by organic acids secreted by white-rot fungi. This metal cation can directly oxidize the (minor) phenolic substructures of lignin and indirectly generate lipid peroxyl radicals able to oxidize the non-phenolic units of this polymer (Hammel and Cullen, 2008). Two MnP subfamilies have been identified. Long/extralong MnPs are specific for Mn^{2+} (Fernández-Fueyo et al., 2014a), whereas members of the short MnP subfamily are also able to oxidize phenols like generic peroxidases (GP, EC 1.11.1.7) (Fernández-Fueyo et al., 2014c). Unlike MnP, LiP displays a catalytic tryptophan exposed to the solvent involved in direct oxidation of such bulky and heterogeneous substrate as lignin is (Doyle et al., 1998; Mester et al., 2001). Versatile peroxidase (VP, EC 1.11.1.16) constitutes the third family of ligninolytic peroxidases, which was described 20-years ago (Martínez et al., 1996; Ruiz-Dueñas et al., 1999). VP combines catalytic properties of the above two families due to the presence of both a Mn-oxidation site (Ruiz-Dueñas et al., 2007) and a catalytic tryptophan (Pérez-Boada et al., 2005) in its molecular structure. This peroxidase also exhibits characteristics of GPs by its ability to oxidize low redox potential substrates (e.g. phenols) at the main heme access channel (Morales et al., 2012).

As a consequence of their wide substrate specificity, ligninolytic peroxidases are able to oxidize not only lignin but also other phenolic and non-phenolic aromatic compounds and different industrial dyes, revealing that these enzymes have a high industrial interest (Martínez et al., 2009; Ruiz-Dueñas et al., 2009). They are suitable and attractive for

different applications such as the production of biofuels, materials and chemicals of added value in lignocellulosic biorefineries, for the bleaching process in the paper pulp manufacture and for the treatment of dye wastewater (Martínez et al., 2009; Ragauskas et al., 2006; Husain, 2010). However, their high biotechnological potential cannot be exploited because some difficulties prevent their industrial application. Some of these drawbacks are insufficient levels of protein production and instability towards different factors such as pH, temperature or hydrogen peroxide concentration (Martínez et al., 2009; Ayala et al., 2008).

In recent years, several genomes of basidiomycete species involved in plant biomass biodegradation have been sequenced (Ohm et al., 2014) and the number is increasing. As a result, the sequences of different types of peroxidases have been identified in these genomes and subsequently expressed and characterized. Some of them have new structural, catalytic and stability properties (Fernández-Fueyo et al., 2014c; Fernández-Fueyo et al., 2014a; Fernández-Fueyo et al., 2012; Fernández-Fueyo et al., 2015). Among these, MnP4 from the *Pleurotus ostreatus* genome exhibits a remarkably high acidic and alkaline stability (Fernández-Fueyo et al., 2014c). The study of this and other new peroxidases will provide us with valuable information about the relationships existing among the structure, the stability and the catalytic properties of these enzymes that will allow the design of new biocatalysts of interest.

In the present work, VP (isoenzyme VPL2) from *Pleurotus eryngii* has been subjected to protein engineering using a rational design strategy. The crystal structures of *P. eryngii* VP and *P. ostreatus* MnP (isoenzyme MnP4 following the genome nomenclature) were compared, and putative stabilizing motifs responsible for the high stability towards pH of this MnP were identified. Subsequently, these motifs and other generally accepted stabilizing structural determinant (i.e. one disulfide bond) were translated to VP with the aim of increasing its pH stability and obtaining a more adequate biocatalyst for industrial applications. The results here presented demonstrate that the use of structural determinants identified in peroxidases obtained from genomic analysis is a useful tool for designing biocatalysts of interest.

2. Materials and methods

2.1 Chemicals

Isopropyl-β-D-thiogalactopyranoside (IPTG), dithiothreitol (DTT), hemin, oxidized glutathione (GSSG), veratryl alcohol (VA), manganese(II) sulphate, Reactive Black 5 (RB5), 2,6-dimethoxyphenol (DMP), sodium tartrate and other chemicals were purchased from Sigma-Aldrich; urea and hydrogen peroxide were from Merck; and 2,2'-azino-bis(3-ethylbenzothiazoline-6-sulfonate) (ABTS) from Roche.

2.2 Design of VP variants

VPi and VPi-br variants were designed *in silico* based on a comparative analysis of the mature *P. eryngii* VP (allelic variant VPL2; GenBank™ AF007222) and *P. ostreatus* MnP4 (ID 1099081 in the *P. ostreatus* PC15 v2.0 genome sequence from the Joint Genome Institute, JGI, at http://genome.jgi.doe.gov/PleosPC15_2/PleosPC15_2.home.html). For this analysis: i) the amino acid sequence alignment of both enzymes was performed using the pairwise sequence alignment tools (Needle, Stretcher, Water and Matcher programs) available at the European Bioinformatics Institute (EMBL-EBI); and ii) the structural alignment of VPL2 (PDB: 2BOQ) and MnP4 (PDB: 4BM1) was carried out with PyMOL (http://pymol.org). From this analysis, the VPi coding sequence was prepared by replacing codons encoding eight amino acid residues in VPL2 with those present at homologous positions in MnP4. The substituted amino acids were Asp69 → Ser (TCC), Thr70 → Asp (GAC), Ser86 → Glu (GAG), Asp146 → Thr (ACC), Gln202 → Leu (CTC), His232 → Glu (GAG), Ser301 → Lys (AAG) and Gln239 → Arg (CGC). The introduction of the following additional mutations in VPi resulted in the VPi-br variant: Thr2 → Lys (AAG), Ala131 → Lys (AAG), Gln219 → Lys (AAA), Leu288 → Arg (CGT), Ala308 → Arg (CGC), Ala309 → Lys (AAG) and Ala314 → Arg (CGT). Both VPi and VPi-br sequences were synthesized by ATG:biosynthetics (Merzhausen, Germany) and cloned into the *Nde*I/*Bam*HI restriction sites of the expression vector pFLAG1 (International Biotechnologies Inc., Cambridge, UK).

Other two VP variants were produced using the QuikChange™ Site-Directed Mutagenesis kit (Stratagene, La Jolla, CA, USA). Each of them was obtained by mutagenic PCR using the expression vector pFLAG1 containing the VPi (pFLAG1-VPi) or the VPi-br (pFLAG1-VPi-br) coding sequences as template, and two primers consisting of a direct and a reverse oligonucleotide designed complementary to opposite strands of the same DNA region containing the desired mutations. To obtain VPi-ss (A49C/A61C), a first PCR was carried out using pFLAG1-VPi as template and primers for A49C mutation, 5'-CC CTT CGT TTG ACT TTC CAC GAT **TGC** ATC GGT TTC TCT CC-3' (only direct sequences are shown here and below, with the changed triplets underlined and the mutations introduced in bold). Then, a second PCR was made using pFLAG1-VPi containing the A49C mutation as template and primers for A61C mutation, 5'-GGC GGA GGA GGA **TGT** GAC GGT TCC ATC ATC GCG-3'. VPi-br-ss was obtained using pFLAG1-VPi-br as template and primers for A49C and A61C mutations in two consecutive PCR reactions.

PCR reactions were carried out in an Eppendorf Mastercycler Pro S using 10 ng of template DNA, 250 μM each dNTP, 125 ng of both direct and reverse primers, 2.5 units of *Pfu* Turbo DNA polymerase AD (Stratagene) and the manufacture´s reaction buffer. Reaction conditions were as follows: (i) a "hot start" of 95°C for 1 min; (ii) 18 cycles at 95°C for 50 s, 55°C for 50 s and 68°C for 10 min; and (iii) a final cycle at 68°C for 10 min. The plasmids obtained from the mutagenic PCR were transformed into *Escherichia coli* DH5α for plasmid propagation. At least one positive clone of each variant was completely sequenced using an ABI 3730 DNA Analyzer (Applied Biosystem), checked and used to transform *E. coli* W3110 for protein expression.

2.3 Enzyme production, activation and purification

Native (i.e. wild-type recombinant enzyme) VP of *P. eryngii* (isoenzyme VPL2) and its mutated variants were expressed in *E. coli* W3110 after transformation with the corresponding expression vectors. Cells were grown in Terrific Broth medium (Sambrook and Russell, 2001) supplemented with 100 μg/ml of ampicillin at 37°C and 180 rpm until OD_{500}~1 (~3 h). Then protein expression was induced with 1 mM IPTG and cells were grown for a further 4 h. The apoenzyme accumulated in inclusion bodies and was recovered by solubilisation in 50 mM Tris-HCl

(pH 8.0) containing 8 M urea, 1 mM EDTA and 1 mM DTT for 1 h at 4°C. The subsequent *in vitro* folding of the solubilized protein was performed overnight at room temperature in a solution of 0.16 M urea, 20 μM hemin, 5 mM $CaCl_2$, 0.5 mM GSSG, 0.1 mM DTT and 0.1 mg/ml protein in 20 mM Tris-HCl at pH 9.5. The refolded enzyme was purified by Resource-Q chromatography using a 0-0.3 M NaCl gradient (2 ml/min flow rate, 20 min) in 10 mM sodium tartrate (pH 5.5) containing 1 mM $CaCl_2$. Finally the enzymes were dialyzed against 10 mM sodium tartrate (pH 5).

The purified native VP and its variants showed an R_z value (A_{407}/A_{280}) ~ 4 indicative of their high purity. Moreover, the UV-visible spectrum obtained in the 300-700 nm range was used to check the correct incorporation of heme into the enzyme (Pérez-Boada et al., 2002). Enzyme concentration was determined from the absorbance of the Soret band (ε_{407}= 150 mM^{-1} cm^{-1}) (Ruiz-Dueñas et al., 1999).

2.4 Kinetic studies

Oxidation of Mn^{2+} was estimated by the formation of Mn^{3+}-tartrate complex (ε_{328}= 6500 M^{-1} cm^{-1}) in 0.1 M sodium tartrate (pH 5) and that of VA by formation of veratraldehyde (ε_{310}= 9300 M^{-1} cm^{-1}) in the same buffer at pH 3 and 2.5. Oxidation of ABTS was followed by generation of its cation radical (ε_{436}= 29300 M^{-1} cm^{-1}) and that of RB5 by its disappearance (ε_{598}= 30000 M^{-1} cm^{-1}) both in 0.1 M tartrate buffer at pH 3.5 (RB5 also at pH 3). H_2O_2 concentration was determined using ε_{240}= 39.4 M^{-1} cm^{-1} (Nelson and Kiesow, 1972). All enzymatic activities were measured as initial velocities taking linear increments (decreases for RB5) in the presence of 0.1 mM H_2O_2 using a Shimadzu UV-1800 spectrophotometer.

Values and standard errors for apparent affinity constant (Michaelis constant, K_m) and maximal enzyme turnover (catalytic constant, k_{cat}) were obtained fitting the experimental measurements to the Michaelis-Menten model with SigmaPlot 12.0 software (Systat. Software Inc, California). Fitting of these constants to the normalized Michaelis-Menten equation $v = (k_{cat}/K_m)[S]/(1+[S]/K_m)$ yielded enzyme efficiency values (k_{cat}/K_m) with their standard errors.

2.5 Optimum pH determination

The optimum pH for oxidation of different substrates was determined by measuring the enzymatic activity of the native VP and its mutated variants at saturating concentrations of VA (20 mM), RB5 (15 μM) and ABTS (7 mM) in 0.1 M Britton-Robinson (B&R) buffer (Britton and Robinson, 1931), and Mn^{2+} (6 mM) in 0.1 M sodium tartrate over the pH range 2.5-5.5, using 0.1 mM H_2O_2 and 0.01-0.03 μM enzyme.

2.6 pH stability studies

The enzymes were incubated at pH 3, 3.5 and 7 in 0.1 M B&R buffer at 25˚C for 120 h. Their residual activity was estimated after 1 min, 1 h, 4 h, 24 h and 120 h incubation by measuring the oxidation of ABTS (2 mM) using 0.1 mM H_2O_2 and 0.01 μM of enzyme in 0.1 M sodium tartrate (pH 3.5). The activity obtained with the sample incubated for 1 min at pH 5 was taken as reference (maximum activity). UV-visible spectra in the 300-700 nm range and absorbance at the Soret band (407 nm) were recorded during the incubation at pH 3, 3.5 and 7 by using an Agilent 8453 diode array spectrophotometer.

2.7 Thermal stability studies

The enzymes were incubated at different temperatures (30-80˚C) in 10 mM sodium tartrate (pH 5) for 10 min using a Thermo Shaker TS-100 BIOSAN, and then chilled on ice for 5 min. Their residual activity was measured by ABTS (2 mM) oxidation using 0.1 mM H_2O_2 and 0.01μM enzyme in 0.1 M sodium tartrate (pH 3.5), at 25 °C. The activity of the enzyme measured before incubation at each temperature was taken as reference (maximum activity) to calculate the percentage of residual activity. Data of residual activity for each temperature were fitted to a sigmoidal model and T_{50} values (temperature at which the activity is half of the initial one after 10 minutes of incubation) were calculated from the fit.

2.8 Crystallization

Crystallization trials were carried out by the sitting drop vapor diffusion method, using 96-well MRC2 plates with 50 μl reservoir solution and the

commercially available screenings from Emerald (Wizard classic crystallization screens I, II and III) and Jena Biosciences (JBScreen Classic Kits 1-10). Drops consisted of 0.2 µl of protein solution (10 mg/ml in 10 mM sodium tartrate buffer at pH 5.0) and 0.2 µl of reservoir solution. Crystallization was carried out at 22°C. Crystals suitable for X-ray data collection were obtained from these initial trials. Crystals of the mutant VPi were obtained in 0.1 M sodium MES buffer at pH 6.5, 25% PEG 4000 and 0.2 M $MgCl_2$; and cryoprotected with 20 % glycerol. Crystals of the mutant VPi-br were obtained in 10 % PEG 4000 and 20% 2-Propanol; and cryoprotected with Paratone-N oil. Crystals of the mutant VPi-ss were obtained in 0.1 M sodium citrate buffer at pH 5.4, 12% PEG 4000 and 0.2 M calcium acetate; and cryoprotected with Paratone-N oil.

2.9 Data collection and processing

Crystals were mounted in nylon loops and flash-frozen in liquid nitrogen in the mother liquor containing the cryoprotectant indicated above. All diffraction data were obtained at 100 K. X-ray diffraction intensities were collected at SOLEIL (Gyf-sur-Yvette, France) and ALBA (Barcelona, Spain) synchrotrons. Diffraction data were indexed, integrated, merged and scaled using the program XDS (Kabsch, 2010). Data collection statistics are shown in **Table 1**.

The structures of the three mutants were solved by molecular replacement using the crystal structure of *P. eryngii* VPL (3FMU) as the search model and the program PHASER implemented in the PHENIX package (Adams et al., 2010). The final models were obtained by consecutive rounds of refinement, performed with the PHENIX package; followed by manual model building, performed with Coot (Emsley et al., 2010) using σ_A weighted 2Fo-Fc and Fo-Fc electron density maps. Solvent molecules were introduced in the structure automatically in the refinement as implemented in the PHENIX package and visually inspected. A total of 5 % of reflections was used to calculate the R_{free} value throughout the refinement process. The structures were validated using MolProbity (Chen et al., 2010; Davis et al., 2007). Refinement and final model statistics are summarized in **Table 1**. The coordinates and structure factors have been deposited with the Protein Data Bank

accession codes 5ABN, 5ABO and 5ABQ. All figures were produced with PyMOL.

Table 1. Data collection and refinement statistics.

Data collection	VPi	VPi-br	VPi-ss
Space group	P 2_1 2_1 2_1	P 2_1 2_1 2_1	P 2_1 2_1 2_1
Cell constants	a=46.6;b=68.5,c=84.9	a=54.8,b=64.2,c=95.4	a=45.9,b=68.8,c=87.8
Resolution range (Å)	50.00-2.20(2.33-2.20)	50.00-1.10(1.16 - 1.10)	50.00-2.30(2.43-2.30)
Nº of total reflections	183536	1331552	134131
Nº of unique reflections	14447	135701	12985
R_{merge} (%)	9.1 (76.9)	6.9 (109.4)	12.0 (56.5)
Completeness (%)	99.9 (99.3)	97.9 (86.7)	99.9 (99.5)
<I/σ(I)>	18.6 (3.2)	15.3 (1.2)	13.9 (3.2)
Multiplicity	12.7 (13.0)	9.8 (6.0)	10.3 (10.7)
CC(1/2)	99.9 (97.4)	99.9 (56.0)	99.8 (97.2)
Solvent content (%)/ Matthews coef.	35.27 / 1.90	47.96 / 2.36	40.87 / 2.08
Subunits per asymmetric unit	1	1	1
Wilson B factor (Å^2)	46.9	15.7	46.3
Refinement			
Resolution range	50.0 - 2.20 Å	50.0 - 1.10 Å	50.00 - 2.30 Å
Working reflections	14361	135667	12942
R_{work} / R_{free}	20.6 / 27.5 %	13.4 / 14.4 %	24.8 / 30.0 %
Protein atoms (non H)	2407	2360	2315
Heme group	1	1	1
Ca^{2+}	2	2	4
Water molecules	31	449	65
Mg^{2+} ions	2	-	-
Mean B factors (Å^2)			
Protein atoms(non H)	67.70	15.69	64.24
Heme group	36.66	11.78	36.64
Ca^{2+}	48.03	10.44	57.35
Water molecules	47.71	27.32	48.27
Mg^{2+} ions	51.11	-	-
Deviations from ideality			
rmsd bond lengths	0.010 Å	0.010 Å	0.003 Å
rmsd angles	1.337°	1.454°	0.772°
Ramachandran plot statistics			
Preferred %	91.67	97.76	91.94
Allowed %	5.25	2.24	7.74
Outliers %	3.09	0.00	0.32
PDB code	5ABN	5ABO	5ABQ

3. Results

3.1 Rational design strategy

P. eryngii VP (isoenzyme VPL2) and *P. ostreatus* MnP4 share a common structural scaffold (**Fig. 1A**). Their crystal structures (PDB entries 2BOQ for VP, and 4BM1 for MnP4) superimpose with a root mean square deviation (rmsd) of only 0.75 Å between the C_α positions over 316 amino acid residues, covering 95% of the mature proteins. This high structural similarity between both proteins was the basis of our strategy aimed to improve the pH stability of VP, which consisted in identifying

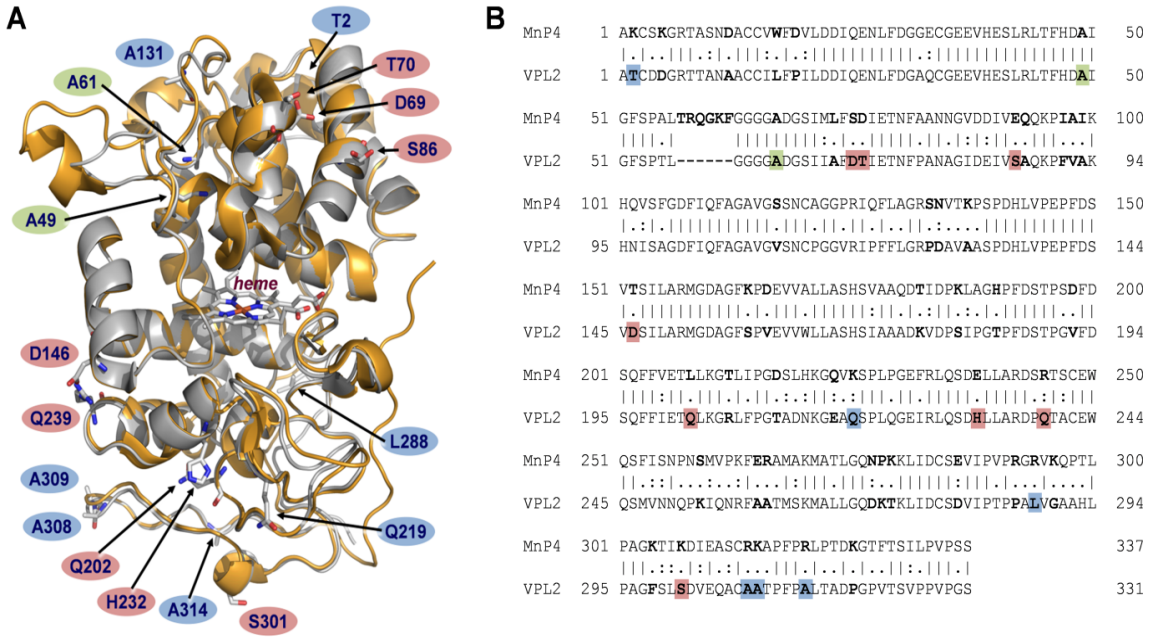

Figure 1. Structural and amino acid sequence alignment of VP (isoenzyme VPL2) from *P. eryngii* and MnP4 from *P. ostreatus*. (A) Superimposition of VP (PDB 2BOQ) (grey) and MnP4 (PDB 4BM1) (orange) crystal structures (shown as cartoons) highlighting the VP amino acid residues mutated in this work (shown together with the heme group as CPK-colored sticks, and labeled according to the color code described below); and (**B**) alignment of their amino acid sequences (labeled using the same color code) (vertical lines denote conserved residues, and colons and periods indicate conservative and semi-conservative substitutions, respectively). Residues explored in the structural comparative analysis of VP and MnP4 searching for putative stabilizing motifs are shown in bold in the amino acid sequence alignment. VP amino acids subsequently substituted with those of MnP4 to generate the VPi variant appear on red background; those substituted by basic residues present in MnP4, introduced into VPi to form the VPi-br variant, are shown on blue background; and alanines substituted by cysteines to form an extra disulfide bridge in VPi resulting in the VPi-ss variant are highlighted on green background.

the stabilizing motifs putatively contributing to the high stability towards pH of MnP4, and their subsequent transfer into VP. First, the amino acid sequences of these two enzymes were aligned (a 63% sequence identity was found) (**Fig. 1B**). They differ in 124 amino acids, 27 being charged residues in MnP4 and non-charged in VP (while VP only has 11 charged residues being neutral in MnP4). In order to identify those contributing to pH stability in MnP4, a comparative analysis of their position in the molecular structures and interaction with surrounding residues was performed by walking on the superimposed crystal structures of MnP4 and VP on the protein surface. The internal regions of the structures were not explored and subsequent changes at these locations were not performed in VP, with only one exception as described below. Our idea was to substitute only a few amino acid residues in the VP molecular structure minimizing the impact on the catalytic sites to maintain the activity. It is well known that a very subtle equilibrium between stability and activity exits and the improvement of one of these properties is often at the expense of the other.

Four regions exposed to the solvent were identified in the MnP4 molecular structure (**Fig. 2**, left column) as hotspots for rational design of a VP with improved stability. These regions exhibit extra ion pairs and hydrogen bond networks in MnP4, compared with VPL2 (**Fig. 2**, middle column), which are responsible for strengthening helix-helix, loop-helix and intra-loop interactions. Based on these observations and considering that most ion pairs have a stabilizing role (Kumar and Nussinov, 2002), a VP variant (VPi) containing eight substitutions (D69S/ T70D/ S86E/ D146T/ Q202L/ H232E/ Q239R/ S301K) was engineered by introducing the residues involved in these interactions in the four targeted regions. After verifying its increased pH stability (studies described below), new putative stabilizing residues were searched in MnP4. A high number of basic residues with their side chains exposed to the solvent, most of them with no movement restrictions by interactions with surrounding amino acids, were identified in MnP4 (31 of a total of 34 present in the protein, including 20 lysines and 11 arginines). Seven of these exposed residues (4 lysines and 3 arginines) were introduced into VPi, and the VPi-br variant

containing the 8 mutations present in VPi plus mutations T2K/A131K/ Q219K/L288R/A308R/A309R/A314R was obtained.

A third approach to improve the stability of VP was the further structural stabilization of the distal Ca^{2+}-binding site, responsible for maintaining the relative position of the distal histidine involved in enzyme activation by H_2O_2. For that, the VPi-ss variant was designed by adding a double mutation (A49C/A61C) to VPi. The two cysteines added

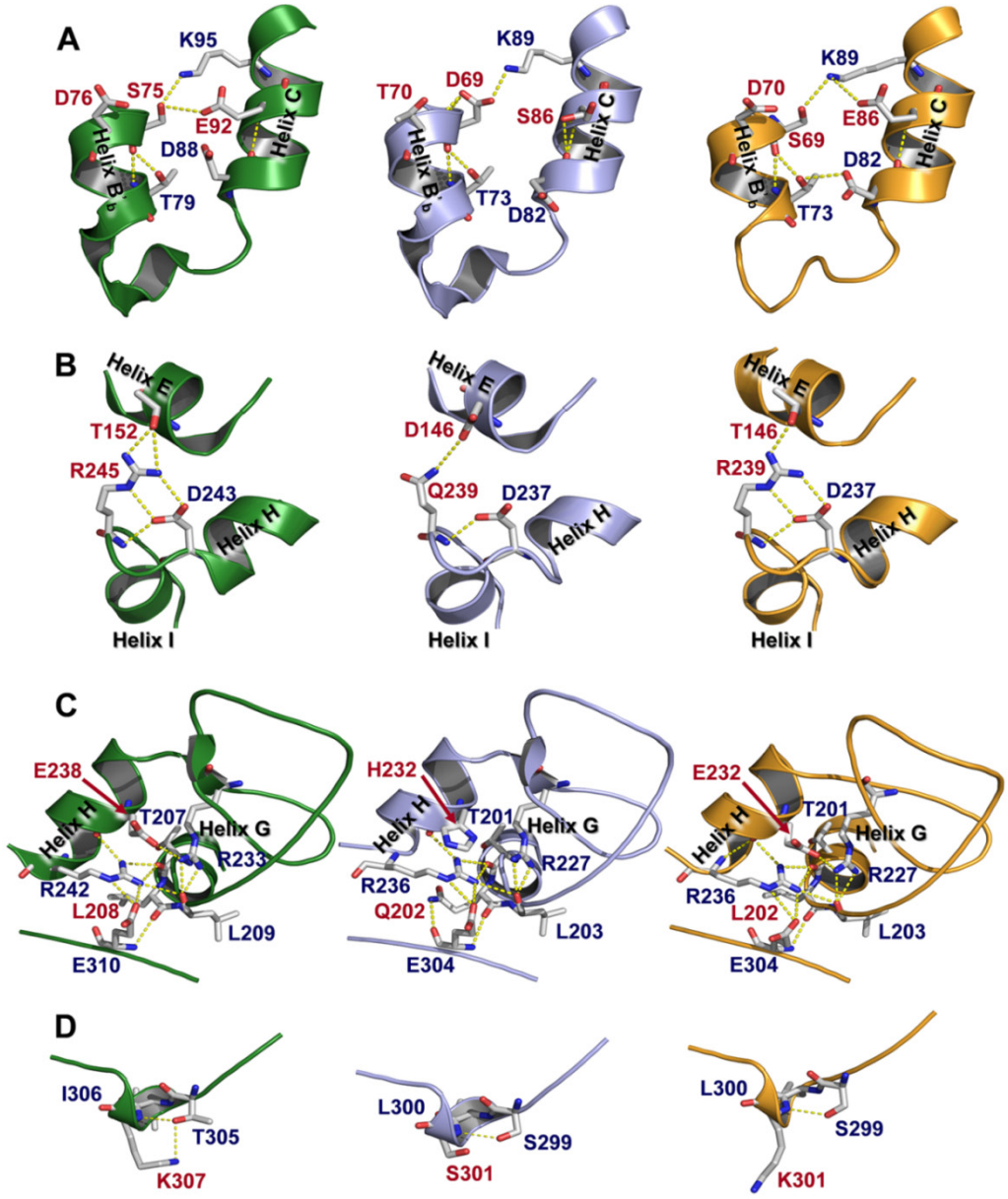

Figure 2. Structural details of four solvent exposed regions (A, B, C and D) in MnP4 (left column), VP (middle column) and VPi variant (right column). Residues mutated in VPi and their homologous in MnP4 and VP are highlighted in red color.

to this variant should form an extra disulfide bond contributing to the structural stabilization of the loop containing two of the four amino acid residues that coordinate the distal Ca^{2+} ion. Finally, the VPi-br-ss variant was designed by combining all the mutations described above in a single VP molecule. The four purified VP variants exhibited the characteristic UV-visible absorption spectrum of the native VP showing relative maxima at 407 nm (Soret band), and at 505 and 637 nm (charge transfer bands CT2 and CT1, respectively) (**Fig. 3**), which is indicative of an active peroxidase with a high-spin ferric heme (Pérez-Boada et al., 2005). These results proved the correct heme incorporation in the recombinant enzymes.

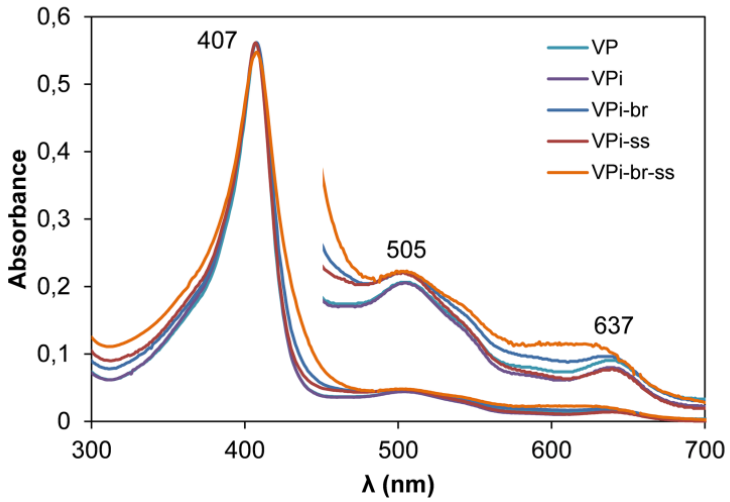

Figure 3. Electronic absorption spectra of native VP and variants VPi, VPi-br, VPi-ss and VPi-br-ss. The spectra were obtained in 10 mM sodium tartrate, pH 5, at 25 °C (details of the 450 nm-700 nm region are shown in x4 scale).

3.2 Effect of the mutations on VP catalytic properties

Native VP and the designed variants were kinetically characterized at the three catalytic sites characteristic of this ligninolytic peroxidase (Mn^{2+} oxidation site, main heme access channel and catalytic Trp exposed to the solvent) (Ruiz-Dueñas et al., 2009) (**Table 2**). The optimum pH for oxidation of four different substrates was also determined (**Fig. 4**), in both cases with the aim of identifying potential effects on the catalytic activity due to the mutations introduced.

Three of the four variants exhibited a catalytic efficiency for Mn^{2+} oxidation similar to that of the native enzyme. VPi-br-ss was the most affected variant, with only a 40% decrease in efficiency, and all of them (including native VP) showed the same pH activity profile with the optimum at pH 4.5-5 (**Fig. 4A**). With respect to the catalytic activity at the main heme access channel, the optimum pH (3.5) for ABTS oxidation did not experience any variation in the four variants (**Fig. 4B**), although their catalytic efficiency suffered a 35-70% decrease at this pH. The activity of native VP (and that of VPi-br and VPi-br-ss) oxidizing ABTS was dramatically reduced at pH 3 (**Fig. 4B**). By contrast, VPi and VPi-ss showed high activity levels with this substrate at this pH, and a 2.7 and 2.3-fold improved catalytic efficiency, respectively, compared with the native enzyme at its optimum pH (**Table 2**).

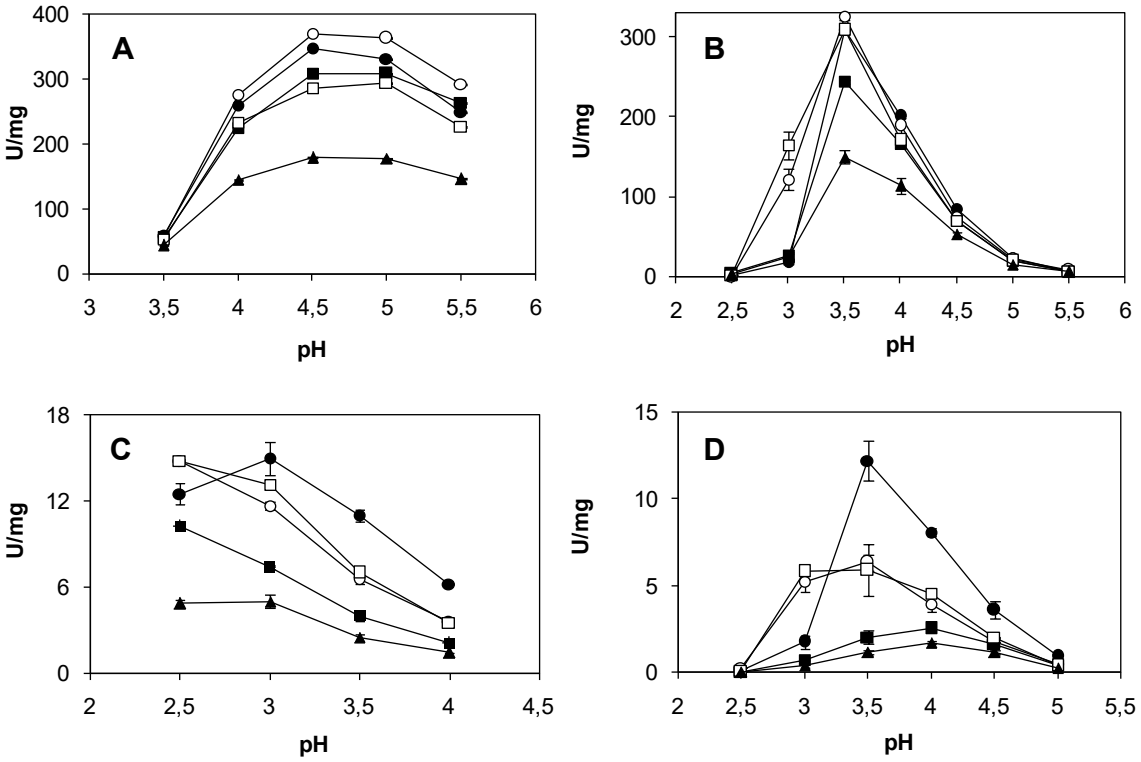

Figure 4. Optimum pH for oxidation of Mn^{2+} (A), ABTS (B), VA (C) and RB5 (D) by native VP (●), VPi (○), VPi-br (■), VPi-ss (□) and VPi-br-ss (▲). Reactions in 0.1 M B&R buffer for ABTS (7 mM), VA (20 mM) and RB5 (15 mM) oxidation; and 0.1 M sodium sodium tartrate for Mn^{2+} oxidation (pH 2.5-5.5), with 0.1 mM H_2O_2 at 25°C. Means and 95% confidence limits are shown.

Table 2. Steady-state kinetic constants [k_{cat} (s^{-1}), K_m (μM), Ef = k_{cat}/K_m (s^{-1} mM^{-1})] of native VP and mutated variants for oxidation of Mn^{2+} (at the Mn-binding site), ABTS (at the main heme access channel), and VA and RB5 (at the catalytic Trp exposed to the solvent)[a].

		VP	VPi		VPi-br	VPi-ss		Vpi-br-ss
Mn^{2+}	k_{cat}	211 ± 4	217 ± 3		160 ± 2	170 ± 2		133 ± 2
	K_m	130 ± 11	106 ± 6		120 ± 7	83 ± 5		134 ± 1
	Ef	**1641 ±132**	**2055 ± 106**		**1340 ± 64**	**2041 ± 112**		**997 ± 73**
ABTS	k_{cat}	208 ± 6	103 ± 4	73 ± 2 [b]	125 ± 4	216 ± 15	264 ± 9 [b]	104 ± 5
	K_m	1020 ± 74	797 ± 86	131 ± 12 [b]	1800± 150	2710 ± 380	575 ± 49 [b]	1660 ± 180
	Ef	**204 ± 10**	**130 ± 10**	**558 ± 39 [b]**	**69 ± 4**	**80 ± 6**	**459 ± 27 [b]**	**62 ± 4**
VA	k_{cat}	5.8 ± 0.1	7.5 ± 0.2	11.1 ± 0.3 [c]	4.7 ± 0.1	9.8 ± 0.2	8.9 ± 0.3 [c]	3.1 ± 0.2
	K_m	2600 ± 190	4000 ± 390	3250 ± 300 [c]	5350 ± 470	3960 ± 250	2470 ± 270 [c]	3850 ± 800
	Ef	**2.2 ± 0.1**	**1.9 ± 0.1**	**3.4 ± 0.2 [c]**	**0.9 ± 0.1**	**2.5 ± 0.1**	**3.6 ± 0.3 [c]**	**0.8 ± 0.1**
RB5	k_{cat}	5.5 ± 0.3	4.5 ± 0.1	8.4 ± 0.3 [b]	3.3 ± 0.2	5.5 ± 0.3	9.0 ± 0.2 [b]	3.5 ± 0.2
	K_m	3.4 ± 0.3	1.4 ± 0.1	0.4 ± 0.05 [b]	2.1 ± 0.3	3.2 ± 0.4	0.45 ± 0.03 [b]	1.8 ± 0.2
	Ef	**1.6 ± 0.1**	**3.1 ± 0.1**	**19.3 ± 1.8 [b]**	**1.5 ± 0.1**	**1.7 ± 0.1**	**19.9 ± 1.0 [b]**	**2.0 ± 0.2**

[a] Reactions at 25 °C in 0.1 M sodium tartrate (pH 5 for Mn^{2+}, pH 3.5 for ABTS and RB5, and pH 3 for VA). Kinetic constants of VPi and VPi-ss for oxidation of ABTS and RB5 were also measured at pH 3[b], and for VA at pH 2.5[c]. Means and 95% confidence limits are shown.

Finally, the catalytic activity at the exposed Trp164 responsible for the oxidation of high redox potential substrates was characterized using VA (simple lignin model compound) and RB5 (recalcitrant diazo dye) as reducing substrates. VPi, VPi-ss and VPi-br shifted their optimum pH from 3 to 2.5 for VA oxidation (**Fig. 4C**), and VPi and VPi-ss widened the optimum pH range with RB5 (between pH 3 and 3.5) (**Fig. 4D**). In addition, with both substrates, the catalytic efficiency of VPi and VPi-ss at the lower pH values (pH 2.5 and 3 for VA and RB5 oxidation, respectively) was higher than that of the native enzyme at its optimum pH (**Table 2**).

This effect was more significant for RB5 oxidation, mainly due to a ~8-fold increased affinity (K_m = 0.4 μM for these variants *vs* 3.4 μM for the native enzyme), and much less important for VA oxidation (k_{cat} /K_m increasing from 2.2 s^{-1} mM^{-1} to 3.4 and 3.6 s^{-1} mM^{-1} in VPi and VPi-ss, respectively).

3.3 pH and thermal stability of VP variants

The stability of native VP and its mutated variants was evaluated during incubation at pH 3, 3.5 and 7, both by measuring the residual activity (**Fig. 5**) and by monitoring the evolution of the UV-visible spectra (**Fig. 7**). The decrease of the Soret band at 407 nm, typical of a stable native VP at pH 5 (Pérez-Boada et al., 2005), was followed as an indicative of the integrity of the heme environment (**Fig. 6**).

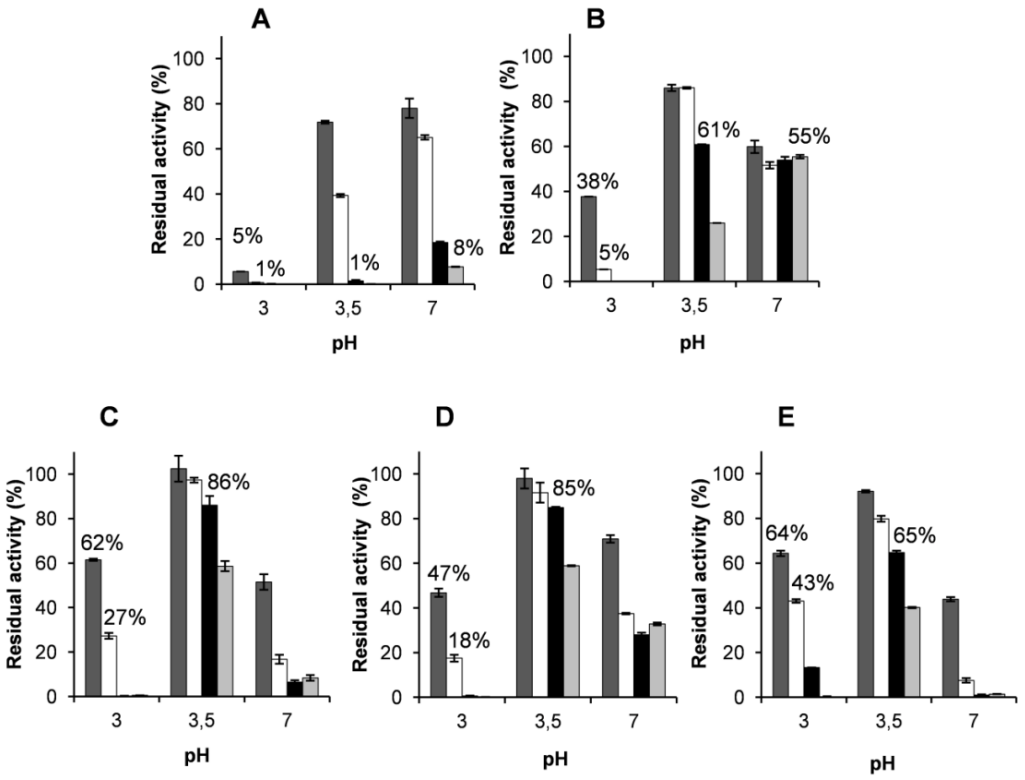

Figure 5. pH stability of native VP (A) and mutated variants VPi (B), VPi-br (C), VPi-ss (D) and VPi-br-ss (E). The enzymes were incubated in 0.1 M B&R buffer (at pH 3, 3.5 and 7) at 25°C, and their residual activity was measured after 1 (■), 4 (□), 24 (■) and 120 h (■), with 7 mM ABTS and 0.1 mM H_2O_2 in 0.1 M sodium tartrate pH 3.5, and referred to activity after 1 min incubation at pH 5. Means and 95% confidence limits are shown.

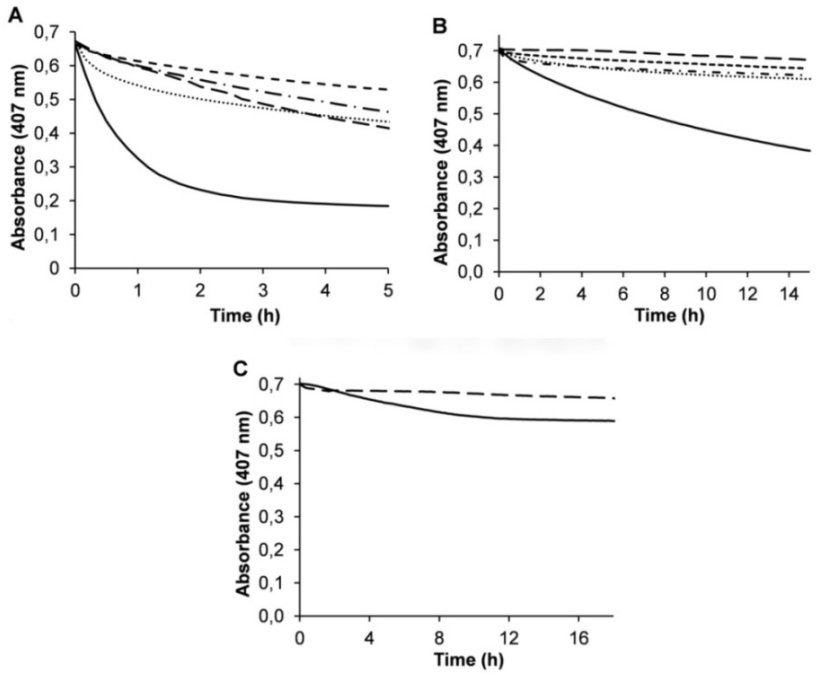

Figure 6. pH stability of native VP and its mutated variants monitored as the absorbance of the Soret band at 407 nm. VP (—), VPi (— —), VPi-br (— · —), VPi-ss (----) and VPi-br-ss (····) were incubated in 0.1mM B&R buffer at pH 3 (**A**), pH 3.5 (**B**) and pH 7 (**C**) and 25°C.

The results revealed that VPi is significantly more stable than native VP at acidic and neutral pH. The 7-fold stability improvement observed after 1 h of incubation at pH 3 was very limited in time since both the native enzyme and the mutated variant were nearly completely inactivated after 4 h of incubation (**Figs. 5A and B**). By contrast, the improvement at pH 3.5 and 7 was more extended in time. VPi retained 61% (at pH 3.5) and 55% (at pH 7) of the initial activity after 24 and 120 h, respectively, compared with the native enzyme which resulted almost completely inactivated under the same experimental conditions.

This stability improvement, measured as a percentage of the initial activity, could be correlated with the increased stability of the heme environment as revealed from the analysis of the electronic absorption spectra obtained for native VP and VPi. Although the two enzymes suffered strong changes in their UV-visible spectra at pH 3 (**Figs. 7A and D**), these changes were quantitatively less significant for VPi. A faster decrease in the intensity at 411 nm (Soret band) and 507 nm (CT2 band) was observed for native VP (**Fig. 7A**), with the Soret maximum progressively blue-shifting (39 nm) to attain a maximum at 372 nm after 5 h.

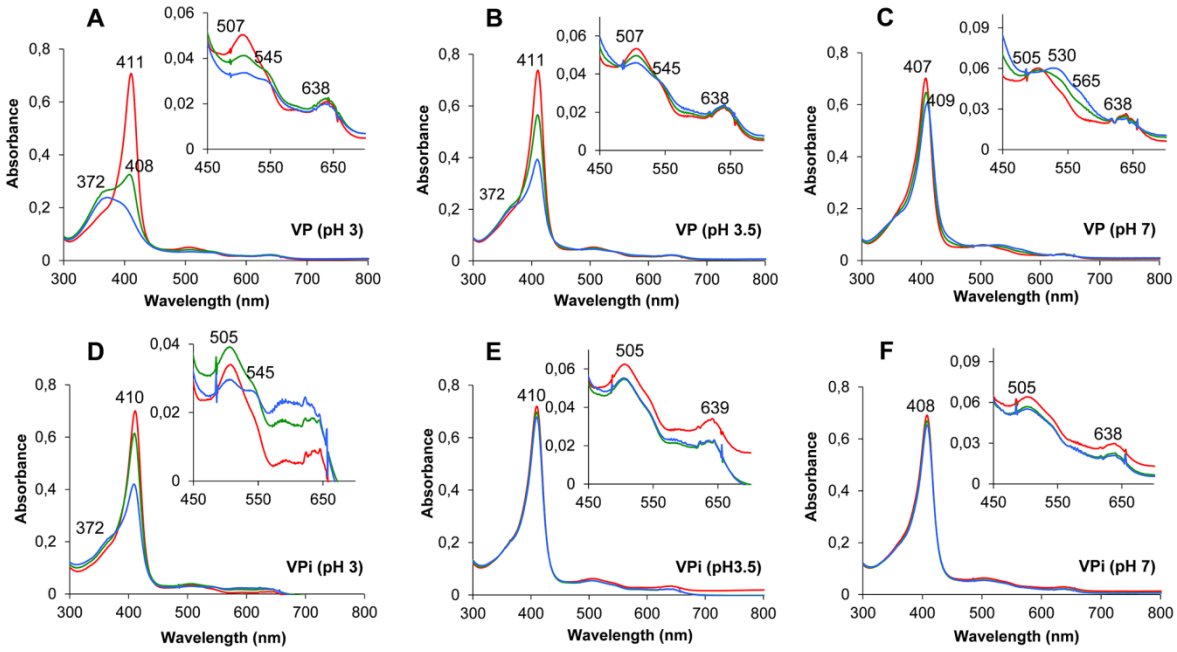

Figure 7. Time course of the electronic absorption spectra of native VP (top) and VPi (bottom) at acidic and neutral pH. UV-visible spectra of native VP and VPi after 0 (red line), 1 (green line) and 5 h (blue line) incubation at pH 3 (**A** and **D**), 3.5 (**B** and **E**) and 7 (**C** and **F**) in 0.1 M B&R buffer, at 25°C.

A shoulder at 545 nm (β band) and a maximum at 638 nm (CT1 band) were observed over the entire time of the experiment in both native VP and VPi. The spectrum described for the native VP after 5 h at pH 3 (exhibiting maxima at 372, 507, 545 and 638 nm) is compatible with that of a four-coordinate heme. During these 5 h, VPi experienced a 38% decrease in the maximum at 410 nm with a shoulder appearing near the 372 nm region (**Fig. 7D**). This spectrum has intermediate characteristics between those of the native VP incubated at pH 3 and those previously described for the native VP at pH 4.5 (maxima at 409, 505 and 638 nm) (Pogni et al., 2006) at which the enzyme has been described to be a stable high-spin heme protein. These spectral characteristics suggest that at least two VPi species are present under these conditions, one with the iron four-coordinated, and the other with the iron also coordinated by the proximal histidine. This indicates that VPi moves much more slowly than the native enzyme towards destabilization of the heme environment at pH 3.

On the other hand, only slight modifications were observed in the spectra of VPi both at pH 3.5 and 7 after 15 h of incubation (**Figs. 7E and**

F) unlike what happened with the native enzyme (**Figs. 7B and C**). Native VP experienced a sharp drop in the Soret band at pH 3.5, following the same spectral evolution described for the enzyme incubated at pH 3, although with less dramatic changes (**Figs. 7B and 6B**). The spectral changes at pH 7 exhibited a different behavior. A slight drop and shift of the Soret band to 409 nm were observed concomitantly with both the progressive disappearance of the CT2 and CT1 bands (at 505 and 638 nm respectively), and the increasing of α and β bands at 565 and 530 nm at this pH (**Figs. 7C and 6C**) suggesting an hexacoordinated heme iron. Interestingly, the almost undetectable changes in the spectrum of VPi at pH 3.5 and 7 contrast with the loss of 39% (at pH 3.5) and 45% (at pH 7) of the initial activity after 24 h. All these results together suggest that the mutations introduced at residues exposed to the solvent in VPi ultimately contribute to increase the stability of the heme environment, necessary for activity of ligninolytic peroxidases. However, this does not seem to be enough to completely stabilize the enzyme.

VPi-br harboring seven additional basic residues exposed to the solvent, and VPi-ss containing two cysteines added to form an additional extra disulfide bond, further improved the stability of VPi at acidic pH (**Figs. 5C and D**, respectively). Both variants retained 86% and 85% of the initial activity at pH 3.5 after 24 h of incubation compared to the 61% retained by VPi and far from the 1% of the native VP. Moreover, although they were not so stable at pH 3 as at pH 3.5, VPi-br and VPi-ss maintained 62% and 47% of the initial activity, respectively, at pH 3 after 1 h compared to the 38% showed by VPi and the 5% of native VP. The analysis of the UV-visble spectra of these two variants over time evidenced an evolution of the Soret band similar to that observed for VPi (**Figs. 6 and 8**). This is indicative of the integrity of the heme and its environment at acidic pH. Unlike what observed at low pH, VPi-ss only exhibited a slight increased stability after 1 h incubation at pH 7 compared with VPi (**Fig. 5D**). Both VPi-br and VPi-ss not only did not show an additional improvement at longer times at neutral pH but, on the contrary, VPi-br significantly reversed the improvement attained in VPi (**Fig. 5C**). The accumulation of all the mutations in the VPi-br-ss variant retained or slightly improved the stability of VPi-br and VPi-ss at

pH 3 (43% of residual activity after 4 h) but worsen at pH 7 being even less stable than the native VP at this pH (**Fig. 5E**).

Regarding thermal stability, VPi, VPi-br and VPi-ss exhibited T_{50} values between 58°C -60°C (**Fig. 9**). These values are similar to that found for the native VP (61°C) and higher than that obtained for VPi-br-ss that showed a T_{50} of 55°C (6° C lower than that of the native VP).

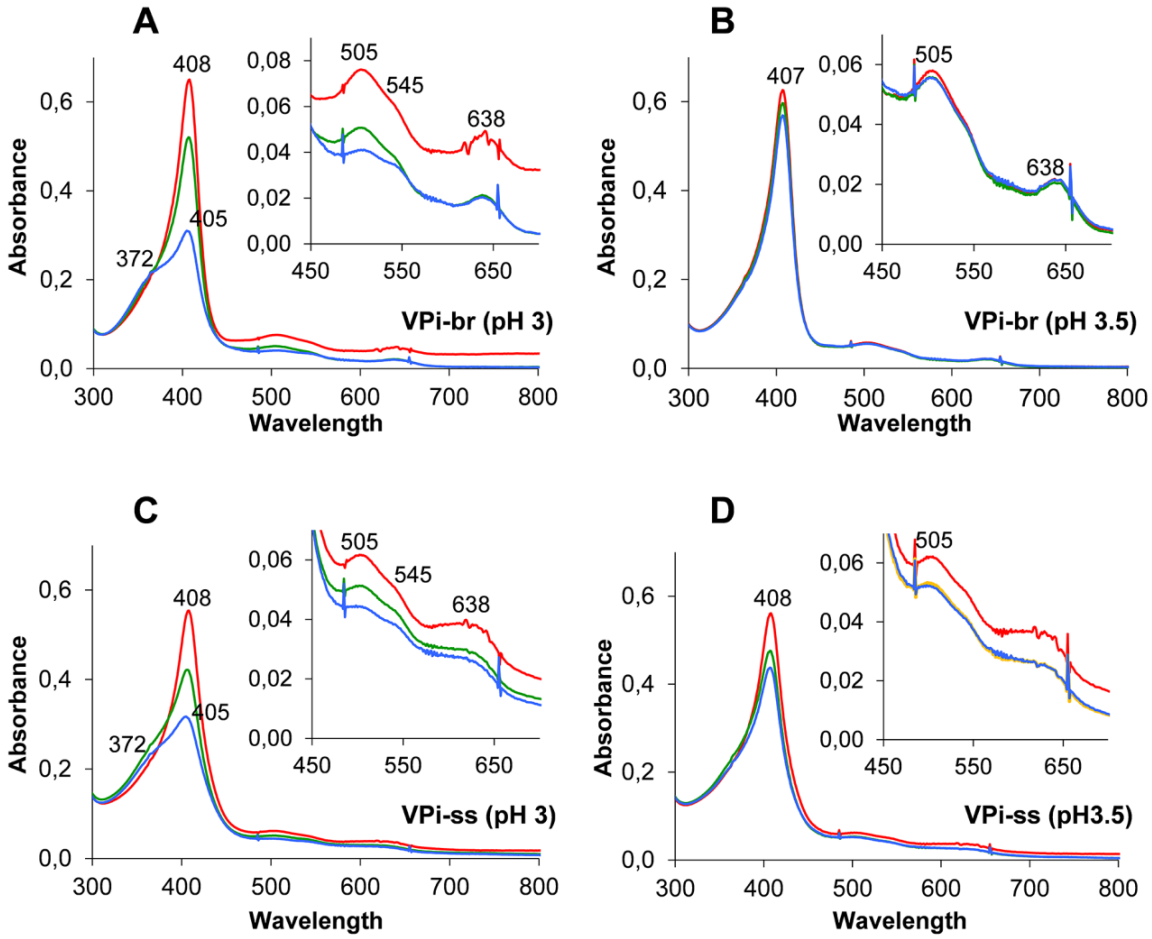

Figure 8. Time course of the electronic absorption spectra of VPi-br (top) and VPi-ss (bottom) at acidic pH. UV-visible spectra of Vpi-br and Vpi-ss after 0 (red line), 1 (green line) and 5 h (blue line) of incubation at pH 3 (**A** and **C**) and 3.5 (**B** and **D**) in 0.1 M B&R buffer at 25°C.

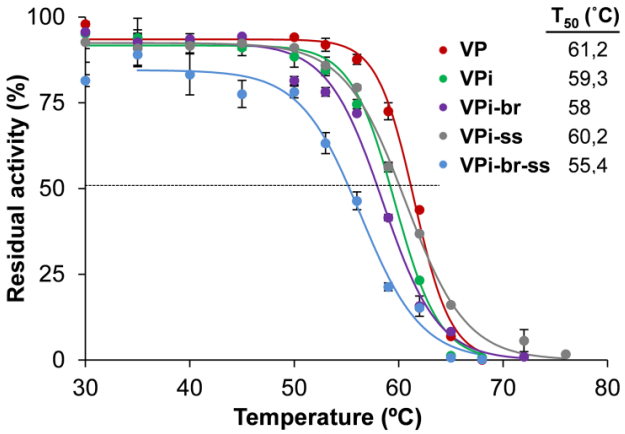

Figure 9. T_{50} profiles of native VP and four designed mutated variants. Residual activity was estimated from ABTS oxidation in 0.1 M sodium tartrate, pH 3.5.

3.4 Crystal structure analysis of the VP variants

Crystal structures of VPi, VPi-br and VPi-ss showing enhanced pH stability were solved (**Table 1**) and subsequently analyzed both to verify that the mutations introduced had generated the expected stabilizing motifs and to explain how these motifs contribute to increase the enzyme stability. The overall folding characterizing the native VP, as well as the key elements that maintain its molecular architecture (i.e. two structural Ca^{2+} ions and four disulfide bonds), and position of the heme group, appear conserved in the three mutated variants (**Fig. 10A** shows these elements in VPi). The structural changes observed are in general restricted to the regions where mutations were introduced.

VPi includes eight mutations distributed into four solvent-exposed regions (named A-D in **Fig. 10A**). Region A (containing mutations D69S/T70D/S86E) is located at the heme distal side above the heme plane, whereas regions B, C and D (containing mutations D146T/Q239R, Q202L/H232E and S301K, respectively) are found at the proximal side below the heme plane. The three mutations introduced in region A fail to emulate the contacts identified in MnP4 (**Fig. 2A**, left). However, compared with the native VP (**Fig. 2A**, middle), they contribute to reinforce the interaction between helices B'_b and C by increasing the H-bond network in this area, as shown in the crystal structure (**Fig. 2A,** right). Similarly, the two substitutions in region B strengthen the loop between helices H and I by interaction of the Arg239 guanidinium group

with the Asp237 carboxylate (**Fig. 2B**, right), mimicking that observed between Arg245 and Asp243 in MnP4 (**Fig. 2B**, left). In addition, the two mutated residues in this region (Thr146 and Arg239) are able to retain the H-bond that connects the loop between helices H and I with the N-terminal end of helix E established between Asp146 and Gln239 in the native VP (**Fig. 2B**, middle).

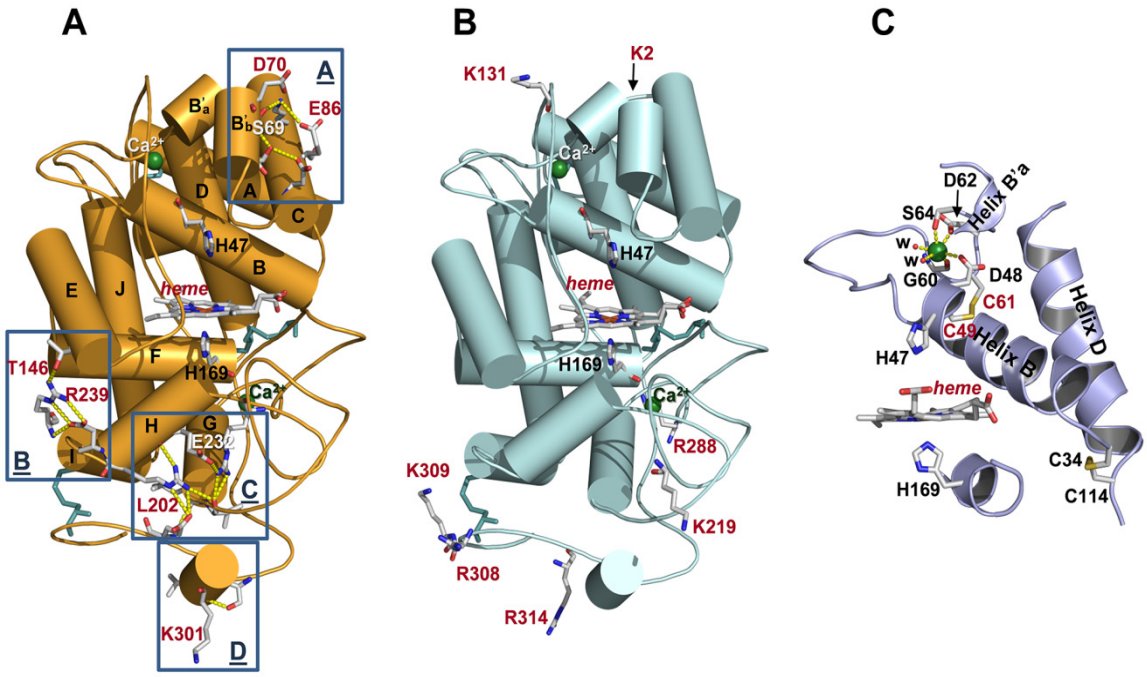

Figure 10. Crystal structures of VPi, VPi-br and VPi-ss variants. (**A**) Molecular structure of VPi (with 12 α-helices named from A to J, shown as cylinders) including general structural elements such as four disulfide bonds (cyan sticks) and two Ca^{2+} ions (green spheres); heme cofactor; the two catalytic histidines above and below the porphyrin plane; and mutated residues (all of them as CPK sticks) generating new H-bond and salt bridge interactions (yellow dashed lines) at four regions (named A to D) described in more detail in Fig. 2. (**B**) Molecular structure of VPi-br, showing the same general elements described for VPi plus the seven solvent-exposed basic residues characterizing this variant (mutations described in VPi are also included in VPi-br but they have not been represented for simplifying purposes). (**C**) Structural detail of the VPi-ss variant showing the extra disulfide bond (formed by Cys49 and Cys61) that connects helices B and B'a (shown as cartoons); the amino acid residues (CPK sticks) and water molecules (w) coordinating the distal Ca^{2+} ion; and one of the four disulfide bonds naturally existing in native VP between cysteine residues 34 and 114 that connects helices B and D (also depicted as cartoon) (heme and axial histidines are also shown).

Regarding the region C, the introduction of a glutamate at position 232 in helix H promotes the formation of a salt bridge between this amino acid and Arg227 (**Fig. 2C**, right) emulating that observed between Glu238 and Arg233 in MnP4 (**Fig. 2C**, left). This interaction, not existing in the native enzyme (**Fig. 2C**, middle), reinforces an extensive H-bond network that anchors the helix H both to the C-terminal end of helix G and to Glu304 located at the C-terminal region of the protein consisting of 66 residues without clearly defined secondary structures (except for two 3-amino acids β strands and a single turn 3_{10} helix). Finally, unlike what was described for the other regions, the S301K substitution included in region D (**Fig. 2D**, right) do not have the expected effect. This should consist in formation of a new H-bond, as observed in MnP4 (**Fig. 2D**, left). By contrast, the side-chain of Lys301 appears exposed to the solvent. Summarizing, three of the four protein regions containing mutations exhibit a modified distribution of hydrogen bonds and salt bridges that can be correlated with the improvement in pH stability previously described for the VPi variant.

VPi-br and VPi-ss crystal structures exhibited minor differences compared with VPi regarding the interactions involving the mutated residues in region A (VPi-br also regarding the interactions of residues in region C), and no significant changes were identified in the other regions described. The analysis of the VPi-br crystal structure also revealed that the seven solvent-exposed basic residues introduced in this variant present a configuration similar to that observed for the homologous residues in MnP4. Their side-chains appear interacting with water molecules through hydrogen bonds or do not present any interaction, and no contacts are observed with surrounding residues (**Fig. 10B**). Finally, the VPi-ss structure confirmed that the two cysteines introduced at positions 49 and 61 form an extra (fifth) disulfide bond next to the distal Ca^{2+} binding site (**Fig. 10C**). This region did not show any additional change compared with the native enzyme even though the two new cysteines occupy positions adjacent to Asp48, Gly60, Asp62 and Ser64 involved, together with two water molecules, in Ca^{2+} coordination.

4. Discussion

Over the last years several approaches have been addressed at molecular level with the aim to solve the main problems preventing the use of ligninolytic peroxidases in biotechnological applications, including high-yield production and stability to different factors (Smith and Doyle, 2006; García-Ruiz et al., 2012). Some properties of the ligninolytic peroxidases have been also improved by introducing structural determinants suggested to be responsible for thermal, pH and oxidative stability (Reading and Aust, 2000; Reading and Aust, 2001; Sáez-Jiménez et al., 2015), and similar results have been attained by directed molecular evolution using appropriate selection pressures (García-Ruiz et al., 2012; González-Pérez et al., 2014).

Recently, the development of next generation sequencing methods has allowed to sequence a large amount of genomes of ligninolytic basidiomycetes and a new array of high redox potential peroxidases has emerged (Martínez et al., 2014). Some of these new peroxidases have proved to be particularly stable under certain conditions and are being used as protein scaffolds that can be redesigned with the aim to provide enzymes with catalytic properties of interest (Fernández-Fueyo et al., 2014b). A recent study focused on the analysis of the *P. ostreatus* genome sequence obtained at JGI enabled the identification and characterization of the complete set of lignin-degrading peroxidases in this white-rot fungus (Fernández-Fueyo et al., 2014c; Ruiz-Dueñas et al., 2011), revealing strong differences in their stability properties and providing enzymes of biotechnological interest. Among these peroxidases, MnP4 has demonstrated to be especially stable at both acidic and moderately alkaline pH, and the same has been shown for a few other MnPs (Fernández-Fueyo et al., 2014a). By contrast, VPs are usually not so stable to pH. An example is VP from *P. eryngii* which is easily inactivated at neutral and basic pH as well as below pH 4 (Lú-Chau et al., 2004). VPs are more interesting than MnPs as industrial and environmental biocatalysts due to their wide substrate specificity (Ayala et al., 2008; Moreira et al., 2007; Marques et al., 2010; Ruiz-Dueñas and Martínez, 2009; Ruiz-Dueñas and Martínez, 2010; Salvachúa et al., 2013). That is the reason why we decided to take advantage of the structural similarities between MnP4 from *P. ostreatus* (Fernández-

Fueyo et al., 2014c) and the best characterized VP from *P. eryngii* (Ruiz-Dueñas et al., 2009) to identify the structural determinants responsible for such stability in MnP4 and transfer them to VP designing a more stable peroxidase of biotechnological interest.

The fact that only minimal changes are produced in the UV-visible spectrum of MnP4 incubated under acidic (pH 3) and moderately alkaline (pH 8) conditions has been reported to be indicative of the high stability of its heme environment (Fernández-Fueyo et al., 2014c). Unlike MnP4, two different pH-induced structural transitions were identified from the analysis of the electronic absorption spectra of the native VP incubated at acidic and neutral pH at which the enzyme is inactivated. On one hand, the spectral changes at low pH suggested that the interaction between the heme iron and the imidazole group of the proximal histidine is broken. This assumption was based on the high similarities observed between the UV-visible spectrum here obtained for native VP (with maxima at 372, 507, 545 and 638 nm) and that reported for an intermediate form of metmyoglobin (maxima at 370, 510, 545 and 640) in which this cleavage is produced during the acid transformation of the native state into an unfolded form (Palaniappan et al., 1994; Sage et al., 1991). Similar spectra were also obtained for horseradish and *Coprinopsis cinerea* peroxidases incubated at very low pH, and the same conclusions regarding the weakening and/or rupture of the histidine-iron bond were reached (Smulevich et al., 1997; Smulevich et al., 1996). On the other hand, the spectrum at neutral pH was characteristic of a VP with an hexacoordinated low-spin heme-iron (Verdín et al., 2006). According to previous studies, this form of the enzyme is the result of the formation of a bis-histidyl heme iron complex, in which both proximal and distal histidines are involved, due to loss of one or the two structural Ca^{2+} ions upon thermal (Nie and Aust, 1997b; Sutherland et al., 1997) or alkaline (George et al., 1999; Timofeevski and Aust, 1997) inactivation. An exhaustive characterization of a Ca^{2+}-depleted VP has been reported revealing that, although it can be activated by H_2O_2, its redox potential and catalytic activity are dramatically affected (Verdín et al., 2006).

Four variants (VPi, VPi-br, VPi-ss and VPi-br-ss) were designed to improve the pH stability of VP by introducing combinations of mutations

at different molecular regions, including: i) the amino acid residues responsible for the structural determinants (extra hydrogen bonds and ion pairs) identified in MnP4 as putatively involved in its high stability towards pH; ii) basic residues surface-exposed in MnP4 that are absent in VP; and iii) two cysteines to form an additional disulfide bond not present in MnP4, nor in other ligninolytic peroxidases, but described to play a stabilizing role at high temperature and pH in an engineered MnP (Reading and Aust, 2000; Reading and Aust, 2001). The analysis of the crystal structures of three of these VP variants (VPi, VPi-br and VPi-ss) confirmed the presence of the mutated residues and the structural determinants engineered. Consequently, they could be definitively related with the changes observed in enzyme stability.

Major improvements in stability at acidic and neutral pH resulted from the mutations introduced in VPi (also included in VPi-br, VPi-ss and VPi-br-ss). These mutations are responsible for extra hydrogen bond and salt bridge interactions in four specific regions exposed to the solvent. The introduced residues are located in key positions, anchoring different elements of the secondary structure. At the heme distal side, the reinforced interactions between helices B'_b and C covering helix B and distal Ca^{2+} binding site seem to stabilize the position of the distal histidine (located at helix B) involved in enzyme activation by H_2O_2 (Hiner et al., 2002). Similarly, the reinforced interactions between helices E, G, H, I, and a portion of random coil, all of them covering helix F at the heme proximal side, seem to be responsible for the stabilization of the proximal histidine (located at helix F) acting as the fifth heme iron ligand. The stabilization of the environment of this residue is critical taking into account that the strength of the interaction between this histidine and the heme iron has been proposed as one of the factors determining the high redox potential of ligninolytic peroxidases (Banci et al., 2003; Banci et al., 1991). In short, this analysis shows how mutations reinforcing specific regions of the overall structure ultimately contribute to stabilize the architecture of the heme pocket located inside the protein. Stabilization of this pocket is crucial since the redox potential and activation of peroxidases by H_2O_2 depend on the precise position of the above two histidines located immediately below and above the heme cofactor. This stabilization was definitively confirmed by the spectral analysis of VPi showing a stable pentacoordinate high-

spin heme-iron state at pH 3.5 and 7 characteristic of an active peroxidase (Pérez-Boada et al., 2005), unlike what observed for the native enzyme, where the breakdown of the proximal histidine-iron interaction (at pH 3-3.5) and iron hexacoordination by proximal and distal histidines (at pH 7) was produced.

In spite of the stabilization of the heme pocket, partial loss of activity was observed for VPi at pH 3.5 and pH 7 over time. Therefore, this is not enough to completely stabilize the enzyme, and structural changes affecting other protein regions are most probably produced both at acidic and neutral pH. The structural changes observed in MnP4 when incubated at pH 8 (Fernández-Fueyo et al., 2014c) support this idea. These changes were related with the loss of ~ 15% activity even though its UV-visible spectrum, and in consequence the heme environment, were completely stable.

A stable heme pocket was also observed in VPi-br, VPi-ss and VPi-br-ss at pH 3 and 3.5 as inferred from the analysis of the spectra and time course of their Soret maximum. These three variants contain those mutations previously described to stabilize the heme environment in VPi plus additional substitutions responsible for further stability improvements at acidic pH (basic residues in VPi-br, an extra disulfide bond in VPi-ss and both basic residues and a disulfide bond in Vpi-br-ss). We decided to design the VPi-br variant because the high number of basic residues exposed to the solvent identified in MnP4 led us to think that they could be also responsible for the stability of this enzyme at low pH. No other ligninolytic peroxidases from *P. ostreatus*, all of them less stable than MnP4 (Fernández-Fueyo et al., 2014c), nor VP from *P. eryngii* (including a total of 9 lysines and 9 arginines), have a similar number of basic residues with their ionizable side chains oriented to the solvent. The introduction of basic residues, mainly arginines, at the molecular surface has been described to improve pH stability (Liu et al., 2012; Sokalingam et al., 2012) as well as thermostability and other enzyme properties, including optimal temperature and pH, catalytic efficiency (Zhou et al., 2011; Deng et al., 2014), and stability to chemical denaturants (Sokalingam et al., 2012). In our case, the increased stability of VPi-br at acidic pH compared with VPi could be explained by a general stabilizing effect of the extra basic residues participating in

charge-charge interactions with other charged amino acids of the protein surface (although these interactions were not observed in the VPi-br crystal structure) and by interacting with the solvent improving the solubility of the protein. It should be also noted that the polar surface of the VPi-br variant is significantly increased with respect to VPi by replacing five hydrophobic residues (four alanines and leucine) with polar charged amino acids (four arginines and one lysine).

Regarding VPi-ss, the extra disulfide bond included in this variant further stabilized the enzyme at pH 3.5 by reinforcing the molecular structure at the distal heme side together with mutations D69S/T70D/S86E, whose stabilizing role in VPi has been described above. Cysteines forming the new disulfide bond (Cys49-Cys61) are located in a critical position. They are next to the residues involved in coordination of the distal Ca^{2+} ion (Asp48, Gly60, Asp62 and Ser64), which are adjacent to the position of the distal histidine (His47) located at helix B. This disulfide bond stabilizes a long 14 amino acids loop connecting helices B and B'a, and gives rigidity to the helix B, which remains anchored by two disulfide bonds (the new one at its N-terminal end, and that formed by Cys34-Cys114 binding the C-terminal ends of helices B and D) (**Fig. 10C**). In short, the extra disulfide bond contributes to stabilize the position of the distal histidine in helix B. This analysis, together with that previously performed for VPi, could explain the accumulative effect due to this disulfide bond and the extra hydrogen bond and salt bridge interactions on the VPi-ss stability improvement observed at pH 3.5. We expected a similar effect at pH 7 according to the results reported for an engineered MnP of *Phanerochaete chrysosporium* including a disulfide bond at the same position (Reading and Aust, 2000). At this pH, the structural destabilization (Reading and Aust, 2000) produced by the release of the distal Ca^{2+} ion should be compensated by the presence of the extra disulfide bond. However, VPi-ss did not show increased stability at neutral pH compared with VPi, unlike what was observed at pH 3.5. These differences again confirm that different mechanisms are eventually responsible for pH inactivation at acidic and neutral pH.

Thermal inactivation of ligninolytic peroxidases has also been correlated with the release of the structural Ca^{2+} ions (Sutherland et al.,

1997; Nie and Aust, 1997a). Increased thermostability has been observed in the aforementioned engineered MnP containing an extra disulfide bond (Reading and Aust, 2000), and electrostatic interactions on the protein surface have also been reported to be involved in thermal stabilization (Kumar and Nussinov, 2001). However, none of the designed VP variants including these structural determinants (VPi, VPi-ss and VPi-br-ss) exhibited a T_{50} value higher than that of the native enzyme (61.2 °C). This value is already high compared with those obtained for other recombinant (expressed in *E. coli*) ligninolytic peroxidases (T_{50} ranging from 56.8 to 38 °C after 10 min incubation) (Fernández-Fueyo et al., 2014a; Fernández-Fueyo et al., 2014c; Nie et al., 1999), and even compared with glycosylated wild-type LiP and MnP from *P. chrysosporium* (Nie et al., 1999). Moreover, thermal stability of native VP (88% residual activity after 30 min incubation at 37 °C, this work) was similar to that of LiP variants containing ancestral residues, which were recently designed with the aim of improving the thermal stability of this enzyme (Semba et al., 2015). This means that VP used in this work is naturally thermostable compared with other ligninolytic peroxidases. However, directed molecular evolution experiments have resulted in a VP variant with a T_{50} improvement of 8 °C over the parental type (García-Ruiz et al., 2012), showing that there is still some room to improve the VP thermal stability by protein engineering.

Something interesting from an applied perspective is the effect observed on the catalytic properties due to the mutations introduced. Affect them as little as possible was a premise of this work, and that was the reason why all substitutions were introduced far from the three catalytic sites present in VP. A small negative impact difficult to rationalize with the data in hand, was observed in some cases. The most noteworthy was the shifting of the optimum pH to a more acidic value for oxidation of high redox potential substrates at the solvent exposed catalytic tryptophan (Pérez-Boada et al., 2005) (VA oxidation by the four VP variants, and RB5 oxidation by VPi and VPi-ss). Two variants (VPi and VPi-ss) also improved its ability to oxidize low redox potential substrates (ABTS) at the main heme access channel (Morales et al., 2012) at a lower pH compared with the native enzyme at its optimum pH. A similar shifting has been reported for a long MnP intrinsically stable at acidic pH transformed into a VP by engineering an exposed

catalytic site (Fernández-Fueyo et al., 2014b). The improvement in affinity for RB5 and ABTS at the new optima pHs suggests a better positioning of these two large sulfonated substrates at the corresponding active sites most probably due to interactions with the distant residues introduced in these variants. On the other hand, the redox potential of heme peroxidases is strongly influenced by pH (Battistuzzi et al., 2010), and different studies have shown that the oxidative activity of these enzymes increases at acidic pH (Gazarian et al., 1996; McEldoon et al., 1995). The fact that the designed variants are more stable at low pH make them of special interest from a biotechnological point of view in processes (e.g. ligninolysis) favored by acidic pH (due to the increased redox potential of the heme cofactor when the pH decreases).

5. Conclusions

P. eryngii VP and *P. ostreatus* MnP4 share the same protein scaffold. The identification and subsequent transfer into VP of the structural determinants putatively responsible for the high stability towards pH of MnP4 allowed us to obtain four variants with an improved pH stability. The analysis of the crystal structures of three of them confirmed that the observed stability improvement is due to the introduction of such determinants, indirectly proving that they should also contribute to the pH stability of MnP4. A significant increased stability at both acidic and neutral pH was achieved by mutations contributing to generate extra hydrogen bond and salt bridge interactions exposed to the solvent. The stabilization of the heme pocket resulting from these interactions was enhanced at low pH by the inclusion of an extra disulfide bond. Further stabilization was also attained at acidic pH by introducing solvent exposed basic residues, probably increasing the protein solubility. In spite of the high number of mutations introduced (seventeen in VPi-br-ss), the VP variants retained the promiscuity of the native enzyme and the catalytic activity was only minimally compromised. The pH stability improvement obtained in this work, together with the intrinsic thermal stability of VP, and the reported possibility to further improve the thermal and oxidative stability of VP by protein engineering (García-Ruiz et al., 2012; Sáez-Jiménez et al., 2015), make this enzyme a promising biocatalyst to oxidize lignin and other high redox potential

aromatic compounds. Currently, a large amount of genomes of ligninolytic basidiomycetes are being sequenced. The characterization of peroxidases encoded by these genomes will provide us with novel enzymes, like MnP4, with new catalytic properties and improved stabilities. The use of these enzymes in comparative structural analyses as that described in this work will allow to design new tailor-made biocatalysts of interest for different applications, including those aimed to the development of the Biorefinery concept that seeks the integral use of plant biomass.

6. References

Adams, P.D., P.V.Afonine, G.Bunkoczi, V.B.Chen, I.W.Davis, N.Echols, J.J.Headd, L.W.Hung, G.J.Kapral, R.W.Grosse-Kunstleve, A.J.Mccoy, N.W.Moriarty, R.Oeffner, R.J.Read, D.C.Richardson, J.S.Richardson, T.C.Terwilliger, and P.H.Zwart. 2010. PHENIX: a comprehensive Python-based system for macromolecular structure solution. *Acta Crystallographica Section D-Biological Crystallography* 66:213-221.

Ayala, M., M.A.Pickard, and R.Vázquez-Duhalt. 2008. Fungal enzymes for environmental purposes, a molecular biology challenge. *J. Mol. Microbiol. Biotechnol.* 15:172-180.

Banci, L., I.Bertini, P.Turano, M.Tien, and T.K.Kirk. 1991. Proton NMR investigation into the basis for the relatively high redox potential of lignin peroxidase. *Proc. Natl. Acad. Sci. USA* 88:6956-6960.

Banci, L., S.Camarero, A.T.Martínez, M.J.Martínez, M.Pérez-Boada, R.Pierattelli, and F.J.Ruiz-Dueñas. 2003. NMR study of Mn(II) binding by the new versatile peroxidase from the white-rot fungus *Pleurotus eryngii*. *J. Biol. Inorg. Chem.* 8:751-760.

Battistuzzi, G., M.Bellei, C.A.Bortolotti, and M.Sola. 2010. Redox properties of heme peroxidases. *Arch. Biochem. Biophys.* 500:21-36.

Britton, H.T.S. and R.A.Robinson. 1931. Universal buffer solutions and the association constant of veronal. *Journal of the Chemical Society*1456-1462.

Chen, V.B., W.B.Arendall, J.J.Headd, D.A.Keedy, R.M.Immormino, G.J.Kapral, L.W.Murray, J.S.Richardson, and D.C.Richardson. 2010. MolProbity: all-atom structure validation for macromolecular crystallography. *Acta Crystallographica Section D-Biological Crystallography* 66:12-21.

Davis, I.W., A.Leaver-Fay, V.B.Chen, J.N.Block, G.J.Kapral, X.Wang, L.W.Murray, W.B.Arendall III, J.Snoeyink, J.S.Richardson, and D.C.Richardson. 2007. MolProbity: all-atom contacts and structure validation for proteins and nucleic acids. *Nucleic Acids Res.* 35:W375-W385.

Deng, Z.M., H.Q.Yang, H.D.Shin, J.H.Li, and L.Liu. 2014. Structure-based rational design and introduction of arginines on the surface of an alkaline alpha-amylase from Alkalimonas amylolytica for improved thermostability. *Appl. Microbiol. Biotechnol.* 98:8937-8945.

Doyle, W.A., W.Blodig, N.C.Veitch, K.Piontek, and A.T.Smith. 1998. Two substrate interaction sites in lignin peroxidase revealed by site-directed mutagenesis. *Biochemistry* 37:15097-15105.

Emsley, P., B.Lohkamp, W.G.Scott, and K.Cowtan. 2010. Features and development of Coot. *Acta Crystallographica Section D-Biological Crystallography* 66:486-501.

Fernández-Fueyo, E., S.Acebes, F.J.Ruiz-Dueñas, M.J.Martínez, A.Romero, F.J.Medrano, V.Guallar, and A.T.Martínez. 2014a. Structural implications of the C-terminal tail in the catalytic and stability properties of manganese peroxidases from ligninolytic fungi. *Acta Crystallogr. D. Biol. Crystallogr.* 70:3253-3265.

Fernández-Fueyo, E., D.Linde, D.Almendral, M.F.López-Lucendo, F.J.Ruiz-Dueñas, and A.T.Martínez. 2015. Description of the first fungal dye-decolorizing peroxidase oxidizing manganese(II). *Appl. Microbiol. Biotechnol.* (online).

Fernández-Fueyo, E., F.J.Ruiz-Dueñas, and A.T.Martínez. 2014b. Engineering a fungal peroxidase that degrades lignin at very acidic pH. *Biotechnol. Biofuels* 7:114.

Fernández-Fueyo, E., F.J.Ruiz-Dueñas, M.J.Martínez, A.Romero, K.E.Hammel, F.J.Medrano, and A.T.Martínez. 2014c. Ligninolytic peroxidase genes in the oyster mushroom genome: Heterologous expression, molecular structure, catalytic and stability properties and lignin-degrading ability. *Biotechnol. Biofuels* 7:2.

Fernández-Fueyo, E., F.J.Ruiz-Dueñas, Y.Miki, M.J.Martínez, K.E.Hammel, and A.T.Martínez. 2012. Lignin-degrading peroxidases from genome of selective ligninolytic fungus *Ceriporiopsis subvermispora*. *J. Biol. Chem.* 287:16903-16916.

García-Ruiz, E., D.González-Pérez, F.J.Ruiz-Dueñas, A.T.Martínez, and M.Alcalde. 2012. Directed evolution of a temperature-, peroxide- and alkaline pH-tolerant versatile peroxidase. *Biochem. J.* 441:487-498.

Gazarian, I.G., M.Lagrimini, S.J.George, and R.N.F.Thorneley. 1996. Anionic tobacco peroxidase is active at extremely low pH: Veratryl alcohol oxidation with a pH optimum of 1.8. *Biochem. J.* 320:369-372.

George, S.J., M.Kvaratskhelia, M.J.Dilworth, and R.N.F.Thorneley. 1999. Reversible alkaline inactivation of lignin peroxidase involves the release of both the distal and proximal site calcium ions and bishistidine co-ordination of the haem. *Biochem. J.* 344:237-244.

González-Pérez, D., E.García-Ruiz, F.J.Ruiz-Dueñas, A.T.Martínez, and M.Alcalde. 2014. Structural determinants of oxidative stabilization in an evolved versatile peroxidase. *ACS Catal.* 4:3891-3901.

Hammel, K.E. and D.Cullen. 2008. Role of fungal peroxidases in biological ligninolysis. *Curr. Opin. Plant Biol.* 11:349-355.

Hiner, A.N.P., E.L.Raven, R.N.F.Thorneley, F.García-Canovas, and J.N.Rodríguez-López. 2002. Mechanisms of compound I formation in heme peroxidases. *J. Inorg. Biochem.* 91:27-34.

Husain, Q. 2010. Peroxidase mediated decolorization and remediation of wastewater containing industrial dyes: a review. *Rev. Environ. Sci. Bio.* 9:117-140.

Kabsch, W. 2010. XDS. *Acta Crystallographica Section D-Biological Crystallography* 66:125-132.

Kishi, K., M.Kusters-van Someren, M.B.Mayfield, J.Sun, T.M.Loehr, and M.H.Gold. 1996. Characterization of manganese(II) binding site mutants of manganese peroxidase. *Biochemistry* 35:8986-8994.

Kumar, S. and R.Nussinov. 2002. Relationship between ion pair geometries and electrostatic strengths in proteins. *Biophys. J.* 83:1595-1612.

Kuwahara, M., J.K.Glenn, M.A.Morgan, and M.H.Gold. 1984. Separation and characterization of two extracellular H_2O_2-dependent oxidases from ligninolytic cultures of *Phanerochaete chrysosporium*. *FEBS Lett.* 169:247-250.

Liu, Y.H., B.Hu, Y.J.Xu, J.X.Bo, S.Fan, J.L.Wang, and F.P.Lu. 2012. Improvement of the acid stability of Bacillus licheniformis alpha amylase by error-prone PCR. *J. Appl. Microbiol.* 113:541-549.

Lú-Chau, T.A., F.J.Ruiz-Dueñas, S.Camarero, G.Feijoo, M.J.Martínez, J.M.Lema, and A.T.Martínez. 2004. Effect of pH on the stability of *Pleurotus eryngii* versatile peroxidase during heterologous production in *Emericella nidulans*. *Bioprocess Biosyst. Eng.* 26:287-293.

Marques, G., J.A.F.Gamelas, F.J.Ruiz-Dueñas, J.C.del Río, D.V.Evtuguin, A.T.Martínez, and A.Gutiérrez. 2010. Delignification of eucalypt kraft pulp with manganese-substituted polyoxometalate assisted by fungal versatile peroxidase. *Bioresource Technol.* 101:5935-5940.

Martínez, A.T., F.J.Ruiz-Dueñas, A.Gutiérrez, J.C.del Río, M.Alcalde, C.Liers, R.Ullrich, M.Hofrichter, K.Scheibner, L.Kalum, J.Vind, and H.Lund. 2014. Search, engineering and applications of new oxidative biocatalysts. *Biofuels Bioprod. Biorefining* 8:819-835.

Martínez, A.T., F.J.Ruiz-Dueñas, M.J.Martínez, J.C.del Río, and A.Gutiérrez. 2009. Enzymatic delignification of plant cell wall: from nature to mill. *Curr. Opin. Biotechnol.* 20:348-357.

Martínez, A.T., M.Speranza, F.J.Ruiz-Dueñas, P.Ferreira, S.Camarero, F.Guillén, M.J.Martínez, A.Gutiérrez, and J.C.del Río. 2005. Biodegradation of lignocellulosics: Microbiological, chemical and enzymatic aspects of fungal attack to lignin. *Int. Microbiol.* 8:195-204.

Martínez, M.J., F.J.Ruiz-Dueñas, F.Guillén, and A.T.Martínez. 1996. Purification and catalytic properties of two manganese-peroxidase isoenzymes from *Pleurotus eryngii*. *Eur. J. Biochem.* 237:424-432.

McEldoon, J.P., A.R.Pokora, and J.S.Dordick. 1995. Lignin peroxidase-type activity of soybean peroxidase. *Enzyme Microb. Technol.* 17:359-365.

Mester, T., K.Ambert-Balay, S.Ciofi-Baffoni, L.Banci, A.D.Jones, and M.Tien. 2001. Oxidation of a tetrameric nonphenolic lignin model compound by lignin peroxidase. *J. Biol. Chem.* 276:22985-22990.

Morales, M., M.J.Mate, A.Romero, M.J.Martínez, A.T.Martínez, and F.J.Ruiz-Dueñas. 2012. Two oxidation sites for low redox-potential substrates: A directed mutagenesis, kinetic and crystallographic study on *Pleurotus eryngii* versatile peroxidase. *J. Biol. Chem.* 287:41053-41067.

Moreira, P.R., E.Almeida-Vara, F.X.Malcata, and J.C.Duarte. 2007. Lignin transformation by a versatile peroxidase from a novel *Bjerkandera* sp strain. *Int. Biodeterior. Biodegrad.* 59:234-238.

Nelson, D.P. and L.A.Kiesow. 1972. Enthalpy of Decomposition of Hydrogen-Peroxide by Catalase at 25 Degrees C (with Molar Extinction Coefficients of H2O2 Solutions in Uv). *Anal. Biochem.* 49:474-478.

Nie, G.J. and S.D.Aust. 1997a. Effect of calcium on the reversible thermal inactivation of lignin peroxidase. *Arch. Biochem. Biophys.* 337:225-231.

Nie, G.J. and S.D.Aust. 1997b. Spectral changes of lignin peroxidase during reversible inactivation. *Biochemistry* 36:5113-5119.

Nie, G.J., N.S.Reading, and S.D.Aust. 1999. Relative stability of recombinant versus native peroxidases from *Phanerochaete chrysosporium*. *Arch. Biochem. Biophys.* 365:328-334.

Ohm, R.A., R.Riley, A.Salamov, B.Min, I.G.Choi, and I.V.Grigoriev. 2014. Genomics of wood-degrading fungi. *Fungal Genet. Biol.* 72:82-90.

Pérez-Boada, M., W.A.Doyle, F.J.Ruiz-Dueñas, M.J.Martínez, A.T.Martínez, and A.T.Smith. 2002. Expression of *Pleurotus eryngii* versatile peroxidase in *Escherichia coli* and optimisation of *in vitro* folding. *Enzyme Microb. Technol.* 30:518-524.

Pérez-Boada, M., F.J.Ruiz-Dueñas, R.Pogni, R.Basosi, T.Choinowski, M.J.Martínez, K.Piontek, and A.T.Martínez. 2005. Versatile peroxidase oxidation of high redox potential aromatic compounds: Site-directed mutagenesis,

spectroscopic and crystallographic investigations of three long-range electron transfer pathways. *J. Mol. Biol.* 354:385-402.

Pogni, R., M.C.Baratto, C.Teutloff, S.Giansanti, F.J.Ruiz-Dueñas, T.Choinowski, K.Piontek, A.T.Martínez, F.Lendzian, and R.Basosi. 2006. A tryptophan neutral radical in the oxidized state of versatile peroxidase from *Pleurotus eryngii*: a combined multi-frequency EPR and DFT study. *J. Biol. Chem.* 281:9517-9526.

Ragauskas, A.J., C.K.Williams, B.H.Davison, G.Britovsek, J.Cairney, C.A.Eckert, W.J.Frederick, J.P.Hallett, D.J.Leak, C.L.Liotta, J.R.Mielenz, R.Murphy, R.Templer, and T.Tschaplinski. 2006. The path forward for biofuels and biomaterials. *Science* 311:484-489.

Reading, N.S. and S.D.Aust. 2000. Engineering a disulfide bond in recombinant manganese peroxidase results in increased thermostability. *Biotechnol. Progr.* 16:326-333.

Reading, N.S. and S.D.Aust. 2001. Role of disulfide bonds in the stability of recombinant manganese peroxidase. *Biochemistry* 40:8161-8168.

Ruiz-Dueñas, F.J., E.Fernández, M.J.Martínez, and A.T.Martínez. 2011. *Pleurotus ostreatus* heme peroxidases: An *in silico* analysis from the genome sequence to the enzyme molecular structure. *C. R. Biol.* 334:795-805.

Ruiz-Dueñas, F.J. and A.T.Martínez. 2009. Microbial degradation of lignin: How a bulky recalcitrant polymer is efficiently recycled in nature and how we can take advantage of this. *Microbial Biotechnol.* 2:164-177.

Ruiz-Dueñas, F.J. and A.T.Martínez. 2010. Structural and functional features of peroxidases with a potential as industrial biocatalysts. *In* Biocatalysts based on heme peroxidases. E.Torres and M.Ayala, editors. Springer-Verlag, Berlin. 37-59.

Ruiz-Dueñas, F.J., M.J.Martínez, and A.T.Martínez. 1999. Molecular characterization of a novel peroxidase isolated from the ligninolytic fungus *Pleurotus eryngii*. *Mol. Microbiol.* 31:223-236.

Ruiz-Dueñas, F.J., M.Morales, E.García, Y.Miki, M.J.Martínez, and A.T.Martínez. 2009. Substrate oxidation sites in versatile peroxidase and other basidiomycete peroxidases. *J. Exp. Bot.* 60:441-452.

Ruiz-Dueñas, F.J., M.Morales, M.Pérez-Boada, T.Choinowski, M.J.Martínez, K.Piontek, and A.T.Martínez. 2007. Manganese oxidation site in *Pleurotus eryngii* versatile peroxidase: A site-directed mutagenesis, kinetic and crystallographic study. *Biochemistry* 46:66-77.

Sáez-Jiménez, V., S.Acebes, V.Guallar, A.T.Martínez, and F.J.Ruiz-Dueñas. 2015. Improving the oxidative stability of a high redox potential fungal peroxidase by rational design. *PLoS ONE* 10, e0124750.

Salvachúa, D., A.Prieto, M.L.Mattinen, T.Tamminen, T.Liitiä, M.Lille, S.Willfor, A.T.Martínez, M.J.Martínez, and C.B.Faulds. 2013. Versatile peroxidase as a valuable tool for generating new biomolecules by homogeneous and heterogeneous cross-linking. *Enzyme Microb. Technol.* 52:303-311.

Sambrook, J. and D.W.Russell. 2001. Molecular cloning. CSHL Press, Cold Spring Harbor, New York.

Semba, Y., M.Ishida, S.i.Yokobori, and A.Yamagishi. 2015. Ancestral amino acid substitution improves the thermal stability of recombinant lignin-peroxidase from white-rot fungi, Phanerochaete chrysosporium strain UAMH 3641. *Protein Engineering Design and Selection* (online).

Smith, A.T. and W.A.Doyle. 2006. Engineered peroxidases with veratryl alcohol oxidase activity. *Patent (International)*WO/2006-114616.

Sokalingam, S., G.Raghunathan, N.Soundrarajan, and S.G.Lee. 2012. A Study on the Effect of Surface Lysine to Arginine Mutagenesis on Protein Stability and Structure Using Green Fluorescent Protein. *PLoS ONE* 7.

Sutherland, G.R.J., L.S.Zapanta, M.Tien, and S.D.Aust. 1997. Role of calcium in maintaining the heme environment of manganese peroxidase. *Biochemistry* 36:3654-3662.

Tien, M. and T.K.Kirk. 1983. Lignin-degrading enzyme from the hymenomycete *Phanerochaete chrysosporium* Burds. *Science* 221:661-663.

Timofeevski, S.L. and S.D.Aust. 1997. Kinetics of calcium release from manganese peroxidase during thermal inactivation. *Arch. Biochem. Biophys.* 342:169-175.

Verdín, J., R.Pogni, A.Baeza, M.C.Baratto, R.Basosi, and R.Vázquez-Duhalt. 2006. Mechanism of versatile peroxidase inactivation by Ca2+ depletion. *Biophys. Chem.* 121:163-170.

Zhou, H.Y., H.Y.Pan, L.Q.Rao, and Y.Y.Wu. 2011. Redesign the alpha/beta Fold to Enhance the Stability of Mannanase Man23 from Bacillus subtilis. *Appl. Biochem. Biotechnol.* 163:186-194.

CHAPTER 3

Investigating the basis of stability of an evolved versatile peroxidase

Abstract

A variant of high biotechnological interest (called 2-1B) was obtained by directed evolution of the *Pleurotus eryngii* VP expressed in *Saccharomyces cerevisiae* (García-Ruiz et al. Biochem. J. 441, 487, 2012). 2-1B shows seven mutations in the mature protein that resulted in significantly improved alkaline stability, a required property for biorefinery applications, together with enhanced oxidation of low redox potential substrates. Here we investigate the structural bases behind the enhanced properties of this evolved enzyme. In order to do this, several VP variants containing one or several of the mutations present in 2-1B were designed, and their stability and biochemical properties determined. In addition, the crystal structures of 2-1B and one of the intermediate variants (both expressed in *Escherichia coli*) were obtained and carefully analyzed. We concluded that the introduction of three basic residues in VP (Lys-37, Arg-39 and Arg-330) led to the formation of a new interaction between the heme cofactor and the helix where distal histidine was located (helix B), and two-three new salt bridges, at the same time that they removed destabilizing (acid-acid) interactions. These new structural determinants stabilized the heme and its environment and maintained the enzyme active (with pentacoordinated heme iron) under alkaline conditions. Moreover, the reinforcement of the solvent-exposed area around Gln-305 in the proximal side, prompted by the Q202L mutation, further enhanced the stability. On the other hand, some of the mutations improved the oxidation of low redox potential substrates at the main heme access channel.

1. Introduction

Lignin is the main reservoir of aromatic compounds in living organisms and a valuable feedstock for the sustainable production of chemicals, materials and biofuels (Ragauskas et al., 2014; Martínez et al., 2009). Due to its aromatic and heterogeneous nature, lignin is highly resistant to chemical and biological degradation (Ruiz-Dueñas and Martínez, 2009). White-rot fungi produce ligninolytic peroxidases involved in lignin degradation, and they are the only organisms in nature being able to extensively mineralize lignin (Martínez et al., 2005; Floudas et al.,

2012). Ligninolytic peroxidases include three families: lignin peroxidases (LiP, E.C. 1.11.1.14), which oxidize high redox potential substrates through an exposed tryptophan radical formed by electron transfer to the heme (Hammel and Cullen, 2008); manganese peroxidases (MnP, E.C. 1.11.1.13), which oxidize Mn^{2+} to Mn^{3+} at a specific Mn-binding site near one of the heme propionates (Gold et al., 2000; Fernández-Fueyo et al., 2014); and versatile peroxidases (VP, E.C. 1.11.1.16), which combine the catalytic properties of LiPs and MnPs (due to the simultaneous presence of the exposed tryptophan and the Mn-binding site, mentioned above) at the same time that they oxidize the typical substrates of generic peroxidases (GPs, E.C. 1.11.1.7; at the main heme access channel) (Ruiz-Dueñas et al., 2009; Morales et al., 2012).

The above enzymes are naturally designed to overcome the recalcitrant nature of lignin taking advantage from their high redox potential, unspecific oxidation mechanism and other catalytic properties. Their use in industrial processes that require the oxidation of lignin and other phenolic and non-phenolic aromatics compounds and dyes is, therefore, very promising (Martínez et al., 2014). In this way, ligninolytic peroxidases could be used in the deconstruction of the lignocellulosic biomass and production of biofuels, materials and chemicals in lignocellulose biorefineries; in bioremediation processes for the treatment of recalcitrant dye wastes; or in bleaching applications in paper pulp manufacture (Martínez et al., 2009; Ragauskas et al., 2006; Husain, 2010). However, there are some drawbacks that prevent the industrial application of these enzymes as they are produced in nature. Among them, it is possible to mention their relative low stability towards some conditions of pH, temperature or hydrogen peroxide concentration, in which industrial processes are often carried out (including the alkaline conditions often used in lignocellulose processing) (Martínez et al., 2009).

2-1B is an enzyme variant obtained by directed evolution of the VP from *Pleurotus eryngii* in *Saccharomyces cerevisiae* (García-Ruiz et al., 2012). During the evolutionary process, seven mutations were introduced in the sequence of mature VP. As a consequence, 2-1B showed increased alkaline stability, and improved oxidation of some

substrates. In the present work, five VP variants containing one or several of the mutations present in 2-1B were designed, and their biochemical properties carefully evaluated, at the same time that the crystal structures of the most relevant variants were solved and used in molecular simulations. The final aim was to understand how the substitutions introduced by directed molecular evolution modulate the stability and catalytic properties of the enzyme, with the aim of using this information in future peroxidase engineering work.

2. Material and Methods

2.1 Chemicals

Isopropyl-β-D-thiogalactopyranoside (IPTG), dithiothreitol (DTT), ethylenediaminetetraacetic acid (EDTA), hemin, oxidized glutathione, veratryl alcohol (VA), manganese (II) sulphate, Reactive Black 5 (RB5), 2,6-dimethoxyphenol (DMP), sodium tartrate and other chemicals were purchased from Sigma-Aldrich; urea and hydrogen peroxide were from Merck; and 2, 2-azinobis-(3-ethylbenzothiazoline-6-sulfonic acid) (ABTS) from Roche.

2.2 Directed mutagenesis

All VP variants but 2-1B (see below) were produced using the QuikChange™ Site-Directed Mutagenesis kit (Stratagene). Each mutation was introduced by PCR using the expression plasmid pFLAG1 (International Biotechnologies Inc.) containing the CDS of *P. eryngii* VPL (allelic variant VPL2; GenBank™ AF007222), named pFLAG1-VPL2, or the same plasmid containing already mutated CDSs as templates and two primers, a direct and a reverse primer designed complementary to opposite strands of the same DNA region containing the desired mutation.

The mutagenic primers $E37K_p$, $H39R_p$ and $G330R_p$ (**Table 1**) were used to obtain the corresponding single variants. The double variant E37K/H39R was obtained using the plasmid pFLAG1-VPL2 as template and the primers $E37K/H39R_p$ containing both E37K and H39R mutations. The double variant E37K/G330R (hereinafter EG) was

obtained using the plasmid pFLAG1-VPL2 harbouring the mutation G330R as template and the primers $E37K_p$. Similarly, the triple variant E37K/H39R/G330R (hereinafter EHG) was achieved using the plasmid pFLAG1-VPL2 containing the E37K and H39R mutations as template and the primers $G330R_p$. In the same way, the multiple variants E37K/H39R/Q202L/G330R (hereinafter EHGQ) and E37K/H39R/ T184M/G330R (hereinafter EHGT) were obtained using the template pFLAG1-VPL2-E37K/H39/G330R with $Q202L_p$ or $T184M_p$ as primers, respectively.

Table 1. Oligonucleotide primers used in mutagenic PCRs for the production of the VP variants

Only the direct sequences are shown with indication of the changed triplets (underlined) and the mutations introduced (bold).

Primer	Sequence 5'-3'	Mutation
$E37K_p$	GCCCAGTGTGGAGAA**A**AGGTGCACGAGTCCC	E37K
$H39R_p$	GGAGAAGAGGTG**CGC**GAGTCCCTTCGTTTGACTTTCCACG	H39R
$G330R_p$	CCCTCCCGTCCCT**AGA**TCGTAAGATCTCTCG	G330R
$Q202L_p$	CTCAATTCTTCATCGAAACG**CTC**CTTAAAGGCAGACTCTTCCC	Q202L
$T184M_p$	CCCATCCGATTCCTGGAA**T**GCCATTCGATTCAACCCCCGG	T184M
$E37K/H39R_p$	GCCCAGTGTGGAGAA**A**AGGTG**CGC**GAGTCCCTTCG	E37K/H39R

PCR reactions were carried out in a Eppendorf Mastercycler Pro S using 10 ng of template DNA, 250 μM each dNTP, 125 ng of both direct and reverse primers, 2.5 units of *Pfu* Turbo AD polymerase (Stratagene) and the manufacture´s reaction buffer. Reaction conditions were as follows: (i) a "hot start" of 95ºC for 1 min; (ii) 18 cycles at 95ºC for 50s, 55ºC for 50s and 68ºC for 10min; and (iii) a final cycle at 68ºC for 10 min. Clones harbouring mutations were transformed into *Escherichia coli* DH5α. One positive clone of each variant was selected, sequenced (Perkin-Elmer ABI PRISM 377) and checked to confirm that the desired mutations had been properly introduced.

2.3 Heterologous expression

Wild-type recombinant (hereinafter native) VP and its directed variants were expressed in *E. coli* W3110 after transformation with the corresponding plasmids. The gene encoding the 2-1B variant was obtained by digesting the plasmid used for *S. cerevisiae* expression

(García-Ruiz et al., 2012), cloned in pFLAG1 (resulting in the pFLAG-VPL2-2-1B construction) and transformed into *E. coli* W3110 for expression.

Cells were grown in Terrific Broth (Sambrook and Russell, 2001) at 37 ºC until OD_{500}~1 (~3 h). Then protein expression was induced with 1 mM IPTG and cells were grown for a further 4 h. The apoenzyme was produced as inclusion bodies and was recovered in a 50 mM Tris-HCl (pH 8.0) solution containing 8 M urea, 1 mM EDTA, and 1 mM DTT. The subsequent *in vitro* folding of the solubilised apoenzyme was carried out in a solution of 0.16 M urea, 20 μM hemin, 5 mM $CaCl_2$, 0.1 mM DTT, 0.5 mM oxidized glutathione and 0.1 mg/ml protein concentration in 20 mM Tris-HCl buffer, at pH 9.5, at room temperature overnight. The refolded enzyme was purified by Resource-Q chromatography using a 0-0.3 M NaCl gradient (2 ml/min, 20 min) in 10 mM sodium tartrate (pH 5.5) containing 1 mM $CaCl_2$. Finally, the purified enzyme was dialyzed against 10 mM sodium tartrate (pH 5). The proteins showed Reinheitszahl values (R_z, A_{407}/A_{280})~ 4 confirming their high purity. Their UV-visible spectra in the 300-700 nm range confirmed that they were correctly folded (Pérez-Boada et al., 2002). Enzyme concentrations were determined from the Soret absorbance (ε_{407}= 150 mM^{-1} cm^{-1}) (Ruiz-Dueñas et al., 1999).

2.4 pH stability studies

Native VP and its directed variants (1 μM) were incubated at different pH values (from 2 to 9) in 0.1 M Britton-Robinson (B&R) buffer (Britton and Robinson, 1931) at 4°C for 120 h. At different times (1 min, 1 h, 4 h, 24 h and 120 h), aliquots were taken and their residual activity was evaluated by measuring the oxidation of ABTS (2 mM) using 0.1 mM H_2O_2 and 0.01 μM of enzyme in 0.1 M sodium tartrate (pH 3.5). The activity obtained after 1 min at pH 5 was taken as reference (maximum activity) to calculate the percentage of residual activity. Native VP and those variants showing improved alkaline stability (2-1B, EHG and EHGQ) (4 μM and 8 μM) were incubated at pH 5 or pH 8 in 0.1 M B&R buffer for 120 h at 4°C, and their electronic absorption spectra (in the 300-800 nm range) were recorded using an Agilent 8453 diode array UV/visible spectrophotometer.

2.5 Kinetic constants

Oxidation of Mn^{2+} (Mn^{3+}-tartrate complex ε_{238} 6500 M^{-1} cm^{-1}) was estimated at pH 5; that of VA (veratraldehyde ε_{310} 9300 M^{-1} cm^{-1}) at pH 3; and those of RB5 (ε_{598} 30000 M^{-1} cm^{-1}), ABTS (cation radical ε_{436} 29300 M^{-1} cm^{-1}) and DMP (coerulignone dimeric product ε_{469} 55000 M^{-1} cm^{-1}) at pH 3.5. All enzymatic activities were measured as initial velocities taking linear increments of absorbance due to the appearance of the reaction product (decreases in the case of RB5). Reactions were performed in 0.1 M tartrate buffer, at 25 ºC, in the presence of 0.1 mM H_2O_2 using a variable wavelength Shimadzu UV-1800 spectrophotometer.

Steady-state kinetic constants were calculated from the estimated oxidation of increasing substrate concentrations until enzyme saturation was observed. Values and standard errors for affinity constant (Michaelis constant, K_m) and maximal enzyme turnover (catalytic constant, k_{cat}) were obtained fitting the experimental measurements to the Michaelis-Menten model using SigmaPlot 12.0 software. Fitting of these constants to the normalized equation $v = (k_{cat}/K_m)$ [S]/ (1+[S]/K_m), where [S] is the substrate concentration, yielded the catalytic efficiency values (k_{cat}/K_m) with their corresponding standard errors.

2.6 Crystallization, data collection and crystal structure determination

Crystallization conditions of the 2-1B and EHG variants were optimized at 22 ºC using the sitting drop vapour diffusion method. Crystals of 2-1B were obtained in 0.1 M Tris-HCl (pH 7.8), 5 % PEG3350, 1.25 M $(NH_4)_2SO_4$ and 7.5 % glycerol, and crystals of EHG were obtained in 0.1 M Na-acetate (pH 4.5), 1.26 M $(NH_4)_2SO_4$ and 0.2 M NaCl. 30 % glycerol and 0.8 M Li_2SO_4 were used as cryoprotectants in 2-1B and EHG, respectively. Diffraction data were obtained and the structures were solved by molecular replacement using the crystal structure of *P. eryngii* VP (PDB entry 2BOQ) as the search model. Data collection statistics, refinement and final model statistics are summarized in **Table 2**. The

structures were analyzed with PyMol (www.pymol.org) and LigPlot software (Wallace et al., 1995).

Table 2 Crystallographic data collection and refinement statistics of VP EHG and VP 2-1B. Data in parenthesis correspond to the last resolution layer.

Data collection	EHG	2-1B
Space group	P 2_1 2_1 2	P 2_1 2_1 2_1
Cell constants (Å)	a = 55.2, b = 104.2, c = 76.6	a = 55.1, b = 106.0, c = 107.6
Resolution range (Å)	50.00 - 1.50 (1.59 - 1.50)	50.00 - 1.80 (1.90 - 1.80)
Nº of total reflections	920257	777990
Nº of unique reflections	71617	59335
R_{merge} (%)	26.6 (324.2)	41.2 (330.8)
Completeness (%)	99.5 (97.2)	98.6 (94.2)
<I/s(I)>	8.5 (0.8)	6.8 (0.7)
Multiplicity	12.8 (12.0)	13.1 (12.0)
CC(1/2)	99.7 (28.8)	99.0 (30.9)
Solvent content (%) / Matthews coef.	55.33 / 2.75	37.48 / 1.97
Subunits per asymmetric unit	1	2
Wilson B factor ($Å^2$)	16.0	26.8
Refinement		
Resolution range	50.0 - 1.50 Å	50.0 - 1.80 Å
Working reflections	71227	58796
R_{work} / R_{free}	19.2 / 22.9 %	18.5 / 21.9 %
Protein atoms (non H)	2440	4740
Heme group	1	2
Ca^{2+}	2	4
Water molecules	367	618
SO_4 ions	10	2
Mean B factors ($Å^2$)		
Protein atoms (non H)	20.07	21.41
Heme group	15.37	17.85
Ca^{2+}	14.63	15.57
Water molecules	30.98	38.23
SO_4 ions	62.93	30.51
Deviations from ideality		
rmsd bond lengths	0.006 Å	0.007 Å
rmsd angles	1.126º	1.104º
Ramachandran plot statistics		
Preferred %	98.47	98.43
Allowed %	1.53	1.57
Outliers %	0.00	0.00
PDB code	----	----

3. Results

3.1 pH stability of the different variants

VP 2-1B (containing E37K/H39R/V160A/T184M/Q202L/D213A/G330R mutations) expressed in *E. coli* showed improved alkaline stability (**Fig. 1D**) compared with native VP (**Fig. 1A**). After 24 and 120 h of incubation at pH 8, it retained 82% and 78% of residual activity, respectively, whereas native VP was inactivated. Moreover, after 1 h of incubation at pH 9, native VP retained only 5% of the initial activity while 2-1B maintained 36% of activity. The differences in stability between both enzymes at neutral and most acidic pH conditions (in the pH 3.5-7 range) were minimal, and 2-1B was less stable at the lowest pH value (pH 3) assayed.

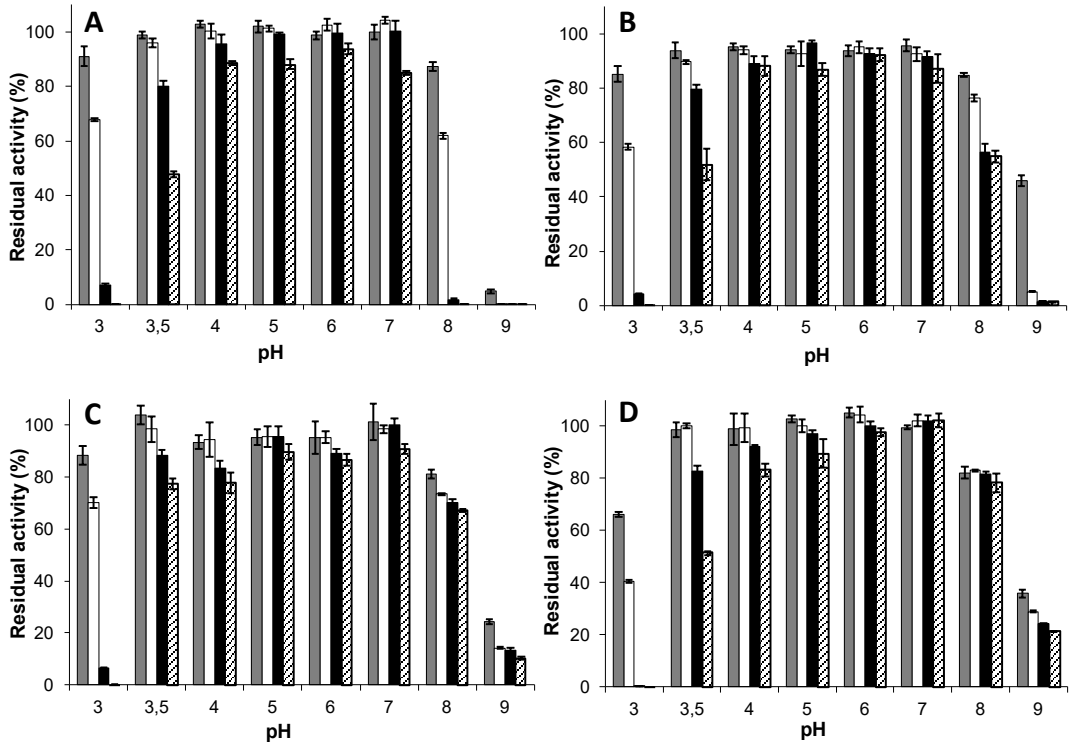

Figure 1 pH stability of native VP and three mutated variants
Residual activities of VP (**A**) and the EHG (**B**) EHGQ (**C**) and 2-1B (**D**) variants, after 1 h (gray bars), 5 h (white bars), 24 h (black bars), and 120 h (striped bars) of incubation in 0.1 M B&R buffer at different pH values (2-9). Residual activity measured as ABTS (2 mM) oxidation in 0.1 M sodium tartrate (pH 3.5) using 0.01 μM enzyme and 0.1 mM H_2O_2. Means and 95% confidence limits of replicate assays. See **Table 3** for the mutations present in each of the variants.

To analyze the effect of each of the individual mutations in 2-1B, and the effect of combining them, several single and multiple VP variants were designed (**Table 3**), expressed in *E. coli* and characterized. The H39R variant showed high instability at acidic and alkaline pH values compared with native VP (**Fig. 2A**). Native VP maintained around 90% of the initial activity in the range of pH 4-7 after 120 h of incubation, while H39R only showed 41%, 68% and 21% activity at pH 4, 5 and 6 respectively (and no activity at pH 7). The following VP variant analyzed, EG containing mutations E37K/G330R, exhibited similar pH stability than native VP and no improvement in the alkaline range was observed (**Fig. 2B**).

Table 3. Seven individual mutations in 2-1B and their combination in the five intermediate variants analyzed in the present study

Variants	Mutations
2-1B	E37K / H39R / V160A / T184M / Q202L / D213A / G330R
H39R	H39R
EG	E37K / G330R
EHG	E37K / H39R / G330R
EHGQ	E37K / H39R / Q202L / G330R
EHGT	E37K / H39R / T184M / G330R

Surprisingly, the EHG variant, which harbours the mutations of the two variants previously analyzed (E37K/H39R/G330R), displayed an increase in the alkaline stability compared with native VP (**Fig. 1B**). This triple variant maintained 55% of the initial activity after 120 h of incubation at pH 8, whereas native VP not only showed no activity under these conditions but it was inactivated after 24 h of incubation (**Fig. 1A**). In a similar way, after 1 h of incubation at pH 9, EHG exhibited a 46% of the initial activity, whereas native VP only retained 5%. Moreover, this variant maintained a similar stability compared with native VP at acidic and neutral pH values. However, the values of pH-stability observed for EHG were not as high as that obtained for 2-1B, which retained 78% of activity after 120 h of incubation at pH 8.

The next VP variant analyzed was EHGQ (E37K/H39R/Q202L/ G330R), which harboured the three mutations of EHG plus the Q202L mutation, also found in 2-1B. EHGQ showed 67% of residual activity after 120 h of incubation at pH 8 (**Fig. 1C**), a value higher than that of

EHG (55% of activity). EHGQ also retained a low percentage of the initial activity (24%) after 1-h incubation at pH 9 compared with native VP, which was completely inactivated. Therefore, it was determined that Q202L substitution also contributed to the enhancement of the pH stability in 2-1B. As previously describe for EHG, its stability at neutral and acidic pH was similar to that of the native VP.

The last variant tested, E37K (EHGT/H39R/T184M/G330R), harboured the three mutations introduced in EHG plus the T184M mutation, also found in 2-1B. After 120 h at pH 8, EHGT displayed 30% of the initial activity (**Fig. 2C**) compared with 55% of activity retained by EHG. In consequence, we concluded that the T184M substitution did not contribute to the alkaline stability of 2-1B.

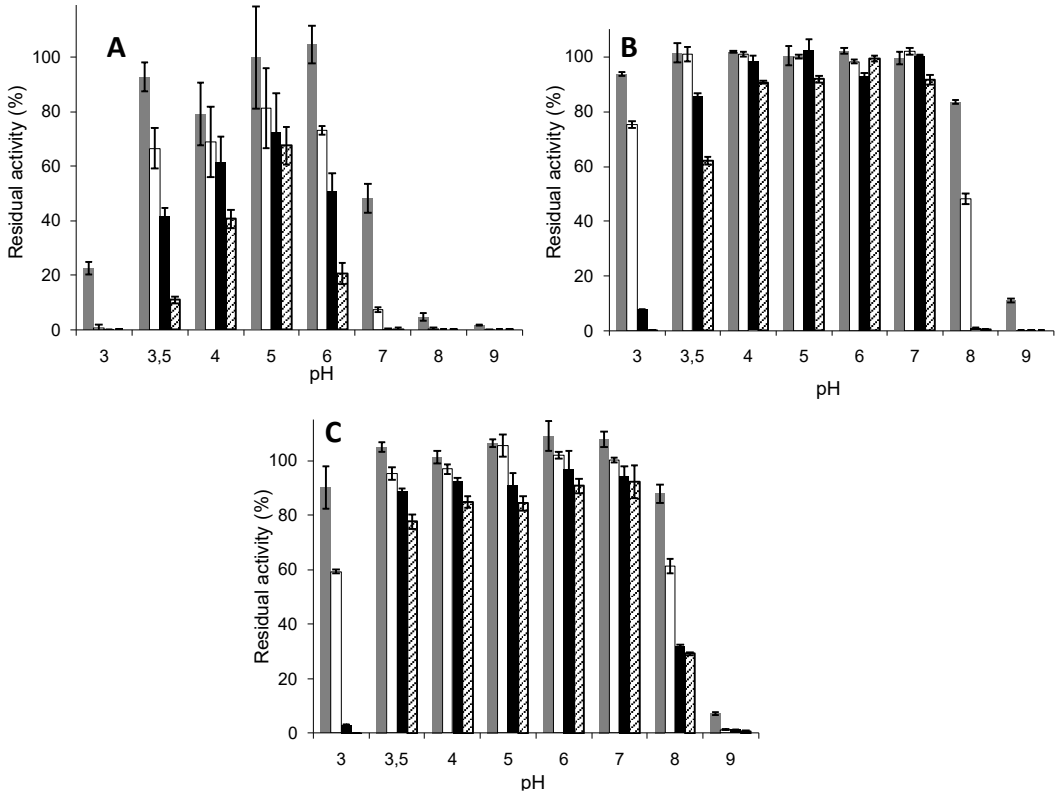

Figure 2. pH stability of H39R, EG (E37K/G330R) and EHGT (E37K/H39R/ G330R/T184M) VP variants

Residual activities of H39R (**A**), EG (**B**) and EHGT (**C**) after incubation in 0.1M Britton & Robinson buffer at different pH values (2-9) during 1 h (gray bars), 5 h (white bars), 24 h (black bars), and 120 h (striped bars). Residual activity measured as ABTS (2 mM) oxidation in 0.1 M sodium tartrate (pH 3.5) using 0.01 μM enzyme and 0.1 mM H_2O_2. Means and 95% confidence limits of replicate assays.

3.2 pH effect on the UV-visible spectra

The electronic absorption spectra of native VP and its variants were recorded after incubation at alkaline pH 8, and at pH 5 at which all of them are stable, to check the eventual modification of the heme interactions with its environment. As expected, all the spectra at pH 5 exhibited a Soret maximum at 407 nm, maxima at 505 nm and 637 nm corresponding to ligand-to-metal charge transfer bands (CT2 and CT1 respectively), and the β band at 541 nm (**Fig. 3**, black lines), which correspond to the typical spectrum of the ferric enzyme with high-spin pentacoordinated heme iron.

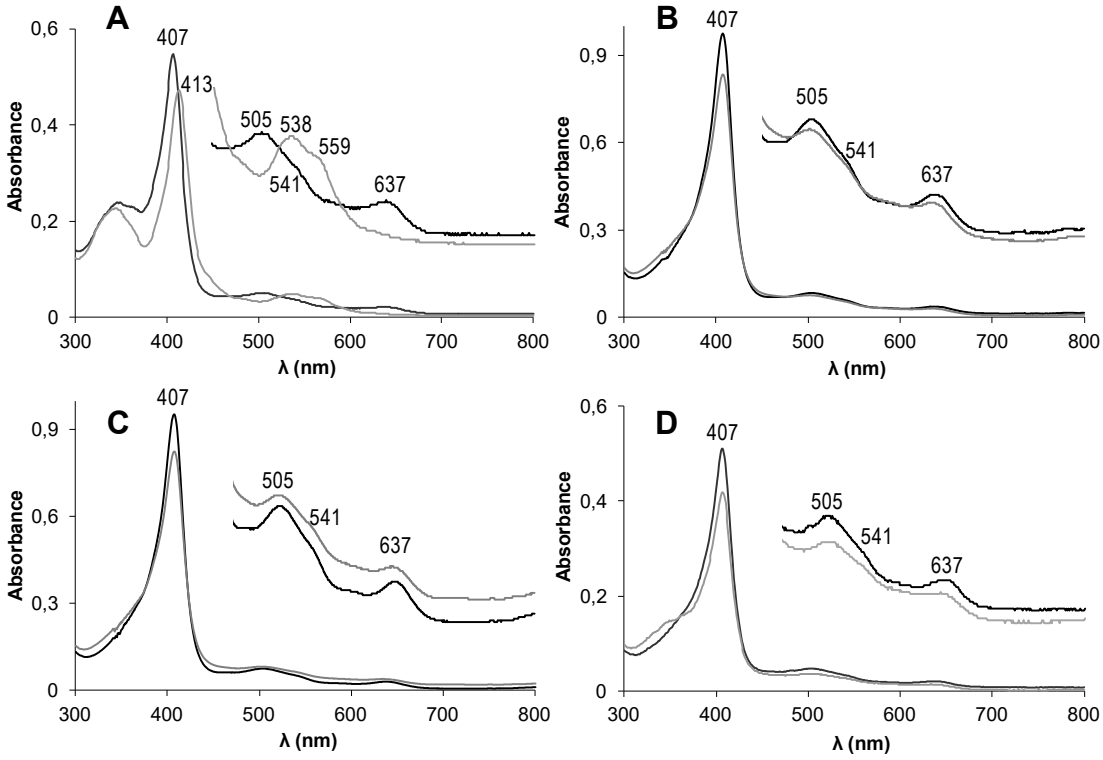

Figure 3. Electronic absorption spectra of native VP and variants after treatments at pH 5 and pH 8

UV-visible spectra of native VP (**A**) and the EHG (**B**), EHGQ (**C**) and 2-1B (**B**) variants incubated for 120 h in 0.1M B&R buffer at pH 5 (black) and pH 8 (gray). Amplified (x 5) 450-800 nm regions are shown. Main maxima are indicated.

However, the spectrum of native VP after incubation at pH 8 suffered important changes (**Fig. 3A**, gray lines). The Soret maximum was red-shifted to 413 nm and showed less intensity, the CT bands at 505 nm and 637 nm disappeared and a new maximum rose at 538 nm (β band)

together with a shoulder at 559 nm (α band). In contrast, 2-1B preserved the spectrum mostly unaltered when incubated at pH 8 (**Fig. 3D**, gray lines), maintaining the Soret maximum at 407 nm, as well as the CT1 , CT2 and β bands at 637, 505 and 541 nm, respectively. In the same way, the EHG and EHGQ variants also preserved the ferric high-spin heme spectrum with all maxima unaffected (**Fig. 3B** and **3C**, gray lines).

3.3 Catalytic properties

Different substrates are oxidized at specific VP sites: i) high redox potential VA and RB5 are oxidized at the catalytic tryptophan; ii) low redox potential ABTS and DMP are oxidized both at the catalytic tryptophan (high efficiency site) and at the heme channel in direct contact with the heme edge (low efficiency site); and iii) Mn^{2+} is oxidized at the Mn^{2+}-binding site, in direct contact with a heme propionate. The steady-state kinetic constants for the oxidation of the above five substrates by native VP and four variants were measured (**Table 4**).

In general, the oxidation of substrates in the catalytic tryptophan was not affected by the substitutions introduced in 2-1B, since the kinetic constants for the oxidation of VA, RB5 and ABTS and DMP (in the high efficiency site) were mostly unaltered in this and the other variants. The only exception was EHGT which exhibited a 3-fold higher catalytic efficiency (559 $s^{-1}{\cdot}mM^{-1}$) for DMP oxidation, compared with that of native VP (186 $s^{-1}mM^{-1}$), due to a decrease in the affinity constant (K_m).

Mn^{2+} oxidation was impaired in 2-1B and the rest of analyzed variants since their efficiency values were decreased around 60-fold, changing from 1640 $s^{-1}mM^{-1}$ in native VP to 25-30 $s^{-1}mM^{-1}$ in the variants. The worsening in the oxidation was mainly due to the increase of the K_m values.

Interestingly, the oxidation of ABTS and DMP at the low efficiency site was improved in 2-1B and EHGT. The efficiency for the oxidation of ABTS showed a 9-12-fold increase in both variants, mainly due to a reduction of the K_m values. In a similar way, the efficiency in the oxidation of DMP exhibited a 5-fold increase. In EHGT, this improvement

was mainly due to the decrease in the K_m. However, in 2-1B, a decrease of the K_m value combined with an increase of the k_{cat} was observed.

Table 4. Kinetic constants - K_m (μM), k_{cat} (s^{-1}) and k_{cat}/K_m (s^{-1} mM^{-1}) - for oxidation of VA, RB5, Mn^{2+}, ABTS and DMP by native VP, 2-1B and three intermediate variants (see Table 3 for mutations in each of them) .[a]

		VP	EHG	EHGQ	EHGT	2-1B
VA	K_m	2600 ± 190	2110 ± 150	1780 ± 60	5910 ± 190	2710 ± 270
	k_{cat}	5.8 ± 0.1	5.2 ± 0.1	4.4 ± 0.04	5.9 ± 0.1	3.8 ± 0.1
	k_{cat}/K_m	2.2 ± 0.1	2.5 ± 0.1	2.5 ± 0.1	1.0 ± 0.02	1.4 ± 0.1
RB5	K_m	3.4 ± 0.3	4.3 ± 0.5	3.5 ± 0.3	2.4 ± 0.1	7.6 ± 0.6
	k_{cat}	5.5 ± 0.3	7.8 ± 0.4	6.7 ± 0.3	5.1 ± 0.1	6.7 ± 0.3
	k_{cat}/K_m	1.6 ± 0.1	1.8 ± 0.1	1.1 ± 0.08	2.2 ± 0.1	0.8 ± 0.04
ABTS (high efficiency)	K_m	3.0 ± 0.2	2.6 ± 0.2	2.3 ± 0.2	12.7 ± 2.8	nd[b]
	k_{cat}	8.1 ± 0.2	8.3 ± 0.3	7.2 ± 0.3	38.8 ± 6.5	nd[b]
	k_{cat}/K_m	2700 ± 140	3128 ± 183	3160 ± 154	3050 ± 160	nd[b]
ABTS (low efficiency)	K_m	1020 ± 74	406 ± 36	278 ± 20	61 ± 3	98 ± 9
	k_{cat}	208 ± 6	89 ± 2	89.5 ± 2	117 ± 2	234 ± 8
	k_{cat}/K_m	204 ± 10	219 ± 15	322 ± 19	1916 ± 73	2370 ± 150
DMP (high efficiency)	K_m	38 ± 4	17. ± 2.1	16.3 ± 2.8	11.2 ± 1.9	27 ± 7.3
	k_{cat}	7.1 ± 0.1	2.9 ± 0.1	4.1 ± 0.1	6.3 ± 0.3	2.9 ± 0.4
	k_{cat}/K_m	186 ± 16	168 ± 18	250 ± 38	559 ± 80	112 ± 18
DMP (low efficiency)	K_m	10500 ± 400	34500 ± 6050	34100 ± 5290	3070 ± 420	7465 ± 375
	k_{cat}	30 ± 0.4	40 ± 4	56 ± 4	46 ± 2	91 ± 2
	k_{cat}/K_m	2.8 ± 0.1	1.1 ±0.1	1.6 ± 0.1	15 ± 1.5	12 ± 0.5
Mn^{2+}	K_m	130 ± 11	7020 ± 190	6790 ± 200	5590 ± 371	5710 ± 350
	k_{cat}	211 ± 4	208 ± 2	188 ± 2	160 ± 4	143 ± 3
	k_{cat}/K_m	1641 ±132	30 ± 0.6	28 ± 0.6	29 ± 1.3	25 ± 1.2

[a]Reactions were carried out at 25 °C in 0.1 M sodium tartrate (pH 3 for VA, pH 5 for Mn^{2+}, and pH 3.5 for RB5, ABTS and DMP). Means and 95% confidence limits of replicate assays. ABTS and DMP oxidation showed biphasic kinetics enabling calculation of two sets of constants (for high and low efficiency sites). [b] Not determined because the kinetic curve of the high efficiency site overlapped with that of the low efficiency site

In contrast to the results obtained for EHGT, EHG showed no improvement in ABTS and DMP oxidation. Since the only difference between these two variants is the T184M mutation present in EGHT, it was concluded that this substitution is involved in the improved oxidation of low redox substrates by EGHT (and probably 2-1B).

3.4 Analysis of crystal structures

The crystal structures of 2-1B and EHG were obtained, analyzed and compared with that of native VP (PDB 2BOQ) to explain, from a structural point of view, both the enhanced alkaline stability and the modified catalytic properties of these variants. H39R, E37K and G330R mutations were determinant for the higher alkaline stability found in 2-1B. Residues 37 and 39 are partially solvent-exposed, close to the heme (at 7.1 and 3.3 Å, respectively, in native VP structure) (**Fig. 4A**) and close to the Mn^{2+}-binding site (formed by Glu-36, Glu-40 and Asp-175).

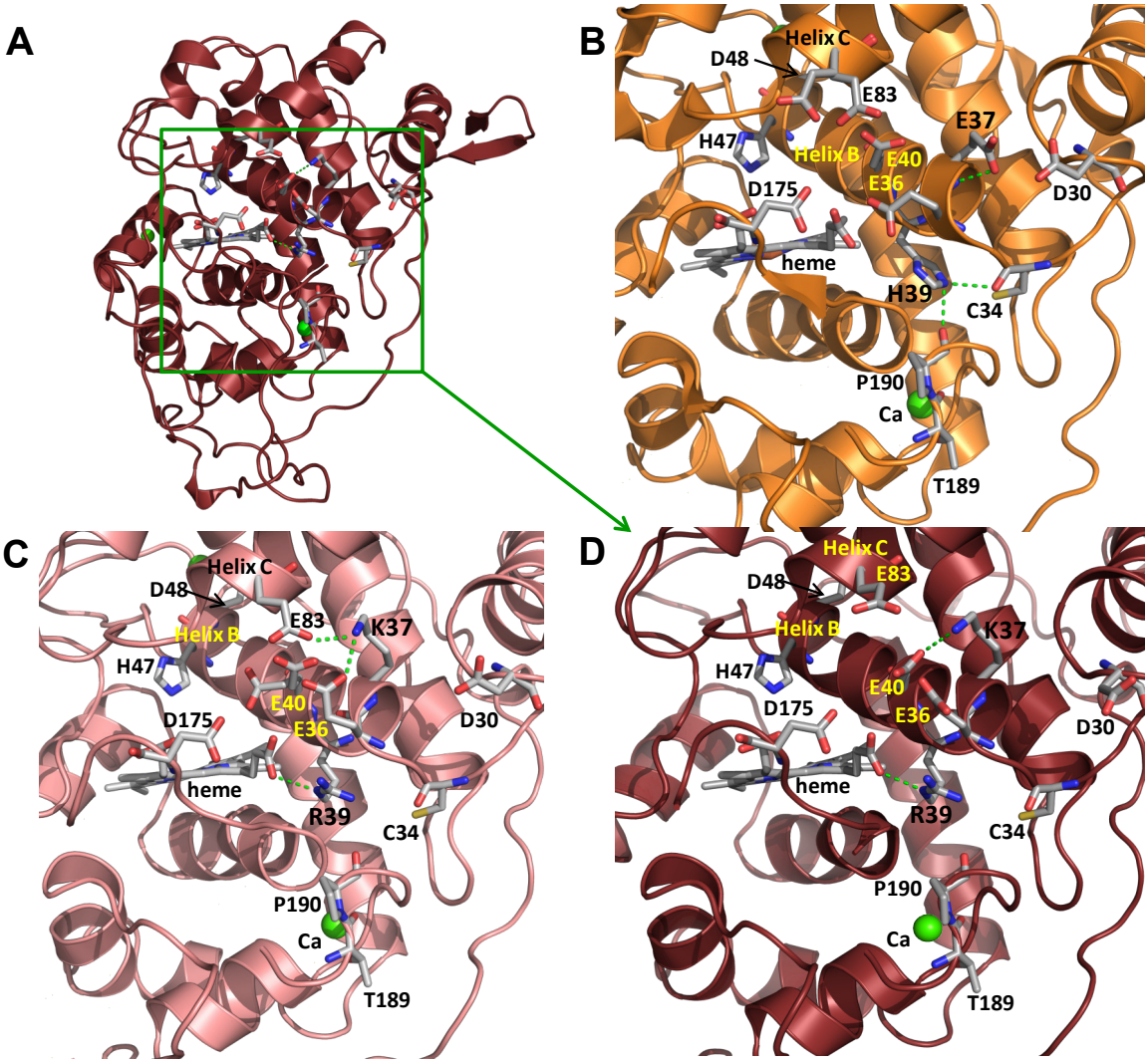

Figure 4. E37K and H39R mutations in 2-1B and EHG crystal structures
Crystal structure of 2-1B (**A**) with details of the region in front of the heme propionates in native VP (**B**) and the EHG (**C**) and 2-1B (**D**) variants showing the heme, the mutated residues at positions 37 and 39, and other surrounding residues (in CPK colours). Hydrogen bonds are shown as green dashed lines, calcium ions as green spheres and secondary structure as colour cartoon.

They belong to helix B, which is located directly above the heme and harbours distal histidine (His-47) and distal arginine (Arg-43) involved in catalysis. Moreover, the distal histidine is involved in the hexacoordination of the heme iron observed at alkaline pH. The new Arg-39 in 2-1B and EHG (**Fig. 4D** and **C**) showed a different orientation of its lateral chain relative to the position of His-39 in native VP. The new orientation enabled the formation of a new H-bond with the distal propionate of the heme, being this interaction absent in native VP. Instead, in VP, His-39 formed two H-bonds with Cys-34 and Pro-190, which were lost in the improved variants.

The E37K substitution changed an acidic residue for a basic residue. The new lysine forms a salt bridge with Glu-40 in 2-1B (**Fig. 4D**) and a double salt bridge with Glu-36 and Glu-83 in EHG (**Fig. 4C**). In contrast, the side chain of Glu-37 in VP did not make this type of interactions (**Fig. 4B**). On the other hand, Glu-37 is close (< 7 Å) to several acidic residues (such as Glu-40 and Glu-36 on helix B, Glu-83 on helix C, Glu-26 on helix A and Asp-30 and Asp-175 on two loops). Among these acidic residues, it is worth noting the position of Asp-30, whose side chain is at only 3.2 Å from residue 37. Therefore, the introduction of the new Lys-37 in 2-1B and EHG variants removed the destabilizing acid-acid interaction between Glu-37 and Asp-30.

G330R was also involved in the pH-stability improvement of 2-1B. It is the penultimate residue in the VP C-terminal tail, and its position could not be determined in the crystal due to the high mobility of this area. For this reason, we could not verify in which way this mutation contributed to enhance the stability. Nonetheless, it is interesting to note that residue 330 is close to residues 37 and 39, all of them around the Mn^{2+}-binding site.

Q202L, at the bottom of the molecule (**Fig. 5A**), was the last mutation identified as stabilizing VP under alkaline conditions. The introduction of Leu-202 in 2-1B led to the disappearance of two H-bonds present in native VP, one with Ala-235 and other with Glu-304 (**Fig. 5B** and **C**). As a consequence, the position of the side chain of some surrounding residues changed in the 2-1B variant, especially that of Gln-305 forming

three new interactions with Gln-245, Cys-307 and Thr-310 in 2-1B. These interactions reinforced and joined two solvent-exposed regions of the protein: i) the helix I; and ii) the loop between the helix 3_{10} (from Leu-300 to Asp-302) and the C-terminal tail. None of these interactions appeared in the native VP.

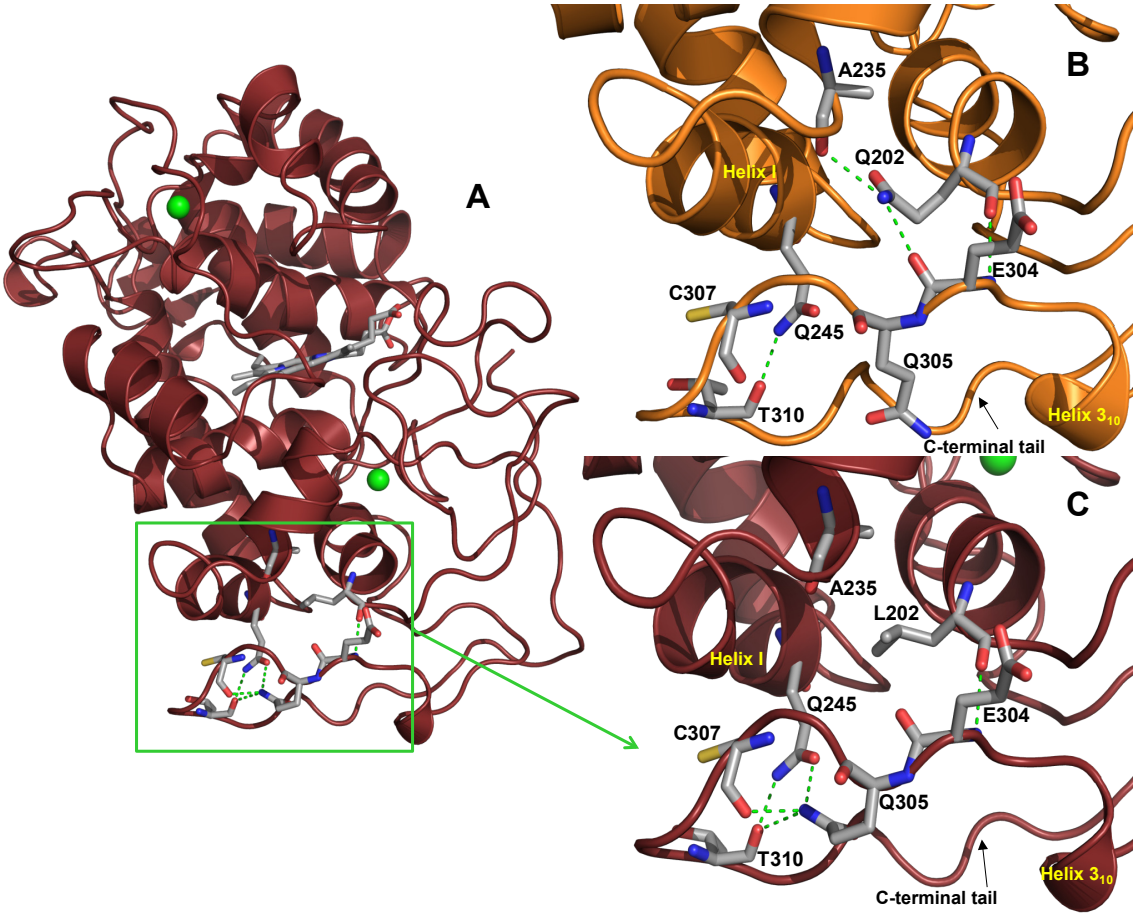

Figure 5. Q202L mutation in 2-1B crystal structure
Crystal structure of 2-1B (**A**) with a detail of the region around residue 202 in native VP (**B**) and the 2-1B (**C**) variant. Analyzed residues are shown as CPK sticks, hydrogen bonds as green dashed lines, calcium ions as green spheres and secondary structure as coloured cartoon.

Regarding the structural calcium ions, described as essential for pH stability, in 2-1B and EHG structures, both of them appeared coordinated in the same way than in the native VP.

Finally, the effects of the T184M mutation were studied in the 2-1B structure (**Fig. 6**), since it was involved in the enhanced oxidation of ABTS and DMP at the low efficiency site. Residue 184 is solvent exposed and located below the Mn^{2+}-binding site, formed by Glu-36, Glu-40 and

Asp-175. In native VP, Thr-184 forms three H-bonds, two with the backbone of Ala-174 and another with Ile-181. On the contrary, Met-184 in the 2-1B variant only formed one H-bond with Ala-174, near Asp-175 at the Mn^{2+}-binding site.

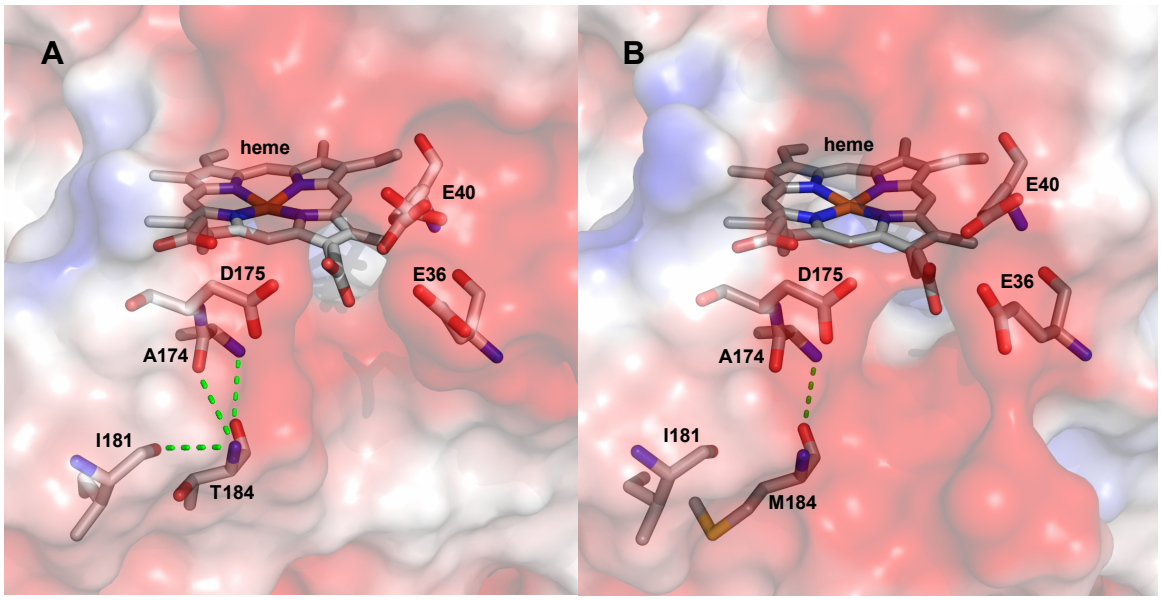

Figure 6. T184M mutation in 2-1B crystal structure.
Detail of the crystal structure of native VP (**A**) and 2-1B (**B**) showing residue 184 and the surrounding region. Residues and heme shown as CPK-coloured sticks, hydrogen bond as green dashed lines, and semitransparent protein surface in CPK colours.

4. Discussion

The 2-1B variant of *P. eryngii* VP contains seven mutations, introduced during the evolution process in *S. cerevisiae*, that conferred significantly improved alkaline stability and enhanced activity on some low redox potential substrates (García-Ruiz et al., 2012). In the present work we identified some of the structural bases of the new properties of this VP variant, by analyzing the stability and catalytic properties of a series of (single and multiple) variants expressed in *E. coli*.

First, we confirmed that 2-1B expressed in *E. coli* retains the improved properties observed when expressed in *S. cerevisiae*. However, it is possible to mention that, although 2-1B produced in *E. coli* showed a significantly increased alkaline stability (retaining 80% and 20% activity after 120 h at pH 8 and pH 9, respectively) compared

with native VP (which was completely inactivated) this improvement was not as high as found when the variant was expressed in *S. cerevisiae* (100% and 60% activity at pH 8 and pH 9, respectively) (García-Ruiz et al., 2012). These differences are likely due to the lack of glycosylation of 2-1B expressed in *E. coli*, as reported for temperature stability of *Phanerochaete chrysosporium* ligninolytic peroxidases (Nie et al., 1999). In general, glycosylation has been described to give robustness and protection against enzyme inactivation (Olden et al., 1985; Tams and Welinder, 1998) and, therefore, could reinforce the stabilizing effect of the mutations introduced in 2-1B.

4.1 Explaining the alkaline stability

During alkaline inactivation, ligninolytic peroxidases lose their structural calcium ions leading to a relaxation of the protein structure and hexacoordination of the heme involving the distal histidine (George et al., 1999). These changes are reflected in the electronic absorption spectrum, which is indicative of the high or low spin states of the heme iron and its coordination state (Youngs et al., 2000). The *P. eryngii* native VP was inactivated in 24 h upon alkaline incubation (pH 8), showing the spectrum of a low-spin hexacoordinated heme iron. This is characterized by the red-shifted Soret band and the appearance of the α and β bands. Similar changes have been reported for *Bjerkandera adusta* VP (Verdín et al., 2006) and other ligninolytic peroxidases, such as LiP (George et al., 1999) and MnP from *P. chrysosporium* (Youngs et al., 2000). In contrast, the EHG variant showed improved alkaline stability and conserved the UV-visible spectrum (including the Soret maximum and the CT1 and CT2 bands) unchanged during incubation at pH 8. This spectrum is indicative of a peroxidase with a high-spin ferric state of the heme iron, which is completely functional (Santoni et al., 2004). From these data, it can be inferred that the three new basic residues present in EHG (Lys-37, Arg-39 and Arg-330) reinforced the heme environment enabling the maintenance of pentacoordinated heme iron at pH 8, as required for the catalytic activity of the enzyme.

The stability improvement achieved with the introduction of these basic residues could be rationalized by comparative analysis of the EHG, 2-1B and native VP crystal structures. The new Arg-39 appeared

hydrogen-bonded to the heme distal propionate in the two variants. The connections of the heme with the apoprotein have been described as essential for stability (Henriksen et al., 2001; Mirza et al., 2000) and engineering new connections with the heme has been proposed as an strategy to increase stability (Kamal and Behere, 2008). The heme in ligninolytic peroxidases is non-covalently bound and shows no polar interactions with the apoprotein, with the exception of those that the propionates make. So, the new connection made by Arg-39 seems important for the stability achieved, as it anchors the heme to the protein (helix B) and contributes to fix the relative position of His-47 with respect to the iron ion. Heme iron coordination by His-47 (at pH 8) would be, therefore, prevented at the same time that the cofactor release will be delayed. Moreover, the stabilizing effect produced by Arg-39 could be related to the packing effect, since the lateral chain of the arginine is taking up more space than the lateral chain of the histidine in native VP, reducing the mobility of the heme and the residues around and, therefore, increasing the stability.

On the other hand, the new Lys-37 forms new salt bridges, which contributed to the improved stability of 2-1B and EHG. Those with Glu-36 in EHG and Glu-40 in 2-1B reinforced the structure of helix B, located directly above the heme and harbouring distal histidine (His-47) and arginine (Arg-43), which are essential in the reaction of the enzyme with H_2O_2 (Hiner et al., 2002) and in the stabilization of the oxidized forms of the heme iron (Erman et al., 1993; Vitello et al., 1993). Moreover, as in the case of H39R mutation, fixing the helix B position will reduce the possibilities of His-47 to approach the heme and generate the inactive form with hexacoordinated iron. Helix B also contains Asp-48, one of the residues coordinating the distal calcium, which is required for pH stability. Additionally, the ion pair between Lys-37 and Glu-83 in helix C (directly above helix B) in EHG, would also contribute to the increased stability, although this interaction would not be determinant as it did not appeared in 2-1B, which showed higher stability than EHG. The presence of salt bridges has been positively correlated with stability in different families of proteins (Vogt et al., 1997; Kumar et al., 2000; Vinther et al., 2011; Gromiha et al., 2013). In addition, a high number of acidic residues were observed around residue 37. At alkaline pH 8, these residues would be deprotonated. In consequence, a high concentration

of negative charge would characterize this region. The introduction of a basic residue (Lys-37) would reduce the negative charge avoiding detrimental interactions and reinforcing the structure of VP at alkaline pH. At acidic pH, however, the acidic residues will be protonated and no accumulation of negative charge would be produced, explaining the lack of acidic stability improvement of EHG and 2-1B.

The G330R mutation also contributed to the improved stability found in 2-1B and EHG. Although the role played by Arg-330 could not be studied in the crystal structures, it is likely that this residue located in the same area as residues 37 and 39 forms new interactions stabilizing the surrounding region containing a high number of acidic residues.

It was remarkable the fact that the stabilizing effect produced by Lys-37, Arg-39 and Arg-330 was only detected when they appeared together, since the H39R variant was unstable and the E37K/G330R variant showed a similar stability to that of the native VP. The sum of the new interactions formed by these residues results in the stabilization of VP but, individually, they make the protein instable due to the vulnerability of the region where they are (near the heme and the Mn^{2+}-binding site).

The EHGQ (E37K/H39R/G330R/Q202L) variant showed higher stability than EHG and almost achieved the alkaline stability found in 2-1B, so it was concluded that: i) the Q202L mutation also contributed to the enzyme stabilization; and ii) the four mutations introduced in EHGQ are responsible for the most part of the enhancement towards alkaline stability found in 2-1B. From the analysis of the crystal structure of 2-1B, it was observed that the Q202L substitution promoted the reorganization of Gln-305 and the formation of new interactions in the area which could explain the improvement observed due to this mutation. Although residue 202 is in the core of the protein, the residues affected by the new interactions are solvent exposed. The solvent exposed regions are very sensitive to pH changes, so the reinforcement of these areas could be determinant to strengthen the structure and avoid the alkaline inactivation at pH 8. Moreover, residue 202 would be an example of a residue located far from the heme and the rest of catalytic sites that is able to increase the stability of the enzyme.

4.2 Explaining the modified catalytic properties

Regarding the catalytic properties of 2-1B, it was found that this variant is more efficient than the native enzyme oxidizing low redox potential substrates, mainly due to an increased affinity (a decreased K_m). The same behaviour was previously reported for 2-1B expressed in *S. cerevisiae* (García-Ruiz et al., 2012). This fact was attributed to the T184M mutation. It is possible that the disruption of two H-bonds produced by the removal of Thr-184, especially the one with Ala-174, next to Asp-175 (that is part of the Mn^{2+} binding site), gives more flexibility to the region between the Mn-binding channel and the main heme-access channel).

The simultaneous worsening in manganese oxidation is explained by the introduction of Lys-37 and Arg-39 (García-Ruiz et al., 2012). These two residues could compromise the Mn^{2+}-binding by forming salt bridges with Glu-36 and Glu-40 (two of the three residues involved in Mn-coordination together with Asp-175) in EHG and 2-1B, respectively. Moreover, it is also probable that the new interaction established between the heme internal propionate and the apoprotein in 2-1B and EHG affects the Mn^{2+} binding and oxidation, considering that this propionate is involved in these two events (Ruiz-Dueñas et al., 2007). Interestingly, the kinetic constants for Mn^{2+} oxidation in 2-1B and the rest of variants were similar to that obtained for VP E36D and E40D variants (Ruiz-Dueñas et al., 2007), which suffered a shortening of the lateral chain of Glu-36 and Glu-40 (substitution by aspartic acid). These substitutions led to a worsening in the Mn^{2+} oxidation reflected in a high increase (25-fold) of the K_m and a consequent decrease in the efficiency. In the same way, 2-1B and derived variants showed K_m values 43-54-fold higher. It is likely that salt bridges formed by Lys-37 in EHG and 2-1B were limiting the mobility of Glu-36 and Glu-40 leading to an impaired activity towards manganese in a similar way as happened with the E36D and E40D variants. Finally, substrate oxidation at the catalytic tryptophan was not impaired by the mutations introduced in 2-1B given that the oxidation of high redox compounds such as VA and RB5 by this variant was similar to that found in native VP. This is indicative of the maintenance of the high redox potential of the enzyme, determined by

the position of the proximal histidine and by the strength of the interaction between this residue and the heme iron (Banci et al., 2003; Banci et al., 1991).

4.3 Conclusions

We were able to provide a structural-functional basis for the improved stability of the 2-1B variant by designing and characterizing several (individual and multiple) intermediate variants with the same mutations found in 2-1B. The *E. coli* expression system used not only facilitated variant generation by site-directed mutagenesis, but also enabled crystallization of the non-glycosylated forms of two of them. In this way, the introduction of three basic residues in VP (Lys-37, Arg-39 and Arg-330) resulted in new interactions at the heme environment that avoided the hexacoordination of the heme iron, which leads to enzyme inactivation at pH 8. Moreover, the reinforcement of the solvent-exposed area around Gln-305, in the proximal side, further enhanced the stability. Interestingly, the biochemical characterization of the intermediate variants revealed discrete stability improvements, and the combination of most of them was required to stabilize VP. This stabilization could be obtained by random combination of mutations using directed molecular evolution, and would be impossible by a rational approach since the basis for the synergistic improvements observed could not be predicted "a priori".

5. References

Banci, L., I.Bertini, P.Turano, M.Tien, and T.K.Kirk. 1991. Proton NMR investigation into the basis for the relatively high redox potential of lignin peroxidase. *Proc. Natl. Acad. Sci. USA* 88:6956-6960.

Banci, L., S.Camarero, A.T.Martínez, M.J.Martínez, M.Pérez-Boada, R.Pierattelli, and F.J.Ruiz-Dueñas. 2003. NMR study of Mn(II) binding by the new versatile peroxidase from the white-rot fungus *Pleurotus eryngii*. *J. Biol. Inorg. Chem.* 8:751-760.

Borrelli, K., B.Cossins, and V.Guallar. 2010. Exploring hierarchical refinement techniques for induced fit docking with protein and ligand flexibility. *J. Comp. Chem.* 31:1224-1235.

Borrelli, K.W., A.Vitalis, R.Alcantara, and V.Guallar. 2005. PELE: Protein energy landscape exploration. A novel Monte Carlo based technique. *J. Chem. Theory Comput.* 1:1304-1311.

Britton, H.T.S. and R.A.Robinson. 1931. Universal buffer soluttions and the association constant of veronal. *Journal of the Chemical Society*1456-1462.

Erman, J.E., L.B.Vitello, M.A.Miller, A.Shaw, K.A.Brown, and J.Kraut. 1993. Histidine 52 is a critical residue for rapid formation of cytochrome *c* peroxidase compound I. *Biochemistry* 32:9798-9806.

Fernández-Fueyo, E., S.Acebes, F.J.Ruiz-Dueñas, M.J.Martínez, A.Romero, F.J.Medrano, V.Guallar, and A.T.Martínez. 2014. Structural implications of the C-terminal tail in the catalytic and stability properties of manganese peroxidases from ligninolytic fungi. *Acta Crystallogr. D. Biol. Crystallogr.* 70:3253-3265.

Floudas, D., M.Binder, R.Riley, K.Barry, R.A.Blanchette, B.Henrissat, A.T.Martínez, R.Otillar, J.W.Spatafora, J.S.Yadav, A.Aerts, I.Benoit, A.Boyd, A.Carlson, A.Copeland, P.M.Coutinho, R.P.de Vries, P.Ferreira, K.Findley, B.Foster, J.Gaskell, D.Glotzer, P.Górecki, J.Heitman, C.Hesse, C.Hori, K.Igarashi, J.A.Jurgens, N.Kallen, P.Kersten, A.Kohler, U.Kües, T.K.A.Kumar, A.Kuo, K.LaButti, L.F.Larrondo, E.Lindquist, A.Ling, V.Lombard, S.Lucas, T.Lundell, R.Martin, D.J.McLaughlin, I.Morgenstern, E.Morin, C.Murat, M.Nolan, R.A.Ohm, A.Patyshakuliyeva, A.Rokas, F.J.Ruiz-Dueñas, G.Sabat, A.Salamov, M.Samejima, J.Schmutz, J.C.Slot, F.St.John, J.Stenlid, H.Sun, S.Sun, K.Syed, A.Tsang, A.Wiebenga, D.Young, A.Pisabarro, D.C.Eastwood, F.Martin, D.Cullen, I.V.Grigoriev, and D.S.Hibbett. 2012. The Paleozoic origin of enzymatic lignin decomposition reconstructed from 31 fungal genomes. *Science* 336:1715-1719.

García-Ruiz, E., D.González-Pérez, F.J.Ruiz-Dueñas, A.T.Martínez, and M.Alcalde. 2012. Directed evolution of a temperature-, peroxide- and alkaline pH-tolerant versatile peroxidase. *Biochem. J.* 441:487-498.

George, S.J., M.Kvaratskhelia, M.J.Dilworth, and R.N.F.Thorneley. 1999. Reversible alkaline inactivation of lignin peroxidase involves the release of both the distal and proximal site calcium ions and bishistidine co-ordination of the haem. *Biochem. J.* 344:237-244.

Gold, M.H., H.L.Youngs, and M.D.Gelpke. 2000. Manganese peroxidase. *Met. Ions Biol. Syst.* 37:559-586.

Gromiha, M.M., M.C.Pathak, K.Saraboji, E.A.Ortlund, and E.A.Gaucher. 2013. Hydrophobic environment is a key factor for the stability of thermophilic proteins. *Proteins* 81:715-721.

Guallar, V., C.Y.Lu, K.Borrelli, T.Y.Egawa, and S.R.Yeh. 2009. Ligand migration in the truncated hemoglobin-II from *Mycobacterium tuberculosis*: The role of G8 tryptophan. *J. Biol. Chem.* 284:3106-3116.

Halgren, T. 2007. New method for fast and accurate binding-site identification and analysis. *Chem. Biol. Drug Design* 69:146-148.

Hammel, K.E. and D.Cullen. 2008. Role of fungal peroxidases in biological ligninolysis. *Curr. Opin. Plant Biol.* 11:349-355.

Henriksen, A., O.Mirza, C.Indiani, K.Teilum, G.Smulevich, K.G.Welinder, and M.Gajhede. 2001. Structure of soybean seed coat peroxidase: A plant peroxidase with unusual stability and haem-apoprotein interactions. *Protein Sci.* 10:108-115.

Hiner, A.N.P., E.L.Raven, R.N.F.Thorneley, F.García-Canovas, and J.N.Rodríguez-López. 2002. Mechanisms of compound I formation in heme peroxidases. *J. Inorg. Biochem.* 91:27-34.

Husain, Q. 2010. Peroxidase mediated decolorization and remediation of wastewater containing industrial dyes: a review. *Rev. Environ. Sci. Bio.* 9:117-140.

Kamal, J.K.A. and D.V.Behere. 2008. Kinetic stabilities of soybean and horseradish peroxidases. *Biochem. Eng. J.* 38:110-114.

Kumar, S., C.J.Tsai, and R.Nussinov. 2000. Factors enhancing protein thermostability. *Protein Eng.* 13:179-191.

Martínez, A.T., F.J.Ruiz-Dueñas, A.Gutiérrez, J.C.del Río, M.Alcalde, C.Liers, R.Ullrich, M.Hofrichter, K.Scheibner, L.Kalum, J.Vind, and H.Lund. 2014. Search, engineering and applications of new oxidative biocatalysts. *Biofuels Bioprod. Biorefining* 8:819-835.

Martínez, A.T., F.J.Ruiz-Dueñas, M.J.Martínez, J.C.del Río, and A.Gutiérrez. 2009. Enzymatic delignification of plant cell wall: from nature to mill. *Curr. Opin. Biotechnol.* 20:348-357.

Martínez, A.T., M.Speranza, F.J.Ruiz-Dueñas, P.Ferreira, S.Camarero, F.Guillén, M.J.Martínez, A.Gutiérrez, and J.C.del Río. 2005. Biodegradation of lignocellulosics: Microbiological, chemical and enzymatic aspects of fungal attack to lignin. *Int. Microbiol.* 8:195-204.

Mirza, O., A.Henriksen, L.Ostergaard, K.G.Welinder, and M.Gajhede. 2000. Arabidopsis thaliana peroxidase N: structure of a novel neutral peroxidase. *Acta Crystallographica Section D-Biological Crystallography* 56:372-375.

Morales, M., M.J.Mate, A.Romero, M.J.Martínez, A.T.Martínez, and F.J.Ruiz-Dueñas. 2012. Two oxidation sites for low redox-potential substrates: A directed mutagenesis, kinetic and crystallographic study on *Pleurotus eryngii* versatile peroxidase. *J. Biol. Chem.* 287:41053-41067.

Nie, G.J., N.S.Reading, and S.D.Aust. 1999. Relative stability of recombinant versus native peroxidases from *Phanerochaete chrysosporium*. *Arch. Biochem. Biophys.* 365:328-334.

Olden, K., B.A.Bernard, M.J.Humphries, T.K.Yeo, K.T.Yeo, S.L.White, S.A.Newton, H.C.Bauer, and J.B.Parent. 1985. Function of Glycoprotein Glycans. *Trends in Biochemical Sciences* 10:78-82.

Pérez-Boada, M., W.A.Doyle, F.J.Ruiz-Dueñas, M.J.Martínez, A.T.Martínez, and A.T.Smith. 2002. Expression of *Pleurotus eryngii* versatile peroxidase in *Escherichia coli* and optimisation of *in vitro* folding. *Enzyme Microb. Technol.* 30:518-524.

Ragauskas, A.J., G.T.Beckham, M.J.Biddy, R.Chandra, F.Chen, M.F.Davis, B.H.Davison, R.A.Dixon, P.Gilna, M.Keller, P.Langan, A.K.Naskar, J.N.Saddler, T.Tschaplinski, G.A.Tuskan, and C.E.Wyman. 2014. Lignin valorization: improving lignin processing in the biorefinery. *Science* 344:1246843.

Ragauskas, A.J., C.K.Williams, B.H.Davison, G.Britovsek, J.Cairney, C.A.Eckert, W.J.Frederick, J.P.Hallett, D.J.Leak, C.L.Liotta, J.R.Mielenz, R.Murphy, R.Templer, and T.Tschaplinski. 2006. The path forward for biofuels and biomaterials. *Science* 311:484-489.

Ruiz-Dueñas, F.J. and A.T.Martínez. 2009. Microbial degradation of lignin: How a bulky recalcitrant polymer is efficiently recycled in nature and how we can take advantage of this. *Microbial Biotechnol.* 2:164-177.

Ruiz-Dueñas, F.J., M.J.Martínez, and A.T.Martínez. 1999. Molecular characterization of a novel peroxidase isolated from the ligninolytic fungus *Pleurotus eryngii*. *Mol. Microbiol.* 31:223-236.

Ruiz-Dueñas, F.J., M.Morales, E.García, Y.Miki, M.J.Martínez, and A.T.Martínez. 2009. Substrate oxidation sites in versatile peroxidase and other basidiomycete peroxidases. *J. Exp. Bot.* 60:441-452.

Ruiz-Dueñas, F.J., M.Morales, M.Pérez-Boada, T.Choinowski, M.J.Martínez, K.Piontek, and A.T.Martínez. 2007. Manganese oxidation site in *Pleurotus eryngii* versatile peroxidase: A site-directed mutagenesis, kinetic and crystallographic study. *Biochemistry* 46:66-77.

Sambrook, J. and D.W.Russell. 2001. Molecular cloning. CSHL Press, Cold Spring Harbor, New York.

Santoni, E., C.Jakopitsch, C.Obinger, and G.Smulevich. 2004. Comparison between catalase-peroxidase and cytochrome c peroxidase. The role of the hydrogen-bond networks for protein stability and catalysis. *Biochemistry USA* 43:5792-5802.

Tams, J.W. and K.G.Welinder. 1998. Glycosylation and thermodynamic versus kinetic stability of horseradish peroxidase. *FEBS Lett.* 421:234-236.

Verdín, J., R.Pogni, A.Baeza, M.C.Baratto, R.Basosi, and R.Vázquez-Duhalt. 2006. Mechanism of versatile peroxidase inactivation by Ca2+ depletion. *Biophys. Chem.* 121:163-170.

Vinther, J.M., S.M.Kristensen, and J.J.Led. 2011. Enhanced Stability of a Protein with Increasing Temperature. *J. Am. Chem. Soc.* 133:271-278.

Vitello, L.B., J.E.Erman, M.A.Miller, J.Wang, and J.Kraut. 1993. Effect of Arginine-48 replacement on the reaction between cytochrome *c* peroxidase and hydrogen peroxide. *Biochemistry* 32:9807-9818.

Vogt, G., S.Woell, and P.Argos. 1997. Protein thermal stability, hydrogen bonds, and ion pairs. *J. Mol. Biol.* 269:631-643.

Wallace, A.C., R.A.Laskowski, and J.M.Thornton. 1995. LIGPLOT: a program to generate schematic diagrams of protein-ligand interactions. *Protein Eng* 8:127-134.

Youngs, H.L., P.Moënne-Loccoz, T.M.Loehr, and M.H.Gold. 2000. Formation of a bis(histidyl) heme iron complex in manganese peroxidase at high pH and

restoration of the native enzyme structure by calcium. *Biochemistry* 39:9994-10000.

CHAPTER 4

Demonstration of Lignin-to-Peroxidase Direct Electron Transfer: A Transient-state Kinetics, Directed Mutagenesis, EPR and NMR Study

Abstract

Versatile peroxidase is a high redox-potential peroxidase of biotechnological interest that is able to oxidize phenolic and non-phenolic aromatics, Mn^{2+}, and different dyes. The ability of VP from *Pleurotus eryngii* to oxidize water-soluble lignins (softwood and hardwood lignosulfonates) is demonstrated here by a combination of directed mutagenesis and spectroscopic techniques, among others. In addition, direct electron transfer between the peroxidase and the lignin macromolecule was kinetically characterized using stopped-flow spectrophotometry. VP variants were used to show that this reaction strongly depends on the presence of a solvent-exposed tryptophan residue (Trp-164). Moreover, the tryptophan radical detected by EPR spectroscopy of H_2O_2-activated VP (being absent from the W164S variant) was identified as catalytically active, since it was reduced during lignosulfonate oxidation resulting in the appearance of a lignin radical. The decrease of lignin fluorescence (excitation 355 nm/emission 400 nm) during VP treatment under steady-state conditions was accompanied by a decrease of the lignin (aromatic nuclei and side chains) signals in 1D and 2D NMR spectra, confirming the ligninolytic capabilities of the enzyme. Simultaneously, size-exclusion chromatography showed an increase of the molecular mass of the modified residual lignin, especially for the (low molecular mass) hardwood lignosulfonate, revealing that the oxidation products tend to recondense during the VP treatment. Finally, mutagenesis of selected residues neighbor to Trp-164 resulted in improved apparent second-order rate constants for lignosulfonate reactions, revealing that changes in its protein environment (modifying the net negative charge and/or substrate accessibility/binding) can modulate the reactivity of the catalytic tryptophan.

1. Introduction

Around 20% of the total carbon fixed in nature is incorporated into lignin. It is the only main component of biomass with an aromatic origin, and a valuable raw material as a source of aromatic simple chemicals

and polymers (Ragauskas et al., 2014). Moreover, due to the recalcitrant nature of the lignin polymer, its removal is a limiting step to access the plant polysaccharides (cellulose and hemicelluloses) as a sustainable industrial feedstock (Himmel et al., 2007; Martínez et al., 2009). Recent studies suggest that some bacterial enzymes are involved in degradation of lignin or lignin decay products (Gall et al., 2014; Ahmad et al., 2011). However, white-rot fungi are the main decayers of wood lignin in nature (Martínez et al., 2005), acting through a battery of secreted oxidoreductases that contribute to a degradation process defined as an "enzymatic combustion" (Kirk and Farrell, 1987). Among these enzymes, high redox-potential peroxidases - of the lignin peroxidase (LiP), manganese peroxidase (MnP) and versatile peroxidase (VP) families – play a central role in lignin attack (Ruiz-Dueñas and Martínez, 2009). The above is in agreement with the presence of ligninolytic peroxidase genes (of the above families) in the genomes in all typical white-rot (lignin-degrading) fungi sequenced to date (poor wood rotters excluded), and their absence from the genomes of all sequenced brown-rot (cellulose-degrading) fungi (Floudas et al., 2012; Riley et al., 2014; Floudas et al., 2015).

VP was first described in *Pleurotus eryngii* (Ruiz-Dueñas et al., 1999; Camarero et al., 1999), and it combines catalytic and structural properties of: i) LiP, characterized by the presence of a surface tryptophan residue involved in oxidation of high redox-potential substrates (such as veratryl alcohol mediating lignin degradation by this enzyme); ii) MnP, characterized by the presence of a Mn-binding site near one of the heme propionates, where Mn^{2+} is oxidized to Mn^{3+} (a diffusible oxidizer acting on lignin phenolic units); and iii) Generic peroxidases, which (as described for plant peroxidases) oxidize low-redox potential compounds at the heme access channel (Ruiz-Dueñas et al., 2009a). These hybrid properties allow VP to oxidize a variety of substrates (Heinfling et al., 1998; Pérez-Boada et al., 2005) that, as recently reported, also include synthetic lignin and model dimers (Fernández-Fueyo et al., 2014).

Ligninolytic peroxidases are of interest for enzymatic delignification processes, enabling the industrial use of biomass polysaccharides, as well as for the transformation of lignin into added-value products

(Martínez et al., 2009). Due to the potential application of these peroxidases as industrial biocatalysts, an in-depth knowledge of the mechanisms underlying and modulating their catalytic properties is of the highest biotechnological importance. During a basic catalytic cycle, similar to that of other peroxidases, the VP resting state (containing a Fe^{3+} heme) is activated by H_2O_2 yielding Compound I (CI, an Fe^{4+}=O·porphyrin radical complex). CI catalyzes an one-electron substrate oxidation and forms Compound II (CII, which contains Fe^{4+}=O). Through another one-electron oxidation of a second substrate molecule, the resting state is recovered. In an extension of the above cycle, VP oxidizes high redox-potential compounds through an exposed catalytic tryptophan which forms a radical (both in the CI and CII transient states) on the surface of the protein through long-range electron transfer (LRET) from this residue to the heme (Ruiz-Dueñas et al., 2009b) (**Fig. 1**).

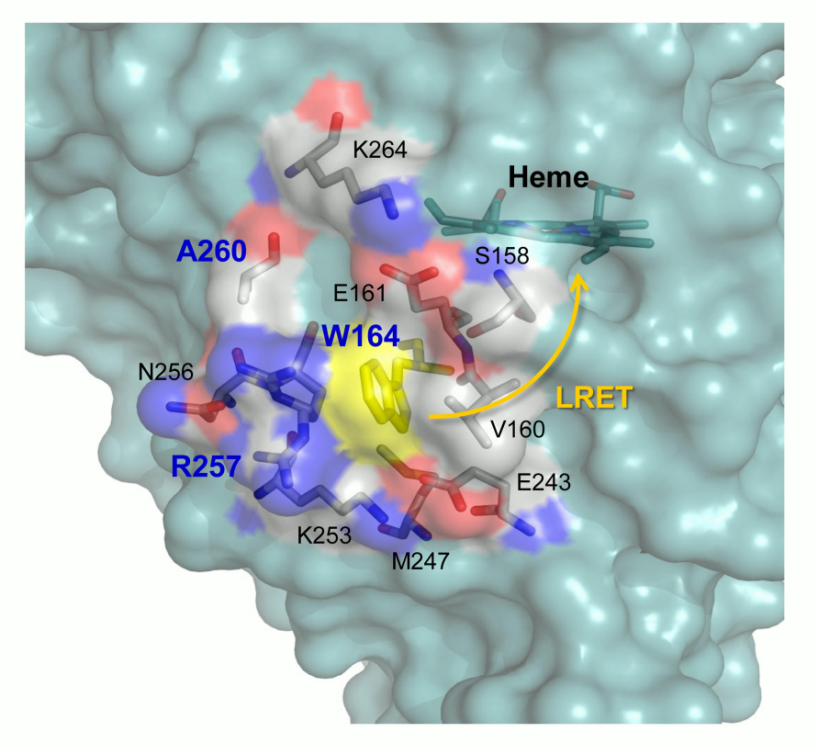

Figure 1. Environment of the exposed catalytic tryptophan acting as starting point for LRET to heme in VP. Trp-164, ten neighbor residues (those changed by directed mutagenesis in bold), heme (all as CPK-colored sticks), and semitransparent protein surface (blue, except for the above tryptophan, in yellow, and the neighbor residues, in CPK colors) are shown.

In this work, the ability of VP to act on the lignin polymer was investigated using water soluble sulfonated lignins. Lignosulfonates are obtained through the sulfite pulping of wood (Gleenie, 1971), being commercialized for a range of applications (http://www.lignotech.com/Industries). Representative softwood lignin, which contains monomethoxylated (guaiacyl) units, and hardwood lignin, which has both monomethoxylated and dimethoxylated (syringyl) units were used in this study. The main aim of the work was to study the transient-state kinetics of VP electron abstraction from the above lignins, the role played by a putative catalytic tryptophan in this redox reaction (through formation of a tryptophanyl free radical), and the modification of lignin during steady-state treatment of lignosulfonates with VP. With this purpose, a combination of site-directed mutagenesis, stopped-flow rapid spectrophotometry, fluorescence spectroscopy, size-exclusion chromatography (SEC), EPR, and NMR studies were performed.

2. Materials and methods

2.1 Enzyme production

VP from *P. eryngii* and its W164S and R257A/A260F mutated variants (Pérez-Boada et al., 2005; Ruiz-Dueñas et al., 2008) were produced in *Escherichia coli* as reported elsewhere (Pérez-Boada et al., 2002). In short, a pFLAG1 expression plasmid (International Biotechnologies Inc., Cambridge, UK) containing the mature protein-coding sequence of isoenzyme VPL2 (GenBank AF007222) was transformed into *E. coli* W3110. The cells were grown in Terrific Broth until optical density ~1. Then, protein expression was induced by addition of 1 mM isopropyl-β-D-thiogalactopyranoside (IPTG), and cells were further grown for 4 h. The apoprotein accumulated as inclusion bodies, and was recovered in a solution of 8 M urea, 1 mM DTT and 1 mM EDTA in 50 mM Tris-HCl (pH 8).

Subsequent *in vitro* reactivation was carried out overnight in a solution of 0.16 M urea,15 μM hemin, 5 mM $CaCl_2$, 0.1 mM DTT, 0.5 mM oxidized glutathione and 0.1 mg·mL^{-1} VP protein in 20 mM Tris-HCl (pH 9.5). Finally, native VP and its variants were purified by anion-exchange chromatography (Resource Q column, GE Healthcare, Uppsala, Sweden)

using a 0-0.3 M NaCl gradient (2 mL·min^{-1}, 20 min) in 10 mM sodium tartrate (pH 5.5) containing 1 mM $CaCl_2$. The R_z (A_{410}/A_{280}~ 4) of the variants was indicative of the purity of the proteins. The UV-visible spectrum was checked to confirm the correct folding and cofactor incorporation in the activated enzymes.

IPTG, DTT, hemin and oxidized glutathione were from Sigma Aldrich (St. Louis, MO, USA) and urea and EDTA were from Merck (Darmstadt, Germany).

2.2 Softwood and hardwood lignins

Two water-soluble sulfonated lignins were used in this study: softwood (*Picea abies*) lignosulfonate and hardwood (*Eucalyptus grandis*) lignosulfonate, both kindly provided by G.E. Fredheim (Borregaard AS, Sapsborg, Norway). The lignosulfonate samples were first dialyzed in 10 mM EDTA, 50 mM Tris (pH 8) with the aim of removing Mn^{2+} traces (which reduce H_2O_2-activated VP), and then in milli-Q water to remove buffer and EDTA. A model for softwood lignosulfonate chemical structure (Areskogh, 2011) is included in **Fig. 2a**, showing guaiacyl units linked by β-O-4' alkyl-aryl ether and other minor bonds. Creosol (Sigma Aldrich) (**Fig. 2b**) and α-sulfonated creosol, kindly provided by R.A. Lauten (Borregaard AS) (**Fig. 2c**), were used as simple models for normal and sulfonated lignin units in stopped-flow experiments.

2.3 Enzyme (transient-state) kinetics

Reduction of CI and CII of wild-type recombinant (hereinafter native) VP and its W164S and R257A/A260F variants in 0.1 M tartrate (pH 3) by softwood and hardwood lignosulfonates, creosol and α-sulfonated creosol was followed using a stopped-flow rapid spectrophotometry equipment (Bio-Logic, Claix, France) with a three-syringe module (SFM300) synchronized to a diode array detector (J&M, Essingen, Germany) and BioKine software.

CI reduction was studied by mixing the enzyme (1 μM final concentration) with H_2O_2 (1 μM final concentration) for 0.6 s, resulting in CI formation. Next, substrates were added at different concentrations, and the reaction was followed at 416 nm (isosbestic point of VP CII and resting state). CII reduction was studied by mixing a solution of enzyme

and ferrocyanide (both at 1 μM final concentration) with H_2O_2 at equimolar ratio. The solution was aged for 6 s, and CII formation was achieved. Then, different excess concentrations of substrate were added, and the reaction was followed at 406 nm (Soret maximum of resting VP). For comparison of the two lignins (and simple substrates) the lignosulfonate concentrations in these and other experiments were referred to the basic phenylpropanoid unit, shown in **Fig. 2** (corresponding to 260 Da and 290 Da in the sulfonated softwood and hardwood lignins, respectively).

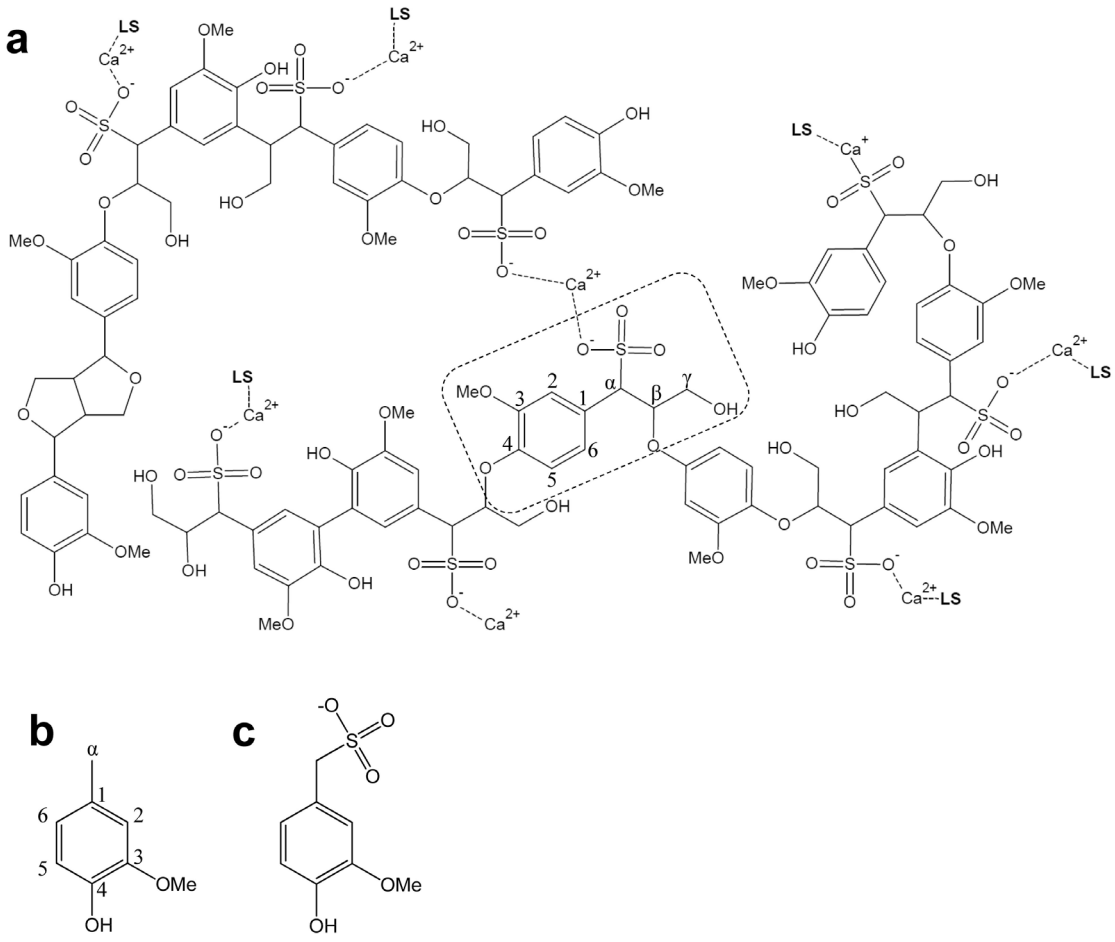

Figure 2. Tentative structure for sulfonated softwood lignin (Areskogh, 2011)**, and simple model compounds.** Structure of softwood lignosulfonate as Ca^{2+} salt (LS, lignosulfonate chains) (**a**); and formulae of creosol (**b**), and α-sulfonated creosol (**c**). The basic phenylpropanoid unit is shown (square), and carbon labeling is indicated. See **Fig. 8e** for the main structures identified in softwood (*P. abies*) and hardwood (*E. grandis*) lignosulfonates.

All kinetic traces exhibited single-exponential character from which pseudo first-order rate constants (k_{2obs} and k_{3obs} for CI and CII reduction, respectively) were calculated. Plots of k_{2obs} *vs* substrate concentration fitted to a linear or hyperbolic model from which apparent second-order rate constants (k_{2app}) were obtained. Plots of native VP k_{3obs} *vs* substrate concentration were fitted to a Michaelis-Menten model from which K_{D3} (dissociation constant of the enzyme-substrate, VP-lignosulfonate, complex) and k_3 (first-order rate constant) were obtained. The corresponding k_{3app} (k_3/K_{D3}) rate constants were calculated with the equation: $k_{3obs}= (k_3/K_{D3})[S]/(1+[S]/K_{D3})$, where [S] indicates substrate concentration. R257A/A260F CII reduction plots were fitted to a sigmoid model from which k_3 and $K_{0.5}$ (substrate concentration resulting in 50% k_3 that, in the present work, was considered equivalent to K_{D3}) constants were obtained. To calculate the k_{3app} values, the following equation was used: $k_{3obs}= K_{D3} (k_3/K_{D3})[S]^b/([S]^b+K_{D3}^b)$, where b is the Hill coefficient. Finally, W164S CII reduction plots were fitted to a linear model from which k_{3app} values were determined.

2.4 EPR of VP reactions with lignin

EPR measurements were performed in solutions containing 0.16 mM VP, 1.3 mM H_2O_2 and 0 (1:8:0 ratio), 0.64 (1:8:4 ratio) or 1.92 mM (1:8:12 ratio) softwood lignosulfonate in 50 mM tartrate (pH 3). The reactions were initiated by addition of H_2O_2 and stopped by immersion in liquid nitrogen after few seconds. CW-X-band (9 GHz) EPR measurements were carried out with a E500 Elexsys Series instrument (Bruker, Karlsruhe, Germany) using the Bruker ER 4122 SHQE cavity, and an ESR900 helium continuous flow cryostat (Oxford Instruments, Abingdon, UK) at 40 K. Measurements with the W164S variant were performed as described above, at 9, 20 and 40 K. Spin quantification was performed by double-integration of the experimental EPR tryptophan radical signal compared with the iron signal of the enzyme in the resting state. To calculate the percentage of lignin radical, the pure tryptophan radical signal was considered as our reference. The area (double integration) of the tryptophan radical signal, with the proper intensity, was subtracted from the area of the mixed signal including the tryptophanyl and lignin radicals (see Results).

2.5 Lignosulfonate treatment under steady-state conditions (fluorescence monitoring)

Softwood and hardwood lignosulfonates (12 g·L^{-1}) were treated with VP (1.3 μM, added in two equivalent doses after 0 and 6 h) and H_2O_2 (12.5 mM, added continuously over 24 h with a syringe pump) in 50 mM phosphate (pH 5), at 25 °C, for different times (3, 12 and 24 h). Control treatments were performed under the same conditions but in the absence of enzyme. Changes in lignin fluorescence were monitored (excitation 355 nm/emission 400 nm) using a Fluorolog-3-221 instrument (Jobin Yvon-Spex, Longjumeau, France) at 25 °C. The lignin samples were diluted to 10 μg·mL^{-1} in 2-methoxyethanol/water (2:1 v/v) before the fluorescence measurement.

2.6 SEC and GC-MS analyses

Changes in the molecular-mass distribution of the VP-treated softwood and hardwood lignosulfonates and controls (described above) were analyzed by SEC using a Superdex-75 column (HR-10/30, 3,000-70,000 Da range; GE Healthcare) with 0.1 M NaOH as the mobile phase, at a flow rate of 0.5 mL·min^{-1}. UV-visible (280 nm), refraction index (RI) and multi-angle laser light scattering (MALLS) detection were compared. Blue dextran (Serva, Heindelberg, Germany) was used to determine the exclusion volume of the column, and a kit of sulfonated polystyrenes sodium salt standards with main peaks (Mp) in the 891-976,000 Da range (PSS, Mainz, Germany) was used for calibration and mass determination (Ve/Vo *vs* Log(Mp), where Ve and Vo are the elution and void volumes.

Low molecular-mass compounds in the reaction mixtures, and controls, were investigated by GC-MS after liquid-liquid extraction with methyl tert-butyl ether (Merck, Darmstadt, Germany) at pH 2. The extracts, with/without N,O-bis(trimethylsilyl)- trifluoroacetamide (Sigma Aldrich) derivatization, were analyzed using a GCMS-QP2010 Ultra instrument (Shimadzu Co., Kyoto, Japan) and a J&W capillary column (DB-5HT 30 m × 0.25 mm I.D., 0.10 μm film thickness). The oven was heated from 60°C (1 min) to 350°C (2 min) at 10°C·min^{-1}. The injector was set at 350 °C and the transfer line was kept at 300 °C.

Helium was used as the carrier gas (1 mL·min^{-1}). Compounds were identified and quantified using authentic standards.

2.7 Lignin NMR

Samples after different times (3, 12 and 24 h) of softwood and hardwood lignosulfonate treatment and the corresponding controls (described above) were freeze-dried for NMR analyses. Solution NMR spectra, including ^{13}C NMR and heteronuclear single quantum correlation (HSQC) 2D-NMR spectra, were recorded at 25 °C on an AVANCE III 500 MHz instrument (Bruker) equipped with a cryogenically cooled 5 mm TCI gradient probe with inverse geometry. The lignosulfonate samples (40 mg initial weight, before treatments) were dissolved in 0.75 mL of deuterated DMSO-d_6. The central solvent peak was used as the internal reference (at δ_C/δ_H 39.5/2.49 ppm), and the other signals were normalized to the same intensity of the DMSO signals (since the same initial sample was used in all the cases).

The HSQC experiment used Bruker's "hsqcetgpsisp2.2" adiabatic pulse program with spectral widths from 0 to 10 ppm (5000 Hz) and from 0 to 165 ppm (20625 Hz) for the ^{1}H and ^{13}C dimensions. The number of transients was 64, and 256 time increments were always recorded in the ^{13}C dimension. The $^{1}J_{CH}$ used was 145 Hz. Processing used typical matched Gaussian apodization in the ^{1}H dimension and squared cosine-bell apodization in the ^{13}C dimension. Prior to Fourier transformation, the data matrices were zero-filled to 1024 points in the ^{13}C dimension. Signals were assigned by literature comparison (Ralph et al., 1999; Lebo et al., 2008; Lutnaes et al., 2008; Rencoret et al., 2009; Prasetyo et al., 2010; Magina et al., 2015). In the aromatic region of the spectrum, the lignin C_2–H_2, C_5–H_5 and C_6–H_6 correlation signals were integrated to estimate the amount of lignins and the syringyl-to-guaiacyl ratio. In the aliphatic oxygenated region, the signals of methoxyls, and C_β–H_β (or C_α–H_α) correlations in the side chains of sulfonated and non-sulfonated β-O-4′ linked, phenylcoumaran and resinol substructures were also integrated. The intensity corrections introduced by the adiabatic pulse program permits to refer the latter integrals to the previously obtained number of lignin units.

Cross-polarization magic-angle spinning (CPMAS) ^{13}C NMR spectra of solid lignosulfonate samples were recorded for 9-72 h on a Bruker AVANCE III 400 using the standard pulse sequence, a time domain of 2 K, a spectral width of 41 Hz, a contact time of 1.5 ms, and an interpulse delay of 5 s.

3. Results

3.1 Transient-state kinetics of electron abstraction from lignin

The transient-state kinetic constants for lignosulfonate reaction with VP were obtained from stopped-flow measurements. Native VP CI/CII were able to react with lignin from both softwood and hardwood (**Fig. 3** top and bottom, respectively) exhibiting similar apparent second-order rate constants (k_{app}) (**Table 1**), although some differences were observed in the CII reduction K_{D3} and k_3 values.

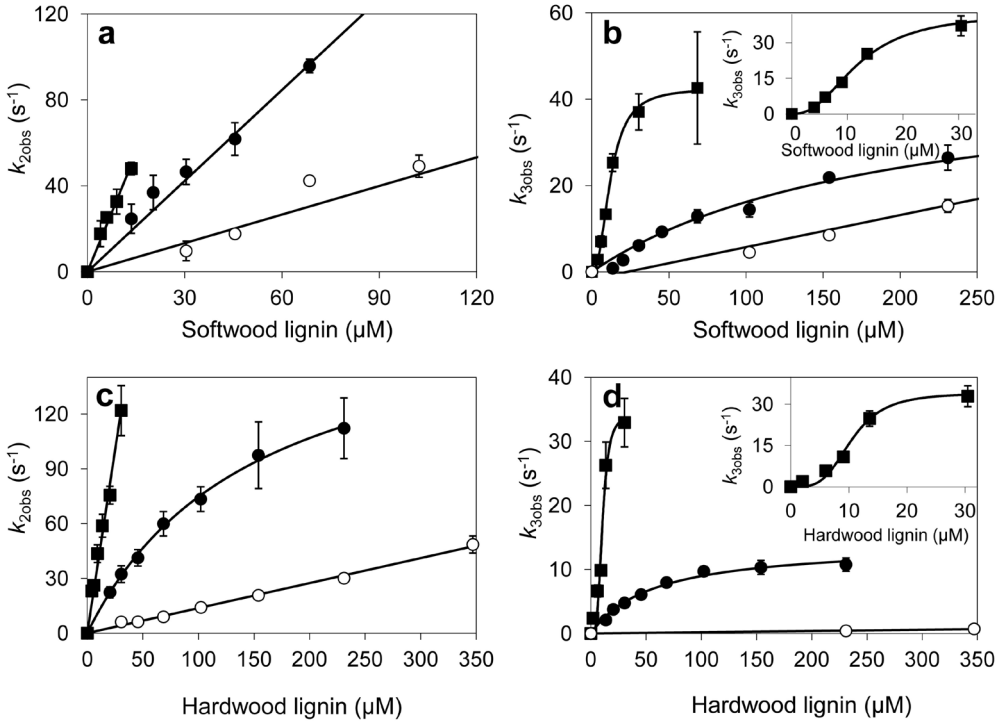

Figure 3. Kinetics of reduction of CI (a, c) and CII (b, d) of native VP (●) and its W164S (○) and R257A/A260F (■) variants by softwood (a,b) and hardwood (c,d) lignosulfonates. Stopped-flow reactions were carried out at 25 °C in 0.1 M tartrate (pH 3). The lignosulfonate concentrations in **Figs. 3-5** refer to the basic phenylpropanoid unit, as explained in Materials and Methods. Means and 95% confidence limits are shown. Insets show the R257A/A260F kinetic curves for a smaller concentration range.

Table 1. Transient-state kinetic constants for the reduction of CI and CII of the native VP and its W164S and R257A/A260F variants by softwood and hardwood lignosulfonates.

Shown are first-order rate constants, k_3 (s^{-1}); equilibrium dissociation constants, K_{D3} (μM); and apparent second-order rate constants, k_{2app} and k_{3app} ($s^{-1}mM^{-1}$). Means and 95 % confidence limits. The lignosulfonate concentrations refer to the basic sulfonated phenylpropanoid unit, as explained in Materials and Methods.

	CI reduction		**CII reduction**					
	Softwood	**Hardwood**	**Softwood**			**Hardwood**		
	k_{2app}	k_{2app}	k_3	K_{D3}	k_{3app}	k_3	K_{D3}	k_{3app}
VP	1410 ± 30	1240 ± 50	48 ± 2	194 ± 21	250 ± 20	14 ± 1	57 ± 7	250 ± 20
W164S	660 ± 90	140 ± 3	-[a]	-	70 ± 10	-	-	2 ± 0.2
R257A/A260F	3680 ± 150	4020 ± 130	40 ± 1	11 ± 1[b]	3540 ± 70	34 ± 3	10 ± 1[b]	3260±240

[a] -, not determined because saturation was not reached.

[b] $K_{0.5}$ values (substrate concentration at which the velocity is half-maximal) obtained using the Hill equation and, in the present work, $K_{0.5}$ was considered equivalent to K_{D3}.

The dissociation constant K_{D3} was 3.4-fold lower for hardwood lignosulfonate than for softwood lignosulfonate, indicating a higher affinity of the enzyme for the former lignin. A similar decrease was observed in the k_3 constant for the hardwood lignosulfonate, this being the reason for the similar efficiency in the oxidation of both lignins. The kinetics for reduction of VP CI/CII by creosol and α-sulfonated creosol was also examined (**Fig. 4**). Although CI seems to be more efficient oxidizing creosol (1560 ± 35 s^{-1}·mM^{-1}) than its sulfonated counterpart (253 ± 8 s^{-1}·mM^{-1}), CII reduction (the limiting step in catalysis) showed similar efficiencies (122 ± 8 and 89 ± 8 s^{-1}·mM^{-1}, respectively), k_3 (21 ± 1 and 13 ± 1 s^{-1}, respectively) and K_{D3} (175 ± 21 and 147 ± 22 μM, respectively) values for the two model substrates.

Besides native VP, two variants were tested for the oxidation of lignosulfonates (**Fig. 3** and **Table 1**). In the W164S variant, the substitution of the putative catalytic tryptophan resulted in impaired oxidation of both lignosulfonates. The strongest effect of the W164S mutation was observed in the case of the hardwood lignosulfonate,

where the k_{2app} and (rate limiting) k_{3app} values experienced 9-fold and 125-fold decreases, respectively, with respect to the native lignin. The remaining reduction of W164S CI and CII is attributed to the minor phenolic units present in the softwood (2.1%) and hardwood (1.4%) lignosulfonates (G.E. Fredheim, personal communication).

The second VP variant (R257A/A260F) harbors two surface mutations near Trp-164 (**Fig. 1**). Interestingly, this variant showed enhanced transient-state kinetic constants (**Fig. 3** and **Table 1**), and sigmoidal kinetics for CII reduction (**Fig. 3b,d**, insets). A 13-14 fold improved (rate limiting) k_{3app} was observed, reveling higher efficiency in the oxidation of both lignosulfonates. This was due to 17-fold and 6-fold decreases of K_{D3} for softwood and hardwood lignosulfonates, respectively, indicative of a higher affinity. CI reduction was also improved, although the increases in k_{2app} were not as high (**Fig. 3a,c** and **Table 1**).

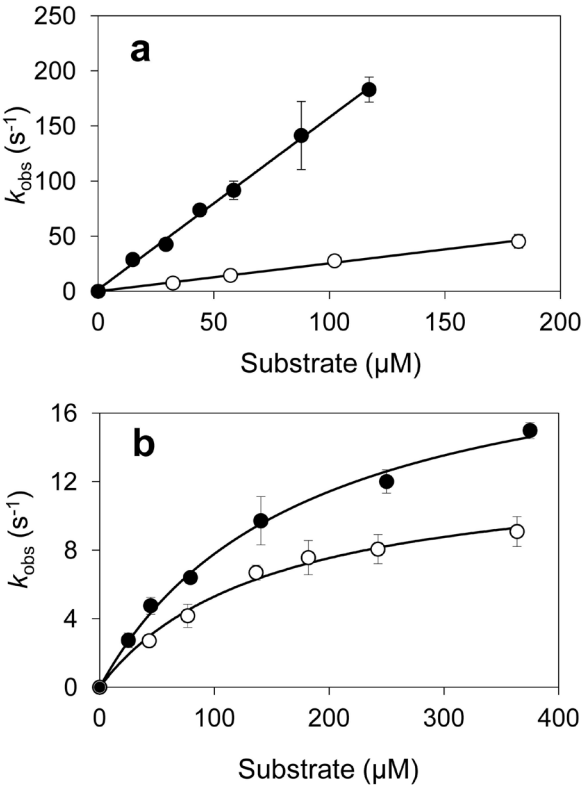

Figure 4. Kinetics of VP CI (a) and CII (b) reduction by creosol (black circles) and the corresponding sulfonate derivative (white circles). Stopped-flow reactions were carried out at 25 °C in 0.1 M tartrate (pH 3). Means and 95% confidence limits.

3.2 EPR detection of VP and lignin radicals

EPR spectra of VP reactions with different concentrations of softwood lignosulfonate were obtained (after enzyme activation by H_2O_2). In the absence of reducing substrate, a protein radical was observed (**Fig. 5**, blue line), whose abundance from EPR signal integration (referred to the iron signal in the resting state enzyme) was estimated to be ~0.25 spin/heme. Under the above conditions (40 K) no protein radicals were detected for the W164S variant, while a porphyrinyl radical, centered at g = 2.00(1) with a ΔH_{pp} ~ 0.22 mT, was observed (at T < 30 K), whose intensity quickly declined when the acquisition temperature increased from 9 to 40 K. When a low amount of lignin was added (VP/H_2O_2/lignin ratio of 1:8:4) a mixed radical signal centered on both the protein and the lignin was detected (**Fig. 5**, red line), whose lignin radical only represented ~0.9% of the tryptophanyl radical signal intensity in the previous VP spectrum without lignin. When a higher amount of lignin was added (VP/H_2O_2/lignin ratio of 1:8:12) the protein radical signal was replaced by the intense lignin radical signal (**Fig. 5**, black line), which represented ~35% of the intensity of the pure tryptophanyl signal in the VP spectrum.

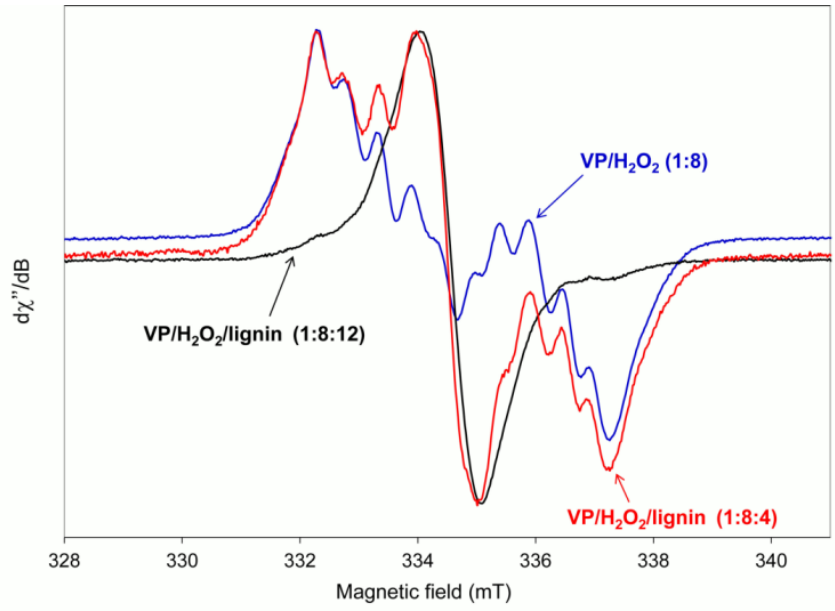

Figure 5. EPR spectra of the reactions of VP with H_2O_2 (at molar ratio 1:8), and of VP with H_2O_2 and softwood lignosulfonate at two different molar ratios (1:8:4 or 1:8:12). All spectra were recorded at 40 K, 9.394 GHz, 1 mW microwave power, and 0.2 mT modulation amplitude, a few seconds after mixing. Intensity normalized spectra are shown (integration values for the tryptophanyl and lignin radical signals in the original spectra are provided in the text).

In the spectrum acquired with the highest lignin content, the residual protein radical contribution was visible on the wings of the lignin radical signal. The protein radical signal (**Fig. 5**, blue line) is characterized by a large doublet splitting centered at g = 2.0027 (± 0.0001), with well resolved subsplittings on each of the two components. This signal has been previously assigned to a tryptophanyl neutral radical (Trp-164) (Pérez-Boada et al., 2005; Pogni et al., 2006) formed through LRET to the H_2O_2-activated heme. On the other hand, the lignin radical (**Fig. 5**, black line) is characterized by a single line at g = 2.0043 (± 0.0001) with a $\Delta H_{pp} \sim 0.1$ mT. This radical was stable for several hours, and could be detected even at 298 K.

3.3 Fluorescence changes during the VP treatments

Changes in lignin fluorescence are easily detectable during steady-state treatments of lignosulfonates with VP. As shown in **Fig. 6**, a decrease of the fluorescence intensity to 40% (compared with the initial intensity) was observed after 3 h of incubation of softwood and hardwood lignosulfonates with VP and H_2O_2. In addition, after 12 h and 24 h of the enzymatic treatment of softwood lignin, the fluorescence was practically undetectable. In the case of the hardwood lignosulfonate, the fluorescence intensity decreased to a 20% after 12h treatment and was mostly inexistent after 24h.

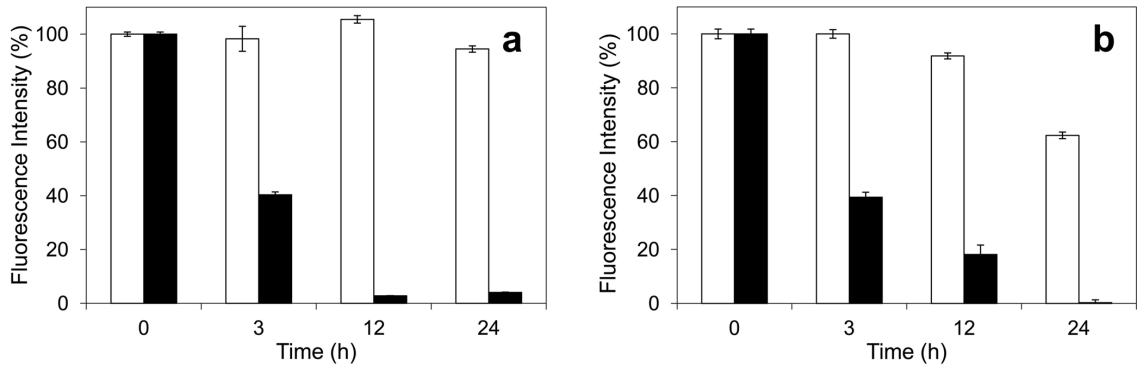

Figure 6. Relative fluorescence of softwood (a) and hardwood (b) lignosulfonates during 24-h treatment with VP and H_2O_2 (black bars) and the corresponding controls without enzyme (white bars). Changes of lignosulfonate (12 g·L-1) fluorescence during treatment with VP (1.3 μM) and H_2O_2 (12.5 mM) in 50 mM phosphate (pH 5) were monitored (excitation 355 nm/emission 400 nm) after different time periods (3, 12 and 24 h). Means and 95% confidence limits.

3.4 Changes of lignin molecular mass

Fig. 7 shows the molecular mass distribution profiles of softwood (**a**) and hardwood (**b**) lignosulfonates after 24-h treatment with VP (red curve) and control treatment without enzyme (green curve) in a Superdex-75 column (with 0.1 M NaOH as eluent, and 280-nm detection).

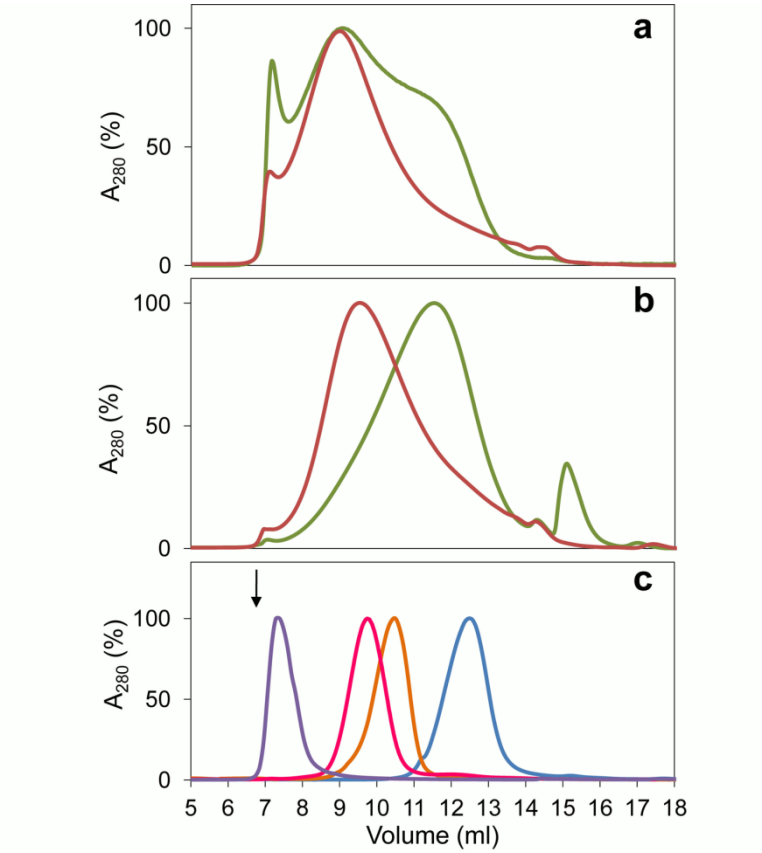

Figure 7. Molecular-mass distribution of VP-treated and control softwood (a) and hardwood (b) lignosulfonates, and sulfonated polystyrene standards (c). Lignosulfonate samples (12 g·L^{-1}) after 24-h treatment with VP (1.2 μM) and H_2O_2 (9.5 mM) (red lines), and the corresponding controls without enzyme (green lines), were analyzed in a Superdex-75 column using 0.15 M NaOH as the mobile phase (0.5 mL·min^{-1}) and UV-visible (280 nm) detection. Sulfonated polystyrenes (Mp 78,400, 29,500, 10,200 and 4,210 Da, from left to right) were used as molecular-mass standards (arrow shows the Blue dextran, BD, elution volume) (**c**).

Using sulfonated polystirene standards (Mp 78,400, 29,500, 10,200 and 4210 Da) (**Fig. 7c**) we estimated Mp of 47,228 Da and 4,342 Da for the control softwood and hardwood lignosulfonates, respectively. The softwood lignosulfonate had a broader distribution with a large

shoulder around 11.7 mL elution volume (9,571 Da) and a small excluded fraction. For hardwood lignosulfonate, a small peak was observed near the column void volume. Similar profiles were observed when the RI and MALLS detectors were used, with the only exception of the low molecular-mass peak that was only detected with the UV-visible detector (suggesting simple compounds with high absorbance at 280 nm).

The enzymatic treatment resulted in a net increase of the average molecular mass of the hardwood lignosulfonate (from Mp of 4,342 Da to 35,742 Da). For the softwood lignosulfonate, the Mp was not significantly modified, but the large shoulder disappeared (most probably being incorporated into the Mp of 48,000 Da). Simultaneously, the small excluded fraction in softwood lignosulfonate disappeared, suggesting some depolymerization activity. Finally, the low molecular-mass peak present in the control hardwood lignosulfonate was not observed after the enzymatic treatment.

The same samples were extracted with methyl *tert*-butyl ether and analyzed by GC-MS, but no low molecular-mass compounds derived from lignin could be identified. Only 2,6-dimethoxy-*p*-benzoquinone, a product from peroxidase oxidation of syringic acid (Shin, 1995) (present in the control sample), was found after VP treatment of the hardwood lignosulfonate.

3.5 NMR analyses of lignosulfonates after VP treatment

The chemical modification of lignin during the above VP treatments was analyzed by 1D and 2D NMR (the main structures identified are indicated in **Fig. 8g**).

The HSQC spectrum of the control softwood lignosulfonate (**Fig. 8a**) shows the C_2-H_2, C_5-H_5 and C_6-H_6 aromatic correlations of the lignin guaiacyl units (green signals). In the aliphatic-oxygenated region, the C_α-H_α, C_β-H_β, and C_γ-H_γ correlations of the lignin side-chains forming inter-unit linkages in the main sulfonated (**A**) and minor non-sulfonated (***A***) β-O-4' substructures (blue signals) were found. Small C_α-H_α, C_β-H_β, and C_γ-H_γ correlations in phenylcoumarans (**B**, cyan signals) and

pinoresinols (**C**, purple signals), whose side chains were not sulfonated due to C_α ether-bond, and the prevalent methoxyl correlations (orange signal) were also observed. The spectrum of the control hardwood lignosulfonate (**Fig. 8d**) includes the above signals, with the only exception of phenylcoumaran signals, plus those of α-sulfonated (**S**), and non-sulfonated normal (***S***) and α-oxidized (***S'***) syringyl units (red signals).

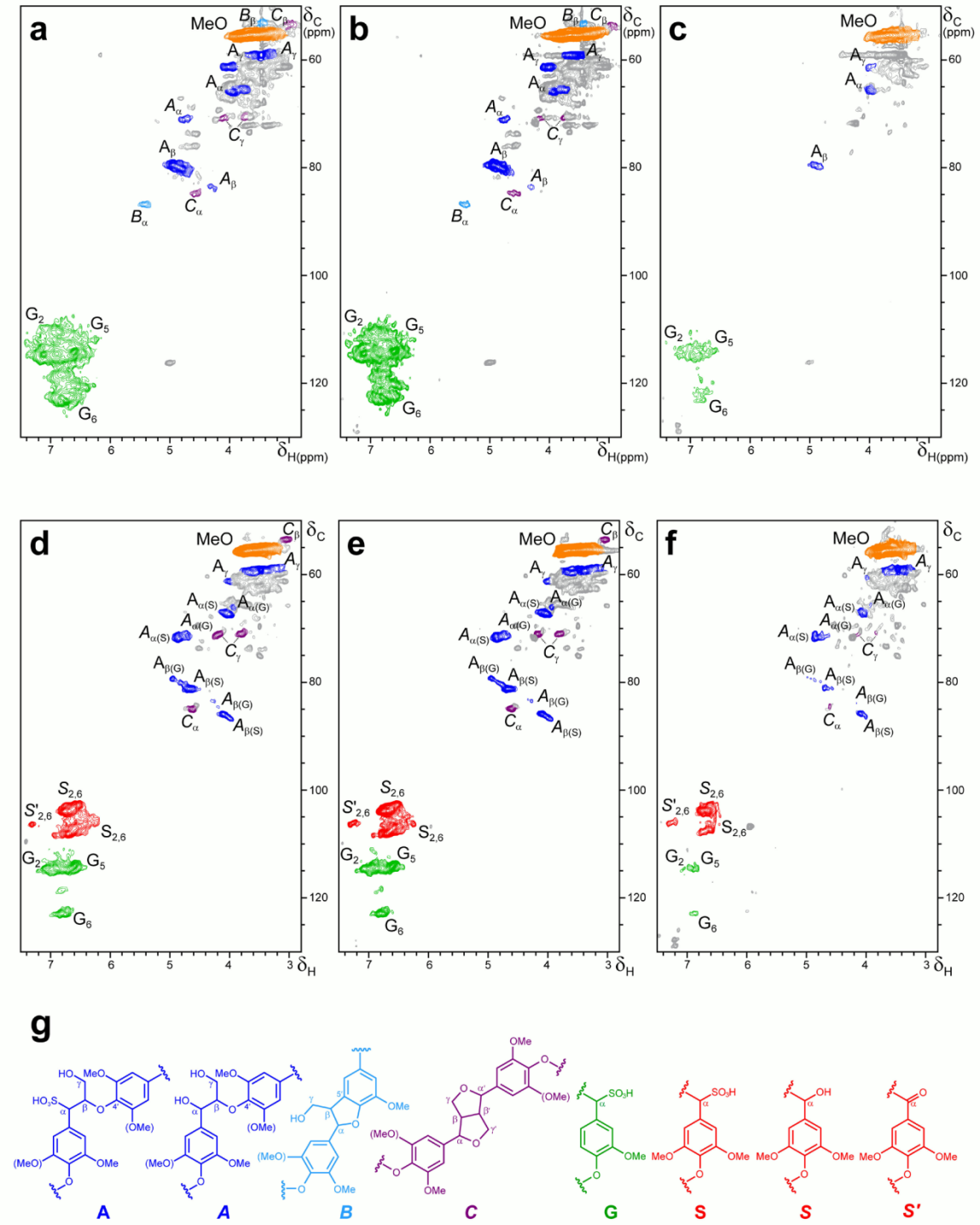

Figure 8 (see legend on the next page)

Moreover, those β-O-4' substructures including a second guaiacyl or syringyl unit could be discriminated. Another difference is the similar amount of sulfonated (**A**) and non-sulfonated (***A***) β-O-4' substructures in the hardwood lignosulfonate, while only minor non-sulfonated β-O-4' substructures (***A***) were found in the softwood lignosulfonate.

During VP treatment of lignosulfonates, the signals of the different side-chain linkages (**A**, ***A***, **B** and **C**) and aromatic (**G**, **S, *S*** and ***S'***) lignin units (**Fig. 8g**) decreased, as shown in the 3-h (**Fig. 8b** and **e**) and especially 24-h treatment spectra (**Fig. 8c** and **f**), and some changes in

Figure 8. HSQC spectra of softwood (a-c) and hardwood (d-f) lignosulfonate after 3-h (b,e) and 24-h (c,f) treatment with VP/H_2O_2, compared with control without enzyme (a,d), and formulae of the main structures identified (g). Signals correspond to ^{13}C-^{1}H correlations at the different positions of lignin normal/α-oxidized syringyl units (red signals), guaiacyl units (green signals), α-sulfonated/non-sulfonated side chains in β-O-4' (blue signals), phenylcoumaran (cyan signals), and pinoresinol (purple signals) substructures, and methoxyls (orange signal) (gray, unassigned signals). Signals of β-O-4' substructures with a second guaiacyl or syringyl unit could be identified. Same amount of sample (40 mg before treatment) and DMSO-d_6 (0.75 mL) were used for all the spectra in **Figs. 8** and **9**, which were normalized to the same intensity of the DMSO signal (not shown) for comparison.

List of signals (δ_C/δ_H ppm): 53.2/3.46, C_β/H_β in phenylcoumarans (**B_β**); 53.4/3.00, C_β/H_β in resinols (**C_β**); 55.5/3.66, C/H in methoxyls (**MeO**); 59.4/3.4 and 3.72, C_γ-H_γ in β–*O*–4′ (***A_γ***); 61.1/4.00, C_γ-H_γ in sulfonated β–*O*–4′ (**A_γ**); 65.6/3.93, C_α/H_α in sulfonated β–*O*–4′ linked to a G-unit (**$A_{\alpha(G)}$**); 67.2/4.02, C_α/H_α in sulfonated β–*O*–4′ linked to a S-unit (**$A_{\alpha(S)}$**); 70.8/4.16 and 3.77, C_γ-H_γ in β-β' resinols (**C_γ**); 71.1/4.72, C_α/H_α in β–*O*–4′ linked to a G-unit (***$A_{\alpha(G)}$***); 71.5/4.85, C_α/H_α in β–*O*–4′ linked to a S-unit (***$A_{\alpha(S)}$***); 79.3/4.91, C_β/H_β in sulfonated β–*O*–4′ linked to a G unit (**$A_{\beta(G)}$**); 80.9/4.67, C_β/H_β in sulfonated β–*O*–4′ linked to a S unit (**$A_{\beta(S)}$**); 83.3/4.24, C_β/H_β in β–*O*–4′ linked to a G unit (***$A_{\beta(G)}$***); 84.9/4.59, C_α/H_α in β-β' resinols (**C_α**); 85.7/4.08, C_β/H_β in β–*O*–4′ linked to a S unit (***$A_{\beta(S)}$***); 86.7/5.41, C_α/H_α in phenylcoumarans (**B_α**); 103.8/6.68, C_2/H_2 and C_6/H_6 in non-sulfonated syringyl units (***$S_{2,6}$***); 106.2/7.29, C_2/H_2 and C_6/H_6 in α-oxidized syringyl units (***$S'_{2,6}$***); 108.0/6.68, C_2/H_2 and C_6/H_6 in sulfonated syringyl units (**$S_{2,6}$**); 114.0/6.60 and 114.3/6.87, C_2/H_2 and C_5/H_5 in guaiacyl units (**G_2/G_5**); and 122.8/6.75, C_6/H_6 in guaiacyl units (**G_6**) (minor, and largely overlapping, signals of C_2/H_2, C_5/H_5 and C_6/H_6 correlations in non-sulfonated guaiacyl units would appear at 110.7/6.93, 114.2/6.65 and 118.6/6.79 ppm, respectively; not shown).

their relative abundances were also observed. The similar decrease of both signal types resulted in only slightly modified numbers of inter-unit linkages per aromatic unit. However, the methoxyl numbers increased (up to 2.5 and 3.5 per guaiacyl and syringyl unit, respectively) suggesting the formation of non-aromatic methoxyl-containing (e.g. muconate type). This was accompanied by the formation of α-oxidized syringyl units, whose relative abundance (with respect to total syringyl units) was two and four-fold higher after 3-h and 24-h treatment, respectively, in the hardwood lignosulfonate (where the S/G ratio also increased).

Concerning lignin side-chain signals, only those present in the sulfonated β-O-4' substructures ($\mathbf{A_\alpha}$, $\mathbf{A_\beta}$ and $\mathbf{A_\gamma}$) remained after 24-h treatment of the sofwood lignosulfonate, and those of phenylcoumaran, resinol and non-sulfonated β-O-4' side chains were not detected. In contrast, those of sulfonated (**A**) and non-sulfonated (***A***) β-O-4', phenylcoumaran, (**B**) and resinol (**C**) side chains, were observed after 24-h treatment of the hardwood lignosulfonate, albeit with low intensities. No changes in the aromatic/aliphatic HSQC signals were observed in the control treatment without enzyme.

Since only protonated carbons appear in the HSQC spectra, ^{13}C NMR analyses were also performed. The solution ^{13}C NMR spectra revealed that the VP treatment (**Fig. 9b,d**) decreased not only the G_2, G_5, G_6 and $S/S_{2,6}$ signals, but also those of quaternary G_1, G_3, G_4, S_1, $S_{3,5}$ and S_4 carbons, compared with the corresponding controls (**Fig. 9a,c**). The minor C_α, C_β and C_γ signals from the main β-O-4' substructures ($A/A_{\alpha/\beta/\gamma}$) in the control spectra (**Fig. 9a,c**), were hardly detectable after the enzymatic treatment (**Fig. 9b,d**). Moreover, a carboxyl signal (R-COOH) was observed in the spectra of the treated lignosulfonates, with the highest intensity in the softwood lignosulfonate spectrum. The above results were confirmed by solid-state CPMAS ^{13}C NMR spectra (not shown) that, albeit of their lower resolution, clearly showed a decrease of the different carbon types in lignin.

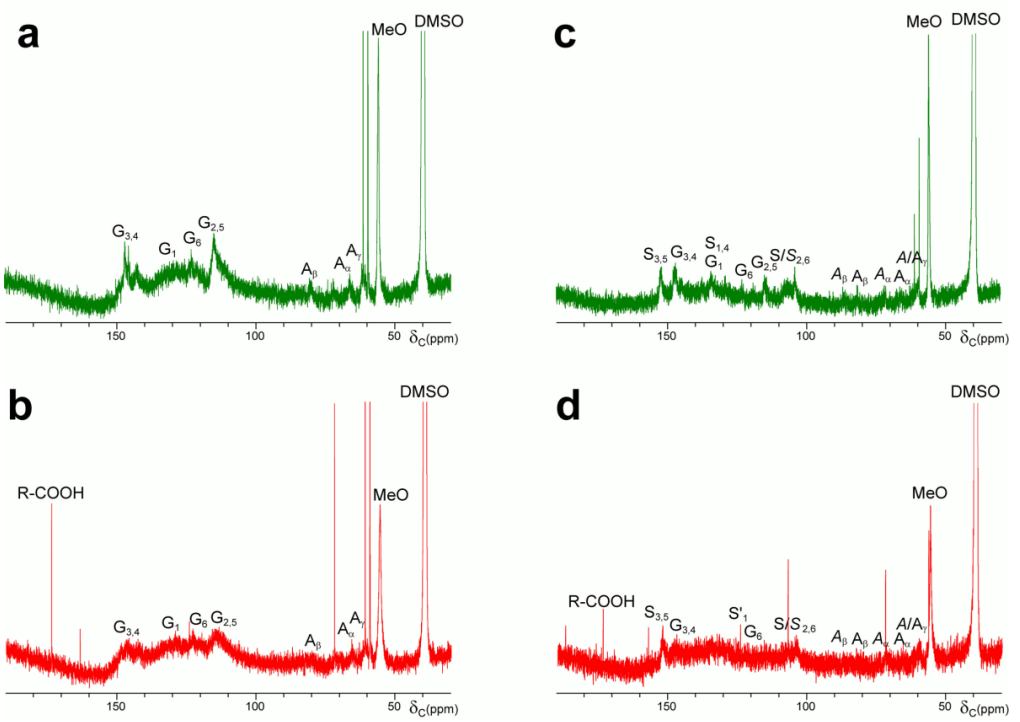

Figure 9. ^{13}C NMR spectra of softwood (a,b) and hardwood (c,d) lignosulfonate after 24-h treatment with VP/H_2O_2 (b,d), compared with control without enzyme (a,c). Signals of protonated (G_2, G_5, G_6, and $S_{2,6}$) and quaternary (G_1, G_3, G_4 and S_1, S_3, S_4 and S_5) carbons in guaiacyl and syringyl lignin units; α/β carbons in β-O-4' linked sulfonated (A_α and A_β) and non-sulfonated (A_α and A_β) lignin side-chains; and methoxyls (MeO) are shown, together with a carboxyl (R-COOH) signal. Two sharp extra signals, at 59.2 and 61.0 ppm (one of them also observed in the HSQC spectra), most probably come from the buffer used in lignosulfonate dialysis (before use), and other in the treated samples remained to be assigned.

List of quaternary carbon signals (δ_C ppm): 134, C_1 in guaiacyl units (**G_1**) and $C_{1,4}$ in syringyl units (**$S_{1,4}$**); 147, $C_{3,4}$ in guaiacyl units (**$G_{3,4}$**); and 152, $C_{3,5}$ in syringyl units (**$S_{3,5}$**) (see **Fig. 8** legend for δ_C of protonated carbons)

4. Discussion

4.1 Lignin oxidation by VP

Phanerochaete chrysosporium LiP was the first enzyme whose ability to depolymerize lignin and cleave non-phenolic lignin model dimers was reported (Tien and Kirk, 1983; Hammel et al., 1993). However, a similar lignin-degrading ability was only recently established for VP (Fernández-Fueyo et al., 2014). In the present study, VP was demonstrated to directly oxidize lignin, and the electron transfer between the polymer and the enzyme was for the first time in a

peroxidase kinetically characterized under transient-state conditions and assigned to the presence of a radical-forming tryptophan residue (Trp-164).

Comparing lignin oxidation with the oxidation of simple compounds, it is interesting to notice that the (rate limiting) reduction of CII by lignosulfonates (250 s^{-1}·mM^{-1}) is (2-fold) better than found for creosol, and much better than the catalytic efficiencies for veratryl alcohol (~60-fold higher) (Pérez-Boada et al., 2005), and 3,4,5-trimethoxybenzyl alcohol (~500-fold higher) (data not shown). The above suggests that lignin, at least water-soluble lignosulfonates, are more efficiently oxidized by VP than simple aromatic compounds. It is interesting to know if sulfonation, in addition of rendering lignin soluble, affects the oxidizability of its aromatic units by modifying the VP binding or turnover rate. With this purpose, creosol and its α-sulfonated form were compared as VP substrates. Although these models differ (in their phenolic nature, etc) from the corresponding lignosulfonate units, the kinetic constants for CII reduction by sulfonated creosol were in the same range of those obtained for the softwood lignin. Moreover, α-sulfonation does not significantly modified oxidation of aromatic compounds (and most probably lignin) by VP since (rate limiting) CII reduction by creosol was only slightly better than found for its sulfonated counterpart.

2D NMR, in HSQC or similar experiments (in combination with ^{13}C NMR) represents the state-of-the-art technique for the structural analysis of the lignin polymer (Ralph et al., 1999; Lu and Ralph, 2011; Rico et al., 2014). During the lignin treatment with VP, a progressive decrease in the intensity of the signals of the lignin aromatic units and side chains was observed, which correlated with the decrease of sample fluorescence. Lignin fluorescence is a well-known phenomenon (Albinsson et al., 1999; Schmidt, 2010), and its decrease has been reported during lignosulfonate treatment with the laccase-mediator system (Prasetyo et al., 2010). The progressive degradation of the different lignin structures was better shown in the HSQC spectra, but could also be observed in solution and solid-state ^{13}C NMR for both protonated and quaternary carbons (the latter not included in the HSQC

analysis). Moreover, a carboxyl signal appeared in the ^{13}C NMR spectra after the VP treatment.

Concomitantly with the lignin degradation shown by the fluorescence and NMR analyses, a net repolymerization of the oxidation products was shown by SEC, which was especially significant for the lower molecular-mass hardwood lignosulfonate. This repolymerization would result from new diaryl C-C or ether substructures formed by aromatic radical condensation, as reported for lignosulfonate treatment with the lignin-degrading laccase-mediator system (Prasetyo et al., 2010). It is interesting that in the VP reactions with lignosulfonates, no veratryl alcohol was added and, in spite of this, significant lignin degradation was produced.

4.2 Role of VP Trp-164

It is assumed that ligninolytic peroxidases oxidize lignin (and other high redox-potential compounds) at a solvent exposed residue, generally a tryptophan, susceptible to form a protein-based radical through LRET to heme (Ruiz-Dueñas et al., 2009a; Martínez et al., 2009; Smith et al., 2009). The involvement of VP Trp-164 in the oxidation of high redox compounds, such as veratryl alcohol and Reactive Black 5, has been demonstrated using the W164S variant that has no activity on these substrates (Ruiz-Dueñas et al., 2009b; Pérez-Boada et al., 2005). However, the implication of Trp-164 in lignin oxidation and, more specifically, in the electron transfer from the polymer to the enzyme has not been demonstrated until now.

The kinetic results obtained for the lignosulfonate reaction with the W164S variant, showed that k_{2app} and k_{3app} decreased to different extents. The residual activity is attributed to minor phenolic units in lignosulfonates (Prasetyo et al., 2010) that would be oxidized at the heme access channel, as reported for simple phenols (Morales et al., 2012). Although electron transfer between synthetic lignin (dehydrogenation polymer, DHP) and *P. chrysosporium* LiP had been previously shown (Johjima et al., 1999), here this transfer is directly related to the presence of the catalytic tryptophan (VP Trp-164 or LiP Trp-171).

Formation of a tryptophanyl neutral radical centered in Trp-164 has been reported after VP activation by H_2O_2 (Pérez-Boada et al., 2005 Pogni et al., 2006) and supported by the absence of such radical in the W164S spectrum, while a porphyrinyl radical signal was observed at 9 K, in agreement with previous studies (Ruiz-Dueñas et al., 2009b). The EPR signal of this tryptophanyl neutral radical is mixed with a lignin radical signal when VP was incubated with a low concentration of lignosulfonate. Interestingly, when a higher concentration was used, the lignin radical signal predominated, and the tryptophanyl signal mostly disappeared. Therefore, we concluded that the Trp-164 radical is active on lignin since its reduction was observed concomitantly to the formation of a lignin radical, as previously shown for veratryl alcohol oxidation by LiP (Smith et al., 2009).

An in-depth analysis of the lignosulfonate radical detected by EPR could not be carried out since no hyperfine structure was observed. However, the g-value and the width of the signal are coherent with a radical formed by oxidation/hydrogen removal from a hydroxyl group of the substrate, in agreement with previously reported data (Taboada-Puig et al., 2013; Gronqvist et al., 2005; Felby et al., 1997). It has been shown that the treatment of kraft lignin with VP leads to formation of phenoxy radicals (Taboada-Puig et al., 2013), and the same has been reported for laccase and horseradish peroxidase (Gronqvist et al., 2005). On the other hand, the long half-life of the lignin radical formed by VP can be due to the fact that the radicals are immobilized in the lignin matrix, rather than to a low reactivity (Felby et al., 1997).

4.3 Importance of the Trp-164 environment

Although the solvent-exposed tryptophanyl radical is responsible for the oxidation of high redox-potential compounds, variations in the radical environment modulate its redox potential and stability (Ivancich et al., 2001). This is most probably responsible for differences between VP and LiP catalysis (Ruiz-Dueñas et al., 2008). Whereas VP is able to oxidize Reactive Black 5 directly, LiP needs of the presence of mediators to oxidize this anionic recalcitrant substrate. On the other hand, LiP is able to oxidize veratryl alcohol more efficiently than VP does. This

ability has been attributed to the acidic Trp-171 environment in *P. chrysosporium* LiP, which would facilitate the stabilization of the veratryl alcohol cation radical (Khindaria et al., 1996).

In this context, the R257A/A260F variant was designed to study in which way residues of the catalytic tryptophan environment could modulate the kinetic properties of VP (Ruiz-Dueñas et al., 2008). This variant showed sigmoidal plots for CII reduction, and improved transient-state kinetic constants for lignosulfonates. Sigmoidal plots in steady-state oxidation of some VP substrates have been related to the existence of two oxidation sites (corresponding to the catalytic Trp-164 and the heme access channel) (Morales et al., 2012). However, taking into account the position of the two mutations, and the molecular size of lignosulfonates, the sigmoidal plots obtained here suggest the existence of two different lignosulfonate binding poses in the environment of the catalytic tryptophan. Similar results were obtained for reduction of CII of the R257A/A260F variant by the sulfonated Reactive Black 5 (Ruiz-Dueñas et al., 2008).

More interestingly, the R257A/A260F variant showed enhanced kinetic constants for both softwood and hardwood lignosulfonates, with 13-14 fold increased k_{3app}. Similar improvements have been reported for veratryl alcohol oxidation (Ruiz-Dueñas et al., 2008) with transient-state constants similar to those described for LiP (Gelpke et al., 2002). In this variant, Ala-260 was substituted by a phenylalanine, the residue at the homologous position in *P. chrysosporium* LiP that has been implicated in substrate binding by aromatic-aromatic interactions with veratryl alcohol oxidation (Gelpke et al., 2002). In the same way, VP interaction with lignin would be improved by this mutation, as suggested by the lower K_{D3} found for the R257A/A260F VP variant. On the other hand, the removal of basic Arg-257 would result in a more acidic catalytic tryptophan environment (as found in LiP) and would enhance VP reaction with lignin (Smith et al., 2009). In conclusion, the results from lignosulfonate oxidation by R257A/A260F VP show that the efficiency of the electron transfer from the polymer to the catalytic tryptophan depends on its surface environment and can be improved by modifying it.

4.4 Concluding remarks

The ability of VP to abstract electrons from softwood and hardwood lignin was demonstrated by stopped-flow spectrophotometry, using water soluble lignosulfonates as substrate. This ability is related to the presence of Trp-164, as shown using site-directed mutagenesis. Moreover, EPR experiments detected the Trp-164 neutral radical and demonstrated that it is catalytically active oxidizing lignin, as summarized in the enzyme cycle presented in **Fig. 10**. Improvements in the VP transient-state reactions with lignosulfonates, after the R257A/A260F double mutation, revealed the importance of the Trp-164 environment in the VP activity on lignin. Finally, NMR, fluorescence and SEC analyses confirmed degradation and residual lignin repolymerization tendency during lignosulfonate treatment with VP under steady-state conditions.

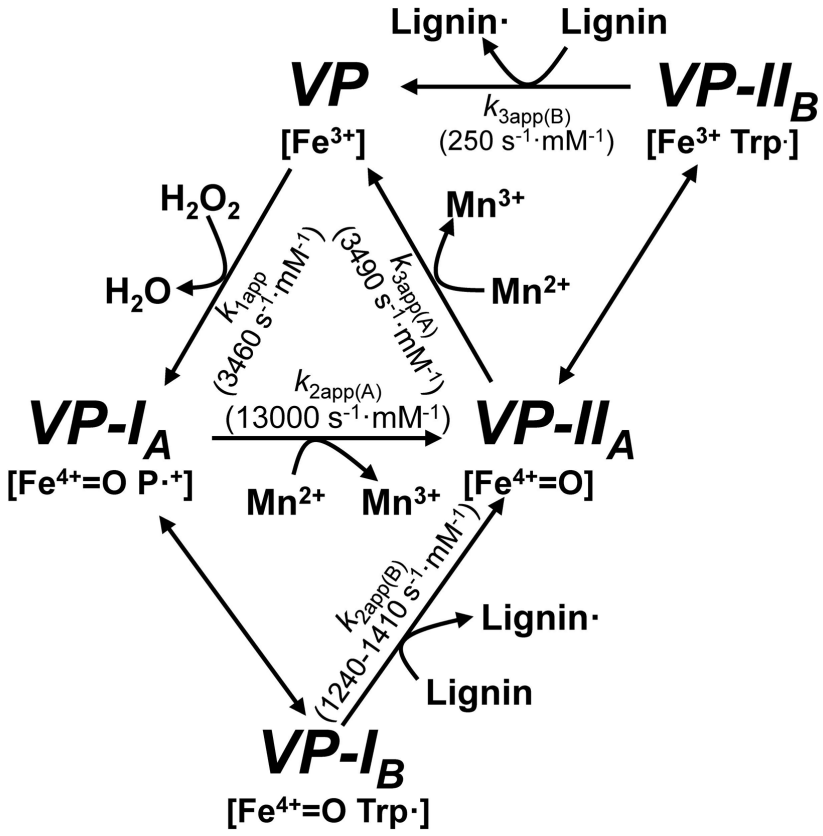

Figure 10 (see legend on the next page)

Figure 10. VP catalytic cycle. Scheme for VP catalytic cycle showing resting state (Fe^{3+}) activation by H_2O_2 and lignin oxidation by a tryptophanyl radical (VP-I_B and VP-II_B) formed by one electron transfer from Trp-164 to VP-I_A (Fe^{IV}=O porphyrin radical, $P^{\cdot+}$) and VP-II_A (Fe^{IV}=O) heme. In contrast, Mn^{2+} is directly oxidized by VP-I_A and VP-II_A. Other VP substrates, like phenols (including the lignin phenolic units) and dyes can be oxidized both at the heme access channel (by VP-I_A and VP-II_A) and at the catalytic tryptophan (by VP-I_B and VP-II_B) (Morales et al., 2012) (not shown for simplicity). The above porphyrin radical was experimentally observed in the EPR spectrum of the W164S variant (at 9 K), while the tryptophanyl radical was observed in the VP spectra acquired at 40 K. The transient state (apparent second-order) rate constants for reactions with sulfonated lignins can be overestimated since some reaction is also produced at the heme channel (by VP-I_A and VP-II_A), probably involving the minor phenolic units in lignin, as shown in **Table 1** (W164S variant). The H_2O_2 and Mn^{2+} rate constants are taken from previous studies (Ruiz-Dueñas et al., 2007; Pérez-Boada et al., 2005). No constants are provided for the pass of VP-I_A and VP-II_A to VP-I_B and VP-II_B, respectively, since electron deficiency is shared between the two redox centers (Ruiz-Dueñas et al., 2009b).

5. References

Ahmad, M., J.N.Roberts, E.M.Hardiman, R.Singh, L.D.Eltis, and T.D.H.Bugg. 2011. Identification of DypB from *Rhodococcus jostii* RHA1 as a lignin peroxidase. *Biochemistry* 50:5096-5107.

Albinsson, B., S.Li, K.Lundquist, and R.Stomberg. 1999. The origin of lignin fluorescence. *J. Mol. Struct.* 508:19-27.

Areskogh, D. 2011. Structural modification of lignosulphonates. PhD thesis, KTH, Stockholm.

Camarero, S., S.Sarkar, F.J.Ruiz-Dueñas, M.J.Martínez, and A.T.Martínez. 1999. Description of a versatile peroxidase involved in natural degradation of lignin that has both Mn-peroxidase and lignin-peroxidase substrate binding sites. *J. Biol. Chem.* 274:10324-10330.

Felby, C., B.R.Nielsen, P.O.Olesen, and L.H.Skibsted. 1997. Identification and quantification of radical reaction intermediates by electron spin resonance spectrometry of laccase-catalyzed oxidation of wood fibers from beech (*Fagus sylvatica*). *Appl. Microbiol. Biotechnol.* 48:459-464.

Fernández-Fueyo, E., F.J.Ruiz-Dueñas, M.J.Martínez, A.Romero, K.E.Hammel, F.J.Medrano, and A.T.Martínez. 2014. Ligninolytic peroxidase genes in the oyster mushroom genome: Heterologous expression, molecular structure, catalytic and stability properties and lignin-degrading ability. *Biotechnol. Biofuels* 7:2.

Floudas, D., M.Binder, R.Riley, K.Barry, R.A.Blanchette, B.Henrissat, A.T.Martínez, R.Otillar, J.W.Spatafora, J.S.Yadav, A.Aerts, I.Benoit, A.Boyd, A.Carlson, A.Copeland, P.M.Coutinho, R.P.de Vries, P.Ferreira, K.Findley, B.Foster, J.Gaskell, D.Glotzer, P.Górecki, J.Heitman, C.Hesse, C.Hori, K.Igarashi, J.A.Jurgens, N.Kallen, P.Kersten, A.Kohler, U.Kües, T.K.A.Kumar, A.Kuo, K.LaButti, L.F.Larrondo, E.Lindquist, A.Ling, V.Lombard, S.Lucas, T.Lundell, R.Martin, D.J.McLaughlin, I.Morgenstern, E.Morin, C.Murat, M.Nolan, R.A.Ohm, A.Patyshakuliyeva, A.Rokas, F.J.Ruiz-Dueñas, G.Sabat, A.Salamov, M.Samejima, J.Schmutz, J.C.Slot, F.St.John, J.Stenlid, H.Sun, S.Sun, K.Syed, A.Tsang, A.Wiebenga, D.Young, A.Pisabarro, D.C.Eastwood, F.Martin, D.Cullen, I.V.Grigoriev, and D.S.Hibbett. 2012. The Paleozoic origin of enzymatic lignin decomposition reconstructed from 31 fungal genomes. *Science* 336:1715-1719.

Floudas, D., B.W.Held, R.Riley, L.G.Nagy, G.Koehler, A.S.Ransdell, H.Younus, J.Chow, J.Chiniqui, A.Lipzen, A.Tritt, H.Sun, S.Haridas, K.LaButti, R.A.Ohm, U.Kües, R.A.Blanchette, I.V.Grigoriev, R.E.Minto, and D.S.Hibbett. 2015. Evolution of novel wood decay mechanisms in Agaricales revealed by the genome sequences of *Fistulina hepatica* and *Cylindrobasidium torrendii*. *Fungal Genet. Biol.* 76:78-92.

Gall, D.L., J.Ralph, T.J.Donohue, and D.R.Noguera. 2014. A group of sequence-related sphingomonad enzymes catalyzes cleavage of b-aryl ether linkages in lignin b-guaiacyl and b-syringyl ether dimers. *Environ. Sci. Technol.* 48:12454-12463.

Gelpke, M.D.S., J.Lee, and M.H.Gold. 2002. Lignin peroxidase oxidation of veratryl alcohol: Effects of the mutants H82A, Q222A, W171A, and F267L. *Biochemistry* 41:3498-3506.

Gleenie, D.W. 1971. Reactions in sulfite pulping. *In* Lignins: Occurence, formation, structure and reactions. K.V.Sarkanen and C.H.Ludwig, editors. Wiley, New York. 597-637.

Gronqvist, S., L.Viikari, M.L.Niku-Paavola, M.Orlandi, C.Canevali, and J.Buchert. 2005. Oxidation of milled wood lignin with laccase, tyrosinase and horseradish peroxidase. *Appl. Microbiol. Biotechnol.* 67:489-494.

Hammel, K.E., K.A.Jensen, M.D.Mozuch, L.L.Landucci, M.Tien, and E.A.Pease. 1993. Ligninolysis by a purified lignin peroxidase. *J. Biol. Chem.* 268:12274-12281.

Heinfling, A., F.J.Ruiz-Dueñas, M.J.Martínez, M.Bergbauer, U.Szewzyk, and A.T.Martínez. 1998. A study on reducing substrates of manganese-oxidizing peroxidases from *Pleurotus eryngii* and *Bjerkandera adusta*. *FEBS Lett.* 428:141-146.

Himmel, M.E., S.Y.Ding, D.K.Johnson, W.S.Adney, M.R.Nimlos, J.W.Brady, and T.D.Foust. 2007. Biomass recalcitrance: Engineering plants and enzymes for biofuels production. *Science* 315:804-807.

Ivancich, A., G.Mazza, and A.Desbois. 2001. Comparative electron paramagnetic resonance study of radical intermediates in turnip peroxidase isozymes. *Biochemistry* 40:6860-6866.

Johjima, T., H.Itoh, M.Kabuto, F.Tokimura, T.Nakagawa, H.Wariishi, and H.Tanaka. 1999. Direct interaction of lignin and lignin peroxidase from *Phanerochaete chrysosporium*. *Proc. Natl. Acad. Sci. USA* 96:1989-1994.

Khindaria, A., I.Yamazaki, and S.D.Aust. 1996. Stabilization of the veratryl alcohol cation radical by lignin peroxidase. *Biochemistry* 35:6418-6424.

Kirk, T.K. and R.L.Farrell. 1987. Enzymatic "combustion": The microbial degradation of lignin. *Annu. Rev. Microbiol.* 41:465-505.

Lebo, S.E., S.M.Braaten, G.E.Fredheim, B.F.Lutnaes, R.A.Lauten, B.O.Myrvold, and T.J.McNally. 2008. Recent advances in the characterization of lignosulfonates. *In* Characterization of lignocellulosic materials. T.Hu, editor. Blackwell Pub., New York. 189-205.

Lu, F.C. and J.Ralph. 2011. Solution-State NMR of Lignocellulosic Biomass. *J. Biobased Mater. Bio.* 5:169-180.

Lutnaes, B.F., B.O.Myrvold, R.A.Lauten, and M.M.Endeshaw. 2008. H-1 and C-13 NMR data of benzylsulfonic acids - model compounds for lignosulfonate. *Magn. Reson. Chem.* 46:299-305.

Magina, S., A.P.Marques, and D.V.Evtuguin. 2015. Study on the residual lignin in *Eucalyptus globulus* sulphite pulp. *Holzforschung* 69:513-522.

Martínez, A.T., F.J.Ruiz-Dueñas, M.J.Martínez, J.C.del Río, and A.Gutiérrez. 2009. Enzymatic delignification of plant cell wall: from nature to mill. *Curr. Opin. Biotechnol.* 20:348-357.

Martínez, A.T., M.Speranza, F.J.Ruiz-Dueñas, P.Ferreira, S.Camarero, F.Guillén, M.J.Martínez, A.Gutiérrez, and J.C.del Río. 2005. Biodegradation of lignocellulosics: Microbiological, chemical and enzymatic aspects of fungal attack to lignin. *Int. Microbiol.* 8:195-204.

Morales, M., M.J.Mate, A.Romero, M.J.Martínez, A.T.Martínez, and F.J.Ruiz-Dueñas. 2012. Two oxidation sites for low redox-potential substrates: A directed mutagenesis, kinetic and crystallographic study on *Pleurotus eryngii* versatile peroxidase. *J. Biol. Chem.* 287:41053-41067.

Pérez-Boada, M., W.A.Doyle, F.J.Ruiz-Dueñas, M.J.Martínez, A.T.Martínez, and A.T.Smith. 2002. Expression of *Pleurotus eryngii* versatile peroxidase in

Escherichia coli and optimisation of *in vitro* folding. *Enzyme Microb. Technol.* 30:518-524.

Pérez-Boada, M., F.J.Ruiz-Dueñas, R.Pogni, R.Basosi, T.Choinowski, M.J.Martínez, K.Piontek, and A.T.Martínez. 2005. Versatile peroxidase oxidation of high redox potential aromatic compounds: Site-directed mutagenesis, spectroscopic and crystallographic investigations of three long-range electron transfer pathways. *J. Mol. Biol.* 354:385-402.

Pogni, R., M.C.Baratto, C.Teutloff, S.Giansanti, F.J.Ruiz-Dueñas, T.Choinowski, K.Piontek, A.T.Martínez, F.Lendzian, and R.Basosi. 2006. A tryptophan neutral radical in the oxidized state of versatile peroxidase from *Pleurotus eryngii*: a combined multi-frequency EPR and DFT study. *J. Biol. Chem.* 281:9517-9526.

Prasetyo, E.N., T.Kudanga, L.Ostergaard, J.Rencoret, A.Gutiérrez, J.C.del Río, J.I.Santos, L.Nieto, J.Jimenez-Barbero, A.T.Martínez, J.B.Li, G.Gellerstedt, S.Lepifre, C.Silva, S.Y.Kim, A.Cavaco-Paulo, B.S.Klausen, B.F.Lutnaes, G.S.Nyanhongo, and G.M.Guebitz. 2010. Polymerization of lignosulfonates by the laccase-HBT (1-hydroxybenzotriazole) system improves dispersibility. *Bioresource Technol.* 101:5054-5062.

Ragauskas, A.J., G.T.Beckham, M.J.Biddy, R.Chandra, F.Chen, M.F.Davis, B.H.Davison, R.A.Dixon, P.Gilna, M.Keller, P.Langan, A.K.Naskar, J.N.Saddler, T.Tschaplinski, G.A.Tuskan, and C.E.Wyman. 2014. Lignin valorization: improving lignin processing in the biorefinery. *Science* 344:1246843.

Ralph, J., J.M.Marita, S.A.Ralph, R.D.Hatfield, F.Lu, R.M.Ede, J.Peng, S.Quideau, R.F.Helm, J.H.Grabber, H.Kim, G.Jimenez-Monteon, Y.Zhang, H.-J.G.Jung, L.L.Landucci, J.J.MacKay, R.R.Sederoff, C.Chapple, and A.M.Boudet. 1999. Solution-state NMR of lignin. *In* Advances in lignocellulosics characterization. D.S.Argyropoulos, editor. Tappi Press, Atlanta. 55-108.

Rencoret, J., G.Marques, A.Gutiérrez, L.Nieto, I.Santos, J.Jiménez-Barbero, A.T.Martínez, and J.C.del Río. 2009. HSQC-NMR analysis of lignin in woody (*Eucalyptus globulus* and *Picea abies*) and non-woody (*Agave sisalana)* ball-milled plant materials at the gel state. *Holzforschung* 63:691-698.

Rico, A., J.Rencoret, J.C.del Río, A.T.Martínez, and A.Gutiérrez. 2014. In-depth 2D NMR study of lignin modification during pretreatment of *Eucalyptus* wood with laccase and mediators. *Bioenerg. Res.* 8:211-230.

Riley, R., A.A.Salamov, D.W.Brown, L.G.Nagy, D.Floudas, B.W.Held, A.Levasseur, V.Lombard, E.Morin, R.Otillar, E.A.Lindquist, H.Sun, K.M.LaButti, J.Schmutz, D.Jabbour, H.Luo, S.E.Baker, A.G.Pisabarro, J.D.Walton, R.A.Blanchette, B.Henrissat, F.Martin, D.Cullen, D.S.Hibbett, and I.V.Grigoriev. 2014. Extensive sampling of basidiomycete genomes demonstrates inadequacy of the white-rot/brown-rot paradigm for wood decay fungi. *Proc. Natl. Acad. Sci. USA* 111:9923-9928.

Ruiz-Dueñas, F.J. and A.T.Martínez. 2009. Microbial degradation of lignin: How a bulky recalcitrant polymer is efficiently recycled in nature and how we can take advantage of this. *Microbial Biotechnol.* 2:164-177.

Ruiz-Dueñas, F.J., M.J.Martínez, and A.T.Martínez. 1999. Molecular characterization of a novel peroxidase isolated from the ligninolytic fungus *Pleurotus eryngii*. *Mol. Microbiol.* 31:223-236.

Ruiz-Dueñas, F.J., M.Morales, E.García, Y.Miki, M.J.Martínez, and A.T.Martínez. 2009a. Substrate oxidation sites in versatile peroxidase and other basidiomycete peroxidases. *J. Exp. Bot.* 60:441-452.

Ruiz-Dueñas, F.J., M.Morales, M.J.Mate, A.Romero, M.J.Martínez, A.T.Smith, and A.T.Martínez. 2008. Site-directed mutagenesis of the catalytic tryptophan environment in *Pleurotus eryngii* versatile peroxidase. *Biochemistry* 47:1685-1695.

Ruiz-Dueñas, F.J., M.Morales, M.Pérez-Boada, T.Choinowski, M.J.Martínez, K.Piontek, and A.T.Martínez. 2007. Manganese oxidation site in *Pleurotus eryngii* versatile peroxidase: A site-directed mutagenesis, kinetic and crystallographic study. *Biochemistry* 46:66-77.

Ruiz-Dueñas, F.J., R.Pogni, M.Morales, S.Giansanti, M.J.Mate, A.Romero, M.J.Martínez, R.Basosi, and A.T.Martínez. 2009b. Protein radicals in fungal versatile peroxidase: Catalytic tryptophan radical in both Compound I and Compound II and studies on W164Y, W164H and W164S variants. *J. Biol. Chem.* 284:7986-7994.

Schmidt, J.A. 2010. Electronic spectroscopy of lignins. *In* Lignin and lignans: Advances in chemistry. C.Heitner, D.R.Dimmel, and J.A.Schmidt, editors. CRC Press, Boca Raton. 49-102.

Shin, K.-S. 1995. Oxidation of syringic acid by extracellular peroxidase of white-rot fungus,*Pleurotus ostreatus*. *Mycoscience* 36:31-35.

Smith, A.T., W.A.Doyle, P.Dorlet, and A.Ivancich. 2009. Spectroscopic evidence for an engineered, catalytically active Trp radical that creates the unique reactivity of lignin peroxidase. *Proc. Natl. Acad. Sci. USA* 106:16084-16089.

Taboada-Puig, R., T.A.Lu-Chau, M.T.Moreira, G.Feijoo, and J.M.Lema. 2013. Activation of Kraft Lignin by an Enzymatic Treatment with a Versatile Peroxidase from Bjerkandera sp R1. *Appl. Biochem. Biotechnol.* 169:1262-1278.

Tien, M. and T.K.Kirk. 1983. Lignin-degrading enzyme from the hymenomycete *Phanerochaete chrysosporium* Burds. *Science* 221:661-663.

DISCUSIÓN GENERAL

Las peroxidasas ligninolíticas producidas por los basidiomicetos de podredumbre blanca son enzimas con un gran potencial biotecnológico debido a su elevado potencial redox y su capacidad para transferir este potencial oxidativo a un residuo expuesto al solvente. Esto les permite oxidar una gran variedad de compuestos aromáticos fenólicos y no fenólicos, incluyendo el polímero de lignina, colorantes industriales e hidrocarburos aromáticos policíclicos entre otros (Martínez et al., 2009). Sin embargo, estas enzimas no se pueden utilizar a nivel industrial tal y como se producen en la naturaleza (Ayala et al., 2008). Previo a su aplicación, algunas de sus propiedades catalíticas y operacionales han de ser optimizadas y adaptadas a las condiciones en las que se llevarán a cabo los distintos procesos industriales en los que se pretendan utilizar.

La peroxidasa versátil (VP) presenta un especial interés debido a que combina propiedades catalíticas de las otras peroxidasas ligninolíticas (lignina peroxidasa, LiP; y manganeso peroxidasa, MnP) y de las peroxidasas genéricas (GP). Además, oxida directamente compuestos que MnP y LiP solo son capaces de oxidar en presencia de manganeso y alcohol veratrílico actuando como mediadores (Ruiz-Dueñas et al., 2009). La disponibilidad de la estructura cristalográfica de la VP de *Pleurotus eryngii* y el conocimiento de las relaciones estructura-función de las peroxidasas ligninolíticas y otras enzimas relacionadas han permitido el abordaje de los estudios de mejora de la VP desde un punto de vista racional. Estos se han centrado en el diseño de diferentes variantes mutadas de esta enzima con objeto de mejorar su estabilidad a peróxido de hidrógeno y pH, así como en la identificación de los determinantes estructurales responsables de dicha estabilidad. Además, se han llevado a cabo estudios de la capacidad ligninolítica de la VP y de la implicación del triptófano catalítico en la oxidación de la molécula de lignina.

1. Estudio y mejora de la estabilidad oxidativa

El peróxido de hidrógeno juega diferentes papeles a lo largo de la *vida* de las peroxidasas ligninolíticas. Así, se ha descrito que induce la producción de estas enzimas en los hongos de podredumbre blanca

(Ruiz-Dueñas et al., 1999a; Li et al., 1995), es el sustrato activador de las mismas y también es responsable del proceso de inactivación oxidativa que sufren estas peroxidasas (Valderrama et al., 2002).

Los estudios llevados a cabo en esta tesis sobre la estabilidad oxidativa de la VP de *Pleurotus eryngii* mostraron que la enzima se inactiva fácilmente en presencia de peróxido de hidrógeno, y que durante el proceso de inactivación sus cuatro metioninas son oxidadas a metionina-sulfona. Considerando su localización en la estructura molecular de la VP, cercanas al cofactor hemo y al triptófano catalítico, es probable que la oxidación de estos residuos altere la conformación del bolsillo del hemo conduciendo a un empeoramiento de la actividad y estabilidad de la enzima. Teniendo en cuenta este razonamiento, la sustitución de estas metioninas fue la primera estrategia diseñada para mejorar la estabilidad oxidativa de la VP. Estos residuos fueron sustituidos por otros más resistentes a la oxidación, lo que llevó a un aumento en la estabilidad oxidativa en las variantes en las que tres o las cuatro metioninas fueron sustituidas.

Como segunda estrategia de mejora de la estabilidad oxidativa, se diseñaron diferentes variantes en las que se introdujeron mutaciones en el entorno de la histidina distal. Este residuo y la arginina distal juegan un papel clave en la reacción con peróxido que lleva a la activación de la enzima (Hiner et al., 2002; Vitello et al., 1993). Las mutaciones pretendieron provocar ligeras modificaciones estructurales que afectaran a la reactividad de la enzima. La variante resultante de esta estrategia mostró una velocidad de activación ralentizada, lo que tuvo un efecto positivo en la estabilidad.

Finalmente, ambas estrategias se combinaron dando lugar a distintas variantes que presentaron una estabilidad oxidativa mejorada, entre las que destacó la mostrada por la variante quíntuple T45A/I103T/ M152F/M262F/M265L. El incremento en la estabilidad de esta variante se relacionó con el aumento de la estabilidad del Compuesto III (generado al reaccionar el compuesto II con peróxido), un intermediario que no forma parte del ciclo catalítico normal, y que conduce a la inactivación y al blanqueo de la enzima (Wariishi and Gold, 1989). Un Compuesto III más estable posiblemente permita a la enzima completar

el ciclo catalítico y volver al estado de reposo en condiciones operacionales evitando su inactivación. Así, la peroxidasa puede comenzar un nuevo ciclo catalítico y prolongar su vida útil. Por otra parte, aunque dar una explicación mecanística que relacione las mutaciones introducidas en la variante quíntuple con el aumento de estabilidad del Compuesto III es especulativa con los datos existentes, es razonable pensar que los cambios introducidos pueden influenciar las interacciones existentes entre los residuos del entorno de la histidina distal con el hemo, con un efecto directo en la formación y estabilidad del Compuesto III y en la estabilidad de la peroxidasa.

2. Estudio y mejora de la estabilidad a pH

La identificación de una manganeso peroxidasa (isoenzima MnP 4) estable en un amplio rango pH a partir del análisis genómico del hongo *Pleurotus ostreatus* (Fernández-Fueyo et al., 2014) y su elevada similitud estructural con la VP de *Pleurotus eryngii* permitió el diseño de una estrategia de mejora de la estabilidad de esta VP basada en la comparación estructural de ambas enzimas.

Tras el análisis estructural se identificaron una serie de motivos, entre los que se incluyen puentes de hidrógeno y un elevado número de residuos básicos expuestos al solvente, que se presentaron como posibles factores determinantes de la gran estabilidad mostrada por la MnP4. Estos motivos se trasladaron a la VP generándose distintas variantes mutadas que mostraron un aumento significativo en la estabilidad a pH ácido y neutro. El análisis de la estructura cristalográfica de estas variantes confirmó que las mejoras observadas se debían a los nuevos motivos estructurales introducidos en la VP.

Este trabajo demostró la posibilidad de trasladar de unas enzimas a otras los determinantes estructurales que modulan determinadas propiedades, definiéndose como una metodología efectiva para el diseño de biocatalizadores de interés. Actualmente se están secuenciando una gran cantidad de genomas de basidiomicetos de podredumbre blanca (Ohm et al., 2014; Floudas et al., 2012). Esto llevará a la identificación de nuevas peroxidasas ligninolíticas, algunas

de ellas con propiedades de interés (Martínez et al., 2014), que podrán usarse en futuros análisis estructurales comparativos con objeto de obtener enzimas diseñadas a la carta.

Por otro lado, el estudio racional de la variante 2-1B, obtenida por evolución dirigida a partir de la VP de *P. eryngii* (García-Ruiz et al., 2012), permitió profundizar en el conocimiento de alguno de los factores responsables de la estabilidad y catálisis en las peroxidasas ligninolíticas. Esta variante contiene siete mutaciones puntuales en su secuencia, como consecuencia del proceso de evolución, que le confieren una mayor estabilidad a pH y una elevada eficiencia catalítica para la oxidación de sustratos de bajo potencial redox. El diseño y caracterización de distintas variantes de VP portadoras de alguna o varias de las mutaciones de 2-1B permitió identificar qué sustituciones son responsables de las propiedades catalíticas mejoradas. Tal como se determinó a partir del análisis de dos estructuras cristalográficas obtenidas por difracción de rayos X, las sustituciones introducidas condujeron a la formación de nuevas interacciones con el hemo, así como la generación de nuevos puentes salinos y de hidrógeno que reforzaron zonas concretas de la arquitectura molecular.

En ambos estudios (análisis estructural comparativo entre VP y MnP4, y estudio racional de la variante 2-1B obtenida por evolución dirigida) se observó que la formación de los nuevos puentes de hidrógeno, puentes salinos o puentes disulfuro, que tuvieron como consecuencia el reforzamiento de la estructura secundaria de la enzima, tanto en áreas internas cercanas al hemo como en áreas más periféricas de la enzima, condujeron a un bolsillo del hemo más estable e imperturbable a cambios de pH. Esto demostró que el mantenimiento de la conformación del hemo y su entorno en el que se ubican residuos catalíticos esenciales, es fundamental para la estabilidad de la enzima. Además, la existencia de un elevado número de residuos básicos expuestos al solvente fue otro de los factores que aumentaron la estabilidad a pH ácido. Las interacciones de estos residuos con el solvente u otros residuos vecinos explicarían el efecto estabilizador producido por los mismos. La estabilidad a pH ácido de alguna de las variantes mejoradas es especialmente importante ya que las peroxidasas ligninolíticas presentan un pH óptimo bajo para la

oxidación de una gran variedad de sustratos (Heinfling et al., 1998; Ruiz-Dueñas et al., 1999b). Por tanto, la mejora en la estabilidad a pH ácido aumenta el potencial biotecnológico de estas enzimas.

3. Demostración de la transferencia electrónica entre la VP y la lignina

Uno de los objetivos de la tesis fue estudiar la capacidad ligninolítica de la VP y el papel que juega el triptófano catalítico en el proceso de oxidación de la lignina. Para ello se utilizaron lignosulfonatos (ligninas técnicas) solubles en agua procedentes del proceso de pasteado al sulfito. La VP fue capaz de actuar sobre lignosulfonatos procedentes de maderas duras y blandas con una eficiencia similar. Por el contrario, la variante W164S, en la que el triptófano catalítico fue sustituido por una serina, mostró constantes cinéticas reducidas para ambas ligninas, demostrando la participación de este triptófano en el proceso de oxidación. Estos resultados concordaron con los obtenidos en estudios anteriores para la oxidación de sustratos de alto potencial redox (Pérez-Boada et al., 2005). Además, los experimentos de resonancia paramagnética electrónica realizados con objeto de conocer qué radicales de VP o de sustrato se forman durante la reacción con la lignina, mostraron la señal de un radical triptófanilo tras la activación de la VP por H_2O_2 (Pogni et al., 2006), que fue sustituido por la señal correspondiente de radical de lignina cuando el sustrato fue añadido a la reacción. Estos resultados demostraron de manera inequívoca, y por primera vez para una peroxidasa ligninolítica, que el radical de triptófano formado en la VP es catalíticamente activo y responsable de la oxidación directa de la molécula de lignina, como ya se había demostrado para la oxidación de alcohol veratrílico con la lignina peroxidasa (Smith et al., 2009).

Asimismo, se llevó a cabo el tratamiento de los lignosulfonatos con VP en estado estacionario y los productos obtenidos fueron analizados. Los espectros de resonancia magnética nuclear mostraron la desaparición de las señales aromáticas de la lignina, confirmando las capacidades ligninolíticas de la VP. Simultáneamente, experimentos de cromatografía de exclusión molecular revelaron un aumento del peso molecular de los

lignosulfonatos, revelando que tras la oxidación de los lignosulfonatos por la VP los productos resultantes tienden a polimerizar, como ocurrió tras el tratamiento de lignosulfonatos con lacasa (Prasetyo et al., 2010).

Finalmente, la variante R257A/A260F, que presenta dos mutaciones en aminoácidos del entorno del triptófano catalítico (Ruiz-Dueñas et al., 2008), mostró una mejora en las constantes cinéticas para la reacción con los lignosulfonatos, lo que indicó que cambios en el entorno del triptófano catalítico modulan la actividad de éste.

El estudio de las diferentes variantes mutadas de VP condujo a la mejora de la estabilidad a peróxido y a pH, algunas de las principales dificultades que superar para la aplicación biotecnológica de esta peroxidasa. Además los estudios realizados en esta tesis han permitido profundizar en el conocimiento de las bases estructurales que determinan estas características y ponen de manifiesto el complejo sistema de factores que modulan la estabilidad. Las mejoras obtenidas en el actual trabajo junto con la estabilidad térmica intrínseca relativamente alta de la VP, así como el conocimiento cada vez más amplio de su mecanismo catalítico hacen de esta enzima un biocatalizador muy prometedor capaz de oxidar lignina y otros compuestos de alto potencial redox de interés.

4. References

Ayala, M., M.A.Pickard, and R.Vázquez-Duhalt. 2008. Fungal enzymes for environmental purposes, a molecular biology challenge. *J. Mol. Microbiol. Biotechnol.* 15:172-180.

Fernández-Fueyo, E., F.J.Ruiz-Dueñas, M.J.Martínez, A.Romero, K.E.Hammel, F.J.Medrano, and A.T.Martínez. 2014. Ligninolytic peroxidase genes in the oyster mushroom genome: Heterologous expression, molecular structure, catalytic and stability properties and lignin-degrading ability. *Biotechnol. Biofuels* 7:2.

Floudas, D., M.Binder, R.Riley, K.Barry, R.A.Blanchette, B.Henrissat, A.T.Martínez, R.Otillar, J.W.Spatafora, J.S.Yadav, A.Aerts, I.Benoit, A.Boyd, A.Carlson, A.Copeland, P.M.Coutinho, R.P.de Vries, P.Ferreira, K.Findley, B.Foster, J.Gaskell, D.Glotzer, P.Górecki, J.Heitman, C.Hesse, C.Hori, K.Igarashi, J.A.Jurgens, N.Kallen, P.Kersten, A.Kohler, U.Kües, T.K.A.Kumar, A.Kuo, K.LaButti, L.F.Larrondo, E.Lindquist, A.Ling, V.Lombard, S.Lucas, T.Lundell, R.Martin, D.J.McLaughlin, I.Morgenstern, E.Morin, C.Murat, M.Nolan, R.A.Ohm, A.Patyshakuliyeva, A.Rokas, F.J.Ruiz-Dueñas, G.Sabat, A.Salamov, M.Samejima, J.Schmutz, J.C.Slot, F.St.John, J.Stenlid, H.Sun, S.Sun, K.Syed, A.Tsang, A.Wiebenga, D.Young, A.Pisabarro, D.C.Eastwood, F.Martin, D.Cullen, I.V.Grigoriev, and D.S.Hibbett. 2012. The Paleozoic origin of enzymatic lignin decomposition reconstructed from 31 fungal genomes. *Science* 336:1715-1719.

García-Ruiz, E., D.González-Pérez, F.J.Ruiz-Dueñas, A.T.Martínez, and M.Alcalde. 2012. Directed evolution of a temperature-, peroxide- and alkaline pH-tolerant versatile peroxidase. *Biochem. J.* 441:487-498.

Heinfling, A., F.J.Ruiz-Dueñas, M.J.Martínez, M.Bergbauer, U.Szewzyk, and A.T.Martínez. 1998. A study on reducing substrates of manganese-oxidizing peroxidases from *Pleurotus eryngii* and *Bjerkandera adusta*. *FEBS Lett.* 428:141-146.

Hiner, A.N.P., E.L.Raven, R.N.F.Thorneley, F.García-Canovas, and J.N.Rodríguez-López. 2002. Mechanisms of compound I formation in heme peroxidases. *J. Inorg. Biochem.* 91:27-34.

Li, D., M.Alic, J.A.Brown, and M.H.Gold. 1995. Regulation of manganese peroxidase gene transcription by hydrogen peroxide, chemical stress, and molecular oxygen. *Appl. Environ. Microbiol.* 61:341-345.

Martínez, A.T., F.J.Ruiz-Dueñas, A.Gutiérrez, J.C.del Río, M.Alcalde, C.Liers, R.Ullrich, M.Hofrichter, K.Scheibner, L.Kalum, J.Vind, and H.Lund. 2014. Search, engineering and applications of new oxidative biocatalysts. *Biofuels Bioprod. Biorefining* 8:819-835.

Martínez, A.T., F.J.Ruiz-Dueñas, M.J.Martínez, J.C.del Río, and A.Gutiérrez. 2009. Enzymatic delignification of plant cell wall: from nature to mill. *Curr. Opin. Biotechnol.* 20:348-357.

Ohm, R.A., R.Riley, A.Salamov, B.Min, I.G.Choi, and I.V.Grigoriev. 2014. Genomics of wood-degrading fungi. *Fungal Genet. Biol.* 72:82-90.

Pérez-Boada, M., F.J.Ruiz-Dueñas, R.Pogni, R.Basosi, T.Choinowski, M.J.Martínez, K.Piontek, and A.T.Martínez. 2005. Versatile peroxidase oxidation of high redox potential aromatic compounds: Site-directed mutagenesis, spectroscopic and crystallographic investigations of three long-range electron transfer pathways. *J. Mol. Biol.* 354:385-402.

Pogni, R., M.C.Baratto, C.Teutloff, S.Giansanti, F.J.Ruiz-Dueñas, T.Choinowski, K.Piontek, A.T.Martínez, F.Lendzian, and R.Basosi. 2006. A tryptophan neutral radical in the oxidized state of versatile peroxidase from *Pleurotus eryngii*: a combined multi-frequency EPR and DFT study. *J. Biol. Chem.* 281:9517-9526.

Prasetyo, E.N., T.Kudanga, L.Ostergaard, J.Rencoret, A.Gutiérrez, J.C.del Río, J.I.Santos, L.Nieto, J.Jimenez-Barbero, A.T.Martínez, J.B.Li, G.Gellerstedt, S.Lepifre, C.Silva, S.Y.Kim, A.Cavaco-Paulo, B.S.Klausen, B.F.Lutnaes, G.S.Nyanhongo, and G.M.Guebitz. 2010. Polymerization of lignosulfonates by the laccase-HBT (1-hydroxybenzotriazole) system improves dispersibility. *Bioresource Technol.* 101:5054-5062.

Ruiz-Dueñas, F.J., F.Guillén, S.Camarero, M.Pérez-Boada, M.J.Martínez, and A.T.Martínez. 1999a. Regulation of peroxidase transcript levels in liquid cultures of the ligninolytic fungus *Pleurotus eryngii*. *Appl. Environ. Microbiol.* 65:4458-4463.

Ruiz-Dueñas, F.J., M.J.Martínez, and A.T.Martínez. 1999b. Molecular characterization of a novel peroxidase isolated from the ligninolytic fungus *Pleurotus eryngii*. *Mol. Microbiol.* 31:223-236.

Ruiz-Dueñas, F.J., M.Morales, E.García, Y.Miki, M.J.Martínez, and A.T.Martínez. 2009. Substrate oxidation sites in versatile peroxidase and other basidiomycete peroxidases. *J. Exp. Bot.* 60:441-452.

Ruiz-Dueñas, F.J., M.Morales, M.J.Mate, A.Romero, M.J.Martínez, A.T.Smith, and A.T.Martínez. 2008. Site-directed mutagenesis of the catalytic tryptophan environment in *Pleurotus eryngii* versatile peroxidase. *Biochemistry* 47:1685-1695.

Smith, A.T., W.A.Doyle, P.Dorlet, and A.Ivancich. 2009. Spectroscopic evidence for an engineered, catalytically active Trp radical that creates the unique reactivity of lignin peroxidase. *Proc. Natl. Acad. Sci. USA* 106:16084-16089.

Valderrama, B., M.Ayala, and R.Vázquez-Duhalt. 2002. Suicide inactivation of peroxidases and the challenge of engineering more robust enzymes. *Chem. Biol.* 9:555-565.

Vitello, L.B., J.E.Erman, M.A.Miller, J.Wang, and J.Kraut. 1993. Effect of Arginine-48 replacement on the reaction between cytochrome *c* peroxidase and hydrogen peroxide. *Biochemistry* 32:9807-9818.

Wariishi, H. and M.H.Gold. 1989. Lignin peroxidase compound III: Formation, inactivation, and conversion to the native enzyme. *FEBS Lett.* 243:165-168.

CONCLUSIONES/ CONCLUSIONS

CONCLUSIONES

1. La sustitución de residuos de metioninas, susceptibles de oxidación por peróxido, y la modificación de la reactividad de la enzima con dicho cosustrato, permitieron incrementar la estabilidad oxidativa de la peroxidasa versátil (VP). Estos cambios repercutieron en un aumento de la estabilidad del compuesto III (Fe^{III}-$O_{2}^{\cdot-}$).

2. La introducción de motivos estructurales, como puentes de hidrógeno, salinos o disulfuro, estabilizó el hemo y su entorno en la VP, lo que se reflejó en un aumento de la estabilidad a pH. Igualmente, la introducción de residuos básicos expuestos al solvente resultó en un aumento de la estabilidad a pH ácido.

3. La transferencia de motivos estabilizantes encontrados en el análisis genómico de peroxidasas de interés se presenta como una buena estrategia para el diseño y optimización de este tipo de biocatalizadores.

4. La nueva conexión con el hemo, los puentes salinos formados y la eliminación de interacciones ácido-ácido desestabilizadoras, fueron fundamentales en la mejora de la variante 2-1B obtenida por evolución dirigida, ya que estabilizaron el bolsillo del hemo y mantuvieron la enzima activa bajo condiciones alcalinas moderadas.

5. La transferencia electrónica producida entre la VP y la lignina durante la oxidación de ésta fue establecida en condiciones de flujo detenido (*stopped flow*) y se relacionó inequívocamente con la presencia del triptófano 164 que forma un radical catalíticamente activo.

6. La capacidad ligninolítica de la VP fue demostrada ya que el tratamiento de ligninas técnicas con la enzima mostró la progresiva degradación de éstas. Por otra parte, los productos de degradación resultantes mostraron una tendencia a polimerizar.

7. Las propiedades catalíticas del triptófano 164 están moduladas por residuos de su entorno y pueden ser optimizadas mediante la modificación del mismo.

CONCLUSIONS

1. The substitution of methionines, sensitive to the oxidative inactivation, and the modification of the reactivity of the enzyme with the aforementioned co substrate, allowed the improvement of the oxidative stability of versatile peroxidase (VP). As a consequence of these changes, the stability of Compound III (Fe^{III}-$O_{2}^{\cdot-}$) was increased.

2. The introduction of structural motifs such as hydrogen bonds, salt bridges or disulphide bridges, stabilized the heme environment en the VP, which led to an improvement of the pH stability. In the same way, the introduction of solvent exposed basic residues enhanced the acidic stability of the enzyme.

3. The transfer of stabilizing motifs found in the genomic analysis of peroxidases of interest was showed as a good strategy for the design and optimization of this kind of biocatalysts.

4. The new connection with the heme, the new salt bridges and the removal of destabilizing acid-acid interactions were fundamental in the improvements observed in the 2-1B variant (obtained by directed evolution), since they stabilized the heme pocket and keep the enzyme active under moderate alkaline conditions.

5. The electron transfer produced between the VP and the lignin during the oxidation this polymer was established under stopped flow conditions, and it was unequivocally related to the presence of the tryptophan 164 which formed a catalytically active radical.

6. The ligninolytic ability of VP was demonstrated since the treatment of technical lignins with the enzyme resulted in the progressive degradation of the polymers. The resulting products of degradation showed a tendency to repolymerization.

7. The catalytic properties of tryptophan 164 are modulated by residues neighbor to this catalytic site and they can be optimized by the modification of the tryptophan environment.

ANEXO I

El presente trabajo ha dado lugar a las siguientes publicaciones y comunicaciones en congresos:

i) Publicaciones relacionadas con la tesis doctoral:

1. Sáez-Jiménez V., Acebes S., Guallar V., Martínez A.T., Ruiz-Dueñas F-J. (2015) Improving the oxidative stability of a high redox potential fungal peroxidase by rational design. *PLoS ONE* 10 (4):e0124750.

2. Sáez-Jiménez V., Baratto M.C., Pogni R., Rencoret J., Gutiérrez A., Santos J.I., Martínez A.T., Ruiz-Dueñas F-J. (2015) Demonstration of lignin-to-peroxidase direct electron transfer: a transient-state kinetics, directed mutagenesis, EPR and NMR study. *Journal of Biological Chemistry* 290, 23201-23213.

3. Sáez-Jiménez V., Fernández-Fueyo E., Medrano F.J., Romero A., Martínez A.T., Ruiz-Dueñas F-J. (2015) Improving the pH-stability of versatile peroxidase by comparative structural analysis with a naturally-stable manganese peroxidase. *PLoS ONE*

4. Sáez-Jiménez V., Acebes S., García-Ruiz E., Romero A., Guallar V., Alcalde M., Medrano F.J., Martínez A.T., Ruiz-Dueñas F-J. (2015) Investigating the basis of stability in an evolved versatile peroxidase (en preparación).

ii) Publicaciones no relacionadas con la tesis doctoral:

1. Baratto M.C., Sinicropi A., Linde D., Sáez-Jiménez V., Sorace L., Ruiz-Dueñas F.J., Martínez A.T., Basosi R., Pogni R. (2015) Redox-active sites in *Auricularia auricula-judae* dye-decolorizing peroxidase and several directed variants: a multifrequency EPR study. *The Journal of Physical Chemistry* doi : 10.1021/ acs.jpcb.5b02961.

2. Linde D., Pogni R., Cañellas M., Lucas F., Guallar V., Baratto M.C., Sinicropi A., Sáez-Jiménez V., Coscolín C., Romero A., Medrano F.J., Ruiz-Dueñas F.J., Martínez A.T. (2015) Catalytic surface radical in

dye-decolorizing peroxidase : a computational, spectroscopic and site-directed mutagenesis study. *Biochemical Journal* 466, 253-262.

iii) Trabajos presentados en congresos :

1. Ruiz-Dueñas, F. J., Fernandez, E., Sáez-Jiménez, V., Martínez, M. J., and Martínez, A. T. (2010) Hemeperoxidases in the *Pleurotus ostreatus* genome *Proc.LignoBiotech-1 Symp*., Reims.

2. Ruiz-Dueñas, F. J., Fernández, E., Lomascolo, A., Uzan, E., Sáez-Jiménez, V., Miki, Y., Martínez, M. J., and Martínez, A. T. (2010) Peroxidasas de interés biotecnológico en genomas de basidiomicetos degradadores de lignocelulosa. *XIII Reunión de la Red Temática de Biotecnología de Materiales Lignocelulósicos*, Valladolid.

3. Ruiz-Dueñas, F. J., Fernández, E., Sáez-Jiménez, V., Martínez, M. J., and Martínez, A. T. (2010) Pleurotus hemeperoxidases of biotechnological interest: a complete inventory form the recently available *P. ostreatus* genome. In Feijoo, G. and Moreira, M. T., editors. *Oxidative enzymes as sustainable industrial biocatalysts*, USC (ISBN-13: 978-84-614-2824-3), Santiago de Compostela.

4. Ruiz-Dueñas, F. J., Fernández-Fueyo, E., Sáez-Jiménez, V., Martínez, A. T. (2013) Genomic analysis in the search for peroxidases of indrustrial interest. *XXVI Congreso de Microbiología SEM.* L'Hospitalet.

5. Morales M., Rencoret J., Sáez-Jiménez V., Gutiérrez A., Martínez M.J., Martínez A.T., Ruiz-Dueñas F.J. (2013) Development of biocatalysts for treatment of complex phenolic mixtures based on fungal versatile peroxidase. *5th Congress of European Microbiologists (FEMS2013)* Leipzig, Germany.

6. Pogni R., Ruiz-Dueñas F.J., Baratto M.C., Sinicropi A., Sáez-Jiménez V., Linde D., Martínez A.T., Basosi R. (2014) From *P. eryngii* versatile peroxidase to *A. auricula-judae* dye-decoloriring peroxidase: an EPR work in progress. *Oxizymes*, Vienna.

7. Sáez-Jiménez V., Fernández-Fueyo E., Medrano F.J., Romero A., Martínez, A.T., F.J. Ruiz-Dueñas (2014) pH stability improvement of a high redox-potential fungal peroxidase based on the analysis of stable peroxidases identified in genomes. *Ninth Annual DOE Joint Genome Institute User Meeting,* Walnut Creek, California.

8. Sáez-Jiménez V., Baratto M.C., Pogni R., Martínez Á.T., Ruiz-Dueñas F.J. (2014) Demonstration of lignosulfonates oxidation by versatile peroxidase from *Pleurotus eryngii*. In J.C. del Río, A. Gutiérrez, J. Rencoret and Á.T. Martínez, editors. *13th European Workshop on Lignocellulosics and Pulp (EWLP2014)* (ISBN : 978-84-616-9842-4), Seville.

9. Sáez-Jiménez V., Fernández-Fueyo E., Medrano F.J., Romero A., Martínez A.T., and Ruiz-Dueñas F.J. (2014) Improving pH-stability of model versatile peroxidase through the search for structural motifs in stable peroxidases from genomes. *12th European Conference on Fungal Genetics (ECFG12)*, Seville.

10. Ruiz-Dueñas F.J., Fernández-Fueyo E., Sáez-Jiménez V., Martínez A.T. (2014) Genomic analysis in the search for oxidoreductases of industrial interest. *12th European Conference on Fungal Genetics (ECFG12)*, Seville.

11. Sáez-Jiménez V., Martínez A.T., Ruiz-Dueñas F.J. (2015) Mejora de la estabilidad oxidativa de una peroxidasa fúngica de alto potencial redox mediante diseño racional. *1as Jornadas Españolas de Biocatálisis*, Madrid.

iv) Comunicaciones orales presentadas en congresos:

1. Sáez-Jiménez V., Fernández-Fueyo E., Medrano F. J., Romero A., Martínez A.T., Ruiz-Dueñas F.J. (2013) Improving pH-stability of versatile peroxidase through search for stabilizing motifs in stable peroxidases from genomes. *XXXVI Congreso Sociedad Española de Bioquímica y Biología Molecular,* Madrid.

2. Sáez-Jiménez V., Fernández-Fueyo E., Medrano F. J., Romero A., Martínez A.T., Ruiz-Dueñas F.J. (2013) Mejora de la estabilidad de la peroxidasa versátil de *Pleurotus eryngii* mediante diseño racional. *XVI Reunión de la Red Lignocel*, Pontevedra.

3. Sáez-Jiménez V., Baratto M.C., Pogni R., Rencoret J., Gutiérrez A., Santos J.I., Ruiz-Dueñas F.J., Martínez A.T. (2015) Demostración de la transferencia electrónica directa entre el polímero de lignina y la peroxidasa versátil. *XVII Reunión de la Red Lignocel*, Madrid.